Controls on and Morphodynamic Effects of Width Variations in Bed-load Dominated Alluvial Channels: Experimental and Numerical Study

Singh, Umesh

UNIVERSITÀ DEGLI STUDI DI TRENTO

Queen Mary University of London

Erasmus Mundus Joint Doctorate School in Science for Management of Rivers and their Tidal System

---

Umesh Singh

Controls on and Morphodynamic Effects of Width Variations in Bed-load Dominated Alluvial Channels:

Experimental and Numerical Study

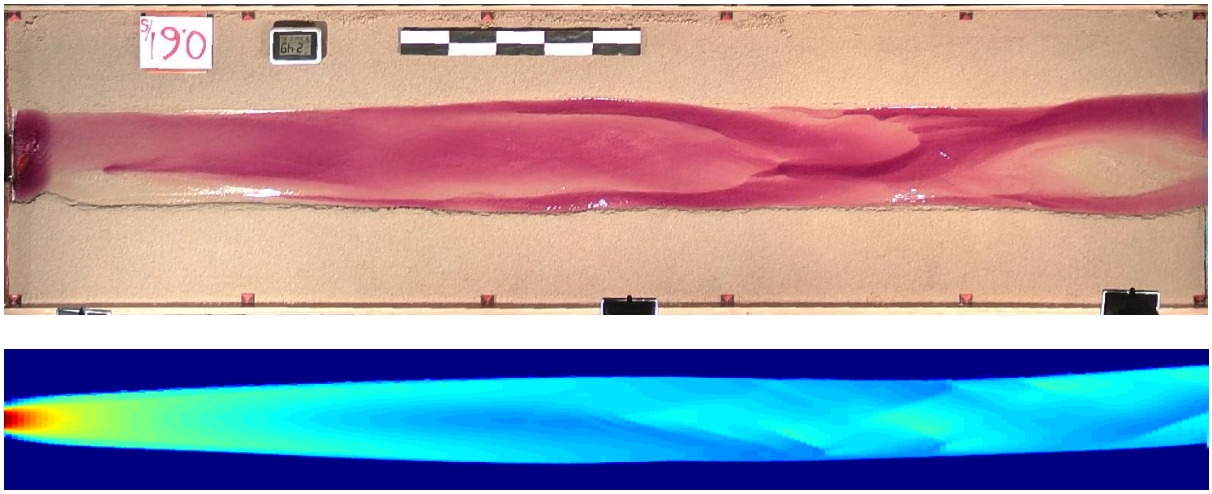

Erasmus Mundus

November 2015

Doctoral thesis in Science for Management of Rivers and their Tidal Systems
Cycle: 2

Primary Institution:
Department of Civil, Environmental and Mechanical Engineering, University of Trento
Secondary Institution:
Department of Physical Geography, Queen Mary University of London
Associate Partner:
UNESCO-IHE, Delft

Supervisors:
Ass. Prof. Dr. Guido Zolezzi, University of Trento
Prof. Dr. James Brasington, Queen Mary University of London
Ass. Prof. Dr. Alessandra Crosato, UNESCO-IHE

Academic Year 2015/16

The SMART Joint Doctorate Programme

Research for this thesis was conducted with the support of the Erasmus Mundus Programme[1], within the framework of the Erasmus Mundus Joint Doctorate (EMJD) SMART (Science for Management of Rivers and their Tidal systems). EMJDs aim to foster cooperation between higher education institutions and academic staff in Europe and third countries with a view to creating centres of excellence and providing a highly skilled 21st century workforce enabled to lead social, cultural and economic developments. All EMJDs involve mandatory mobility between the universities in the consortia and lead to the award of recognised joint, double or multiple degrees. The SMART programme represents collaboration among the University of Trento, Queen Mary University of London, and Freie Universität Berlin. Each doctoral candidate within the SMART programme has conformed to the following during their 3 years of study:

i. Supervision by a minimum of two supervisors in two institutions (their primary and secondary institutions).
ii. Study for a minimum period of 6 months at their secondary institution.
iii. Successful completion of a minimum of 30 ECTS of taught courses.
iv. Collaboration with an associate partner to develop a particular component / application of their research that is of mutual interest.
v. Submission of a thesis within 3 years of commencing the programme.

[1] This project has been funded with support from the European Commission. This publication reflects the views only of the author, and the Commission cannot be held responsible for any use which may be made of the information contained therein.

This page is left intentionally blank

Acknowledgements

I feel blessed to have received support and guidance of many wonderful people who have contributed in various ways during the course of my PhD. Words are not enough to express my gratitude but being able to thank them in this platform is just a small gesture of appreciation towards their belief and support. This work has been carried out at University of Trento (UNITN), Queen Mary University of London (QMUL) and UNESCO-IHE/ TU Delft.

I would like to start by expressing my gratitude to European Commission who supported me financially to carry out this PhD. It would not be possible for me to undertake this research without their financial support.

I am highly indebted to my supervisor at UNITN, Ass. Prof. Dr. Guido Zolezzi for his continuous support, valuable feedback and guidance throughout my research period. My sincere thanks goes to Dr. Walter Bertoldi for providing me experimental data to carry out numerical simulations and Dr. Annunziato Siviglia for supervising the numerical simulations. Also, many thanks to Davide Vanzo for helping me setup numerical simulations using GIAMT2D and Dino Ritz for carrying out analytical computations.

I want to express my gratitude to my supervisor at QMUL Prof. Dr. James Brasington for providing me opportunity to carry out numerical study. I would also like to thank Richard Williams for providing me Delft3D software with updated bank erosion module and Richard Measures for explaining the new bank erosion implementations.

My deep sense of gratitude goes to my supervisor at UNESCO-IHE Ass. Prof. Dr. Alessandra Crosato for having faith in me and giving me an opportunity to carry out laboratory experiments. It has been a great learning experience for me. She has been a great source of inspiration and her optimism has always pushed me towards better pathway.

I would like to express my special thanks to Prof. Dr. Wim Uijttewaal for providing facilities for the experiments. Also, many thanks to technical staff of laboratory of fluid mechanics, TU Delft, specially to Sander De Vree and Ruben for their creative suggestions in design and development of the flume facility.

I want to express my gratitude to Andres Vargas Luna and Protogene Byshimo for helping me to adapting to the working environment at TU Delft. My special thanks to Jairo Angel Escobar and Harmen Schölvinck, without their help it would not have been possible to carry out the experiments. Also, many thanks to Meles Tewodke and Dibesh Shrestha for their valuable support in experimental work.

My sincere thanks goes to Marina Rogato (UNITN), Aureliano Cerreti (UNITN), Claudia Frazinger (UNITN), Lara Fiamozzini (UNITN), Aysha Sabri (QMUL), Jennifer Murray (QMUL) and Otti Kievits (TU Delft) for sharing the heavy burden of bureaucracy. Research life without their support would have been much more difficult.

I am very thankful to all my friends and colleagues from SMART program and 28th PhD cycle for always being there, for the moments we spent together and for their fruitful discussions, unconditional support and encouragement. In particular, I would like to thank Luca Adami - who has been there not only as a friend but also as a guardian, Tesfaye Tarkeign, Marco Redolfi, Jean-Philips Belliard, Simone Zen and Sepideh Ramezani. Thank you so much guys for your invaluable presence in my life!

Finally, and most importantly, I would love to express my sincere and heartfelt gratitude to my family, especially to my lovely wife Shreya who has equally shared the highs and lows of research life with me.

"Gita and Ganga constitute, between themselves, the essence of Hinduism: one its theory and the other is practice."

Swami Vivekananda

Abstract

Understanding and predicting the effects of width variability and the controls on width adjustment in rivers has a key role in developing management approaches able to account for the physical, ecological and socio-economical dimensions of a river system.

Width adaptation in a river occurs due to erosion and accretion of banks, within various geomorphic, environmental and anthropogenic contexts, which set the most relevant factors controlling the morphological dynamics of the river corridor. In turn, changes in channel width imply alterations of the river channel morphodynamics at a variety of space and time scales, implying, for instance, modifications of important controlling parameters, like the width-to-depth ratio, which is closely related to the planform morphology of alluvial rivers. Width adaptation bears crucial implications for river management: on one hand, channel widening may result in loss of valuable land and in the increase of the damage risk of infrastructures in surrounding areas, which are often subjected to increasing pressures related to human settlements and economic activities. On the other hand, several approaches to river restoration are based on the concept of "giving more room to the river", and thus allow the banks to erode and widen, to increase morphological and physical habitat diversity. In view of these implications, the prediction of width adaptation, understanding of its main causes and controlling factors, and quantification of the riverbed morphodynamic response to width variability is of crucial importance to support effective river management.

The practical and engineering interest on stable cross-sections of alluvial channels has attracted a considerable amount of scientific research since late 19th century. Much of the research has focused in developing width prediction tools mostly based on empirical approaches and methods based on extremal hypothesis and to lesser extent on mechanistic methods. In the past two decades, research has advanced in developing numerical models including geotechnical as well as fluvial processes to simulate bank failure mechanism more accurately. Despite significant development on the width predictors, research in controls on width evolution of river channels cannot still be considered a fully settled issue.

The study of the morphodynamic response of the riverbed to width variability in space and time is somehow more recent, and has focussed on the dynamics of large-scale bedforms (river bars) that produce a variety of riverbed configurations and planform morphologies. The effect of spatial width variability on river bars has mainly been based on assessing the role of such planform forcing effects to the bed topography, both in case of straight and meandering river channels. The amplitude of width variability has been related to fundamental questions as those behind the transition between single- and multi-thread river morphologies, and most studies consider regular spatial variations of the channel width. Research on the response of channel bed to spatial width variability has mostly consisted of modelling and theoretical approaches, which point out the limit cases of a purely "free" system response, associated with morphodynamic instability, an of purely "forced" bedform pattern by spatial planform non-homogeneity. The large spectrum of mixed configurations between those two theoretical limits has been so far seldom investigated, despite its strong relevance for real river systems. The limits of what can actually be considered a "planform forcing" effect, or has instead a too small variability have never been clarified, a well as its role on the resulting channel morphodynamics. For instance, the effects of small amplitude width variations on straight channels, which may be due to imperfect bank lines or protrusion due to vegetations, on morphodynamics of river bed has been neglected so far.

This study has two main scientific goals. The first goal is to quantitatively investigate the role of potentially controlling factors on the width evolution of bedload-dominated straight river channels, including the initial channel width, the flow regime and the sediment supply regime. The major question driving the research is whether a river would attain the same width independently of the initial conditions and whether this would be true for all types of discharge regimes of water and sediment supply. The study is carried out using both laboratory experiments (Chapter 3), analytical model (Chapter 4) and numerical model (Chapter 5) tested with reference to real river data. Integrating the results of the experiments with those of analytical and numerical models allows deriving a more robust and complete understanding of the processes involved, including transient width evolution, time scales to morphodynamic equilibrium, equilibrium conditions and role of each controlling factor. In Chapter 3 a set of controlled laboratory experiments have been performed to study channel adjustments in a movable-bed, erodible-bank channel under different flow and sediment regimes and different initial widths. The long-term width evolution is observed to be independent of initial channel width under uniform formative discharge without upstream sediment supply. Width evolution rate is observed to depend on the initial channel width when the sediment is supplied from upstream with the narrowest initial channel evolving at the highest widening rate and resulting into the widest channel. A physics based analytical model of channel adjustment (Chapter 4) has been applied to some of the experiments described in Chapter 3. Furthermore, in Chapter 5 a field scale numerical model was setup using the flow and topographic data of gravel bed reach of Upper Severn River near Abermule (UK). The trend of width evolution computed by analytical model is also qualitatively in agreement with the observations in the experiments. The results of numerical modeling have further supported the observations in the experiments which reinforce the findings in agreement with laws of physics.

The second goal of the present PhD research is to analyze the morphodynamic response of the riverbed to small-scale spatial variability of the channel width, focusing on alternate bars. The main question driving the investigation (Chapter 6) is to which extent small-amplitude, irregular width variations in space affect the morphodynamics of river bars, the fundamental riverbed patterns at the scale of the channel width. The key theoretical question behind this investigation is to which extent "small amplitude" width variations can be considered as a planform forcing, for the channel bed morphodynamic response, and whether it is possible to establish a threshold amplitude below which they may act as a near bank-roughness element. The study is based on hydraulic conditions typical of bedload-dominated piedmont streams, often having flows with Froude numbers around 1 or higher at bar-forming or channel-forming conditions. The study is developed through a numerical modeling approach. Because of the considered hydraulic conditions (close to critical-Froude number) first, a comparison is made between one semi-coupled numerical morphodynamic model, expected to be most suitable for sub critical flows, and one fully-coupled numerical morphodynamic model which can handle Froude-critical flows to assess the potential shortcomings of applying a semi-coupled model under close-to-critial Froude conditions. Such test, (Appendix B) supports the use of both models, and the semi-coupled model is eventually preferred for the advantages in computational speed. Such model is used for the numerical investigations performed in Chapter 6 and to some extent also in Chapter 5. The comparison is based on the reproduction of alternate bars morphodynamics observed in existing sets of flume experiments with fixed banks and super-critical flow conditions. The results of numerical modeling have shown that the small width variations have accelerated the development of the steady bars suppressing the free bar instability. Further investigations reveal that the effects of small width variations to a certain extent can be captured by parameterizing them in the form of increased roughness close to the banks or as small obstructions along the banks.

Contents

List of Figures

List of Tables

1 INTRODUCTION

Most ancient civilizations existed along rivers like the Jordan, the Euphrates, the Tigris, the Nile, the Indus and the Yellow River, from as early as the 11th Millennium BC. The earliest uses of the river water for irrigation with a developed canal systems occurred around the 7th century BC along the Tigris River. Navigation started in the Euphrates in the 4th millennium BC and the first dams were constructed in Jawa in the 3rd millennium BC [*Pierre-Louis*, 2005]. An exponential increase in use and modification of natural water resources, especially in Europe, occurred after the 16th century AD [*Nienhuis and Leuven*, 2001]. Human-made physical changes in rivers include canalization, narrowing and straightening to reclaim riparian land for settlement and economical activities. Dams and reservoirs are made for flood control, hydropower generation and storage of water for irrigation and drinking purposes [*Nienhuis and Leuven*, 2001]. Extraction of sand and gravel from rivers is mainly carried out for construction purposes [e.g. *Surian and Rinaldi*, 2003]. Such interventions change both discharge and sediment regimes of rivers, which then lead to river channel adaptation through morphological changes [*Jansen et al.*, 1979]. At the basin scale, also the change in land use result in river discharge and sediment regimes alterations [*Walling*, 1999; *Foley*, 2005]. The on-going exponential growth of human population and economic development is expected to further increase the number of human interventions in rivers, also in developing nations. *Zarfl et al.* [2015] report that about 3,700 dams are presently under construction or at the planned stage in developing countries. *Church and Ferguson* [2015] point out the need to understand the morphological impact of such human interventions in rivers. At the same time there is an increasing trend of rehabilitating modified rivers to achieve a more natural state in the developed nations [*Nienhuis and Leuven*, 2001]. River rehabilitation is generally carried out to allow higher dynamics in the morphological processes [*Shields et al.*, 2003]. However, increased bed and bank dynamics may lead to undesirable channel widening, resulting in loss of flood plains [*Amiri-Tokaldany et al.*, 2003] and damage to hydraulic structures [*Simon*, 1995], transportation and flood defense infrastructures [*Iwasaki et al.*, 2015]. Channel reconfiguration (Figure 1) and flow restoration are key activities in river rehabilitation [*Wohl et al.*, 2015]. These interventions need quantitative process-based knowledge of channel geometry and planform evolution on the long term [*Shields et al.*, 2003; *Niezgoda and Johnson*, 2005].

After a permanent change of flow, sediment regimes and morphology, caused for instance by human interventions or by a natural event, rivers evolve towards a new morphodynamic equilibrium. At the reach scale, this is characterized by adjusted values of longitudinal slope, channel width and depth. Oscillations around the averaged values of these variables can be expected due to short-term fluctuations related to the variation of discharge and sediment input occurring at the event time scale. The path to the adjusted values, or value ranges, starts from the conditions at which the intervention is made (initial conditions). Early width adaptation occurs over a relatively short time-scale, years to decades, whereas slope adaptation occurs over much longer time-scale, decades to centuries. In turn changes of longitudinal slope influence the width, resulting in long-term width adaptation [*Wilson*, 1973; *Parker et al.*, 2007]. The depth adaptation is governed by both the evolving slope and width. Due to the shorter time-scale of the width adaptation, the effects of changes in hydrological and sediment supply conditions are often described in terms of width and depth [*Huang et al.*, 2014; *Kaless et al.*, 2014] or equivalently, in terms of width and bed level adjustments [*Surian and Rinaldi*, 2003] . However, the slow river slope adaptation can result in additional important long-term channel adjustments.

Figure 1. Images showing examples of river restoration projects a) re-meandering of the straightened reach of River Brede at Logumkloster, Denmark and b) local widening along the straight reach of River Emme at Aeflingen, Switzerland (Courtesy: Dr. Alessandra Crosato)

The channel geometry has historically represented a fundamental topic in river geomorphology. It includes channel planform, width and depth. The planform can be studied by means of planform predictors. The predictors based on channel classifications [*Schumm*, 1985] and physics [*Crosato and Mosselman*, 2009] require prior estimation of the channel width, whereas empirical planform predictors [*van den Berg*, 1995; *Kleinhans and van den Berg*, 2011]. Planform predictors based on extremal hypotheses [*Millar*, 2000; *Eaton et al.*, 2010] rely on their width predictors. So, channel width prediction has an important role in the possibility to predict the pattern of unconfined alluvial channels, with key implications for the design of river restoration measures that forsee "more room to the rivers" and for the sustainable management of the "erodible river corridor" [*Piégay et al.*, 2005; *Rinaldi et al.*, 2009].

The width adaptation has been studied so far by using:

- Reach-averaged width predictors: empirical hydraulic geometry relations [*Leopold and Maddock*, 1953; *Andrews*, 1984; *Hey and Thorne*, 1986; *Parker et al.*, 2007], mechanistic approaches [*Parker*, 1978a, 1978b; *Vigilar, Jr. and Diplas*, 1998] and extremal hypothesis approaches [*Millar and Quick*, 1993; *Cao and Knight*, 1996; *Millar*, 2005; *Eaton and Church*, 2007].
- Numerical models (reach scale or depth scale) [*Langendoen and Simon*, 2008; *Rinaldi et al.*, 2008; *Jia et al.*, 2010; *Langendoen et al.*, 2015]; analytical models [*Tealdi et al.*, 2011].

Reach-averaged width predictors are widely used. They compute the hydraulic geometry of a channel cross-section, based on discharge and sediment properties, irrespective of the initial conditions. However, *Mosselman* [2004] argue that the equilibrium hydraulic geometry may depend also on initial and boundary conditions. *Cao and Knight* [1996] highlight the width-to-depth ratio as an important parameter to define the equilibrium hydraulic geometry. *Blench* (*Blench* 1969, cited by *Mosselman* 2004) state that the equilibrium hydraulic geometry can take any value within a range of values. More in general, the effect of initial channel width on the long-term channel configuration still represents an open issue that requires further investigation.

The discharge of both natural and modified rivers varies at a variety of time scales. Bank-full discharge is widely used as the channel-forming hydraulic condition in most width-prediction models. The channel-forming discharge is an idealized concept, defined as a single value of the discharge which results in a channel configuration comparable to the one obtained with variable discharge [*Shields et al.*, 2003]. In general, this may not be satisfied by a single value of the discharge, because of the non-linear relations between river flow and morphology [*Prins and De Vries*, 1971]. *Van Der Klis* [2003] and *Tubino* [1991], among others, highlight the importance of discharge variation in modelling of river morphology. *Visconti et al.* [2010] found out that discharge variations has a key role in maintaining certain river patterns, such as transitional morphologies between single and multi-thread rivers. Few experimental studies showed that the initial bank-full discharge leads to wider channels, so that the final bank-full discharge is not the channel forming condition [*Valentine et al.*, 2001; *Bertoldi and Tubino*, 2005; *Byishimo*, 2014]. So, better understanding is required on the role of variable discharge and bank full discharge on the evolution of the channel width.

The flow over alluvial beds causes morphodynamic instability, resulting in bed waves at different scales, depending on the width-to-depth ratio and flow characteristics [*Colombini and Stocchino*, 2012]. The morphological characteristics of the smallest bed waves, ripples, scale with the sediment size, the larger dunes and anti-dunes scale with the flow depth. Bars, the largest of all, scale with the cross-section of the river. Ripples form at low Shields numbers, corresponding to hydraulically smooth or transitional regimes. Also dunes and anti-dunes form at hydraulically smooth or transitional flow regimes, but at higher Shields numbers [*Colombini and Stocchino*, 2011]. Dunes are dominant at subcritical flow conditions whereas anti-dunes appear at super-critical flow conditions [*Colombini and Stocchino*, 2008]. Bars occur at shallow water conditions i.e. at large width to depth ratio, irrespective of the flow being sub critical or super critical [*Tubino et al.*, 1999; *Colombini and Stocchino*, 2012].

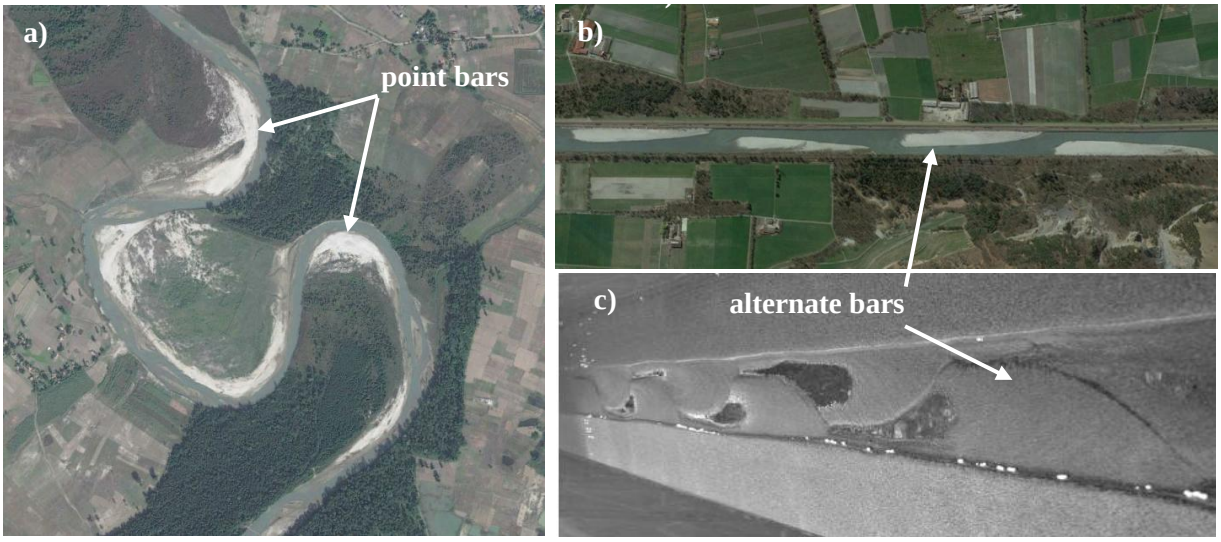

Figure 2: Images showing a) Point bars (forced bars) in the meandering reach of Mohona River at Bordadi, Nepal, from Google Earth, b) alternate bars (free bars) in the straight reach of the Rhine at Sargans, Switzerland, from Google Earth and c) alternate bars formed during the early stage of channel development in laboratory experiments of *Bertoldi and Tubino* [2005].

Bars are commonly present in natural rivers, affect and are strongly affected by variations of the channel width (Figure 2). Bars can be classified as free [*Tubino et al.*, 1999], forced [*Zolezzi and Seminara*, 2001] and hybrid [*Duró et al.*, 2015] i.e. resulting from free-forced interactions [*Seminara and Tubino*, 1989]. Free bars originate by morphodynamic instability caused by the flow over a

mobile channel bed at sufficiently high width-to-depth ratios and have a periodic character, whereas forced bars appear due to forcing by a local flow perturbation and may have spatially variable amplitude. Free bars migrate mainly in downstream but forced bars don't move. Free bars have been studied since long by means of "bar instability theories"; linear [*Callander*, 1969; *Engelund*, 1970; *Parker*, 1976; *Fredsøe*, 1978] and weakly non-linear models [*Colombini et al.*, 1987; *Schielen et al.*, 1993]. Forced bars mostly occur by local forcing (e.g. groynes, bend) or boundary conditions (e.g. width variations) that can be viewed as distributed planform forcing effects. Hybrid bars are periodic steady bars that form due to a combination and/or interaction of morphodynamic instability and steady forcing. Morphodynamic instability may affect their geometrical characteristics whereas steady forcing determines their spatial location and celerity (= 0), as well as their growth rate and, to some extent, geometry. Hybrid bars have been studied using linear models [*Struiksma et al.*, 1985; *Struiksma and Crosato*, 1989] and weakly nonlinear bar models [*Seminara and Tubino*, 1992].

Besides analytical theories, alternate bars have been studied in laboratory flumes [e.g. *Fujita and Muramoto*, 1985; *Lanzoni*, 2000a, 2000b; *Crosato et al.*, 2012] and to lesser extent using physics-based numerical morphodynamic models [*Defina*, 2003; *Jang and Shimizu*, 2005b; *Bernini et al.*, 2006]. The evolution of alternate bars in models are mostly discussed in the light of the analytical theories and most of the times qualitatively, compared with laboratory experiments [*Defina*, 2003; *Bernini et al.*, 2006]. *Jang and Shimizu* [2005] present one of the scarce examples where laboratory experiment data is used to calibrate a numerical model and quantitative comparison of the bar evolution is made.

Numerical modelling of alternate bars in laboratory experiments remains a challenge for a number of reasons. Flow in laboratory experiments is often close to critical or is at super critical conditions [*Peakall et al.*, 1996] which might induce errors if semi-coupled numerical models are used. Due to shallow flows, in laboratory experiments other forces, such as surface tension can have effects. Properties of bars in the experiments may not be fully captured by numerical models which often do not take into account such forces. Equations for flow field and bed evolution are solved using various numerical schemes in numerical models. Numerical solutions may contain additional diffusion due to the numerical schemes, which makes it difficult to simulate morphological phenomena at the same time scale of that in the laboratory experiments.

Another aspect, related to the channel width that needs further investigation is the morphodynamic response of the river bed to a specified spatial distribution of an imposed channel width. Research on the response of channel bed to spatial width variability has mostly consisted of modelling and theoretical approaches, which point out the limit cases of a purely "free" system response, associated with morphodynamic instability, an of purely "forced" bedform pattern by spatial planform non-homogeneity. The effect have been studied in the symmetric settings [*Bittner*, 1994; *Repetto et al.*, 2002; *Wu and Yeh*, 2005; *Wu et al.*, 2011] which are known to develop symmetric forced bedforms such as mid-channel bar. Most of these studies attempt to establish the threshold amplitude of width variation at which the fully forced bed forms are developed. . Other studies like *Duro et al.* [2015] explore the effect of spatial change in reach averaged width on the evolution of bars. The large spectrum of mixed configurations between those two theoretical limits has been so far seldom investigated, despite its strong relevance for real river systems The limits of what can actually be considered a "planform forcing" effect, or has instead a too small variability have never been clarified, as well as its role on the resulting channel morphodynamics.For instance, free bars in the laboratory experiments or channelized rivers can be affected by minor width variations (two orders of magnitude less than the channel width) due to imperfections along the straight banks. Such small width variations have been mostly neglected in studies of bar evolution so far. A question needs to be

answered about the actual planform forcing role of these "small" width variations. Can a threshold amplitude of these spatial width variations be defined below which free bars instability develops almost unaffected by any forcing effects? To which extent apparently small amplitude (at the scale of flow depth) spatial width variations might interact with free bar instability altering properties of free alternate bars?

1.1 Aim of the study

This research has two main aims. The first one is to investigate the role of controlling factors on the long-term reach-averaged channel geometry, focusing on the width evolution of alluvial, bedload-dominated rivers. The second aim is to analyze the morphodynamic response of the riverbed to small-scale spatial variability of the channel width, focusing on the dynamics of alternate bars.

A river reach is defined here as longitudinal river stretch that i) is several times longer than its width and ii) has rather uniform cross-sectionally averaged longitudinal slope, channel sinuosity and width, and iii) has uniform type of bars and other morphological features at the width scale. The long-term evolution refers to the time scale at which the reach-averaged value of the morphological variable of interest (width, sediment transport rate, bar properties) reaches a dynamic equilibrium, whereby event-scale fluctuations are superimposed over an average value that does not change with time under steady external conditions.

1.2 Research questions

To summarize, this research aims to answer the following research questions:

Hydro-morphological controls of reach-averaged evolution of alluvial channel geometry

- Does the long-term equilibrium alluvial channel geometry depend upon the initial channel width?
- Which are the roles of variable discharge and upstream sediment supply on the long-term evolution of the channel width?

Effects of small width variations on the bed morphodynamics of alluvial channels

- To what extent can the alternate bars observed in laboratory experiments be reproduced by a state-of-the-art numerical model?
- Do small-amplitude, irregular, width variations in space affect the morphodynamics of alternate bars?
- To which extent do small-amplitude width variations act as a planform forcing on riverbed topography?

1.3 Methodology

Phenomena in geosciences are studied by i) field observations, ii) physical experiments and iii) numerical models. These methods provide understanding in different ways since they have different strengths and limitations. *Kleinhans* [2010], *Zolezzi et al.*[2012] and many others agree that an understanding based on all three approaches is more robust and complete than one based on a single approach. This study is carried out using laboratory experiments, numerical and semi-analytical models. Field observations or field-scale experiments are not part of the study, though they might support follow-up of the present research in the future.

Laboratory experiments (Chapter 3) are carried out to study the effects of starting and boundary conditions on the river channel formation (width, depth and slope). Several tests are carried out starting with different initial channel widths with both constant or variable discharges and sediment inputs at the upstream boundary. Discharge hydrographs are designed to explore the amplitude and duration of discharge variability on the width evolution. The evolutions of reach-averaged channel width and channel bed level are then analyzed based on the experimental observations. The channel width evolution is also analysed using the semi-analytical model of *Tealdi et al.*[2011] which allows computing the channel adjustment under varying discharge and sediment supply conditions (Chapter 4). For the experiments, a small laboratory experimental facility was available. Its small size represented a limiting factor for long duration experiments. So, the experimental results are integrated with the results of numerical modelling of a similar river for a longer time scale. The numerical simulations (Chapter 5) are designed similar to the scenarios explored in the laboratory experiments. The Delft3D numerical morphodynamic model, which includes a module for bank erosion process is used for the investigations. The flow and sediment characteristics in the laboratory experiments when up scaled represent those in the gravel-bed rivers. Simulations are carried out using the longitudinal slope, sediment and discharge characteristics of River Severn near Abermule as an illustrative case study, which is a gravel bed river. The results of the numerical model are then discussed in the light of the results of the laboratory experiments.

Considering that natural rivers always present some width discontinuities, the effects of small width variations on river bed evolution are analysed by numerical modelling (Chapter 6), with reference to a set of existing laboratory experiments. A fully non-linear numerical model allows studying the long-term bar development when non-linear processes are dominant. Laboratory experiment data of *Garcia Lugo et al.*,[2015] are used for the investigation and for numerical model setup. This allows for comparison between the bars evolved in numerical models and in the experiments. Laboratory experiments were carried out at Froude super-critical or near-critical flow conditions. So, first comparison needs to be made between semi coupled models (Delft3D) and fully coupled model (GIAMT-2D) to assess the appropriateness of each tool for the numerical investigation. Semi-coupled model is most suitable for sub-critical flows whereas fully coupled model can also handle super-critical flows. The coupling strategy greatly affects the computational time since the semi coupled model is significantly faster than the fully coupled model. Model comparison is made based upon the ability of the models to reproduce alternate bars observed in the flume experiments. As both models had similar outcomes, the faster running, semi-coupled model has been chosen for the numerical investigations on bar dynamics in chapter 6. The effects of small-amplitude width variations on channel bed evolution are then explored by imposing small-amplitude width variations of known amplitude and wavelength along one bank, to isolate the effect. The amplitude of width variations is varied among different scenarios. The bed topography evolution of these scenarios is analyzed and compared with the constant-width scenario. This allows quantifying the effects of small-amplitude width variations in the evolution of the channel bed topography and to answer the research questions presented in the previous section.

1.4 Outline of the thesis

This thesis is outlined in 7 chapters. Chapter 2 presents the state of the art on the channel formations, focusing on the channel width and channel bed formation. The review is made on the channel forming processes and the prediction methods. Chapter 3, Chapter 4 and Chapter 5 present investigations of the effects of different controls on the channel evolution focusing on the width. Chapter 3 presents the results of the laboratory experiments, Chapter 4 presents the results of the semi-analytical modelling and Chapter 5 presents the results of numerical modelling. The numerical modelling study of the river

bed topography adaptations to small amplitude width variations, focusing on alternate bars are presented in Chapter 6. Finally, Chapter 7 concludes the key findings of this doctoral thesis, discusses the key limitations encountered in the research and suggests the key investigations for the future.

2 STATE OF THE ART ON RIVER CHANNEL FORMATION

2.1 Channel width formation

A self-formed river flowing through an alluvium adapts its width, depth and slope based on hydrological conditions, sediment characteristics, riparian vegetation and bank material [*Parker et al.*, 2007]. The river channel interacts with its flood plain by width adaptation by bank erosion and accretion. This defines evolution of the river channel and flood plains and their habitats [*Rinaldi and Darby*, 2007]. During the evolution of natural rivers, the width adaptation occurs over a relatively short time-scale, years to decades, whereas slope adaptation occurs over much longer time-scale, decades to centuries [*Wilson*, 1973; *Parker et al.*, 2007]. The depth adaptation is governed by the adaptation of slope and the width. Due to the shorter time-scale of width adaptation, the effects of changes in hydrological conditions are often seen in terms of width and depth adaptation [*Huang et al.*, 2014; *Kaless et al.*, 2014].

2.1.1 Process

River adjusts width within a wide range of geomorphic context which is summarized well in a review paper by *Thorne et al.* [1998]. Widening of river occurs due to erosion of both banks or erosion of one bank due to bar growth on other banks. Widening in meandering rivers occur when the erosion rate of the outer banks exceeds the accretion rate of the inner bank [e.g. *Zolezzi et al.*, 2012]. In rivers in transition widening occurs due to growth of mid-channel bars which deflects the flow towards the banks [e.g. *Leopold and Wolman*, 1957]. In braided rivers widening is caused by avulsions or bank erosion by channels close to the flood plains [e.g. *Klaassen et al.*, 1993]. The bed aggradations may also lead to widening caused by increase in the flow velocity due to steepening of bed [*Ikeda*, 1989] and flow deflection around the growing bars [e.g. *Simon and Thorne*, 1996]. Incision of river bed increase height and steepness of banks which beyond certain threshold cause failure of banks and thus widening of the river. The lowering of the water surface due to incision of river bed level also contribute to bank erosion due to higher pore water pressure induced by higher ground water level in the flood plain [e.g. *Simon et al.*, 2000]. Geomorphic context of river widening is illustrated in Figure 3 and summarized in Table 1.

Table 1. Summary of geomorphic context of river width adjustment

Width adaptation	Geomorphic context			
	Bed aggradations	Bed incision	Planform	Vegetation
Widening	[*Ikeda*, 1981; *Simon and Thorne*, 1996]	[*Osman and Thorne*, 1988; *Simon et al.*, 2000; *Langendoen and Alonso*, 2008]	[*Leopold and Wolman*, 1957; *Klaassen et al.*, 1993; *Zolezzi et al.*, 2012; *Klösch et al.*, 2015]	[*Huang and Nanson*, 1997; *Anderson et al.*, 2005]
Narrowing		[*Simon*, 1989; *Pizzuto*, 1994]	[*Nanson and Hickin*, 1983; *Klaassen et al.*, 1993]	[*Simon*, 1989; *Tal and Paola*, 2010; *Crosato and Saleh*, 2011; *Gurnell et al.*, 2012]

Narrowing of the river occurs due to formation of in-channel berms during the incision of the river bed. In meandering rivers, narrowing occurs when the accretion rate of inner bank exceeds the erosion rate of the outer banks. Riparian vegetation colonization strengthens banks by root reinforcements [e.g. *Tal and Paola*, 2010], increases the hydraulic roughness and deflects the flow towards main channel [e.g *Crosato and Saleh*, 2011] making the cross-section narrower and deeper. In rivers with multi thread channels, narrowing occurs due to the abandonment of channels caused by instability at the bifurcations [e.g. *Klaassen et al.*, 1993]. Within braided corridor the colonisation and growth of vegetation on bars creates islands which are more stable. By trapping fine sediments, vegetation also plays a key role in pioneer landform development which can enlarge and combine together to become larger islands [*Gurnell et al.*, 2012] and may also become the part of the flood plain. Geomorphic context of channel narrowing is illustrated in Figure 4 and summarized in Table 1.

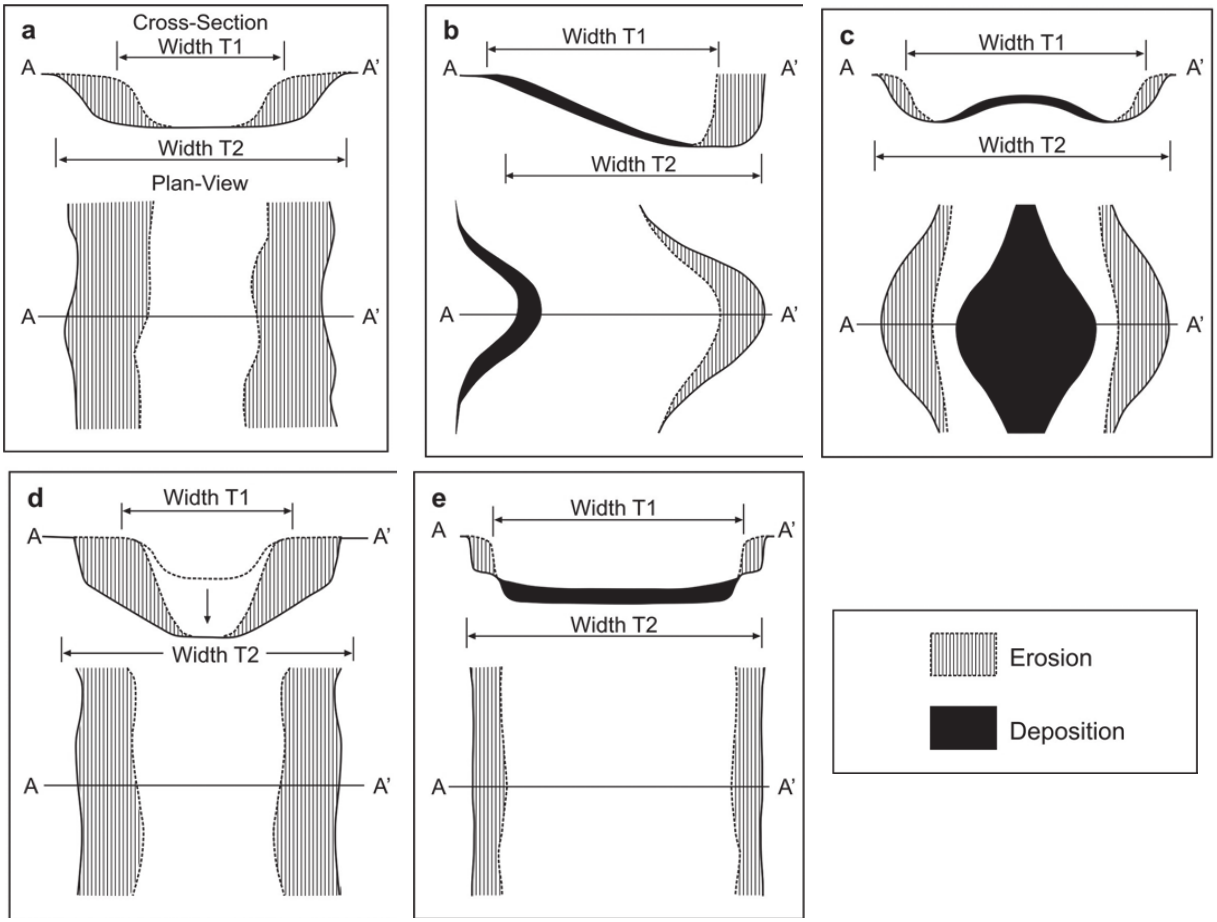

Figure 3. Geomorphic context of river widening a) channel enlargement without bed incision, b) outer bank retreat at faster rate than the rate of accretion of the inner bank in a sinuous channel, c) bank erosion induced by flow deflection due to mid-channel bar growth, d) bank failure due to over steepening of banks due to channel incision and e) bank erosion due to acceleration flow due to channel aggradation (Source: *Thorne et al.*, 1998)

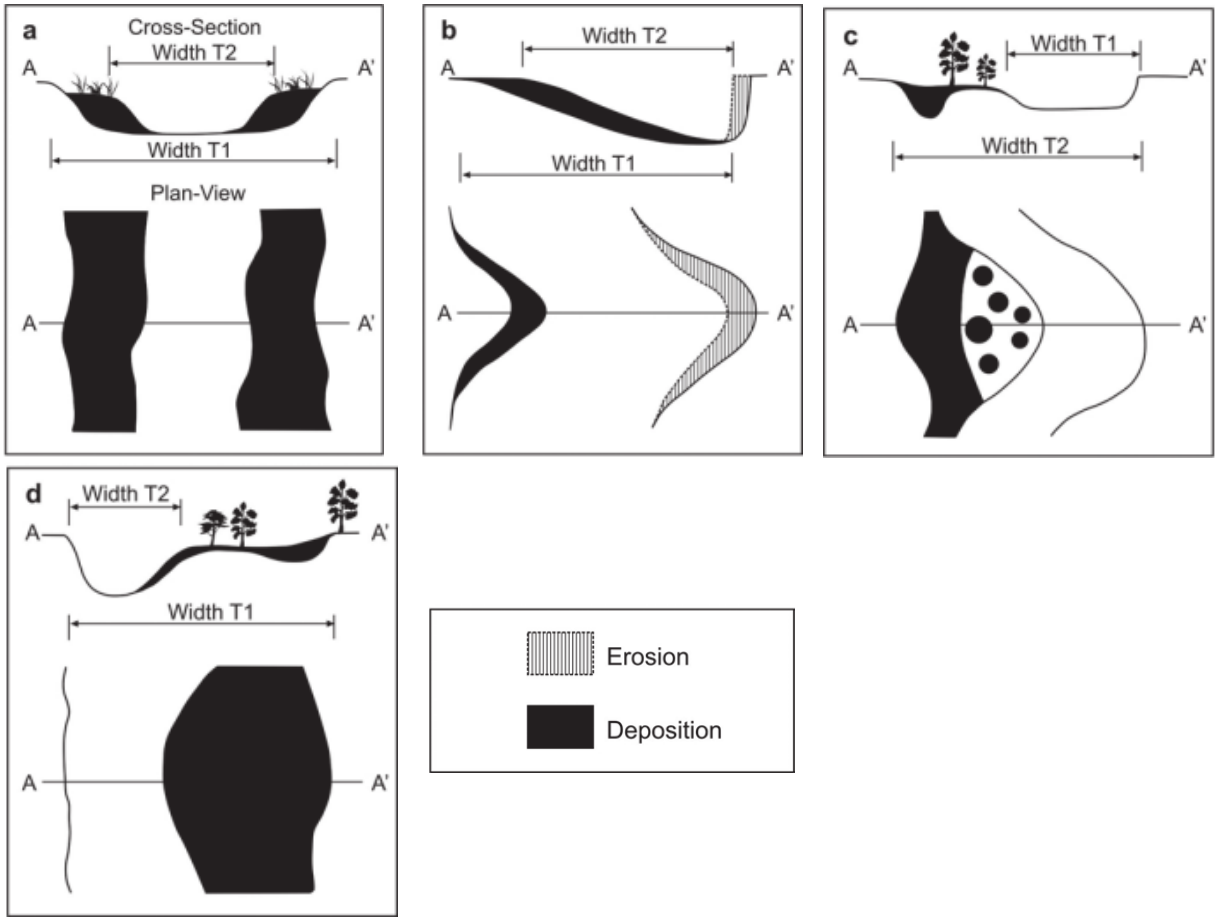

Figure 4. Geomorphic context of channel narrowing a) reduction of channel area by berm formation, b) inner bank accretion at faster than the retreat rate of outer banks in sinuous channel, c) abandonment of the anabranch in multi-thread channels and d) closure of the channel when it gets attached to the flood plain. (Source: *Thorne et al.*, 1998)

2.1.2 Predictions

There has been a considerable research on prediction of stable cross-section of alluvial channel since late 19th century [*Kennedy*, 1895], even before the *Exner*'s [1925] sediment balance principle, the fundamental principle of river morphodynamics, existed. Width adaptation of a river is studied at a reach scale. The longitudinal stretch of river having similar morphological characteristics (e.g. slope, sinuosity) is considered as a river reach. Width prediction methods consist of hydraulic geometrical relations, relations derived from extremal hypothesis approach, Mechanistic approaches, laboratory modelling and numerical modelling.

Hydraulic geometry relation

Empirical methods, also refered as Regime theories, were the first methods developed to predict hydraulic geometry of stable irrigation canals. *Kennedy* [1895] proposed the first regime relation. *Lindley* [1919] revisited Kenedy's work and expressed width, depth and longitudinal slope as design outputs for stable sediment transporting canals. *Lacey* [1930] further build upon works of *Kennedy* [1895] and *Lindley* [1919], using data of stable irrigation canals, developed the quantitative empirical relationship between wetted width, depth, slope and discharge. *Leopold and Maddock* [1953], using data of natural rivers and laboratory experiments, developed an empirical power law relation of hydraulic geometry of river (top width, depth and average velocity) relating with the bank full discharge. Several regime equations were developed further using different dataset of natural rivers

and laboratory experiments [e.g. *Blench*, 1969; *Hey and Thorne*, 1986]. Regime theories are expressed in the form of power law and its general form is expressed in equations (1) (2) and (3).

$$W_{bf} = X_w Q_{bf}^{nw} \quad (1)$$

$$H_{bf} = X_h Q_{bf}^{nh} \quad (2)$$

$$S = X_s Q_{bf}^{-ns} \quad (3)$$

where, W_{bf}, H_{bf} and S are bankfull channel width and depth, and longitudinal slope respectively; Q_{bf} is the bank full discharge, m^3/s; X_w, X_h and X_s are regression coefficients for width, depth and longitudinal slope of channel respectively; n_s, n_h,n_s are exponents for width, depth and longitudinal slope of channel respectively.

Table 2 Values of exponents n_s, n_h,n_s proposed in different empirical hydraulic geometry relations

Source	Year	n_w	n_h	n_s
Lacey	1930	0.5	0.33	0.11
Bose	1936	0.5	0.33	0.21
Glover et al.,	1951	0.46	0.46	0.46
Leopold et al.,	1953	0.45-0.56	0.37-0.45	0.19-0.50
Leopold et al.,	1956	0.50	0.28	0.0667
Blench, sand	1957	0.50	0.33	0.167
Blench, gravel	1957	0.50	0.4	0.40
Inglis	1957	0.50	0.33	0.167
Nash	1959	0.54	0.27	0.12
Nixon	1959	0.50	0.38	0.10
Simons et al.,	1960	0.51	0.36	0.40
Ackers, cohesive	1964	0.53	0.35	0.29
Ackers, experiments	1964	0.42	0.43	
Kellerhals	1967	0.50	0.40	0.40
Lapturev	1969	0.50	0.33	0.10
Bray, regression	1982	0.53	0.33	0.334
Bray, threshold	1982	0.50	0.48	0.482
Hey	1982	0.54	0.41	0.53
Hey and Thorne	1983	0.50	0.39	0.57
Ghosh	1983	0.46	0.46	0.46
Chang	1988	0.50	0.30	0.51
Yalin, sand	1991	0.50	0.33	0.11
Yalin, gravel	1991	0.50	0.43	0.43

(Source: Cao and Knight, 1996)

Bank full discharge is consistently used in the regime theories. Bank full discharge is cross-section dependant so in the absence of gauge data bankfull discharge is estimated as 2 years recurrence interval flood [e.g. *Bray*, 1982] for single thread rivers. The third regime equation of *Leopold and Maddock* [1953] was relation between cross-section average flow velocities and bank full discharge.

Most regime theories (Summarized by *Ferguson*, 1986) use longitudinal slope as surrogate to the cross-section average flow velocity. *Cao and Knight* [1996] provide the summary of exponents of width, depth and longitudinal slope of channel provided in different regime theories:

The value of exponent n_w among most of regime theories remain 0.5 whereas the exponent of slope shows most variation. The value of exponent n_h also shows variation but within a narrow range compared to n_s. One of the reason of high variance of ns compared to n_w and n_h could be the longer geomorphic time scale required for the slope adaptation *Parker et al.* [2007].

The regression coefficients X_w, X_h and X_s also vary widely among the regime theories. *Hey and Thorne* [1986] show that the value of regression coefficient X_w varies within the range of 2.33-4.34 among channels with different vegetation class. The variation in X_w is due to the effects of bed material, bank material properties, vegetation and sediment supply conditions [summarized by *Millar*, 2005].

The regime equations, discussed above, are empirically derived based upon data of specific regions which might restrict their validity to the region where they are derived from. They are also dimensionally inhomogeneous so they cannot provide good explanation on the underlying physics. *Parker et al.* [2007] present the dimensionless bankfull hydraulic relationship for single thread gravel bed river. Since the relationship is derived in dimensionless form, it has been used to develop the physics based explanation of the "quasi-universal" effects of bank strengths, roughness and sediment supply on the width of the rivers which are expressed in equations (4) (5) and (6).

$$\tilde{W} = 4.63\tilde{Q}^{0.0667} \quad (4)$$

$$\tilde{H} = 4.63\tilde{Q}^{-0.0004} \quad (5)$$

$$S = 4.63\tilde{Q}^{-0.344} \quad (6)$$

where, S is the longitudinal channel slope; $\tilde{W}$, $\tilde{H}$ and $\tilde{Q}$ are dimensionless width, depth and bank full discharge respectively using equations (7) (8) and (9).

$$\tilde{W} = \frac{g^{1/5} W_{bf}}{Q_{bf}^{2/5}} \quad (7)$$

$$\tilde{H} = \frac{g^{1/5} H_{bf}}{Q_{bf}^{2/5}} \quad (8)$$

$$\tilde{Q} = \frac{Q_{bf}}{\sqrt{g D_{50}} D_{50}^2} \quad (9)$$

In which, W_{bf}, H_{bf} and Q_{bf} are bankfull width, m, bankfull depth, m, and bankfull discharge, m^3/s, respectively; D_{50} is the median sediment diameter, m, of the surface; g is the acceleration due to gravity, m/s^2. Some other approaches use only median sediment diameter (D_{50}) to make bank channel

width and bankfull depth dimensionless [e.g. *Parker*, 1979; *Andrews*, 1984]. A similar non dimensional relation is also suggested by *Bray* [1982] for gravel bed river which is expressed in equations (10) (11) and (12).

$$\frac{W_{bf}\, g^{0.2}}{Q_{bf}^{\ 0.4}} = 4.73\left(\frac{D_{50}\, g^{0.2}}{Q_{bf}^{\ 0.4}}\right)^{-0.241} \qquad (10)$$

$$S = 0.0449\left(\frac{H_{bf}}{D_{50}}\right) - 0.945 \qquad (11)$$

$$\frac{V}{\sqrt{gH_{bf}\, S}} = 1.97 S^{-0.256} \qquad (12)$$

where, V is the cross-sectional velocity, m/s.

Extremal hypothesis

One dimensional problem of a flow in a alluvial channel can be formulated in the form of six sets of equation which define the conservation of mass and momentum of water and conservation of mass of sediment in one dimension, relation between flow and the cross-sectional area, flow resistance closure relationship and empirical sediment transport rate predictor. The six set of equations contain seven variables if width is allowed to adjust. So, additional constraint or closure relationship should be defined to obtain the steady state solution of the system.

In an Extremal hypothesis approach additional hypothesis is used to define the additional constraint or closure relationship required to obtain the solution of the system. The hypotheses are based upon assumptions which do not have physics based explanation. *Griffiths* [1984] and *Singh* [2004] provide a detailed review on the Extremal hypothesis used to predict the hydraulic geometry of alluvial channels. Minimum unit stream power rate, minimum stream power, minimum energy dissipation rate, maximum friction factor, maximum sediment transport efficiency, maximum sediment transport rate, least channel mobility, least resistance, minimum Froude number, thermodynamic entropy, minimum variance, maximum entropy, maximum entropy-minimum energy, maximum flow efficiency, equal probability of width and depth adjustment, least action principle, and maximum flow resistance are some of the common examples.

Cao and Knight [1996] based upon equal mobility of width and depth adjustment probability hypothesis showed that width to depth ratio as an important parameter in determining the channel geometry in regime theories. *Eaton and Millar* [2004] used the *Millar and Quick* [1993] model based upon maximum sediment transport capacity (MSTC) hypothesis to analyze the effects of the bank strength on the channel prediction. The MSTC approaches that do not include the bank strength [e.g. *Valentine et al.*, 2001] predicted narrower channels compared to the MSTC approaches including bank strength. The analysis also suggest that influence of bank vegetation on river width is more in the case of small channel but less as the size of the channel becomes larger. Based on extremal hypothesis approach of *Eaton and Millar* [2004], *Millar* [2005] derived the hydraulic geometry relation for gravel bed rivers which is expressed in equations (13) (14) and (15).

$$\hat{W} = 16.5\hat{Q}^{0.7} S^{0.6} \qquad (13)$$

$$\hat{H} = 0.125\hat{Q}^{0.16}S^{-0.62} \quad (14)$$

$$\frac{W_{bf}}{H_{bf}} = 155\hat{Q}^{0.53}S^{1.23} \quad (15)$$

where,

$$\hat{Q} = \frac{Q_{bf}}{D_{50}^2\sqrt{gD_{50}\Delta}} \quad (16)$$

$$\hat{W} = \frac{W_{bf}}{D_{50}} \quad (17)$$

in which, Δ=1.65 is the relative density of the sediment.

Mechanistic approaches

Mechanistic models are derived based on laws of physics. Earlier mechanistic model developed were threshold channel theories [*Glover and Florey*, 1951; *Lane*, 1955] which were based on the tractive force approach. The theory assumes a flow in a straight channel, neglecting secondary flows, over non-cohesive sediment. Flow momentum balance equation is then solved to calculate the local boundary shear stress. Tractive force and gravity force on a particle along the banks are balanced by friction force among the particles. The local boundary shear stress or tractive force is then limited to such that it is just sufficient to move the particles without scouring. Balance between the forces then provides relationship between flow depth, the maximum depth, side slopes and the friction angle. From these a stable channel with the cosine profile is obtained.

One of the big limitations of the threshold channel theories iss that they did not allow sediment transport through the stable cross-section. The observations from field and laboratory experiments however show that a cross-section with stable banks transport sediment along the bed. *Parker* [1978] derived the cross-section with stable banks and mobile beds by using the momentum balance equation proposed by *Lundgren and Jonsson* [1964], which allowed the turbulence diffusion of the momentum along the lateral direction, to compute the bed shear stress. The solution is only obtained in the bed region. The stress near the centre of the channel allow bed load transport and vanishes towards the direction of bank to the value close to critical shear stress for bed load transport. The bank profiles were solved separately, to obtain the stress conditions close to critical stress conditions, in a similar approach of the threshold channel theories to obtain a cosine profile. *Parker* [1978] model was further extended to assess the effect of sediment heterogeneity [*Ikeda et al.*, 1988], bank vegetation [*Ikeda and Izumi*, 1990] and suspended sediment [*Parker*, 1978a; *Ikeda and Izumi*, 1991] on the geometry of the stable channel. *Diplas and Vigilar* [1992] used the approach similar to *Parker* [1978] but solved the bank and bed profile numerically. The solution of *Diplas and Vigilar* [1992] resulted the channel cross-section profile defined by a fifth order polynomial. The channel was with larger top width compared to the cosine channel obtained by threshold channel theory.

Pizzuto [1990] extended the model of *Parker* [1978] including a heuristic bank failure model to simulate the evolution of stable channel cross-section starting from an unstable channel. *Kovacs and*

Parker [1994] further included a mechanistic vectorial bedload transport formulation on bed slopes, upto angle of repose, to simulate the time evolution of unstable channel cross-section to a stable cross-section. Both *Pizzuto* [1990] and *Kovacs and Parker* [1994] models were able to simulate the time evolution of cross-section as observed in experiments of *Ikeda* [1981].

Mechanistic models discussed above were developed assuming channel to be in equilibrium, neither deposition nor erosion. Mechanistic models of *Jansen et al.* [1979], *Bolla Pittaluga et al.* [2014] and *Redolfi and Tubino* [2014] can predict hydraulic characteristics at non-equilibrium conditions. However these models can only assess the change in longitudinal slope of a channel with known width. *Tealdi et al.* [2011] extended the model of *Cantelli et al.* [2007] to obtain a mechanistic model which can predict the change in reach averaged width and slope of channel, at non-equilibrium conditions, due to change in discharge and sediment regime. *Tealdi et al.* [2011] model is the only model known of its type which can predict the change in width and bed level/slope in response to change in sediment and discharge regime.

Laboratory modelling

Scaled laboratory experiments of real rivers require scaling of the bed sediment as well as the bank strength properties. The scaling of bank strength is very difficult to obtain at a reduced scale [*Young and Warburton*, 1996] because the cohesion properties of clay are scale independent [*Peakall et al.*, 1996]. So, small scaled laboratory experiments of real rivers with cohesive banks to investigate widening cannot be performed. Alternatively, it is a common practice to investigate morphodynamic processes and phenomena considering 1:1 scaling in physical experiments.

Experiments have been commonly performed in the framework of studying evolution of channel patterns [*Fredkin*, 1945; *Leopold and Wolman*, 1957; *Schumm and Khan*, 1972], to develop empirical width predictors [e.g. *Wolman and Brush*, 1961], to validate the width predictors [e.g. *Valentine et al.*, 2001]. Channel width evolution is studied in some cases by conducting experiments in a channel with half trapezoidal cross-section to avoid sinuosity development [*Ikeda*, 1981; *Diplas*, 1990]. *Fujita & Muramoto* [1982] conducted experiments to study width and bed evolution of channel, with both erodible banks, at different discharges and sediment regimes. *Byishimo* [2014] carried experiments to study width evolution in different sediment types and discharge regimes.

Numerical models

Bank retreat and bank accretion are two important morphological processes leading to river width adjustment. These processes vary both in space and time resulting in longitudinal variation of channel width, which can be modelled using numerical models. Spatial variation of bank strength and geomorphic context of width adaptation mainly contribute to the variation of the river width [*Thorne et al.*, 1998]. Rivers with multi thread channels show more longitudinal width variation compared to rivers with single thread channels.

At process scale, bank retreat occurs due to the interaction between near bank processes: weathering, fluvial erosion and mass failure of banks [e.g. *Leyland et al.*, 2015]. The fluvial erosion process contributes to the widening by i) eroding sediment near the bank and ii) triggering mass failure mechanism. Secondary flow structures near the banks play important role in bank erosion [*Papanicolaou et al.*, 2007]. The intensity of secondary flow velocities are very high along the curved channels [*Blanckaert and de Vriend*, 2003]. The total boundary shear stress near the banks can be divided into two components: flow stress on the surface called “skin drag”, and an additional shear stress due to irregularities along natural banks called “form drag” [*Kean and Smith*, 2006a, 2006b]. Former contributes to bank erosion and latter contributes to bank stabilization [*Darby et al.*, 2010;

Leyland et al., 2015]. The form drag shows temporal variation as a function of bank erosion [*Leyland et al.*, 2015]. The fluvial entrainment at the bank occurs if the flow shear stress (skin drag) is higher than the critical shear stress required for the entrainment [*Leyland et al.*, 2015]. Fluvial erosion process, near the banks, triggers the mass failure by increasing the height of the banks or by increasing the slope of the banks [*Thorne et al.*, 1998].

Mass failure is a geotechnical process which is governed by the balance between the driving forces and resisting forces, which are summarized in table 2. Bank fails if the driving forces exceed the resisting forces. Bank failure by mass failure mechanism occurs by i) rotational failure, ii) toppling failure or iii) cantilever failure.

Rotational failures occurs both in the non-cohesive and cohesive banks. In non-cohesive materials the failure occurs along shallow curved surface compared to cohesive materials. Toppling and cantilever failures occur only in the case of very steep cohesive banks. The bank failure progresses further if the flow is able to erode all the accumulated material near the toe of the bank, due to bank erosion, and continue to erode the toe of the bank. If the flow is not able to erode the accumulated material the berm or bench of the failed material forms thus protecting banks from further erosion [*Thorne et al.*, 1998].

Table 3. Summary of driving forces and stabilizing forces contributing to mass failure process

SN	Components	Forces		Remarks	References
		Driving	Stabilizing		
1	Weight of bank material	■			[*Osman and Thorne*, 1988]
2	Frictional force		■		
3	Pore water				
a)	Increase in unit weight of soil	■			
b)	Shear strength reduction	■			[*Rinaldi and Darby*, 2007]
c)	Negative seepage		■	Direction towards flood plain	
d)	Positive seepage	■		Direction towards river channel	
4	Vegetation				
a)	Weight	■	■	Stabilizing: increase in normal stress	[*Rinaldi and Darby*, 2007]
b)	Root reinforcement		■		
c)	Hydrologic effect	■	■	Soil moisture regulations	[*Simon and Collison*, 2002; *Rinaldi and Darby*, 2007]
d)	Roughness		■		[*Crosato and Saleh*, 2011]

Based upon the complexity of the process included, the numerical modelling approach can be classified into two different types of models.

- *Bank erosion process model*

Bank erosion process models are mainly developed for cohesive banks and include only the geotechnical processes to model the bank failure process. The models perform the stability analysis of the slide failures by using a Limit Equilibrium Method. In Limit Equilibrium Method factor of safety is computed as the ratio between the resisting forces to the driving forces. If the factor of safety is less than one, the bank failure occurs along the assumed failure plain. The methods have improved significantly from simple forms (Thorne et al, 1981) to including more realistic bank geometry[*Osman and Thorne*, 1988], including more processes influencing both driving and resisting forces like pore water pressure, vegetation [*Simon et al.*, 1991; *Rinaldi and Casagli*, 1999; *Simon and Collison*, 2002] and including more complexities to analyze rotational and cantilever failiures [*Dapporto et al.*, 2001; *Simon et al.*, 2002]. *Rinaldi and Darby* [2007] provide detail summary of the developments on the bank erosion process models.

- *Flow model with coupled bank stability model*

At longer time scales, the hydraulic erosion at the toe of the bank is the dominant process governing the bank erosion rate [*Leyland et al.*, 2015]. However, it is not necessarily the cause of bank erosion. The geomorphic context of width adjustment dominant role in controlling the bank erosion process [*Thorne et al.*, 1998]. So, morphodynamic models coupled with bank stability model are used to simulate the temporal evolution of width, slope and depth of channels.

In such models, the flow continuity and momentum equations are solved in one dimension [*Alonso and Combs*, 1986; *Borah and Bordoloi*, 1989; *Darby et al.*, 2007; *Langendoen and Alonso*, 2008] and quasi two dimensions [*Simon et al.*, 1991; *Darby and Thorne*, 1996] in detailed bank erosion models at depth scale which neglects the planform effects on bank erosion. Solution in two dimensions depth averaged [*Mosselman*, 1998; *Jang and Shimizu*, 2005a] and three dimensions [e.g. *Jia et al.*, 2010] are implemented in modeling width evolution at reach scale where bank erosion model is implemented in less detail but the effects of planforms in bank erosions can be modelled. Bed load and suspended sediment transport are modelled separately. Sediment continuity is modelled by using the Exner equation accounting the sediment influx from bank erosion.

In reach scale modeling, mass failure of the cohesive banks is modelled using bank erosion process sub models. Bank erosion is non-cohesive banks are modelled using heuristic or rule based approach. In the heuristic approach the bank erosion is modelled based upon friction angle of particles (angle of repose). The bank failure occurs if the bank becomes steeper than the angle of repose of the bank material [*Jang and Shimizu*, 2005a]. In rule based approach models the bank erosion is implemented in a crude form and is based upon some set of rules which are prescribed to distribute the amount of toe erosion to the adjacent bank cells [*Wang et al.*, 2010; *Crosato and Saleh*, 2011; *Nicholas et al.*, 2013]. The failed mass is then moved to the river bed where it is reworked entirely by fluvial erosion. The accumulated mass should be eroded and toe erosion should continue to trigger the next mass failure of the banks.

2.2 Channel bed formation

The flow over alluvial beds causes morphodynamic instability, resulting in bed waves at different scales, depending on width-to-depth ratio and flow characteristics [*Colombini and Stocchino*, 2012]. Morphodynamic instability is related due to the interaction between the flow-induced bed shear-stress

and gravity. The bed forms occurring due to morphodynamic instability are in the form of ripples, dunes and anti dunes, and bars, respectively in an increasing characteristics spatial scale.

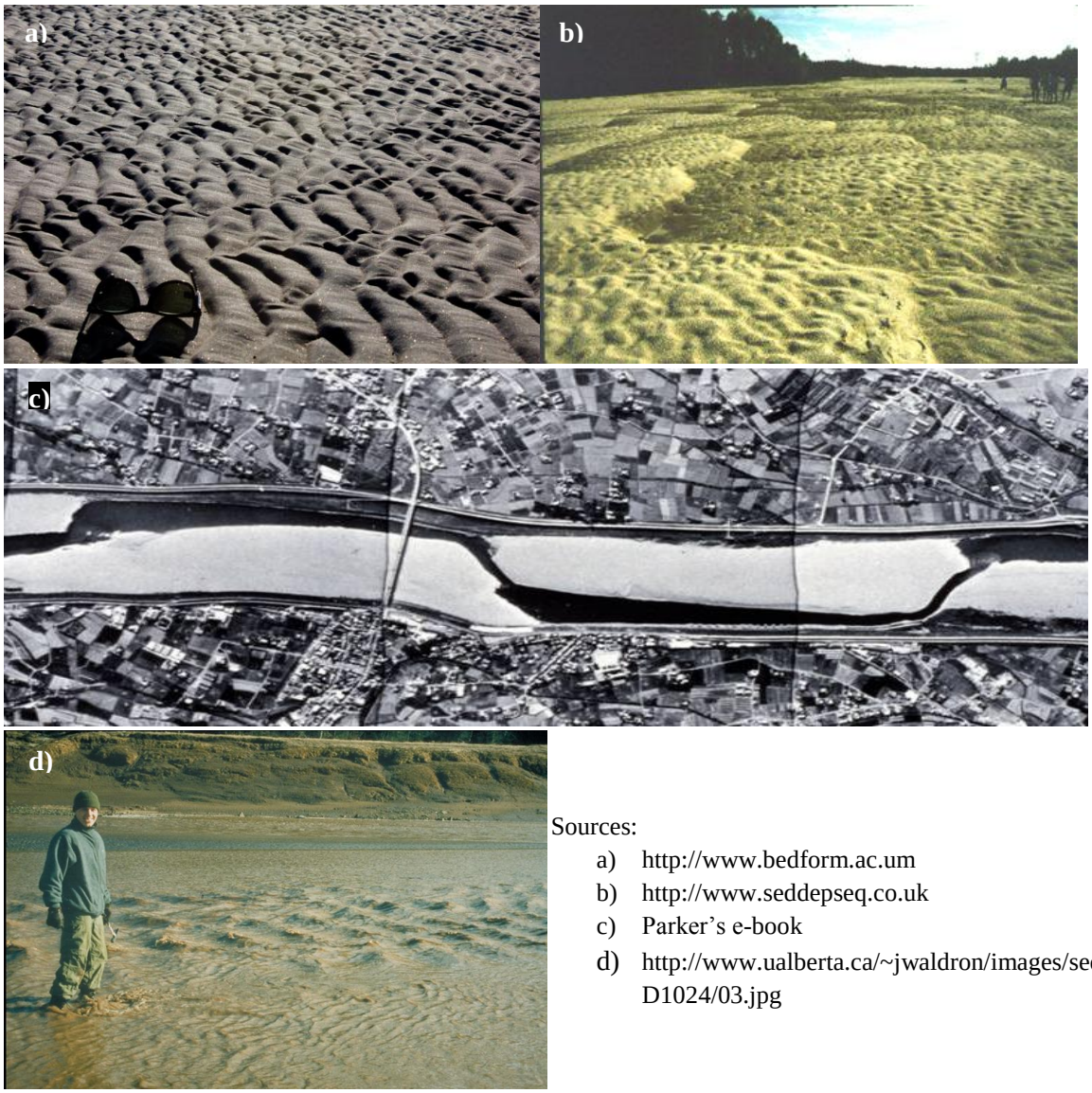

Sources:

a) http://www.bedform.ac.um
b) http://www.seddepseq.co.uk
c) Parker's e-book
d) http://www.ualberta.ca/~jwaldron/images/sedCD1024/03.jpg

Figure 5, Images showing a) ripples, b) dunes, c) alternate bars in the Naka river, Japan and d) antidunes

2.2.1 Processes

Ripples, dunes and anti dunes

Ripples are the smallest bed form waves, scaling with the sediment size, occurring due to morphodynamic instability at a very low transport rates, at smaller values of Shields number, in a hydraulically transitional flow regime (Figure 6). Ripples do not interact with the free water surface. Dunes and antidunes are larger bed form waves, scaling with the flow depth, occurring due to morphodynamic instability at a hydraulically transitional flow but at higher sediment transport rates, higher Shields number. Dunes occur at the lower Froude numbers and migrate downstream. Antidunes occur at Froude number close to 1 or higher and typically move upstream. Both dunes and antidunes interact with water surface with former out of phase with the free surface and latter in phase with the free surface waves (Figure 7).

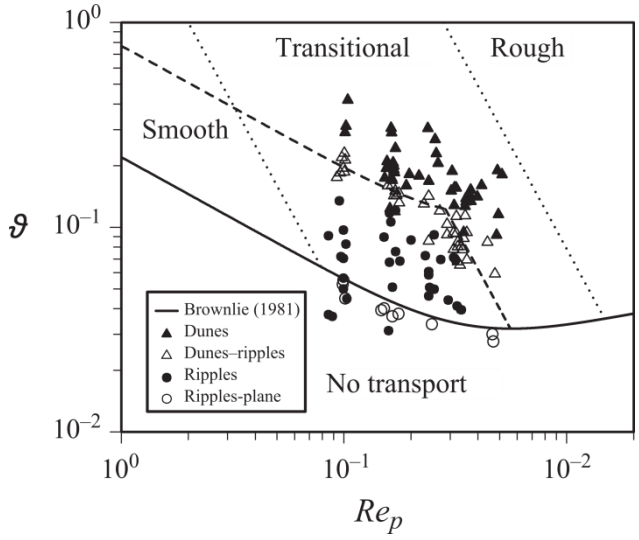

Figure 6. Shields diagram showing the regions of formation of ripples and dunes, [*Colombini and Stocchino*, 2011]

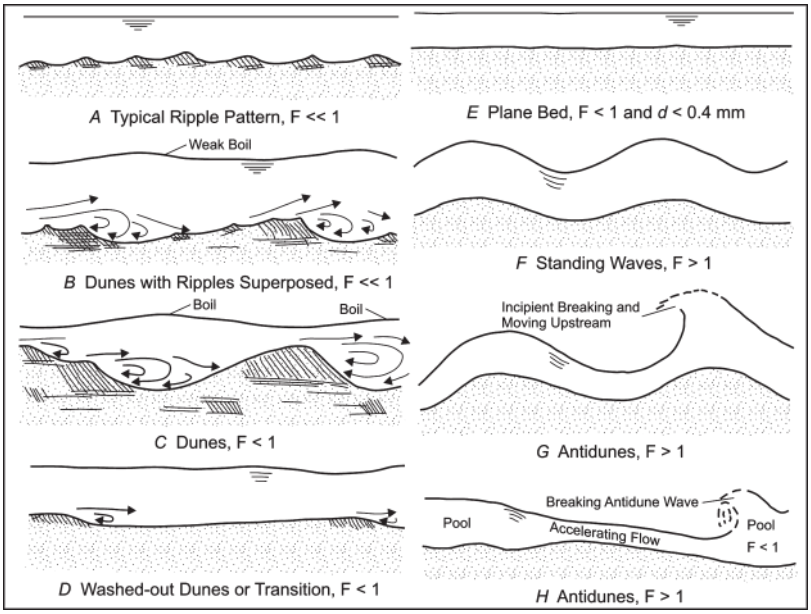

Figure 7. Illustrations of ripple, dunes and antidunes occurring at different flow regime characterized by the Froude number, [*García*, 2008]

Bars

Bars are the largest bed forms, scaling with the channel width, occurring due to morphodynamic stability at shallow water conditions: high width to depth ratio, irrespective of the flow characteristics, sub critical or super critical [*Tubino et al.*, 1999; *Colombini and Stocchino*, 2012]. They are large deposits of sediment contoured by channels that become exposed during low flow stages. Bars have been classically classified as free and forced which has been subject of debate. Free bars originate by morphodynamic instability, and have a periodic character. They migrate in channel in downstream or upstream directions. Forced bars appear due to the forcing by local perturbations (e.g. downstream of a groyne, curvature of meanders) and do not show periodic character. Bars that form due to a combination of steady forcing and morphodynamic instability (forced-free interactions)

are classified as hybrid bars [*Duró et al.*, 2015]. Hybrid bars have periodic characteristics. Morphodynamic instability governs their geometrical characteristics whereas steady forcing determines their spatial location and celerity (= 0).

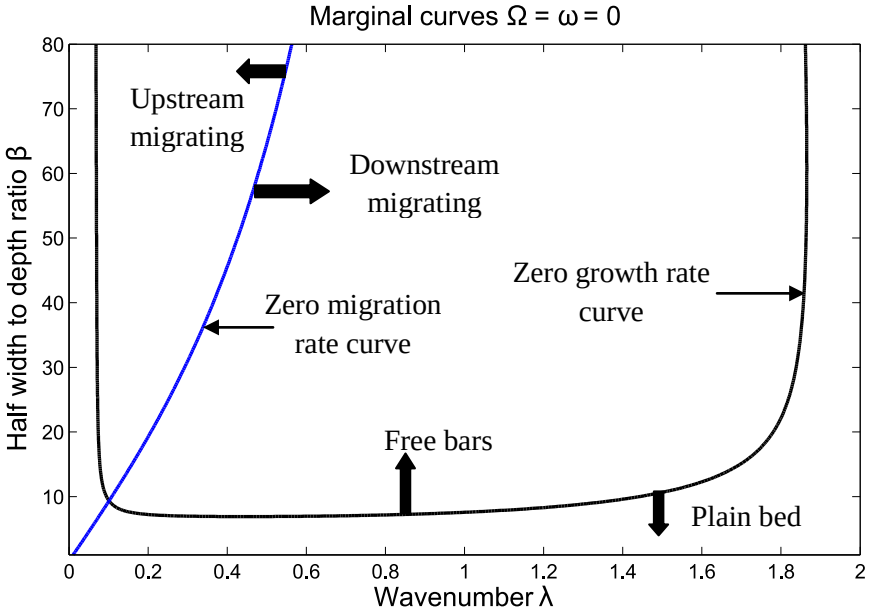

Figure 8 Illustration of free bar instability curve (black) and migration curve (blue) for alternate bars obtained at experimental conditions: shields stress equal to 0.072 and dimensionless sediment diameter equal to 0.017. The curves are derived from linear bar theory of *Colombini et al.* [1987]. *(Courtesy: Luca Adami)*

Among the bed forms, bars strongly interact with the channel width. So within the framework of this thesis the scope is limited to the bars, in particular alternate bars, which are discussed in the following section.

2.2.2 Prediction

Alternate bars have been studied with combinations of analytical theories, experiments and numerical models.

Analytical studies

Alternate bars have been widely studied using analytical theories. Free bars have been studied since long by means of "bar instability theories "linearly [*Callander*, 1969; *Engelund*, 1970; *Parker*, 1976; *Fredsøe*, 1978] and weakly non-linear models [*Colombini et al.*, 1987; *Schielen et al.*, 1993]. Forced bars mostly occur by local forcing (e.g. groynes, bend) or boundary conditions (e.g. width variations). Hybrid bars have been studied using linear models [*Struiksma et al.*, 1985; *Struiksma and Crosato*, 1989] and weakly nonlinear bar models [*Seminara and Tubino*, 1992] as well.

Morphodynamics of bars can be considered as "unit processes" to understand the dynamics of whole alluvial system [*Zolezzi et al.*, 2012]. Although these analytical bar models are based upon simplified assumptions, they provide relevant knowledge on bar dynamics in single channels. They have been employed as reliable physics based tool to predict single and multi-thread channel patterns based upon the calculation of the most likely number of bars in a cross-section represented by the number of transverse half bar wave lengths in the river cross-section, known as "bar mode m" [e.g. *Tubino et al.*, 1999; *Crosato and Mosselman*, 2009]. Meandering rivers are mostly characterized by point bars and alternate bars in their straight parts with typical bar modes (m) less than 1.5. Braided rivers are characterized by the presence of multiple bars (m>2.5). A single mid-channel bar (1.5<m<2.5) can be

observed at transition planforms between meandering and braiding [*Crosato and Mosselman*, 2009]. The number of bars in rivers is crucially controlled by the width to depth ratio of the channel. Higher bar modes require higher width to depth ratios. Literature suggest that a river channel starts to braid at width to depth ratio between 40 [*Fredsøe*, 1978] and 50 [*Crosato and Mosselman*, 2009].

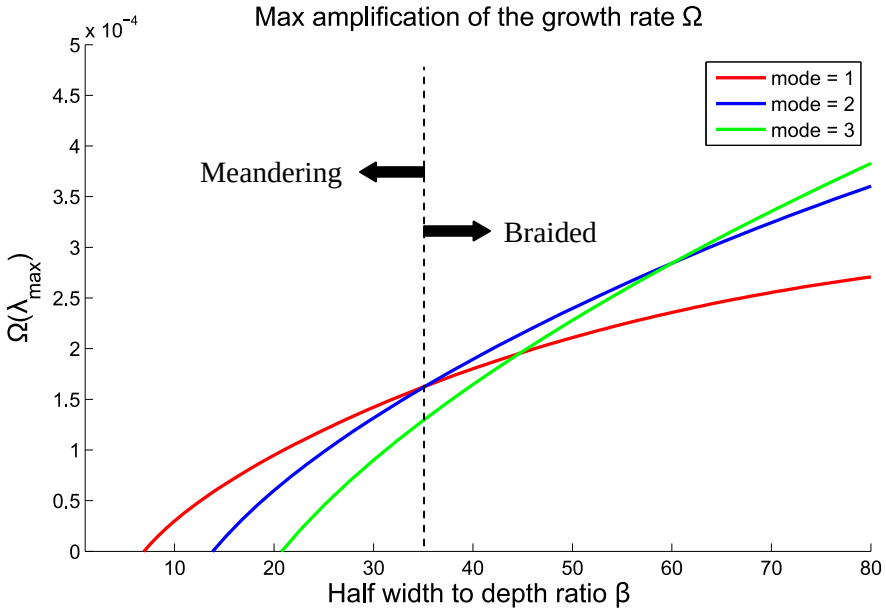

Figure 9 Growth rate of the fastest growing bars plotted against half width to depth ratio of the channel for experimental conditions: shields stress equal to 0.072 and dimensionless sediment diameter equal to 0.017. Mode =1 denotes alternate bars, mode = 2 and 3 denote multiple bars. The curves are derived from linear bar theory of *Colombini et al.* [1987]. *(Courtesy: Luca Adami)*.

Experimental studies

Laboratory experiments models have been extensively used to study alternate bars. For instance, *Jaeggi* [1984] carried out several experiments to derive the empirical relation on formation of alternate bars, *Fujita and Muramoto* [1985] studied the developments of alternate, *Tubino* [1991] studied development of alternate bars in varying discharge conditions, *Lanzoni* [2000a, 2000b] studied alternate bar formation in uniform and non-uniform sediment, *Crosato et al.* [2011] studied long-term development of alternate bars. Laboratory experiments have been widely used to validate the analytical theories and numerical models.

Numerical studies

Numerical studies have been carried out using two different types of models: a) physics based model and b) rule based models. Physics-based numerical models are based on established laws of physics and have been widely used to investigate morphodynamic process. This research has been designed integarating the laboratory experiments and Physics based models. So the scope of the review is limited to physics-based numerical models. However, rule based models are also briefly discussed.

- *Physics-based models*

Physics based morphological models solve Navier-Stokes equations (most commonly with shallow water approximations) to compute the flow field, and sediment transport equations and Exner equations for sediment mass balance to compute morphodynamic development. Physics-based models can be further classified as fully coupled and semi coupled on the basis of solving strategy of flow field and bed level updating. In fully-coupled model, flow-field equations and sediment transport equations are solved together in single time steps. Whereas in semi-coupled models, the sediment

transport equation and flow-field equations are solved separately assuming that the bed level changes occuring at a small computational time steps is small and does not affect the flow field [*Kassem and Chaudhry*, 1998]. At trans-critical flow conditions the bed level change rates are higher affecting the flow field. The fully-coupled solution of flow field and sediment transport in a single time step allows incorporating the interaction between the flow field and the bed level changes establishing them as accurate tools in investigating morphodynamic phenomena in trans-critical flow conditions. Solving flow-field and sediment transport equations separately introduces errors in the semi-coupled models. GIAMT-2D model [*Siviglia et al.*, 2013] is one of the scarce examples of the fully coupled model used to investigate morphodynamics of bars. Semi-coupled models for instance, Delft3D [*Lesser et al.*, 2004] are widely used to investigate bar morphodynamics in single thread as well as multi-thread channels [*Crosato et al.*, 2012; *Schuurman et al.*, 2013; *Duró et al.*, 2015].

Linear analytical theories can approximate the characteristics of the bars during the early phase of their development. Nonlinear effects become dominant as the bar starts to grow higher. In particular, assumptions of fully transporting cross-section made in analytical models, may not be valid anymore as bars start to emerge from the water surface. Experiments have shown that complex alternate bar patterns can be observed in a channel after long-term evolution, despite the early stage of channel evolution is dominated by mid channel bars [*Fujita*, 1989]. The observed decrease in number of bars is due to bar merging during the evolution which can be attributed to the dominance of non-linear effects.

Laboratory-scale morphological models are powerful tools to study morphological process as well. However, quantifying the effects of processes in experiments is often limited due to the difficulty in measurements, like flow characteristics and depth, at such small scales. Since the system evolves rapidly, the time scale in laboratory experiments is very short with respect to real rivers. The measurement of hydraulic parameters over space at a certain time, theoretically representing a state is very difficult in such cases.

Physics-based numerical models are promising tools for the investigation of the long-term evolution of bars. Although models often include a rather simplified description of the complex physical processes, they solve fully non-linear equations for flow field and bed evolution, which compared to analytical models allow to better understand the later stages of the bar evolution when the non-linear interactions are dominant. Numerical models also provide a great flexibility to investigate the bar morphodynamics for different boundary and initial conditions. They allow analysing morphological evolution almost continuous in space and time. Recent studies have shown that 2D numerical models are capable of simulating the plan-form dynamics of both single-thread and multi-thread channels [e.g. *Nicholas*, 2013], at least qualitatively.

Alternate bars are studied less frequently using numerical compared to analytical theories and laboratory experiments. For instance, *Nelson* [1990] used model to explore growth of finite amplitude alternate bars. *Defina* [2003] and *Bernini et al.* [2006] investigate the bar evolution in a straight channel in light of analytical and empirical theories and provide sensitivity of the bar evolution to physical parameters. *Takebayashi and Okabe* [2008] studied alternate bars in non-uniform flow including the process of vegetations. *Wu et al.* [2011] investigated the effects of symmetric width variations on bar morphodynamics. *Crosato et al.* [2012] studied the long-term development of alternate bars. *Verbruggen* [2012] studied the upstream influence of bends in bars.

Physics-based-numerical models have been used less to reproduce the alternate bars observed in the specific cases. When used in specific cases, physics-based modelling requires calibration of

parameters because several combinations of parameters may provide similar results. *Sloff and Mosselman* [2012] suggest that calibrating on different morphological processes can reduce the associated uncertainty. *Jang and Shimizu* [2005] present one of the scarce examples where laboratory experiment data is used to calibrate a numerical model and quantitative comparison of the bar evolution is made.

- *Rule-based models*

Rule-based models are founded on simple rules, representing required physics, to route the discharge and sediment carried by the discharge. Such models were first introduced by *Murray and Paola* [1994] to simulate basic phenomena in braided rivers. Being computationally faster they are powerful exploratory tools for phenomena occurring at larger spatial scale (10^3 km) over longer time scales (century scale) where the physics-based models cannot be applied due to their high computational cost [*Coulthard and Van De Wiel*, 2013]. Continued development in the rule based model which involve improvement of flow and sediment routing [e.g. *Thomas and Nicholas*, 2002], representing more physics, and addition of more complexities like lateral erosion in bends [*Coulthard and Wiel*, 2006] have improved their predictability. As such one of the few examples of rule based model used to explore evolution of alternate bars is presented by *Nicholas* [2010].

3 LABORATORY EXPERIMENTS OF ALLUVIAL CHANNEL ADJUSTMENT

3.1 Introduction

This chapter describes the results of flume experiments carried out at the laboratory of Fluid Mechanics of Delft University of Technology, Delft, the Netherlands, with the general aim to investigate the effects of several controlling factors on the evolution of the width and bed level of an alluvial channel. The specific objectives of the experiments were to investigate the role of initial width (initial condition), discharge and sediment supply regimes (boundary conditions) on the long-term width and bed evolution of bedload dominated channels. The experiments were conducted by starting from different initial channel widths, with either constant or variable discharges at the upstream boundary under two different sediment regimes: i) with sediment feeding and ii) without sediment feeding. Sediment transport rate, channel width and bed levels at different locations where measured and analyzed during the experiments. The comparison between the measured data provide an increased knowledge on the role of the different controlling factors on channel evolution.

3.2 Methodology

3.2.1 Experimental setup

The experiments were performed in a 5 m long, 1.24 m wide and 0.4 m deep wooden flume, setup in a horizontal position on top of a wooden frame (Figure 10). At the upstream end of the flume, a 0.2 m wide notch was used as an inlet to the flume. The inlet notch is located in the middle of the width and the top level of the notch was set at 0.1 m above the bottom. At the downstream end of the flume, an overflow weir was provided throughout the width of the flume. The top level of the weir was set at 0.05 m from the bottom. The flume was filled with sand which was made moist to provide cohesion (apparent). A straight initial channel with rectangular cross-section, having the desired width and depth, was excavated at the centre of the flume, such that the bottom level of the channel started at the top level of the inlet notch and ended at the top level of the weir at the downstream end of the flume, providing 1% longitudinal bed slope to the initial channel. The initial cross-section of the channel was measured using a laser scanning device. A video recording camera was setup in a platform approximately 7 m higher than the flume. From this platform, the camera was able to record videos of the experiments along the entire length of the flume from a nearly orthogonal position. Control point targets were setup along both sides of the flume at 1m interval from the inlet. A meter long graphic scale and a digital clock were also setup on the flume.

An electrical surface pump was used to supply the water discharge to the inlet of the flume. The flow rate of the pump was controlled by adjusting the frequency of the current supplied to the pump. The details of the calibration and setup of the pump are presented in Appendix-A. The flume was extended further upstream of the inlet by 0.3 m to provide a pool collecting the water from the pump and reducing the turbulence at the inlet so as to maintain uniform flow throughout the cross-section of the inlet notch. A hopper shaped sediment feeder was also setup at the inlet to supply the sediment at the desired rate during the experiments. A bucket was placed at the downstream end of the flume to collect the discharge flowing over the weir. The bucket comprised a submerged basket, placed beneath the overflow, to collect the sediments exiting the flume. The basket was made out of a plastic net with opening smaller than the size of the smallest fraction of the sediment used in the flume. It was suspended on a weighing machine which continuously measured the cumulative weight of the collected sediment. The water collected in the bucket, after exiting the basket, was free of sediment

and was re-circulated to the flume inlet by the pump. To ensure the same level of submergence of the sediment collection basket, even during the variable discharge experiments, the water level in the bucket has to be maintained at a constant level. A constant water level was maintained in the bucket by providing an over flow and a constant inflow of water from an external tap into the bucket.

A potassium permanganate solution (purple colour) was fed at the flow inlet to distinguish the wet part of the channel bed topography from the dry part. The feeding rate was every 30 minutes for the constant flow case and at the end of each flow stage for the variable discharge cases.

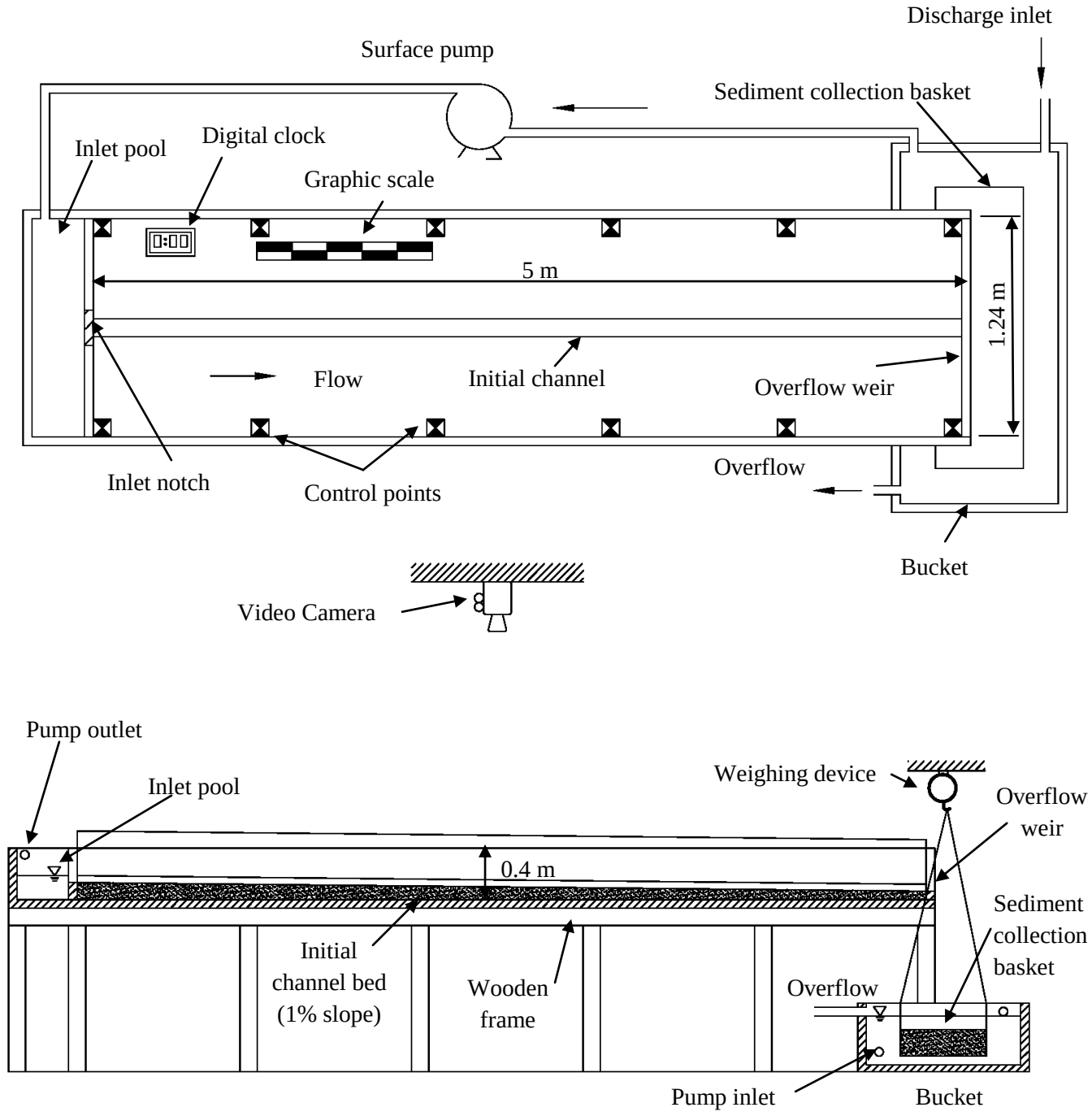

Figure 10. Details of the flume used in the experiment showing a) top view (above) and b) side view (below)

To start the experiment, the bucket at the downstream end of the flume was first filled with water at the constant inflow rate. Meanwhile the frequency of the current supplied to the pump was set to the

value corresponding to the required discharge. As soon as the water started to overflow, the pump was switched on to circulate the discharge from the bucket to the inlet of the flume. The timer in the clock was set to zero. The cumulative weight of the sediment exiting the flume was continuously recorded. In the experiments with sediment feed, the sediment feeder was turned on to supply sediment at the desired rate. In the case of very low discharge the sediment was supplied manually. After 2 hours, the experiments were stopped to measure the cross-sections of the evolved channel. The cross-sections were measured approximately at every 0.5 m from the inlet of the flume using the laser device. Experiments were then restarted and the water levels were measured at each cross-sections by measuring the elevation of the point where the water level intersects the banks. The experiments were then finally stopped after 7 hours and the cross-section and water level measurements were repeated. The experiments had to be stopped earlier if the channel touched the sides of the flume because the width adaptation process in such cases is not fluvial anymore.

3.2.2 Experiment design and test scenarios

Several tests scenarios were designed to explore the effects of initial channel width in the long-term width adaptation of the bed-load dominated channel under different hydraulic and sediment supply regimes. The initial cross-section of the channel and the flow conditions were designed such that the hydraulically smooth regime is avoided to prevent ripple formations at least during the initial part of the experiments. The experimental conditions of constant flow cases were checked by plotting the initial experimental conditions on the modified shields diagram by *Garcia* [1999] (Figure 11).

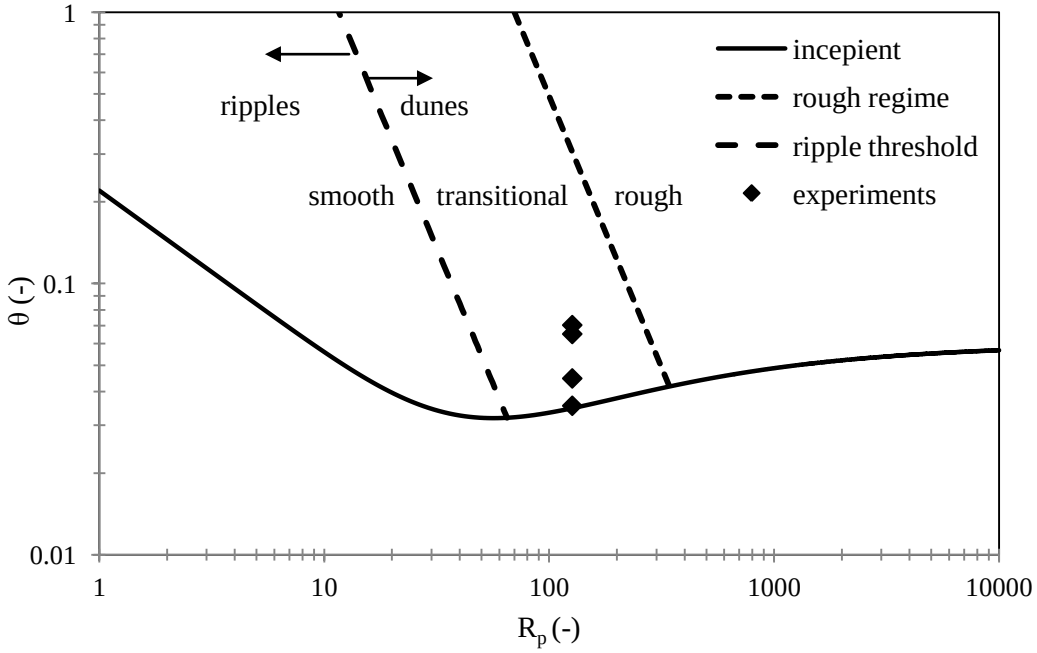

Figure 11. Shields diagram showing the experimental conditions of the constant flow experiments. R_p denotes the particle Reynolds number and θ denotes the Shields number.

A first set of experiments (Table 4 and 5) was carried with four different initial widths, 0.04 m, 0.1 m, 0.25 m and 0.4 m, and supplying a constant discharge of 0.4 l/s without sediment feed at the inlet. Three different rectangular, idealized discharge hydrographs, H1, H2 and H3, were then designed to explore the effects of the variable discharge regime (Figure 12). All hydrographs were designed such that during each cycle of the discharge hydrographs, the total water volume was the same as the total volume of water corresponding to the same duration of the constant flow case. Hydrograph H1 had low and high discharge of 0.3 l/s and 0.5 l/s (+/- 25% of constant flow), respectively. Hydrograph H2

had low and high discharge of 0.2 l/s and 0.6 l/s (+/- 50% of constant flow), respectively. The duration of both the high and low discharge was for 21 minutes, these discharge hydrographs differing only in the flow wave amplitude. For discharge hydrograph H3, the low discharge of 0.28 l/s had duration of 32 minutes and the high discharge of 0.8 l/s had duration of 10 minutes, such that this hydrograph represents a very intense high flow but with a relatively short duration (see Table 4 and 5 and Figure 12).

Table 4. Scenarios explored differed in initial channel width, discharge and sediment input.

Width (m)	No sediment feed				Sediment feed			
	Discharge regime				Discharge regime			
	UNI	H1	H2	H3	UNI	H1	H2	H3
0.04	UNI-0.04				UNI-0.04*			
0.1	UNI-0.10	H1-0.1	H2-0.1	H3-0.1	UNI-0.10*	H1-0.10*	H2-0.10*	H3-0.10*
0.25	UNI-0.25				UNI-0.25*			
0.4	UNI-0.4	H1-0.4	H2-0.4	H3-0.4	UNI-0.4*	H1-0.4*	H2-0.4*	H3-0.4*

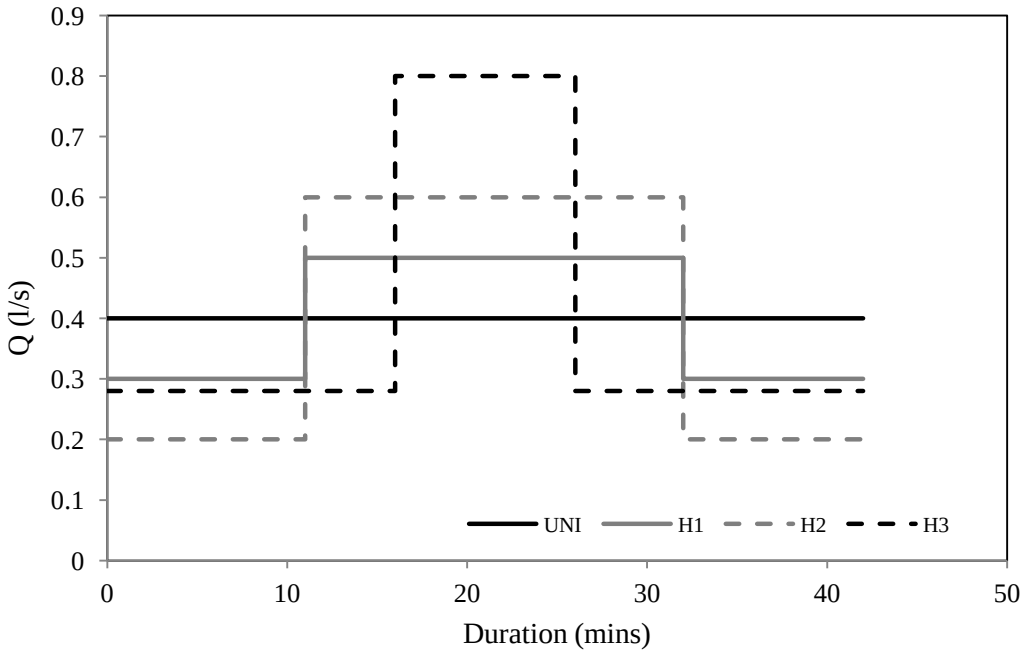

Figure 12. A cycle of the discharge regimes used in the experiments

The experiments with variable discharge were carried only for the initial widths of 0.10 m and 0.4 m. The experiment sets were first carried out without sediment supply and then repeated with the sediment supply. The experiments are labelled with the discharge regime followed by initial channel width. "UNI" represents constant discharge and "H1", "H2" and "H3" denote the hydrographs as shown in Figure 12. The experiments with sediment feed were then followed by "*". Details of the experiments carried out are presented in Table 4 and Table 5.

Table 5. List of all experimental scenarios.

Experiment	W (m)	Low discharge (variable discharge runs)			Constant discharge		High discharge (variable discharge runs)			Remarks
		Q (l/s)	Qs (g/min)	T (min)	Q (l/s)	Qs (g/min)	Q (l/s)	Qs (g/min)	T (min)	
UNI-0.04	0.04	-	-	-	0.4	-	-	-	-	
UNI-0.1	0.1	-	-	-	0.4	-	-	-	-	
UNI-0.25	0.25	-	-	-	0.4	-	-	-	-	
UNI-0.4	0.4	-	-	-	0.4	-	-	-	-	
UNI-0.04*	0.04	-	-	-	0.4	90	-	-	-	
UNI-0.1*	0.1	-	-	-	0.4	90	-	-	-	
UNI-0.25*	0.25	-	-	-	0.4	90	-	-	-	
UNI-0.4*	0.4	-	-	-	0.4	90	-	-	-	
H1-0.1	0.1	0.3	-	21	-	-	0.5	-	21	
H2-0.1	0.1	0.2	-	21	-	-	0.6	-	21	
H3-0.1	0.1	0.28	-	32	-	-	0.8	-	10	
H1-0.1*	0.1	0.3	90	21	-	-	0.5	90	21	
H2-0.1*	0.1	0.2	20	21	-	-	0.6	20	21	
H3-0.1*	0.1	0.28	90	32	-	-	0.8	90	10	
H1-0.4	0.4	0.3	-	21	-	-	0.5	-	21	
H2-0.4	0.4	0.2	-	21	-	-	0.6	-	21	
H3-0.4	0.4	0.28	-	32	-	-	0.8	-	10	
H1-0.4*	0.4	0.3	90	21	-	-	0.5	90	21	
H2-0.4*	0.4	0.2	20	21	-	-	0.6	90	21	
H3-0.4*	0.4	0.28	90	32	-	-	0.8	90	10	

Q = flow discharge (l/s), Qs = sediment supply rate (g/min), T= duration of flow during individual hydrograph cycle (min), an asterisk (*) denotes runs with upstream sediment supply.

3.2.3 Measurement and data processing

Several measurements were carried out before, during and after the experiments using standard and designed measurement techniques. Details of the design, calibration and measurement techniques are discussed in Appendix-A. The data were then processed to obtain a quantitative understanding of the width and bed level evolution of the channel averaged over the reach. The measurements included:

Sediment properties

Sediment properties were measured before setting up of the experiments. The grain size distribution of sediment used in the experiments was determined by performing the DIN-4188 standard sieve analysis. The granulometric distribution of the sediment size was determined using the data from the sieve analysis (Figure 13). The sediment resulted poorly sorted having bimodal distribution of sizes. The 10^{th}, 50^{th} (median) and 90^{th} percentile of the sediment sizes were 0.27 mm, 1 mm and 1.48 mm respectively. The geometric mean and geometric standard deviation of the distribution is 0.78 mm and 1.95 mm, respectively.

The grain density of the sand was 2365 kg/m^3. A Quantachrome ultrapycnometer 1000 (version 2.12) was used to determine the grain density of the sand. The grain density of the sand is necessary to compute the volumetric sediment transport rate of the sand exiting the flume.

Porosity of the sand needed to be computed as well, to convert the volumetric changes of the channel bed and banks (erosion and deposition) during channel formation, to weight of sand. Porosity is the measure of the amount of voids in the sand and is computed as the ratio between bulk density and grain density of sand. The bulk density of the sand is the density of the sand including the voids between sediment particles. The porosity depends upon the level of compaction of the sand. Since the level of compaction may vary between the experiments, both maximum and minimum porosity of the sand was determined using the Japanese standard test. The maximum and minimum porosity of the sand resulted 45.34% and 36.08%, respectively, for an average value of 40.71% ≈ 41%.

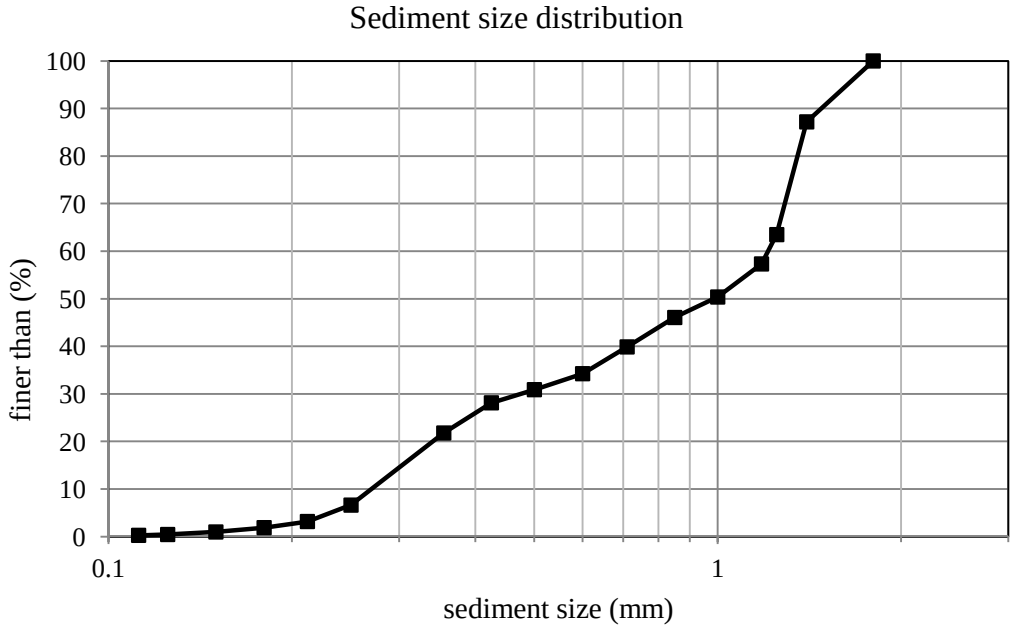

Figure 13. Cumulative grain size distribution of the sediment used in the experiment

Width

The width of the channel is here defined as the distance between the opposite wet-area margins of the channel at a cross-section perpendicular to the flow direction (Figure 14). The temporal evolution of the channel width was computed from the images captured by the video camera. The images of the constant flow experiments were extracted at the interval of 30 minutes from the start of the experiments, whereas the images of the variable discharge experiments were extracted at the end of each low and high flow stages. The width was then extracted from the images using Arc GIS 9.1. The details are presented in Appendix-A.

The images of the experiments showing the evolution after 2 hours and at the end of the experiments are presented in Appendix-A.

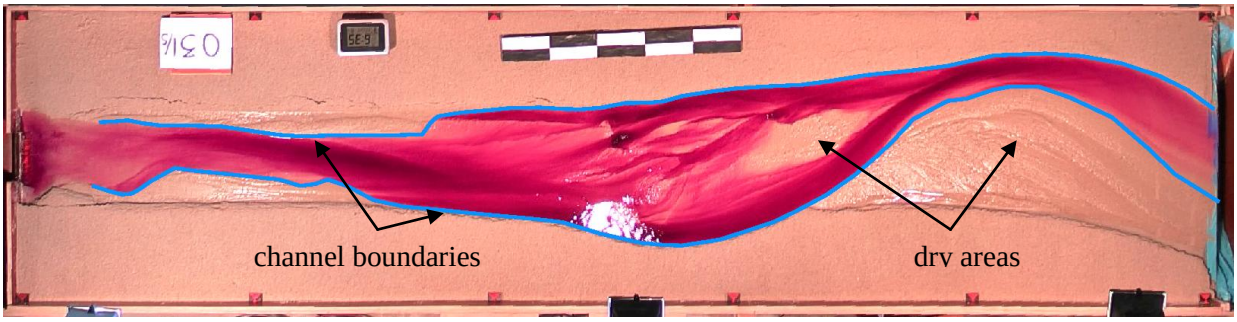

Figure 14. Extraction of channel width from the images showing the extent of the wet channel used for width computation. Flow is from left to right.

Sediment transport rate

The sediment exiting the flume was collected in a submerged basket. The weighing machine recorded weight of the basket in voltage at frequency of 1/10th of second during the entire experiment. The voltage was then used to convert to weight using equation obtained from the calibration of the weighing device. The details of the sediment weight measurement device is presented in Appendix-A. Since the sand was collected in a basket, submerged at a constant level, the measured weight is the relative weight of the sand. The sediment transport rate was computed at a minute interval from the recorded cumulative weight of the sediment which is presented in Appendix-A.

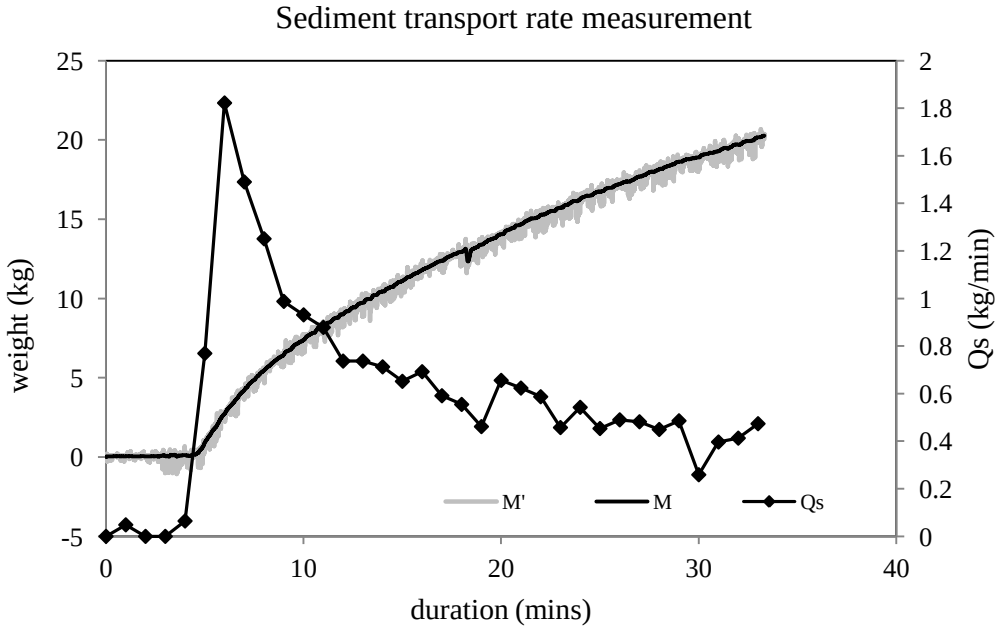

Figure 15. Example of cumulative weight measurement recorded during the experiment (M'), the filtered weight (M) signal and the sediment transport rate computed using the filtered weight signal, during an experiment.

Cross-sections

The evolution of the channel cross-sections was measured to have quantitative assessments of the change in width and bed level. A simple laser topography measuring device was designed to measure cross-sections of channel. The laser device measures distance between the target and the device in terms of voltage. The voltage was then converted to distance. Details on design and calibration of the laser device are presented in Appendix-A.

The cross-sections were measured at 0.28, 0.58, 1.08, 1.58, 2.08, 2.58, 3.15, 3.58, 4.08, 4.58 and 4.98 m from the inlet of the flume. Cross-section measurements were carried out in the channel at 1) initial stage, 2) after 2 hours of evolution and 3) at the end of the experiments. The experiments were stopped for cross-section measurements. After the cross-sections were measured, the experiments were restarted and the water levels were recorded in each cross-section by using the laser device. A typical cross-section with marked water level is presented in Figure 16.

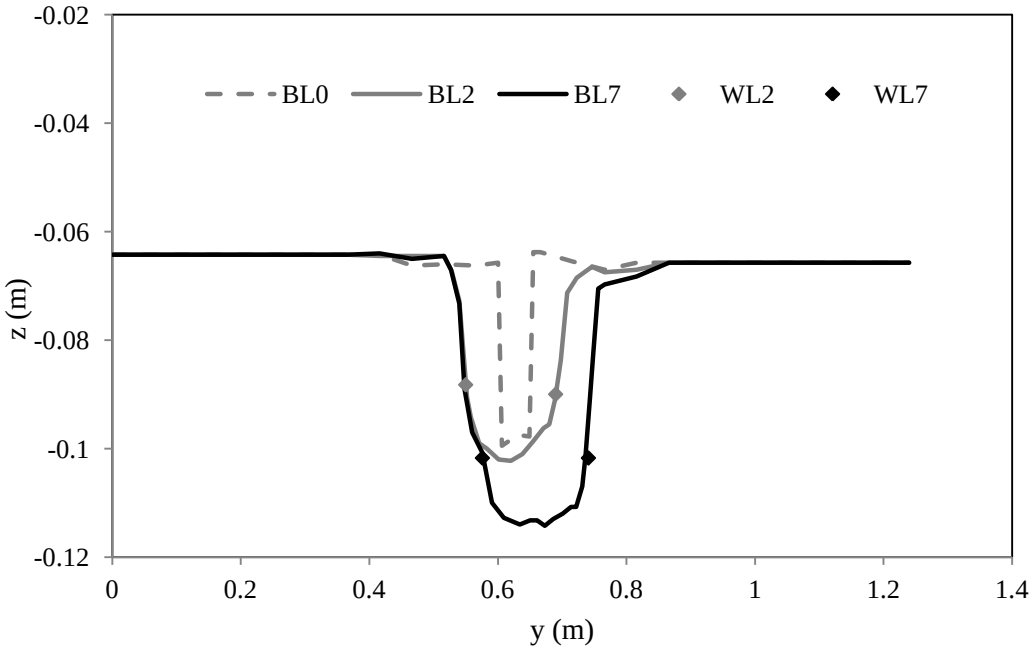

Figure 16. A typical cross-section and water level measurement in experimental channel. BL0, BL2 and BL7 are bed level measured before and after 2 and 7 hours of experiments, respectively. WL2 and WL 7 are the water level measurements carried out at 2 and 7 hours, respectively. "y" is the lateral distance from the right wall of the flume and "z" is the depth with respect to the top level of the flume.

A "bed portion" and a "bank portion" of the channel has been distinguished within each cross-section to analyze the width and bed evolution of the channel. The following algorithm has been used. The transverse slope was computed along the cross-section based on the surveyed topography. The Point where the highest change of the transverse slope occurs starting from the centre of the channel was marked along both left and the right bank of the cross-sections. The part of the cross-section between these points was considered as the bed and the rest as banks. The channel depth (not the wetted depth) was then computed as the elevation difference between the top of the banks and the average bed level of the channel. The average bed level of the channel was then subtracted from the average bed level of the initial channel to compute the average change in the bed level of the cross-section. The cross-section average channel bed level was finally used to compute the longitudinal slope of the channel.

Alternative criteria to distinguish between the bed and bank could be based upon the water level. The perimeter of the wetted area can be considered as bed, and the part above as bank. However, such criteria neglects the terraces of the channel bed formed due to channel incision, over estimating the cross-sectional average depth of the channel.

The cross-sections data were then used to quantify the volume of sediment reworked during the experiment. The channel adjusts its width as well as its bed level during its development. A simple model was developed to quantify reworking of sediment from the banks and the bed of the channel which is presented in Appendix-A.

3.3 Results

3.3.1 Channel width evolution

The evolution of channel width was analysed from the pictures extracted from the video. The channel width had spatial as well as temporal variations during the evolution. Along the longitudinal direction, the channel closer to the upstream flow inlet was narrower compared to the reach of the channel near to the downstream boundary of the flume. To minimize the effects of the boundaries, the measurements were conducted on a 3 m long reach obtained by removing the first and the last meter of close to the boundaries. The reach-averaged channel width was computed by averaging channel width along longitudinal direction at 0.2 m interval for one instance of time during the evolution.

Constant discharge conditions

The width evolutions of the channels were computed every 30 minutes and are presented in Figure 17. Experiments without sediment feed evolved in narrower channels (Figure 17-a) compared to the respective experiments with sediment feed (Figure 17-b). Despite starting from different initial widths, the experiments without sediment feed evolved in single-thread channels with final reach averaged width close to 0.2 m (Figure 17-a). UNI-0.04 and UNI-0.10 represent cases with narrower initial width. UNI-0.25 and UNI-0.4 represent the cases with wider initial widths compared to the final width obtained for the respective cases. Experiments with narrower initial width rapidly widened in the first half an hour and continued to evolve with lower widening rate. The channels started to be slightly sinuous after 2 hours. The amplitude of the channel bend, closer to the downstream boundary, gradually increased. The rate of bank retreat was not completely followed by slightly lower bank advance rate (due to incision), causing the channel to widen but at a slower rate.

In the UNI-0.25 case, the channel widened up to 0.3 m during the first 3.5 hours of evolution, and then eventually narrowed down to 0.2 m towards the end of the experiments (Figure 17-a). Migrating alternate bars developed within the channel in the first half an hour, the weak deflection of flow towards the banks caused little bank erosion and thus slight widening of the channel. As the widening of the channel progressed at a lower rate, mid-channel bars also appeared within the channel. Growth of mid channel bars deflected the flow towards the banks enhancing bank erosion and widening of the channel (e.g. Thorne et al. 1998). After 2 hours, the channel started to widen in the downstream part of the flume whereas incision occurred at the upstream part of the flume. Eventually the channel incision advanced further downstream, which constricted the channel along the left bank leaving the area close to right bank dry forming a narrower channel.

The channel in the UNI-0.4 case continued to narrow throughout its evolution. Due to the higher width to depth ratio, mid channel bars of low amplitude were developed during the first half an hour. The bars did not grow in amplitude. The channel close to the upstream inlet started to incise from the early stages of development (after 1 hour), resulting in a constricted channel closer to the right bank. Channel incision advanced further downstream forming a channel constricted along the right bank leaving the area close to left bank dry along most reach of the flume. Channel widening was observed close to the downstream boundary after 2 hours, due to the growth of a mid channel bar. However, channel narrowing was the dominant process along the most part of the flume (Figure 17-a).

Experiments with sediment feed (Figure 17-b) all evolved into wider multi thread channels at the end of the experiments. UNI-0.04* and UNI-0.1* evolved with higher widening rates compared to UNI-0.25* and UNI-0.4*. During first half an hour of the development UNI-0.04* and UNI-0.1* widened by rapid bank erosion. Alternate bars start to appear after half an hour, when the channel was wide enough to exceed the critical width to depth ratio, defining their formative conditions (e.g. Colombini,

Seminara, & Tubino, 1987). The bank erosion was observed along the pools, resulting in a sinuous and wider channel. The evolution continued to increase the amplitude of the bends. The bank retreated at faster rate than the bank advance rate causing rapid widening of the channel. As the channel continued to widen, complex mid-channel bars formed. Both UNI-0.04* and UNI-0.1* experiments had to be terminated earlier because the channel margins touched the sides of the flume.

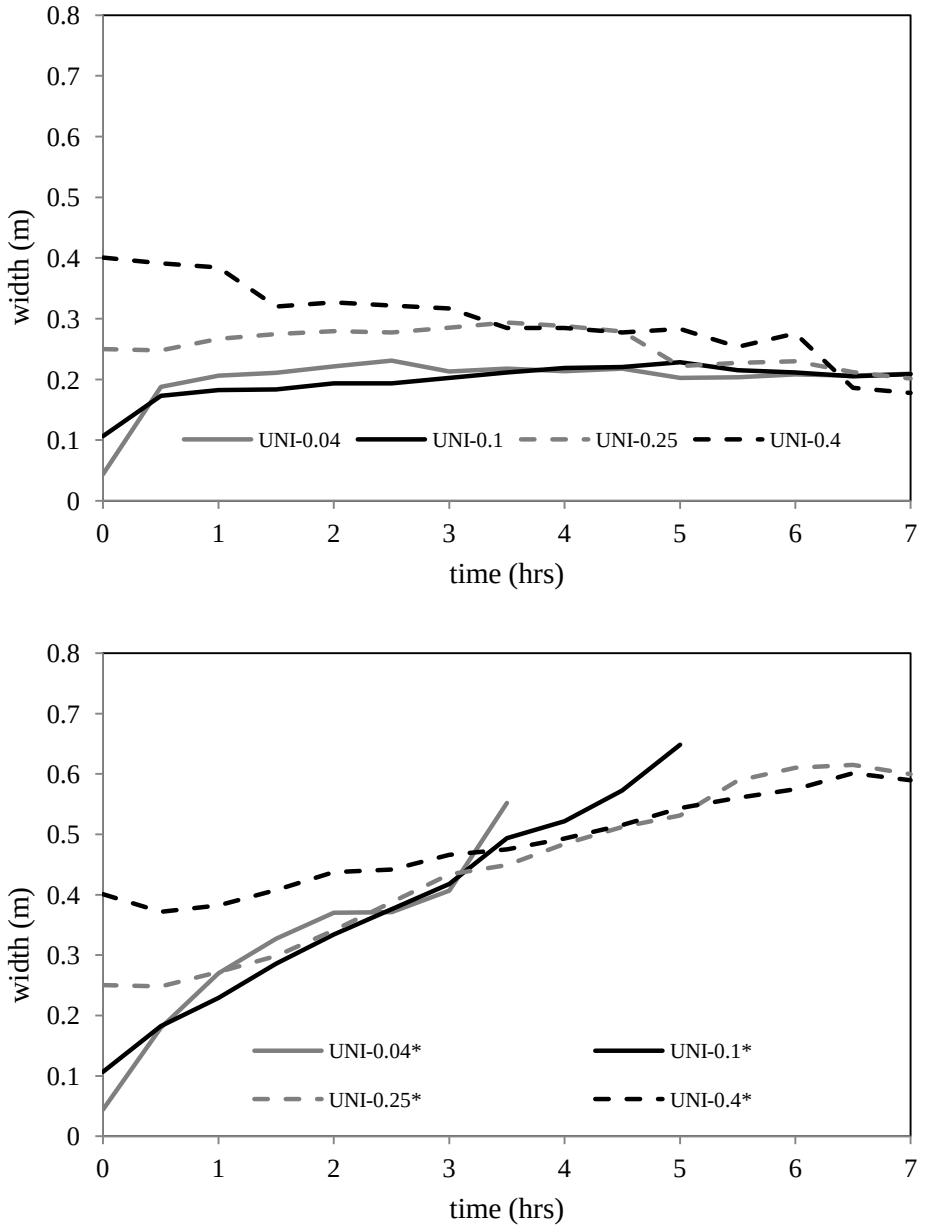

Figure 17. Width evolution in time for the experiments with constant flow of 0.4 l/s but different initial channel widths, 0.04 m, 0.1 m, 0.25 m and 0.4 m a) without sediment feed and b) with sediment feed at the upstream boundary

Since UNI-0.25* and UNI-0.4* cases had higher width to depth ration, the first half and hour were characterized by the development of alternate and mid-channel bars, respectively. The growth of bars caused deflection of flow towards the bank causing bank erosion, resulting in wider and multi-thread channels. Similar phenomena of channel widening was observed by Ashmore (1982) in laboratory channels and Jang & Shimizu (2005) in numerical simulations. As the widening of the channel progressed, complex mid-channel bars were observed migrating along the channel. UNI-0.25*

presented higher widening rate than UNI-0.4*, but after 4 hours both evolved at similar widening rates to resulting in channels with reach averaged widths of 0.6 m.

The final channel width was predicted using some of the width prediction methods presented in chapter 2. Empirical approaches of *Bray* [1982] and Parker et al. [2007] and regime equations based upon extremal hypothesis [*Millar*, 2005] were chosen, because they were developed for the gravel bed rivers. Using the experimental conditions, as input, the channel width of 0.29 m, 0.22 m and 0.29 m was obtained respectively. Even though these methods were developed for gravel bed river channels under equilibrium conditions, they predict the width closer to the width of the channels without sediment supply. The channels obtained by sediment supply, instead, were much wider compared the results from the prediction methods. These channel prediction methods use bank-full discharge as the formative discharge. Since channels in the experiments had different initial widths, the initial bank-full discharges would be different. The UNI-0.04 and UNI-0.04* cases represents almost the bank full condition at the start of the experiments. The final bankfull discharge would be much higher due to channel widening.

Variable discharge conditions

With variable discharge, the width was measured at the end of each discharge stages. Figure 18 compares the width development for the scenarios with 0.1 m wide initial channel and different discharge regimes. Since the channel width consists of the extensions of the wet area at the margins, the spreading and the shrinking of the wet area during the high and low discharge stage is reflected in the computed width of the channel. Discharge regimes H2 and H3 have higher variation among the discharge stages so high width fluctuation were observed between the high and low discharge for these scenarios.

The experiments without sediment feed (Figure 18-a) evolved into channels with a narrower width compared the respective experiments with sediment feed (Figure 18-b). All discharge regimes evolved into single thread channels without sediment feed and to multi-thread channels with sediment feed. The variable scenarios without sediment feed (Figure 18-a) evolved into wider channels compared to the constant discharge scenarios. Even though the constant and variable scenarios have the same total volume of flowing water, the discharge variation plays a role in the width evolution of the channels. The initial half an hour of evolution were characterized by rapid widening followed by slower widening rates in all scenarios. The long-term width development shows that H3-0.1 and H2-0.1 scenarios are grouped together and result similar widths (0.35 m), towards the end of the experiment. H3-0.1 and H2-0.1 are the scenarios with the higher discharge amplitudes. UNI-0.1 and H1-0.1 show similar trends but the H1-0.1 results in a wider channel (0.25 m) compared to the UNI-0.1(0.2 m).

The role of variable discharge was different at the early and later stages of the channel evolution. During the first four cycles of the discharge hydrographs, the channels mostly widened due to bank erosion at the high discharge stage. During the low flow stages, erosion occurred mostly in the channel bed and the flow was concentrated towards the centre of the channel. Bank erosion appeared to have ceased at the lower stage discharge during this period and no bars formed. The following adjacent high discharge stage during this period then eroded the banks and flattened the incised part of the channel bed. However, after 4 cycles of discharge hydrographs, the channel had widened sufficiently to allow for the formation of bars at lower discharge stage. Bars grew in amplitude deflecting the flow towards the banks (as observed in the constant discharge cases) so that the bank erosion was then also observed during the low-stage discharge.

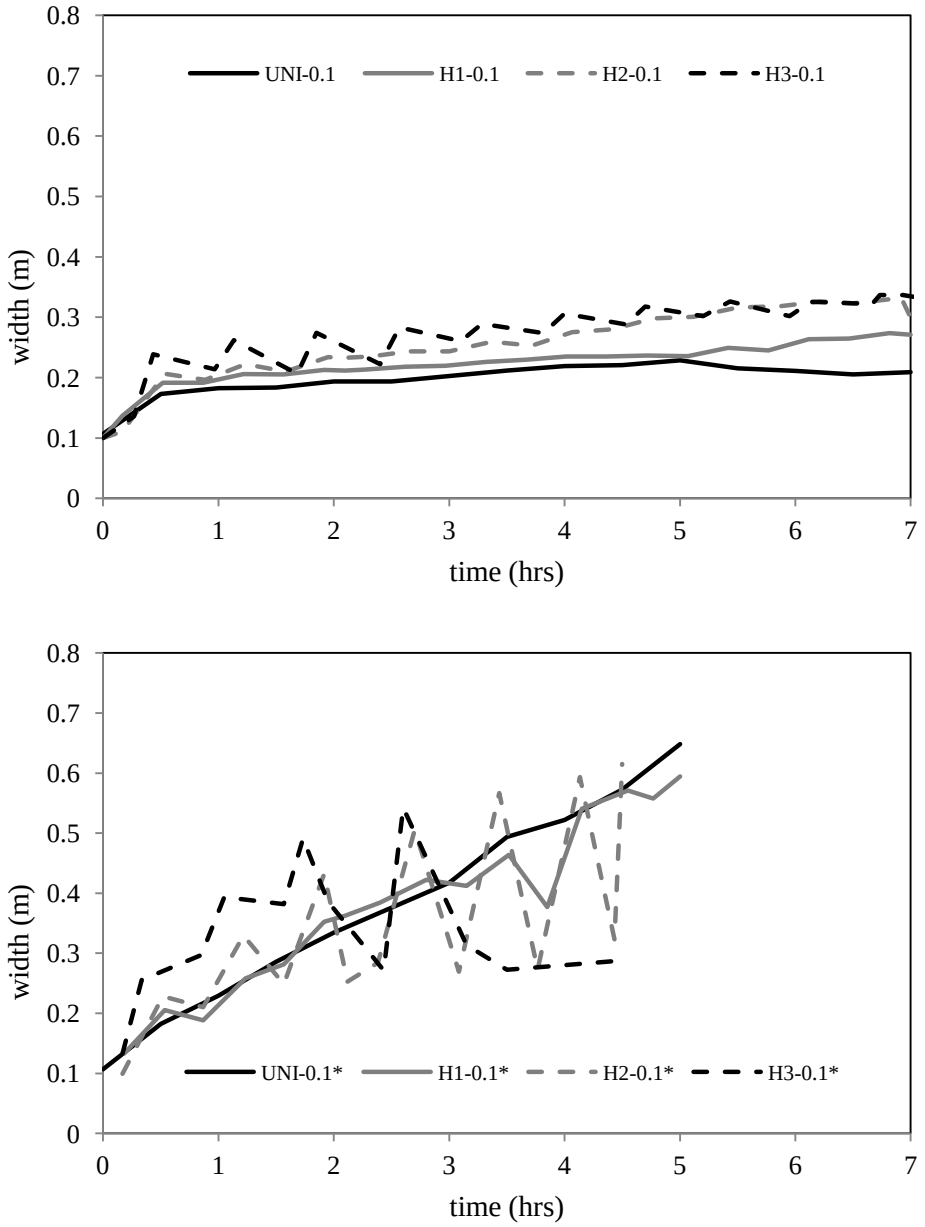

Figure 18. Width evolution in time of experiments starting with initial channel width of 0.1m under discharge regime, Constant, H1, H2 and H3 a) without sediment feed and b) with sediment feed at the upstream boundary

As widening progressed, the bank erosion rate at the high discharge stages also gradually decreased. Thus the difference in channel width between high and low discharge stages decreased as the channel evolution continued. In the H1-0.1 scenarios, the channel started to widen at a higher rate after 5 hours. This was caused by the growth of a bar near the downstream part of the flume.

For variable flow with sediment feed (Figure 18-b) the evolution trend of UNI-0.1* and H1-0.1* appear similar. The evolution trends of H2-0.1* and H3-0.1* scenarios appear also similarThe lower discharges also contributed to the widening of the channels and alternate bars formed already during the first cycle of high discharge stage. The following low discharge stage eroded the banks around the pools increasing the sinuosity of the channel. The following higher discharge then widened the channel and increased the amplitude of the channel bend. The low discharge then concentrated within the sinuous deeper part of the channel further eroding the banks and making channel more sinuous.

Experiments were terminated after 5 hours because the channel continued to widen and touched the sides of the flume.

Since the evolved channel towards the end of the experiments is multi thread and very wide, the discharge during the low stage was concentrated among few channels. The variation among the discharge stage caused spreading and shrinking of the water surface extent within the channel. Scenarios with the highest discharge amplitude, H2-0.1* and H3-0.1*, showed high width variations between the high and low discharge stages towards the end of the experiments (Figure 18-b).

Figure 19 shows the channel width starting from 0.4 m under different discharge regimes. Similar to the previous scenarios, experiments without sediment feed (Figure 19-a) evolved into narrower channels compared to the respective experiments with sediment feed (Figure 19-b). The evolution of channels without sediment feed show that the H1-0.4 and H3-0.4 scenarios evolved into wider channels following similar evolution trends. The H2-0.4 and UNI-0.4 scenarios, however, evolved into narrower channels. The width of channel formed in H2-0.4 case is wider than the channel formed in UNI-0.4 case.

Experiments started with a wide channel, low amplitude migrating bars developed already in the first cycle of discharge hydrographs. During the growth stage of these migrating bars no significant erosion was observed along the banks. The H1-0.4 and H3-0.4 cases have similar lower discharge (0.3 and 0.28 l/s respectively). The lower stage discharge was able to rework the bars formed during the high discharge stage and erode the banks along certain stretch of the channel. The following high discharge reworked the bed and eroded the banks in these regions, resulting in channel widening. Similar phenomena were repeated during the channel evolution in H1-0.4 and H3-0.4 scenarios, under each cycle of discharge hydrograph. Channel incision was observed at the upstream part. The discharge during the high stage spread almost along the entire width of the channel. However, the low flow discharge was confined within the narrow incised part of the channels. So the variation of channel width between the high and low discharge stage was mostly due to the expansion and shrinking of the water surface area within the channel, which is evident at the later stage of evolution.

In H2-0.4 scenario, the lower discharge (0.2 l/s) was not sufficient to rework the bars formed during the high stage discharge. So, the low discharge eroded only some portion of the channel bed, confining the flow to the narrower width of the channel. The following higher discharge reworked the bed along the entire width of the flume but also further deepened the incised part of the channel. The channel incision started near the upstream boundaries and advanced further downstream with evolution, reducing the width of the channel.

With sediment supply, all discharge regime scenarios starting from a 0.4 m wide channel widened even further (Figure 19-b). H1-0.4* scenario resulted in the widest channel and H2-0.4* in the narrowest channel. H3-0.4* and UNI-0.4* resulted in channels with similar width. A scour just downstream of the inlet was observed in scenarios H2-0.4* and H3-0.4*, which indicates that the supplied sediment was less than the transport capacity of the channel. This might have affected the channel evolution for scenarios H2-0.4* and H3-0.4*, resulting in the narrower channels compared to scenario H1-0.4*.

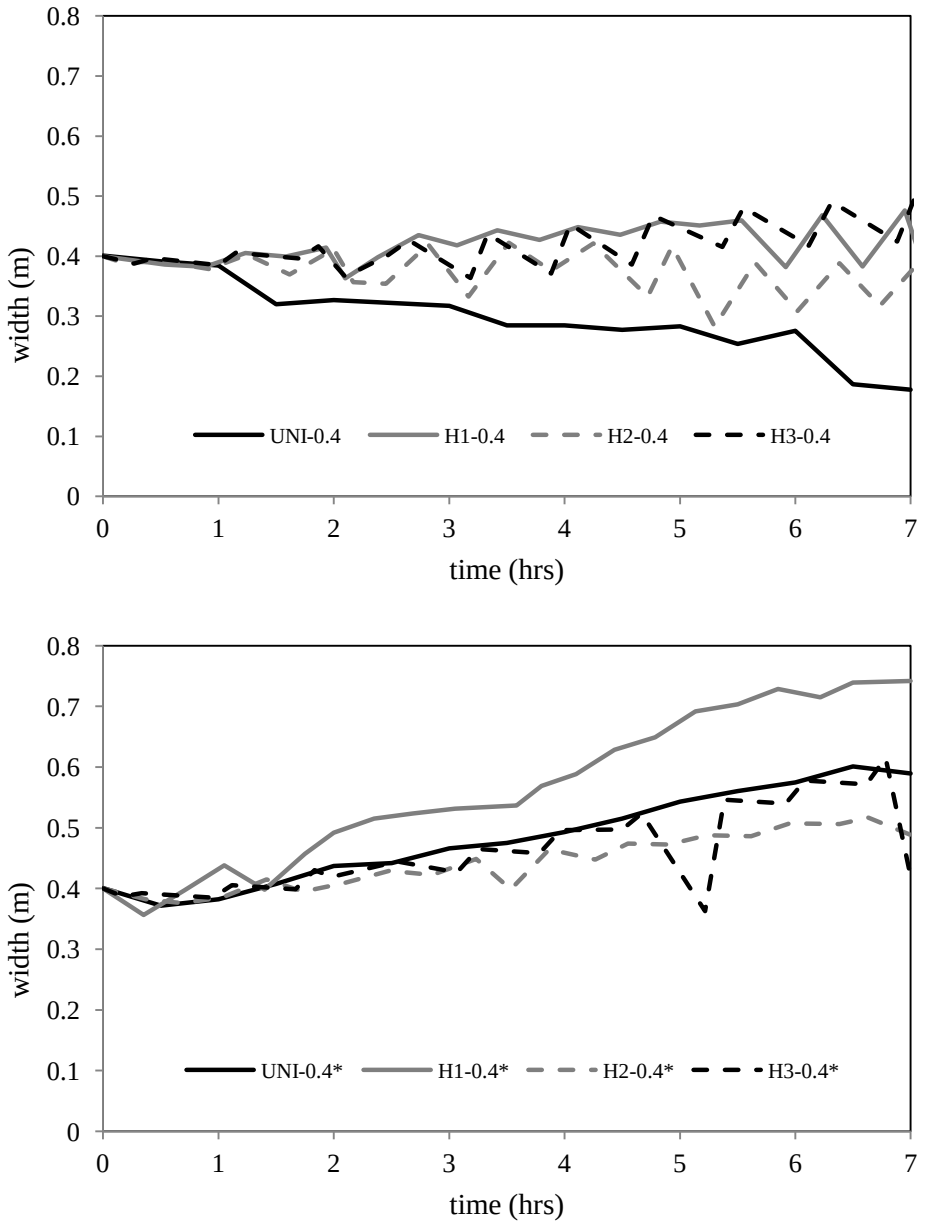

Figure 19. Width evolution in time of experiments starting with initial channel width of 0.4m under discharge regime, Constant, H1, H2 and H3 a) without sediment feed and b) with sediment feed at the upstream boundary

Bars with higher amplitude formed within the channels starting from the early stage of the developments in all scenarios with sediment supply. The growth of bars deflected the flow towards the bank resulting in eroding banks and channel widening. All experiments evolved into multi-thread channels and remained multi-thread also during the low discharge stages, so there was no significant width variation observed among the low and high stage flows. After about 5 hours, however, the low-flow discharge was concentrated in one of the branches, leaving the other branch at the bifurcation dry, thus causing the sudden reduction of channel width in H3-0.4* scenario.

3.3.2 Sediment transport rate evolution

The measured sediment transport rate exiting the flume (output rate) is compared with the width and bed level evolution to understand the correlation between the change in sediment transport rate behaviour and width adjustment. The width evolution and sediment transport rates are shown in

Figure 20for experiments with different initial width at constant flow and without sediment supply condition.

The trends of sediment output rate in the experiments starting with a narrower initial width, UNI-0.04 and UNI-0.1, are similar (Figure 20-a and b). A high rate is observed in the early stage of the channel evolution which gradually decreases to a dynamic equilibrium value towards the end of the experiment. Towards the end of the experiments the average sediment output for these scenarios is 0.16 kg/min and 0.14 kg/min, respectively. Both scenarios showed rapid widening during the first half an hour leading to a similar channel width. Since in UNI-0.04 the flow eroded more sediment from the banks than in UNI-0.1, the initial sediment output rate was higher. The sediment output rate after two hours of development showed a wave like pattern which was caused by bank erosion related to the increasing sinuosity near the downstream part of the channel. Since bank retreat was followed by bank advance, no significant channel widening is observed during this phase.

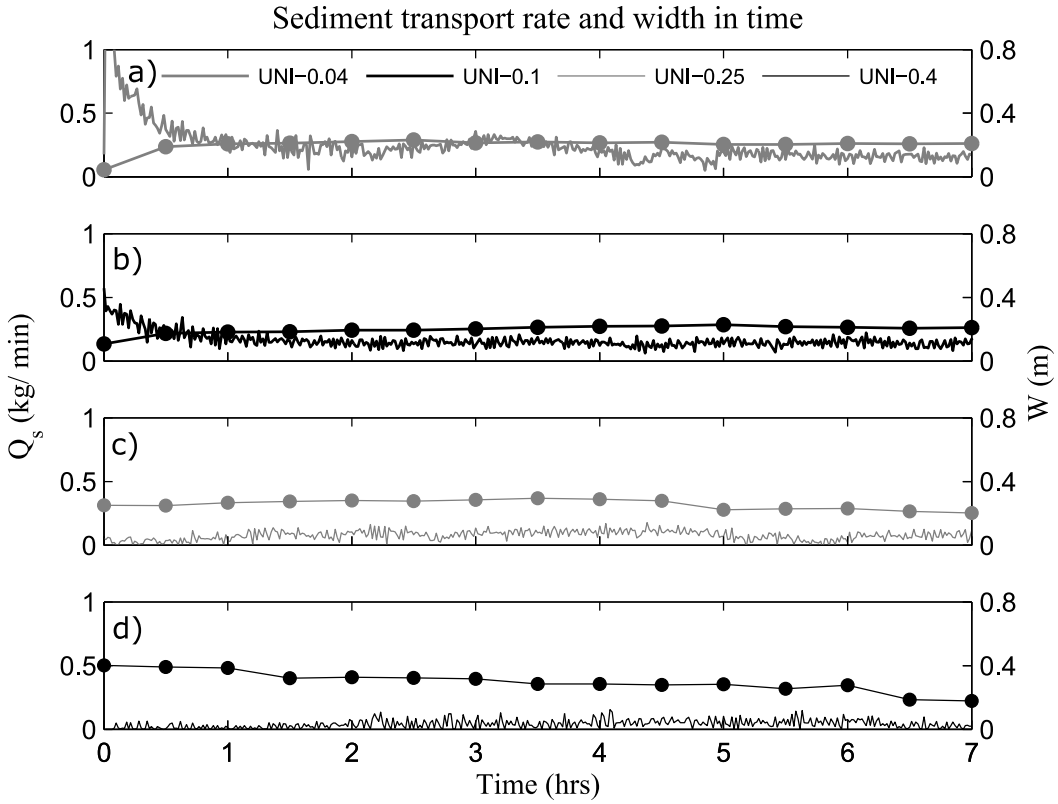

Figure 20. Evolution of width and sediment transport rates exiting the flume for the scenarios a) UNI-0.04, b) UNI-0.1, c) UNI-0.25 and d) UNI-0.4. Continuous lines represent the sediment transport rate and the lines with filled symbols denote the width evolution in time.

In the experiments with a wider initial width : UNI-0.25 and UNI-0.4, the sediment output rate was low at the beginning. After 1 hour the banks started to erode and widening progressed at a slow rate in UNI-0.25 scenario. The sediment output rate increased too because of the input from bank erosion. After 4.5 hours the incision became more dominant which is reflected in sediment output rate decrease. A brief increase in sediment output rate is observed after 6 hours, which is due to channel shifting, near the downstream boundary, from right to left.

For the UNI-0.4 scenario, the sediment output rate starts to increase only after 1.5 hours. Even though, the incision was already evident near the upstream boundary, but the eroded material was deposited more downstream. The increase in sediment output rate after 2 hours is due to bank erosion, caused by

the evolution of the mid channel bar near the downstream boundary, as discussed in section a-1. Bank erosion stopped and the channel incision was also observed near the downstream boundary after 6.5 hours.

The width evolution and sediment output rate for experimental scenarios with constant flow and sediment supply are shown in Figure 21. The sediment output signal of UNI-0.04* case and UNI-0.1* case was not long enough to understand its behaviour during the width evolution (Figure 21-a and b). However it is worth to mention that the channels in both UNI-0.04* and UNI-0.1* remained single thread during the first hour after which they develop a braided planform. The high fluctuations of sediment output observed after 2 hours is typical of a braided channel which is attributed to local degradation and aggradation within the channels (e.g. Ashmore 1991; Hoey & Sutherland 1991).

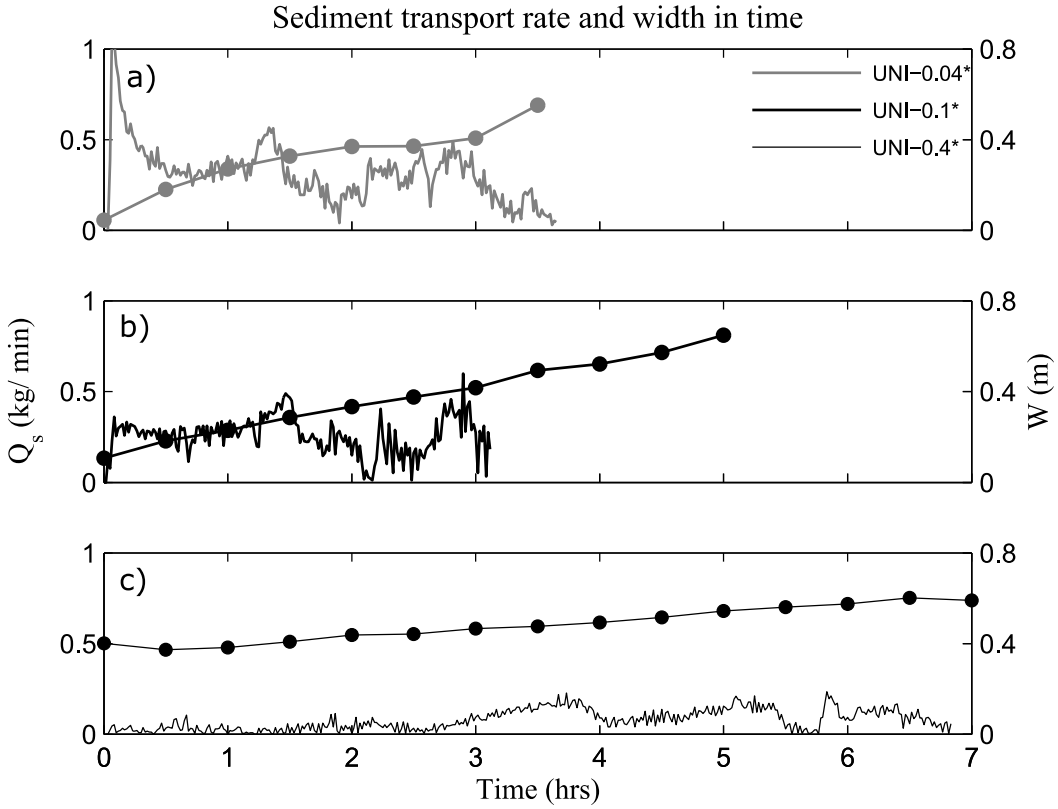

Figure 21. Evolution of width and the sediment output rate exiting the flume for the scenarios a) UNI-0.04*, b) UNI-0.1* and c) UNI-0.4*. Continuous lines represent the sediment output rate and the lines with filled symbols denote the width evolution in time.

For UNI-0.4* (Figure 21-c), even though sediment was supplied, its initial sediment output rate was very small. The migrating bars developed from the beginning of the experiments, but the bars reached the downstream boundary only after half an hour. So, sediment output increased only after the initial period of time. The channel started to widen and form a braided pattern from the upstream boundary, but the reach near the downstream boundary did not widen for the first 2.5 hours. So the sediment output observed between 0.5 hours to 2.5 hours corresponds to the sediment output exiting the upstream braided reach. The reach of the channel near the downstream boundary started to widen and develop the braided planform after 2.5 hours. The channel continued to rework its bars and the banks maintaining the gradual rate of widening.

The width evolution and sediment output rate for channels with 0.1 m initial width without sediment supply is shown in Figure 22. The difference between the sediment output rate during the high flow

stages and low flow stages is clearly observed for the variable discharge scenarios (Figure 22-b, c and d). Like in the case of UNI-0.1 (with constant flow), the average value of sediment output rate decreases asymptotically with the evolution. The average sediment output rate, towards the end of experiment (after 5 hours), in the cases UNI-0.1, H1-0.1, H2-0.1 and H3-0.1 is 0.14 kg/min, 0.12 kg/min, 0.15 kg/min and 0.11 kg/min, respectively. The average sediment output rate is the lowest for H3-0.1 because the duration of low stage discharge is 3.2 times longer than the high stage discharge.

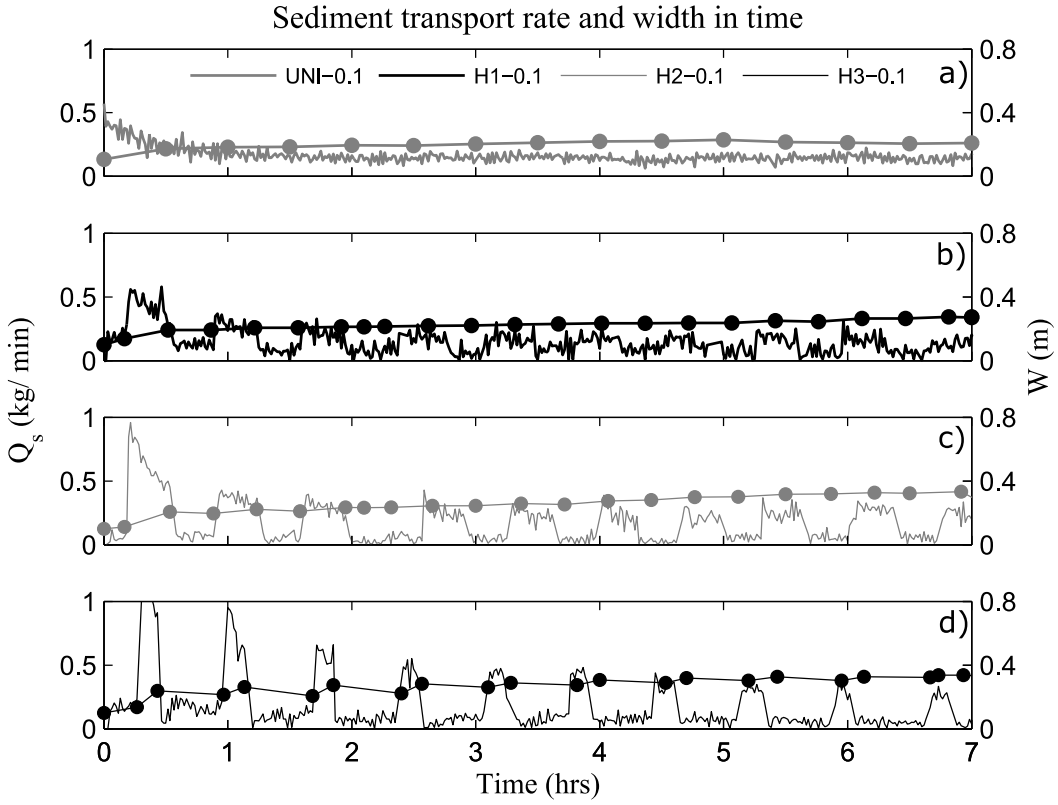

Figure 22. Evolution of width and the sediment output rate exiting the flume for the scenarios UNI-0.1, H1-0.1, H2-0.1 and H3-0.1. Continuous lines represent the sediment output rate and the lines with filled symbols denote the width evolution in time.

The trend of sediment output rate during the channel width evolution is similar in all variable discharge cases (H1-0.1, H2-0.1 and H3-0.1). The highest rate is observed during the first high stage discharge because of rapid widening. The sediment output rate correlates well with the rate of widening. H3-0.1 scenario has the highest sediment output rate at the first stage because of the highest widening rate.

Among the variable discharge regimes, H1-0.1 has the smallest and H3-0.1 has the highest ratio between the high and the low discharges. So the ratio of sediment output rate between the high stage and low stage discharge was observed smallest for H1-0.1 and the highest for H3-0.1. The sediment output ratio is also affected by the rate of widening among the discharge stages. The ratio was minimum during the evolution of H1-0.1 between 3 and 5 hours, because the channel widened at a very small rate. The channel started to widen at a higher rate after 5 hours, which caused the increase in the ratio between the sediment output rate at high discharge stage and low discharge stage. For scenarios H2-0.1 and H3-0.1, the decrease in ratio of sediment output during the high and the low flow stage is correlated with the decrease in ratio between the high and low stage channel width observed during channel evolution.

The width evolution and sediment output rates for the experiments with 0.1 m initial width with sediment supply is shown in Figure 23. The experiments were not long enough to analyze the sediment output with the long-term width evolution. The sediment output rates followed the discharge hydrographs during the early stage of the development when the channel was still single thread (Figure 23-b, c and d). After the second cycle of the discharge hydrographs, the channels started to form a braided planform. After 2 hours, sediment output started to develop a temporal lag with the discharge hydrograph, which might be due to bed aggradation and degradation occurring during the morphodynamic evolution of the braided channels.

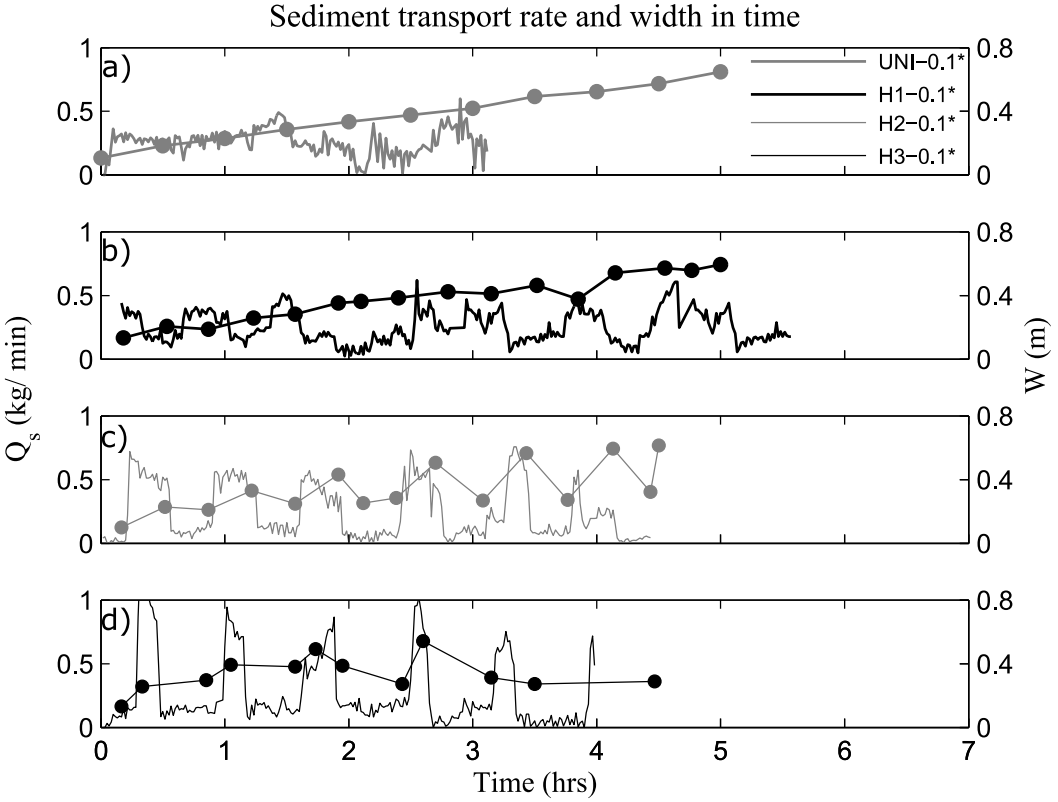

Figure 23. Evolution of width and the sediment output rate exiting the flume for the scenarios a) UNI-0.1*, b) H1-0.1*, c) H2-0.1* and d) H3-0.1*. Continuous lines represent the sediment output rate and the lines with filled symbols denote the width evolution in time.

The width evolution and sediment output rates for the experiments with 0.4 m initial width without sediment supply condition is shown in Figure 24. Alternate high and low sediment output rates correspond to the high and low stage of the discharge hydrograph cycles. No significant sediment output rate was measured for the experiments UNI-0.4, H1-0.4 and H2-0.4 during the early stages until the developed low amplitude mid channel bars reached the downstream boundary of the flume. The sediment output rate was recorded after the high stage discharge for both the experiments. H3-0.4 has the highest discharge amplitude, so significant amounts of sediment output were measured already during the first cycle of hydrograph. The magnitude of bank erosion decreased during the evolution of the channels for the scenarios H1-0.4 and H2-0.4 between 3 and 5 hours. More incision of the channel was observed between 3 and 5 hours, which greatly reduced the sediment output rate. Bank erosion resumed after 5 hours increasing the sediment output rate in both the scenarios. The bank erosion occurred towards the centre of the channel for H1-0.4 which contributed to increase the width. While for H2-0.4, bank erosion occurred close to the downstream boundary, increasing the sediment output. The central part of the channel continued to incise. While for H3-0.4 even though the channel incised

near the upstream boundary, bank erosion continued during the high flow stage near the downstream boundary causing the sediment output rate to increase compared to the early stages of development.

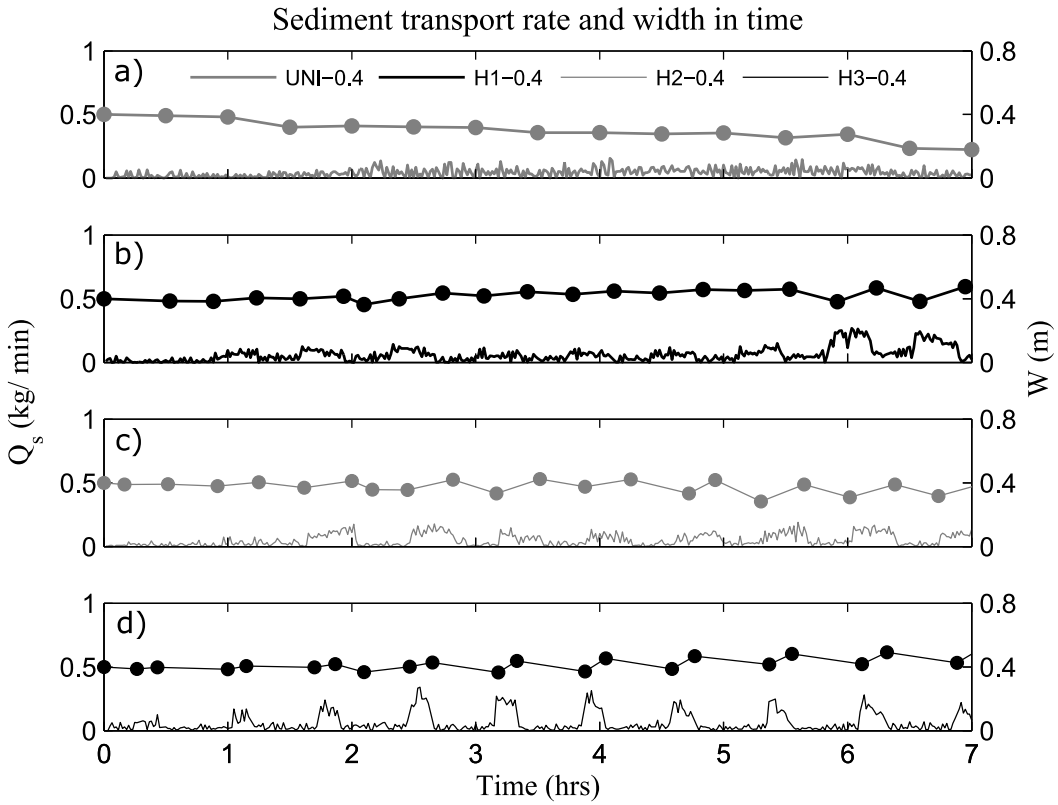

Figure 24. Evolution of width and the sediment output rate exiting the flume for the scenarios UNI-0.4, H1-0.4, H2-0.4 and H3-0.4. Continuous lines represent the sediment output rate and the lines with filled symbols denote the width evolution in time.

3.3.3 Sediment reworking during channel evolution

A fluvial channel evolves by reworking its bed and banks simultaneously. The channel evolution is better understood by identifying the dominant processes involved such as: bed erosion, sedimentation, bank erosion etc. A simple model based on the cross-section measurements was used to compute the volume of reworked bed sediment and the volume of sediment eroded from the banks during the channel evolution. The calculations were performed to study the first two hours of evolution and the subsequent five hours representing the early and the final stages of channel formation, respectively. The experiments with sediment feed were terminated earlier, so for these scenarios the analysis covers the initial stages only. The percentage of volume (Fs) reworking at the bed or bank was computed with respect to the total sediment volume reworking within each sub-reach (0.5 m long). The positive value of F_s denotes erosion and the negative value denotes deposition. Figure 25 summarizes the results for the constant-flow scenarios without sediment feed. The continuous lines and dashed lines are the results at 2 hours and 7 hours respectively and the black and grey lines are the sediment reworked along channel bank and bed, respectively.

The experiments starting from narrower initial width (UNI-0.04 and UNI-0.1) show similar sediment reworking trends (Figure 25-a and b). The sediment reworked during the initial stage of the evolution is dominated by the bank erosion processes whereas in the middle part of the flume the bed aggraded. The later stage of the evolution show that both bed and bank erosion contribute to sediment

reworking. The amount of sediment reworked due to bed incision is the highest at the upstream boundary and decreases to zero at the downstream boundary, where the sediment is reworked entirely by bank erosion. Since scenarios UNI-0.04 and UNI-0.1 produced similar widths, the banks were reworked more for UNI-0.04 than for UNI-0.1, which means that bank erosion is higher in UNI-0.04 scenario, during the complete evolution of the channel.

The experiments starting from a wider initial channel width (UNI-0.25 and UNI-0.4) have similar sediment reworking trends (Figure 25-c and d). During the first stage of development the upstream part of the channel is characterized by channel bed erosion, whereas the downstream part is characterized by the bed aggradation. Sediments reworking by bank erosion is only observed in a reach starting 1.5 m after the inlet of the flume. During the later stage of the development, the channel incision advanced further downstream. In scenario UNI-0.4, the sediment reworking was dominated by the channel bed incision along 80% of the channel length. In scenario UNI-0.25, instead, sediment reworking is dominated by channel bed erosion at the upstream half of the channel and by bank erosion at the downstream half of the channel.

Figure 25 shows the distribution of sediment reworked from channel banks and bed, for the experiments with constant flow and sediment supply. The distributions of reworked sediments are similar for the experiments starting with narrow initial channels (UNI-0.04* and UNI-0.1*). Sediment reworking is dominated by bank erosion along the entire length of the channel. Significant amounts of deposition are observed along most part of the flume (Figure 25-e and f).

In scenario UNI-0.25*(Figure 25-g), the reworked sediment involves both bank erosion and bed deposition. The volumes of sediment deposited are higher than the volumes of sediment originating from bank erosion, except near the downstream boundary of the channel. In the scenario UNI-0.4* (Figure 25-h) deposited sediment volumes are larger than the volume of sediment eroded from the banks near the upstream and the downstream boundaries. The volume of the sediment eroded from the banks are nearly equal to the volume of sediment deposited along the middle portion of the channel.

Sediment reworked during channel evolution of the experiments starting from 0.1m wide initial channel without sediment supply is presented in Figure 26. Sediment reworking in all of the scenarios were dominated by bank erosion during the early stage. Channel bed along the middle part of the flume aggraded. Scenario H3-0.1 had the most aggraded channel bed. Both bank erosion and bed incision contributed to the sediment reworking during the later stage of the development. Bank erosion had higher contribution compared to bed incision. Channel bed incised near the upstream boundary and magnitude of incision decreased moving towards the downstream boundary. Channel bed incision had the highest contribution to sediment reworking in scenario H3-0.1.

Sediment reworking trend in the variable discharge scenarios (H1-0.4, H2-0.4 and H3-0.4) were different from the constant flow scenario (UNI-0.4) in the experiments starting from 0.4 m wide initial channel without sediment supply (Figure 26). Bank erosion occurred along the entire length of the flume in variable discharge scenarios during the early stage of development. Banks did not erode in the first 1.5 m reach of the flume in the UNI-0.4 scenario. Bed aggradation was dominant along the most part of the flume in all of the scenarios. The volumes of sediment deposited were higher than the volumes of sediment eroded from the banks along the reach. Channel bed incision occurred along a short reach close to the upstream boundary. Bed incision progressed further downstream during the later stage of development.

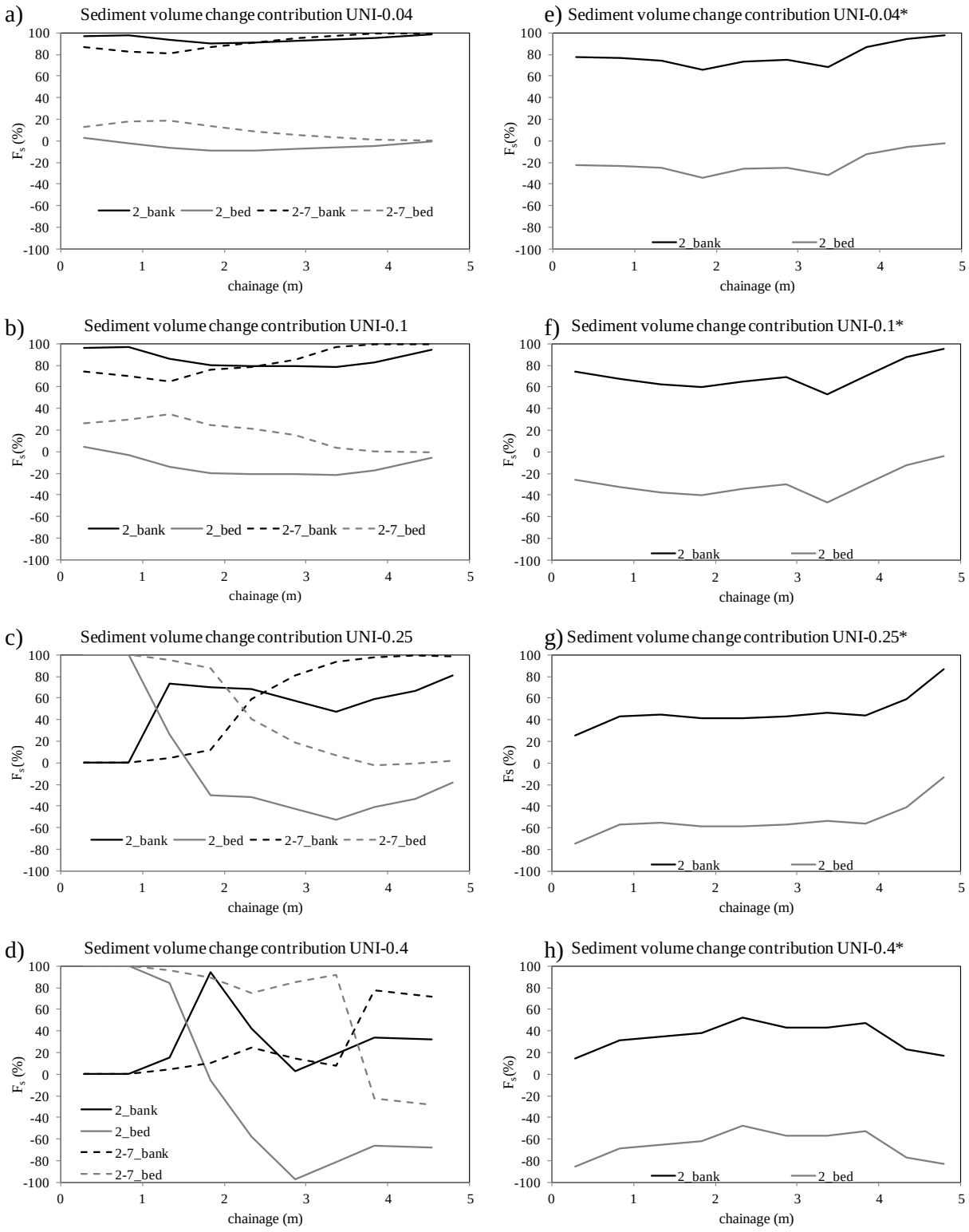

Figure 25. Distribution of sediment reworked from bank and bed along the length of the flume during the evolution of the channel between 0-2 hours and 2-7 hours for cases a) UNI-0.04, b) UNI-0.1, c) UNI-0.25, d) UNI-0.4, e) UNI-0.04*, f) UNI-0.1*, g) UNI-0.25* and h) UNI-0.4*.

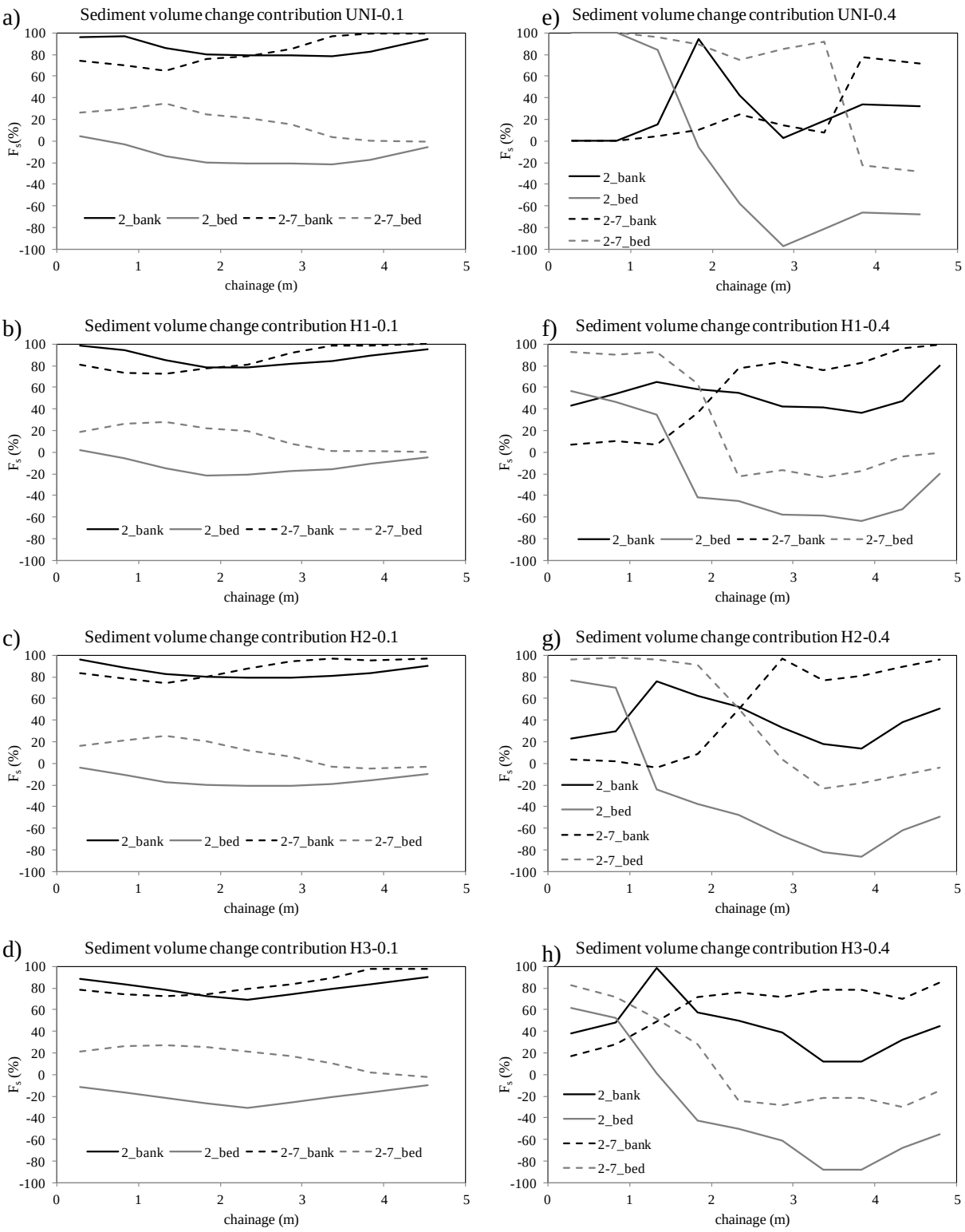

Figure 26. Distribution of sediment reworked from bank and bed along the length of the flume during the evolution of the channel between 0-2 hours and 2-7 hours for cases a) UNI-0.1, b) H1-0.1, c) H2-0.1, d) H3-0.1, e) UNI-0.4, f) H1-0.4, g) H2-0.4 and h) H3-0.4.

Bed incision occurred along first half followed by bed aggradation along the second half of the flume in the variable discharge scenarios. Incision occurred along most part of the flume in the constant-discharge scenario. Bank erosion was negligible along first 1.5 m part of the flume in H1-0.4 and H2-0.4 scenarios whereas banks eroded along the entire flume in H3-0.4 scenario. In constant flow

scenario bank erosion was negligible along most part of the flume except along the 1.5 m reach close to the downstream boundary.

The accuracy of simple sediment reworking model was assessed by comparing the equivalent weight of the estimated net volume of the reworked sediment by the model with the weight of sediment collected at the downstream end of the flume. The percentage of the difference between the estimated and observed net sediment weight was computed. The negative and the positive values denote the lower and higher prediction of the net sediment volume changes, respectively. Figure 27 shows the estimation error in different scenarios. The model performed well for the scenarios where sediment reworking occurred with higher net erosion. Highest errors were observed during the early stage development of the scenarios starting from 0.4 wide initial channels. The resolution of the cross-sections measurements were not fine enough to capture the observed small net change of sediment volume. Estimation error was less for H1-0.4 scenario because the bank erosion had higher contribution to sediment reworking along the entire length of the flume (Figure 26-f). The estimation significantly improved during the later stage of the development when the net change in sediment volume was higher. The model was capable to predict the net sediment reworking with reasonable accuracy despite using cross-section measured 0.5 m apart. The model performed well when channel evolution was dominated by bank erosion.

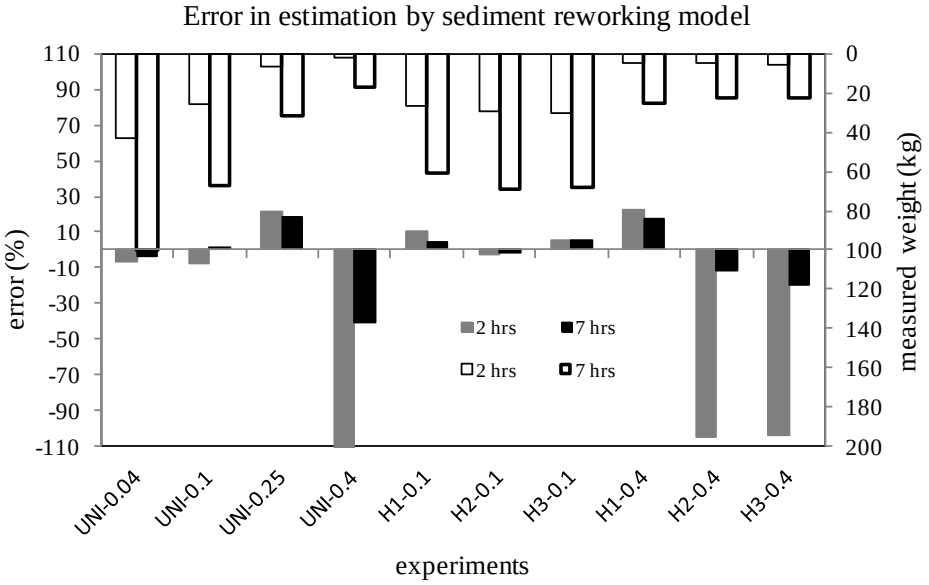

Figure 27. Error in the estimation of net sediment budget from the flume by simple sediment budget model. Filled histograms are the estimation error and void histograms are the weight of sediment measured at the downstream end of the flume.

3.3.4 Combined evolution of channel width and bed

Channel width and bed evolution are simultaneous and interact during channel formation. Channel aggradation and incision result in widening or narrowing. The measured cross-sections were compared to their initial configuration to analyze the change in width and bed level. Reach-averaged relative width change (ΔW) and relative bed-level change ($\Delta\eta$) were computed subtracting the evolved channel width and bed from initial width and bed, respectively. Plotting ΔW against $\Delta\eta$ allows analyzing the combined evolution of channel width and bed. The threshold lines of the width change ($\Delta W = 0$) and bed level change ($\Delta\eta = 0$) subdivide the plot in four parts (Figure 28). In anticlockwise direction, the upper right part represents widening and aggradation; the upper left part represents widening and incision; the lower left part represents narrowing and the incision; the lower

right part shows narrowing and aggradation. Due to the limited number of cross-sections measurements during the experiments, the combined evolution of channel width and channel bed can be analysed only for the conditions occurring after 2 hours and at the end of the experiments.

Figure 28 shows the relative changes in width and bed elevation of the channels with constant flow and without sediment supply. After 2 hours, the channels with a narrower initial width (UNI-0.04 and UNI-0.10) widened and aggraded. Widening increases the sediment influx into the channel and reduces the sediment transport capacity at the same time, causing bed aggradations [*Eaton and Millar*, 2004; *Langendoen and Alonso*, 2008]. Since rapid widening is observed in scenarios UNI-0.04 and UNI-0.1, these scenarios also have the most aggraded channels. Scenario UNI-0.25 also slightly widened (Figure 17-a) and slightly aggraded. Even though the width of the UNI-0.4 scenario has narrowed, the reach-average channel bed was still aggraded. This is because only the reach near the upstream boundary is incised, the major part of the channel is still aggraded (Figure 25-d) resulting the aggradation of the reach-average bed level.

Since sediment is not supplied in all the scenarios, the channel bed level is incised compared to the respective channel bed levels after 2 hours (Figure 28). Channel narrowing also occurs due to the formation of higher terraces within channel during the incision [*Thorne et al.*, 1998]. So, scenarios UNI-0.04, UNI-0.25 and UNI-04 resulted in narrower channels and only scenario UNI-0.1 resulted in wider channel compared to the respective channels after 2 hours. Even though bed incision is observed throughout the length of the channel during the evolution between 2 and 7 hours (Figure 25-a, b, c and d), the reach-averaged channel bed level is slightly aggraded. The channel bed level at the upstream part is incised whereas it is aggraded more downstream, thus counter balancing the reach average channel bed level. Thus, at the end experiments UNI-0.04 and UNI-0.1 resulted in wider and slightly aggraded channels and UNI-0.25 and UNI-0.4 resulted in narrower channel that is slightly aggraded.

Channels with sediment supply, all widened and aggraded after 2 hours (Figure 29). Channel bed aggradations leads to widening caused by an increase in the flow velocity due to steepening of bed (Ikeda, 1989) and flow deflection around bars [*Simon and Thorne*, 1996]. Thus the channel continued to widen and aggrade until the end of the experiments

Figure 30 shows relative change in width and bed level of the channels starting from 0.1 m initial width without sediment supply. All of the scenarios resulted in wider and aggraded channel after 2 hours. Scenario with the highest discharge intensity (H3-0.1) resulted in the widest and most aggraded channel. UNI-0.1 scenario resulted in the narrowest and the least aggraded channel. Since sediment was not supplied, channels incised but widened after 7 hours compared to the channels at 2 hours. Scenarios with higher discharge intensity: H3-0.1 and H2-0.1 resulted in channels with similar reach-averaged width and bed level. These scenarios also resulted in the widest and most aggraded channels. UNI-0.1 scenario resulted in the narrowest channel that was slightly aggraded.

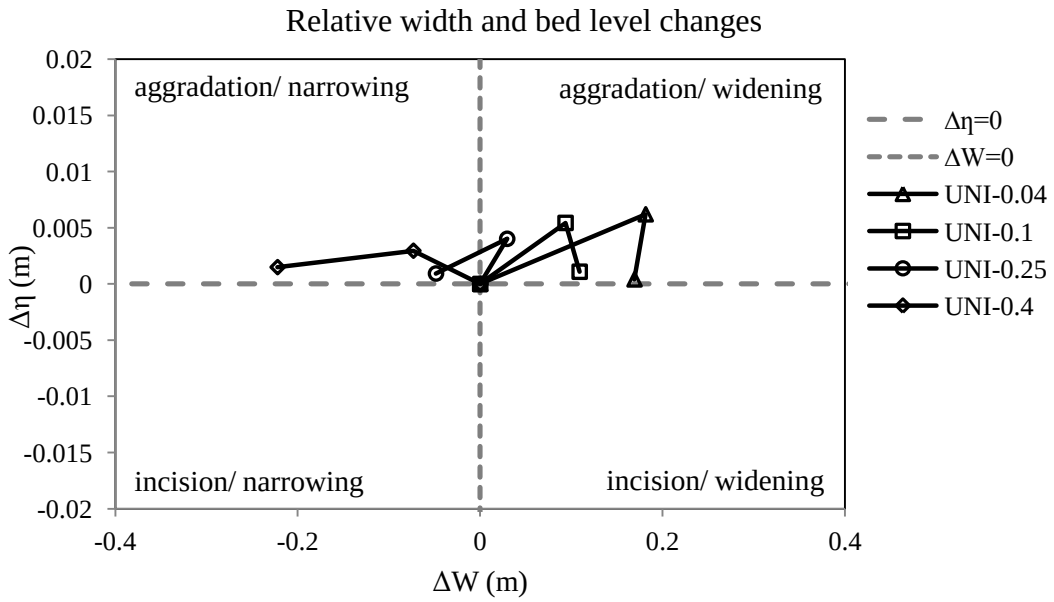

Figure 28. Relative channel-width and bed level changes in scenarios UNI-0.04, UNI-0.1, UNI-0.25 and UNI-0.4 after 2 hours (void symbols) and 7 hours (filled symbols) of the experiments.

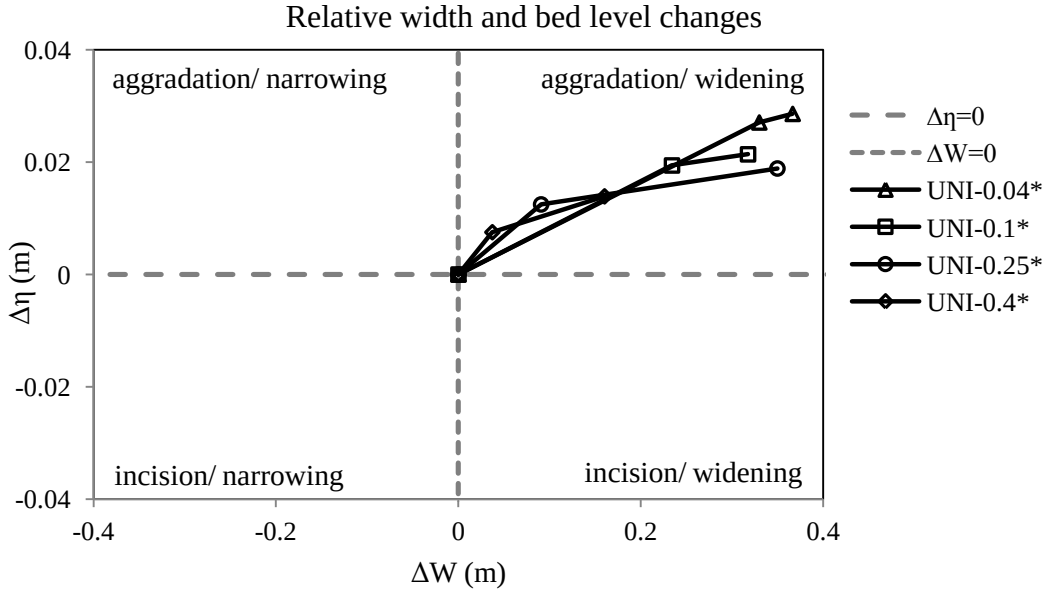

Figure 29. Relative channel-width and bed level changes in scenarios UNI-0.04*, UNI-0.1*, UNI-0.25* and UNI-0.4* after 2 hours (void symbols) and end of the experiments (filled symbols).

The experiments starting from 0.4 initial width without sediment supply resulted in narrower and aggraded channels after 2 hours (Figure 31). In the variable discharge scenarios (H1-0.4, H2-0.4 and H3-0.4) channel widths after 2 hours were measured during the low-stage discharge. So, narrowing of the channels is partly due to the shrinkage of the wetted perimeter during the low flow stages. After 7 hours, scenarios H3-0.4 and H1-0.4 resulted in wider and aggraded channels. H1-0.4 and H3-0.4 had similar low-stage discharge 0.3 l/s and 0.28 l/s, respectively. Scenarios UNI-0.4 and H2-0.4 resulted in narrower and slightly aggraded channels.

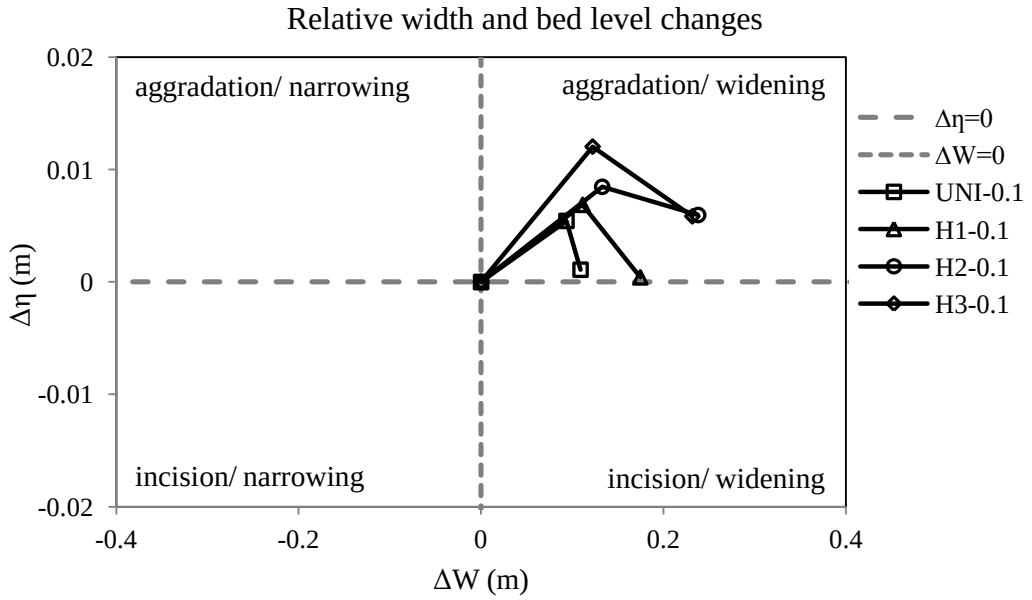

Figure 30. Relative channel-width and bed level changes in scenarios UNI-0.1, H1-0.1, H2-0.1 and H3-0.1 after 2 hours (void symbols) and 7 hours (filled symbols) of the experiments.

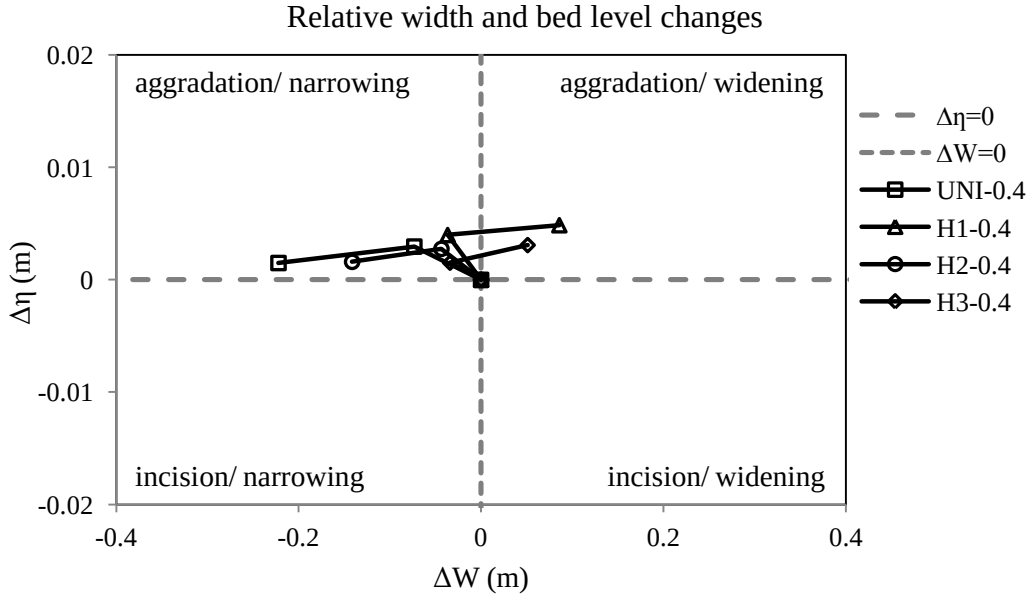

Figure 31. Relative channel-width and bed level changes in scenarios UNI-0.4, H1-0.4, H2-0.4 and H3-0.4 after 2 hours (void symbols) and 7 hours (filled symbols) of the experiments.

3.4 Summary of results

The objectives of this study are to understand the reach-averaged width and bed level evolution of bed-load dominated alluvial channels under different controlling factors. Controlling factors in this study refer to initial channel width, discharge regimes and sediment supply regimes. The results are interpreted to develop a general understanding on width evolution rather than reproducing characteristics of a specific bed-load dominated river. The results from the experimental investigations can be summarized as follows:

Effects of initial channel width

The long-term equilibrium channel widths were independent of the initial channel width in the experiments with constant flow and without sediment supply regimes. The experiments starting from narrower initial width widened and the experiments starting from wider initial width narrowed by bed incision all resulting in similar long-term equilibrium width. With the sediment supply at the upstream boundary, the experiments starting from narrower initial channel widths were terminated earlier because they aggraded and widened rapidly touching the fixed side walls of the flume. The scenarios starting from wider initial channel widths could evolve for longer period of time before approaching the side walls. They resulted in similar long-term channel width despite of the differences during the early stage of the development.

The long-term equilibrium channel widths were observed to be dependent on the initial channel width in variable discharge regimes. At similar variable regimes, the experiments starting from wider initial widths without sediment supply resulted in wider channels. The width evolution in channels with sediment supply could not be compared because the experiments starting from narrower initial channel had to be terminated before reaching an equilibrium condition.

Effects of flow regime

Channels evolved to different equilibrium widths under different flow regimes. Although all flow regimes conveyed same volume of water during the experiments, the variable discharges resulted in wider channels compared to constant flow. Flow regimes resulted in different channel widths depending upon the initial width of the channels. In the experiments starting from narrower initial channel width without sediment supply, regimes with the higher amplitude discharge variation resulted in similar channel width. Regime with the lower amplitude flow variations resulted in channel width similar to constant flow. Wider channels were obtained for the discharge regimes with higher amplitude of discharge variation. The experiments with sediment supply were not long enough to analyze the evolution trend.

In the experiments starting from wider initial channel width without sediment supply, regimes with similar low stage flow resulted in similar width. The regime with higher low-stage flow resulted in wider channels. The channel widened mostly during the high flow stage but low flow stage had an important role in reworking of the channel bed which also controlled the path of the bank erosion during successive high flows.

In the experiments with sediment supply, regime with higher amplitude discharge variation resulted in similar channel width compared to constant flow scenario. Bed scour was observed near the upstream boundary in these variable discharge scenarios which indicate less amount of sediment supplied compared to the sediment transport capacity of the channel at the upstream boundary. This might have caused less bed aggradation and widening of the channels. The variable discharge scenario where no upstream bed scour was observed resulted in wider channel than the constant flow.

Effects of sediment supply regime

Sediment supply from at the upstream boundary played a major role in the channel evolution. Experiments with sediment supply resulted in much wider channels compared to those without sediment supply. Channel predictors developed for gravel-bed rivers which were developed under the assumption of equilibrium conditions estimated widths that were closer to the constant flow experiments without sediment feed carried out in the framework of this study.

All experiments with sediment supply widened and aggraded rapidly resulting in braided channels. Most of the experiments were terminated earlier because they widened rapidly touching the sides of the flumes. So the long-term width evolutions could not be analysed in sediment supply scenarios. The trend of the measured sediment output rate from the flume correlated well with the observed width evolution when the channel was single thread. The correlation became weaker when multi-thread channels started to evolve.

4 ANALYTICAL MODELLING OF ALLUVIAL CHANNEL FORMATION

4.1 Introduction

A simple mechanistic semi-analytical model of *Tealdi et al.* [2011] (here after referred as TCR model) was used to investigate the width evolution trend of channel using laboratory experimental conditions. It is the only analytical model which can quantitatively predict the change in width and bed level/slope in response to change in sediment and discharge regime (non-equilibrium conditions). Data of laboratory experiments reported in Chapter-3 were used to calibrate the model. Due to many simplified assumptions, the model could be used to investigate evolution of the experimental channel starting from 10 cm initial width. Experiment UNI-0.1 was used to calibrate the model. The calibrated model was then used to investigate the width evolution in channels starting from different initial channel widths. The width evolution was also analysed in non-uniform flow scenarios with reference to laboratory experiments H1-0.1, H2-0.1 and H3-0.1. Objective of the use of analytical model was to physically explain the evolution trend of the width rather than to closely reproduce the experiments in detail.

4.2 Description of the model

TCR model is derived by solving a 1D moment conservation equation and sediment continuity equation integrated over a channel cross-section. A bed load transport predictor and linearized bed shear stress formulations are used as closure relations to obtain analytical solutions. A second order governing ordinary differential equation system in time is obtained which relates the temporal rate of change of bed level and of channel width with the temporal variability of the input flow and sediment discharges, the sediment transport relation used, the bank and sediment properties which is illustrated by equation (18) and (19). The model is derived assuming a trapezoidal cross-section (Figure 32).

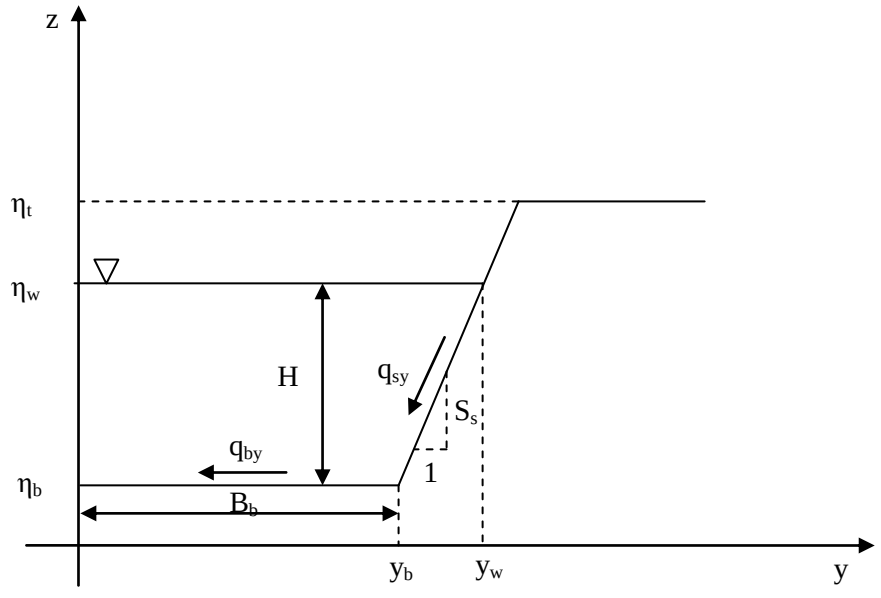

Figure 32. Trapezoidal section showing the notations used in Tealdi model.

$$(1-\lambda_p)\frac{d\bar{\eta}_b}{dt} = \frac{q_{bx,0} - q_{bx,Lx}}{L_x} + \frac{\hat{q}_{syb}}{\bar{B}_b} \qquad (18)$$

$$(1-\lambda_p)(\eta_t-\bar{\eta}_b)\frac{d\bar{B}_b}{dt}=\frac{\eta_t-\bar{\eta}_b}{S_sL_x}(q_{bx,0}-q_{bx,Lx})+\frac{H}{S_sL_x}(q_{sx,Lx}-q_{sx,0})+\left(1+\frac{\eta_t-\bar{\eta}_b}{S_sB_b}\right)\hat{q}_{syb} \quad (19)$$

Where, $\bar{\eta}_b$ is the reach averaged bed level of the channel, m; η_t is the top level of the channel, m; L_x is the length of the reach, m; B_b is the bottom width of the channel, m; S_s is the side slope of the channel; H is the water depth, m; q_{bx} sediment transport rate in bed along longitudinal directions obtained using Wong and Parker formulations (equation (20)), $m^3/s/m$; qsx is the sediment transport rate in side slopes along longitudinal direction obtained using Wong and Parker formulations (equation (21)) $m^3/s/m$; $\hat{q}_{syb}$ is the sediment transport rate in the side slope integrated between y_w and y_b computed using equation (22), $m^3/s/m$.

$$q_{bx}=4.93D_s\sqrt{\Delta gD_s}\left(\theta_b-0.047\right)^{1.6} \quad (20)$$

$$q_{sx}=4.93D_s\sqrt{\Delta gD}\left(\theta_s-0.047\right)^{1.6} \quad (21)$$

$$q_{sy}=4.93D\sqrt{\Delta gD}\left(\theta_s-0.047\right)^{1.6}\left(\frac{V_t}{U}-\frac{r}{\sqrt{\theta_s}}S_s\right) \quad (22)$$

$$\theta_b=\frac{Q_w^2S_s^2\left[\frac{H\left(1-\frac{H}{2B_b}\right)}{k_s}\right]^{-2n_r}}{D_sgH^2\Delta\alpha_r^2(2B_bS_s+H)^2} \quad (23)$$

$$\theta_s=\frac{HS_0\left[30S_s^2\log\left(\frac{H}{k_s}\right)+469S_s^2+312\right]^2}{219024D_s\Delta\left(S_s^2+1\right)^2} \quad (24)$$

Where, θ_b and θ_s are shields stress in channel bed and side slopes, respectively; D_s is the sediment diameter, m; Q_w is the discharge, m^3/s; g is the acceleration due to gravity, m/s2; V_t is the transversal mean velocity along side walls, m/s; U is the mean flow velocity in the cross-section, m/s; r is the coefficient weighing the sediment transport in side slopes in the transverse direction; $k_s=n_kD_{90}$ is the roughness height, m, nk is the coefficient, D90 is the 90th percentile sediment diameter, m; n_r and α_r are the exponents and exponents in the formulation of dimensional roughness coefficient $C_f=\alpha_r(\frac{R_b}{k_s})^{n_r}$. Formulation of θ_b and θ_s illustrated in equation (23) and equation (24) respectively are obtained after linearising the formulation of shear stress in channel bed and banks.

4.3 Choice of parameters

To compute the channel evolution following physical parameters were prescribed in the model during the calibration:

Table 6. Values of parameters used in the analytical model.

Parameters	Value	Remark
Geometrical parameters		
Bb	0.05	Half initial channel bottom width
Ss:1	1.2	Side slope of the banks (Vertical:Horizontal)
Sb	0.01	Longitudinal bed slope of the channel
Ht	0.04 (m)	Top level of the channel
Hydraulic parameters		
nk	2.50	Coefficient weighing roughness height
αr	8.50	Coefficient weighing dimensionless friction factor
nr	0.167	Exponent of dimensionless friction factor
Sediment parameters		
D_{90}	1.48 (mm)	90^{th} percentile of grain size distribution
D_{50}	1 (mm)	Median grain size diameter
Θcr	0.047	Critical shields stress in bed load formula
Δ	1.65	Relative density of sediment
r	0.1	Coefficient weighing the lateral sediment transport on banks
λp	0.4	Porosity of the bed
Discharge		
Qw	0.4 (l/s)	Uniform flow (calibration case)

Values of hydraulic and sediment parameters required in the model were not directly measured in the experiments. The values used in the model were varied within the range reported in the literature to obtain the results closest to experimental observations. The combination of parameters listed in Table 6 resulted in width evolution trend reasonably close to that observed in the experiment UNI-0.1. Values of the parameters were increased and decreased each at a time (keeping others constant) to assess the sensitivity in the results. The sensitivity analysis was carried out for n_k, α_r and r by increasing and their values by 10%. The calibrated model was then used to analyze the effects of initial channel widths and non-uniform discharge on the width evolution of the channel.

4.4 Results

Sensitivity analysis

Figure 33 shows the width evolution in scenarios with different values of α_r. The values α_r equal to 8.50 was chosen for the model setup. Width evolution in the model was sensitive to the value of α_r. Higher value of α_r resulted in narrower channels. Higher values of α_r resulted in higher channel roughness which decreases the flow velocity. Decrease in flow velocity decreases the bed shear stress which reduces the sediment transport capacity thus resulting in narrower channels. Channels became wider with the smaller values of α_r. Smaller values of α_r resulted in lower channel roughness which increases the flow velocity. Increase in flow velocity increases the bed shear stress which increases the sediment transport capacity thus resulting in wider channels.

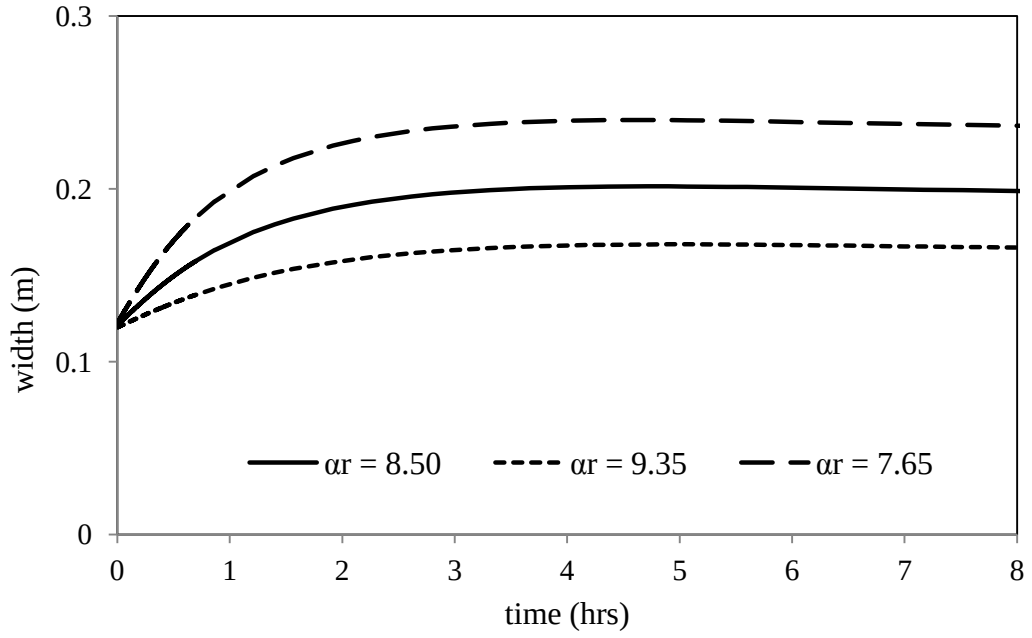

Figure 33. Channel width evolution with values of α_r= 8.50, 9.35 and 7.65.

The sensitivity of the model to the values of parameter "r" are presented in Figure 35. Since the parameter r controls the sediment transport rate along the bank slopes, the model results were sensitive to the choice. Increasing the value of "r" resulted in the widening of the channel because more sediment was transport along the side slope towards channel bed. The value of r equal to 0.1 was used in the model setup.

Figure 34 shows the width evolution with different values of n_k. The values n_k equal to 2.50 was chosen for the model setup. Width evolution in the model was less sensitive to the value of n_k. The values of n_k between 2.25 to 2.75 resulted in similar channel widths.

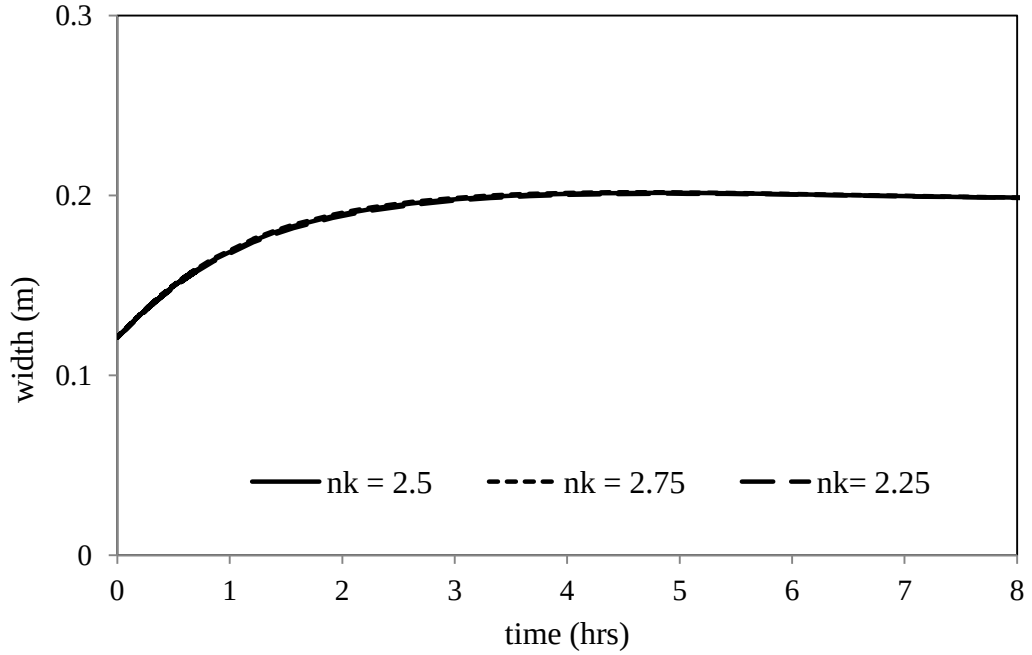

Figure 34. Channel width evolution with values of n_k= 2.5, 2.75 and 2.25.

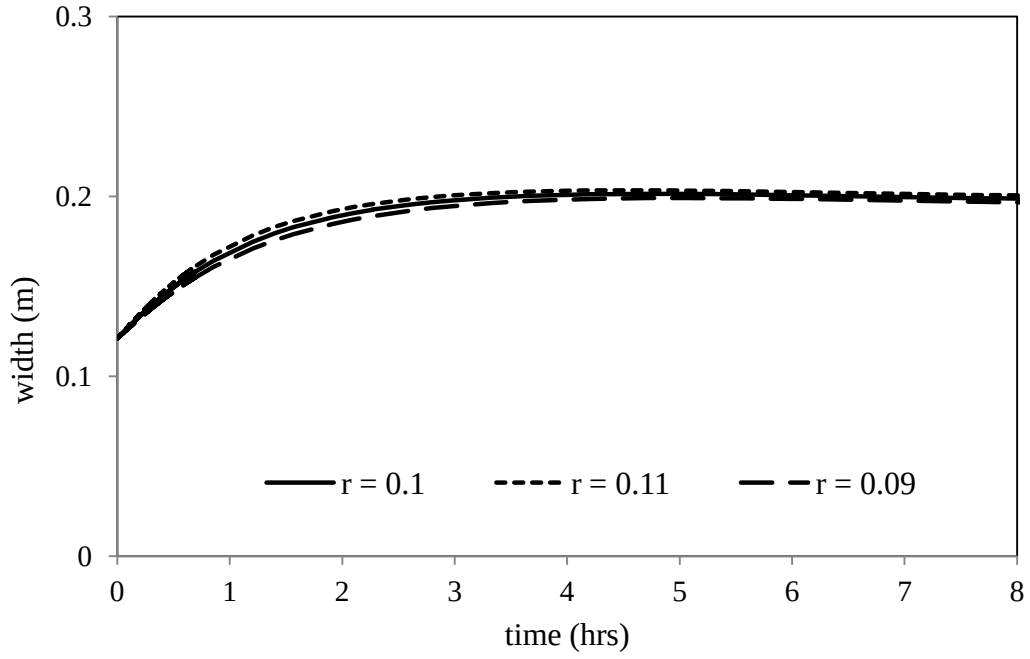

Figure 35. Channel width evolution with values of r = 0.1, 0.11 and 0.09.

Uniform flow

Despite several simplifications, Tealdi model was able to compute the width evolution of a channel reasonably close to those observed in the experiments UNI-0.1 (Figure 36) using the values of the parameters listed in Table 6. Channel width evolution trend was computed for the scenarios starting from different initial channel widths. The scenario starting from narrowest initial channel (0.09 m) resulted in the widest channel whereas the channel starting from the widest initial channel (0.11 m) resulted in the narrowest channel.

Non-uniform flow

Channel width evolution computed by Tealdi model in non-uniform flow scenarios, using conditions of laboratory experiments H1-0.1, H2-0.1 and H3-0.1, were analyzed. Channel widths were computed for non-uniform flow regime (Mod) and for uniform flow regimes using discharge at high flow stage (Mod_high), low flow stage (Mod_low) and average discharge (Mod_uni). Width evolution computed by Tealdi model using the experimental conditions of H1-0.1 is presented in Figure 37. The width evolution trend computed by Tealdi model in non-uniform flow scenario is similar to that observed in the experiment. Channel widened rapidly during early development stage and widening rate decreased with the progress in channel evolution. Channel widening occurred during the high flow stage. The low-stage discharge did not contribute to the channel widening. Equilibrium channel width was achieved after long-term development. The width computed by Tealdi model was higher than channel width in the experiments during the intermediate stage development. The computation made for uniform flow using higher-stage discharge resulted in similar width to that of non-uniform flow after long-term development. Channel width during the intermediate development stage was higher for the uniform flow. This is because the Channel widening did not occur during the low-stage discharge of non-uniform flow scenario, thus lowering the rate of channel widening. Computations carried out at

uniform discharge regime using average discharge (Mod_uni) and low-stage discharge resulted in narrower channels.

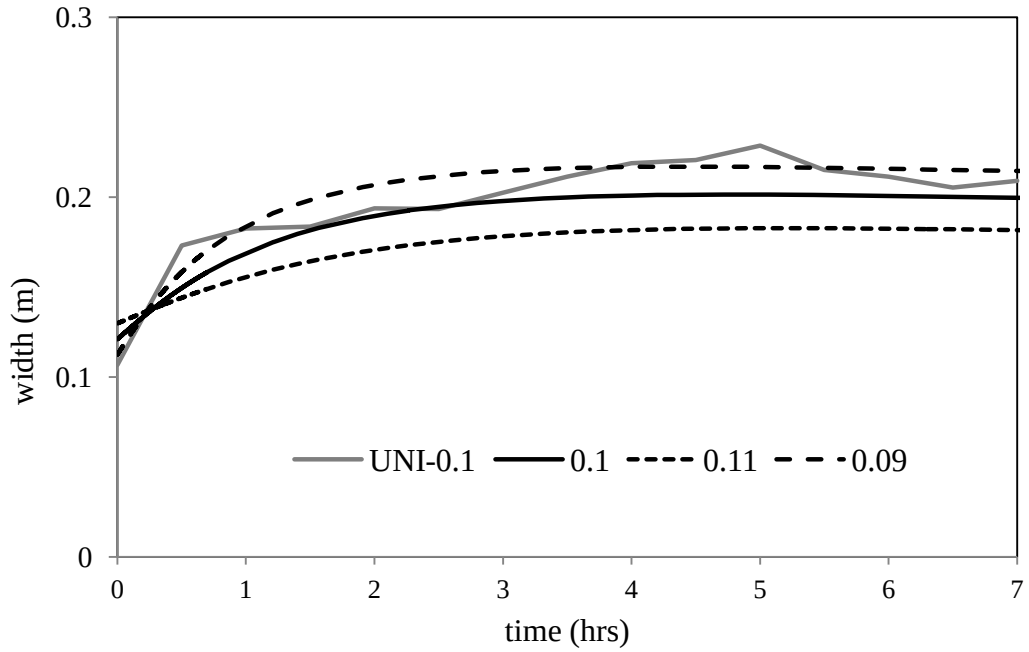

Figure 36. Channel width evolution in scenarios starting from initial channel width 0.1 m, 0.11 m and 0.09 m compared with the experiment UNI-0.1.

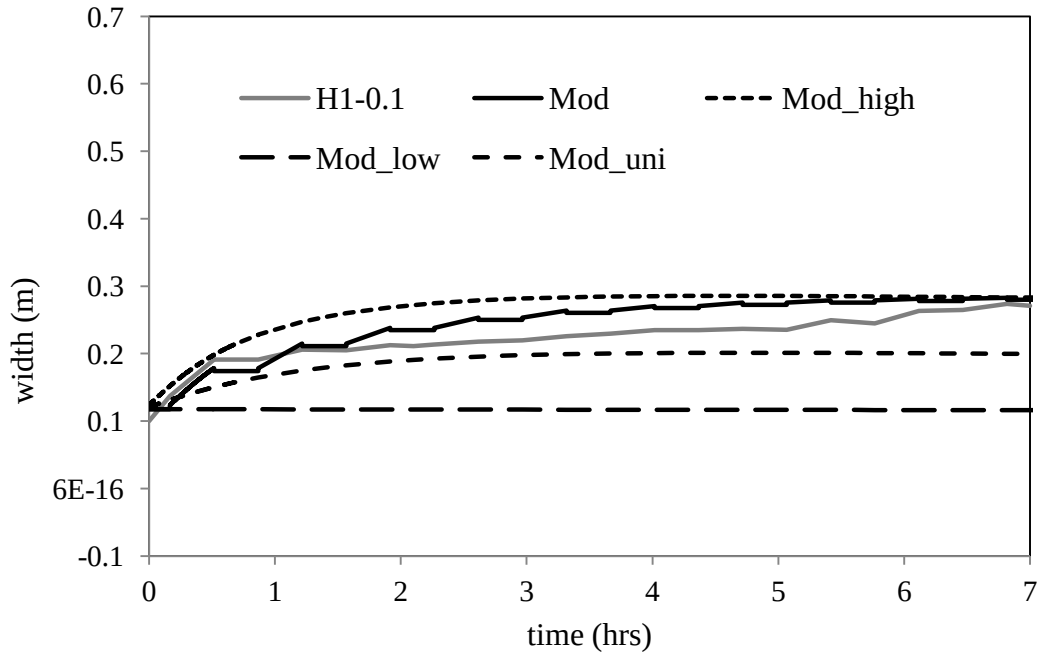

Figure 37. Channel width evolution in the model for the experimental scenario of H1-0.1 (Mod), with high flow stage discharge (Mod_high), low flow stage discharge (Mod_low) and average discharge (Mod_uni).

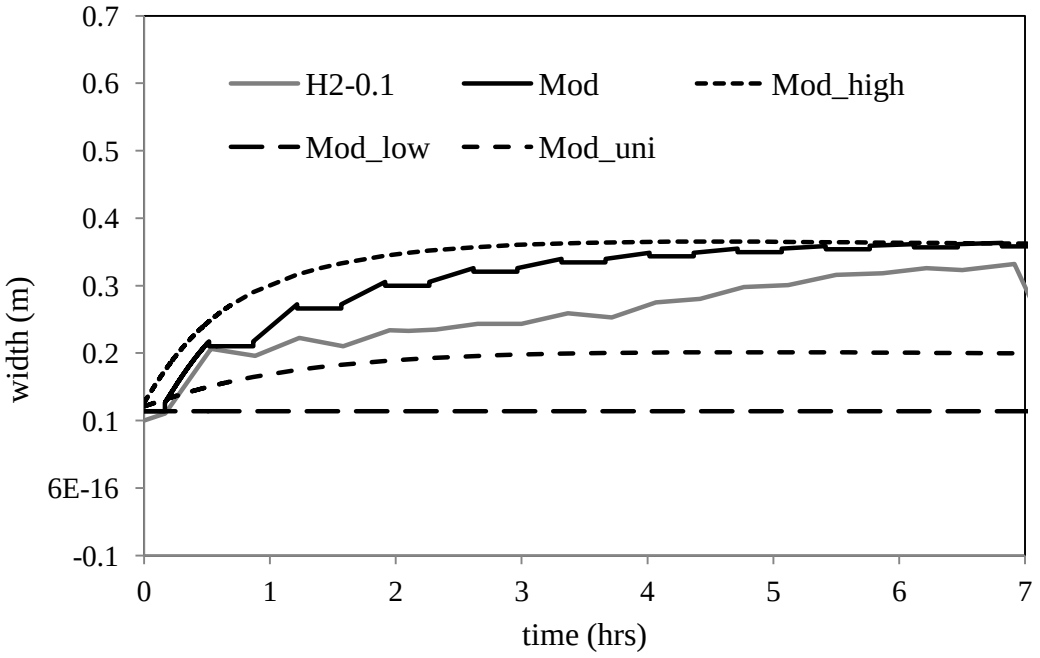

Figure 38. Channel width evolution in the model for the experimental scenario of H2-0.1 (Mod), with constant high flow stage discharge (Mod_high), low flow stage discharge (Mod_low) and average discharge (Mod_uni).

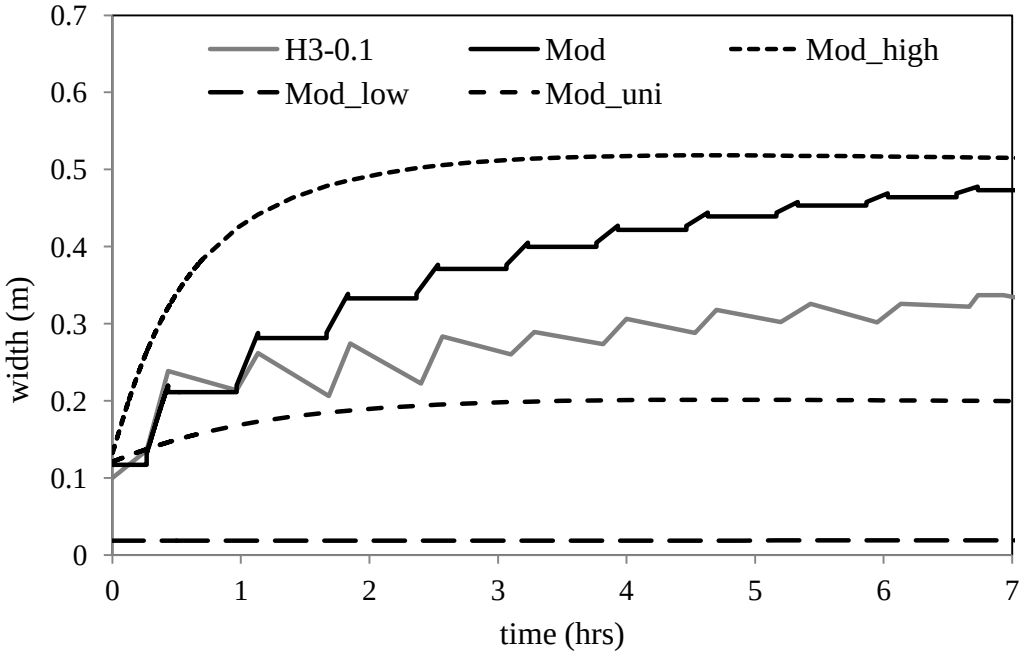

Figure 39. Channel width evolution in the model for the experimental scenario of H2-0.1 (Mod), with high flow stage discharge (Mod_high), low flow stage discharge (Mod_low) and average discharge (Mod_uni).

Figure 38 shows the width evolution computed by Tealdi model for the experimental conditions of H2-0.1. In the non-uniform flow scenario the width evolution trend computed by the model is similar to that in the experiment. The channel computed by the model (Mod) was wider compared to the experiment. The computations at uniform flow using high stage discharge (Mod_high) resulted in the

long-term equilibrium width similar to the non-uniform flow. Channel widths computed at uniform flows using average (Mod_uni) and low stage discharge (Mod_low) were smaller.

Figure 39 shows the width computed by Tealdi model using the experimental conditions of H3-0.1. The width in non uniform flow scenario during the early stage of the development was similar to the experiment. The computed channel was significantly wider at the later stage of the development. The computation carried out at uniform flow using high stage discharge (Mod_high) was similar to the non-uniform flow scenario after long-term development. The uniform flow using average (Mod_uni) and low stage discharge (Mod_low) resulted in narrower channels.

4.5 Summary of the results

The effects of controlling factors: Initial channel width and discharge were investigated using analytical model. The channel evolution was computed using the experimental data. The results from the investigations can be summarized in the following sections.

Effects of initial channel width

The long-term evolution of channel width in scenarios with uniform flow without sediment supply is affected by the initial channel width. Evolution of channels starting from narrower initial channels resulted in wider channels.

Effects of discharge regimes

The long-term width evolution is different for different discharge regimes. Channels evolving with higher amplitude discharge variations result in wider and more aggraded channels. Channel widening occurred mostly during the higher flow stage. The long-term equilibrium width of channels evolving in non-uniform flow scenarios could be predicted using high-stage discharge as uniform flow regime.

5 NUMERICAL MODELLING OF ALLUVIAL CHANNEL FORMATION

5.1 Introduction

This chapter presents results of the investigations on the effects of controlling factors on the alluvial channel formation carried out using numerical. The objectives of numerical modelling were to investigate the role of initial channel width, discharge and sediment supply regimes on the long-term width and bed evolution of bedload dominated channels. Numerical modelling allowed investigating channel evolution in a longer domain and for longer period of time which were not feasible due to smaller facility in the laboratory experiments presented in Chapter 3. It also allowed better understanding of variability of morphodynamic phenomena in both space and time which were difficult to quantify in experiments due to the difficulty in measurements, like flow characteristics and depth, at small scales. Numerical modelling allowed explanation of certain experimental observations on channel evolution based on established laws of physics (flow, sediment transport, bank erosion).

5.2 Numerical modelling

A two dimensional physics-based fully non-linear numerical model (Delft3D) was used to investigate the effects of different controlling factors on channel evolution of a field scale gravel-bed river with (River Severn). Data of the experiments on channel evolution carried out in this study (Chapter 3) were not used because the experimental channels evolved very fast due to rapid widening which caused the instability in the model. Standing surface waves were also observed during the channel evolutions which indicate the occurrence of super-critical flow. The model used is more accurate to study the morphological phenomena at sub-critical flows. Choice of the field scale study allowed having slower evolution of the channel (width and bed) in the model avoiding sudden changes causing model instabilities. The flow characteristics used in the model were similar to those in the experiments at the start up condition.

5.2.1 Model description

Delft3D (open source version - 3.28.50.01) was used for the investigation. Delft3D is a fully nonlinear numerical model that solves the unsteady shallow-water equations with hydrostatic approximation in two dimensions. The bed evolution is modelled by solving sediment transport equations and Exner's sediment balance equations [*Lesser et al.*, 2004]. Channel bed evolutions occur at much slower time scale compared to flow time scale which immediately adapts to the changes in the channel bed. To reduce the computational cost during long-term simulations, the bed development were accelerated by using a coefficient, Morphological Acceleration Factor (MF), to multiply the bed level updates after each flow time-step [*Lesser et al.*, 2004].

A heuristic bank erosion numerical scheme based upon angle of repose, defining critical-failure slope, is implemented which allows to simulated channel widening phenomena. Bank erosion occurs when the lateral slope of the banks exceed the angle of repose. Evolution of channel with erodible banks have been simulated using similar bank erosion scheme by *Jang and Shimizu* [2005]. Detail features of flow model and morphological model in Delft3D are presented in Appendix B.

5.2.2 Model setup

Twelve numerical runs have been performed, according to the conditions summarized in Table 4. The runs differ in discharges and sediment supply regimes, and sediment sizes. The details of the numerical simulation settings are provided in the sections below.

Choice of model river

River Severn was chosen for the model setup because of its data availability and its size which allowed studying its channel evolution at a reasonable amount of computational time. Topographic, flow and sediment characteristics of a 2km meandering reach of the River Severn near Fron (Figure 40), about 2 km downstream of Abermule was used to setup the model. The selected reach of River Severn is single-thread with an average width of 30 m and longitudinal slope of 0.14%. A 2m resolution Lidar topographic data made available by UK Environmental Agency was used to compute the longitudinal slope. The cross-section measured in 1990 was used to calculate the average width of the river. Mean annual flood of the river was computed as 217 m3/s using annual peak flow data monitored at Abermule gauging station between 1962 and 2013. Median grain size sediment diameter (D50) in river bed of the reach near Abermule is 40 mm [*Couperthwaite*, 1997].

Figure 40. Reach of River Severn near Fron showing locations of measured cross-sections (Source: Google Earth).

Model domain and grid size

Two different model domains with rectangular shape were used to simulate channel evolution (Figure 41). The first domain (SD) was 1000 m long and 120 m wide including flood plains. The second domain (LD) was 2000 m long and 300 m wide. Both domains were discretized using rectangular grid cells 1 m long in lateral direction and 5 m long in longitudinal directions. The lateral dimensions of the grids were chosen based upon the sensitivity analysis.

Smaller dimension of grids along lateral directions allowed representing bank slopes higher than the critical value required for bank erosion, thus allowing continuous width evolution in the model. A 5 m deep initial channel with trapezoidal cross-section of desired width and longitudinal slope of 0.0014 was provided at the centre of the domain. Model domains and width of the initial channels used in different scenarios are presented in Table 4. Computational time step was chosen as 0.3 seconds which ensured the stability in the model.

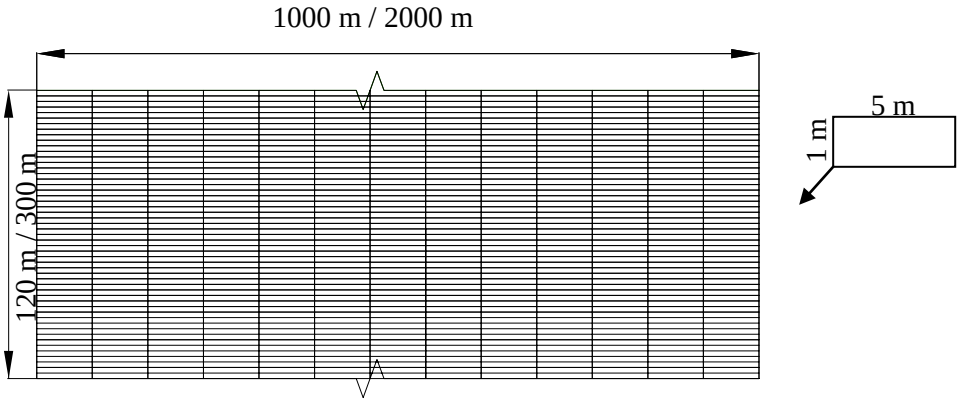

Figure 41. Computational domain used in the model setup showing details of the grid cells.

Hydrodynamics

Channel bed roughness and turbulence diffusion coefficient were prescribed to model the flow field. Chezy's roughness coefficient based upon Colebrook and White roughness formulation was used in the model (equation (25)).

$$C = 18\log\left(\frac{12h}{k_s}\right) \qquad (25)$$

Where, C is the Chezy's roughness, $m^{1/2}/s$; h is the water depth, m; $k_s \approx 6.8\ D_{50}$ is the roughness height, m, computed using formulation suggested by *Julien* [2002]; D_{50} is the median sediment diameter, m. The roughness formulation is water depth dependent representing shallower parts rougher than the deeper parts. Turbulence diffusion is modeled using eddy viscosity coefficient. The value depends upon grid size and flow characteristics. The value of 0.1 m^2/s was chosen based upon the values reported in the hydrodynamic modelling studies carried out in the field scale rivers [*Williams et al.*, 2013].

Boundary conditions

The effects of different discharge and sediment supply regime on the channel evolution were explored. Different discharge and sediment regimes were prescribed along the initial channel cross-section at the upstream boundary. Discharge regimes used in the model for different scenarios are presented in Figure 42 and Table 4. In sediment supply scenarios the sediment transport rate capacity of the flow at upstream boundary was supplied. A constant water level corresponding to normal depth of the discharge imposed at the upstream boundary, computed using the initial channel (width) configuration, was prescribed at the downstream boundary.

Sediment transport and morphodynamic

Sediment transport rate in the model was computed using *Wong and Parker* [2006] formulation (equation (26)).

$$q_s = 4.93\sqrt{\Delta g D_s^3}\,(\theta - 0.047)^{1.6} \qquad (26)$$

Where, q_s is the sediment transport rate, $m^3/s/m$; $\Delta = (\rho_s - \rho)/\rho$ is the relative sediment density in which ρ_s is the density of sediment and ρ is the density of water, kg/m^3; D_s is the sediment diameter, m; g is the acceleration due to gravity, m/s^2; $\theta = u^2/(C^2 \Delta D_s)$ is the Shields stress, u is the depth-averaged velocity (m/s), C is the Chezy's roughness coefficient ($m^{1/2}/s$).

Sediment transport rate in the channel was very low when sediment diameter of 40 mm, corresponding to the mean sediment diameter of the river bed, was used. Channel widening was very small due to low sediment mobility. So the sediment diameter was reduced to increase widening rate in the model. Sediment diameter of 30 mm and 10 mm were used in different scenarios (Table 4).

The transverse-bed slope effect on the direction of bed-load transport is modelled using *Ikeda* [1982] formulation modified by *van Rijn* [1993], which is presented in equation (27).

$$q_{s,n} = q_s \alpha_{bn} \sqrt{\frac{\theta_{cr}}{\theta}} \frac{\partial z}{\partial y} \qquad (27)$$

Where, $q_{s,n}$ is the bed load transport on lateral direction (m3/s/m); α_{bn} is the calibration parameter; θ_{cr} is the critical Shield's stress; θ is the Shield's stress and $\partial z/\partial y$ is the transverse bed slope. Bed topography in the model is sensitive to the transverse bed slope effects on the direction of bed load transport [*Nicholas et al.*, 2013; *Schuurman et al.*, 2013]. *Nicholas et al.* [2013] argue that the general evolution trend of the channel bed is less affected by the value of the parameter. α_{bn} equal 1.5 (default value in the model) was used in the model setup.

To accelerate the bed evolution in long-term simulations, Morphological Acceleration Factor (MF) equal to 10 was used in the model setup which was chosen based on the sensitivity analysis.

Bank erosion

A bank erosion numerical scheme based on angle of repose is used in the model setup. Angle of repose is the limiting lateral slope, above which bank failure occurs. The formulation focuses to compute the slope along each side of a computational cell. Bank erosion occurs if the slope along any of the sides exceeds the angle of repose. The new slope value after bank failure is set equal to the angle of repose. The volume of eroded sediment previously stored in the bank and representing the excess bank volume when compared to the angle of repose, was computed and multiplied by the Morphological-Acceleration-Factor (MF) value to obtain the total volume of sediment associated with bank failure. The total volume of failed sediments was then moved to the adjoining cell in the downstream direction of the slope [*personal communication with Richard Measures, NIWA]*.

The angle of repose is generally assumed equal to the frictional angle of the sediment. *Li and Millar* [2011] report the value of 40° for loose gravel banks. In numerical models, bank erosion is controlled by the value of angle of repose and size of grid cells. Angle of repose equal to 35.6° was implemented in the model which in combination with 1m grid cells allowed continuous widening of channel. The choice was based on the results of the sensitivity analysis, which is described in detail in the following section.

5.2.3 Sensitivity analysis

Sensitivity analyses were performed to assess the effects of MF, grid size and angle of repose on the channel evolution. The effects were analyzed in terms of channel width evolution. A model with smaller domain was setup to perform simulations at less computational time.

5.2.4 Analysis of model simulation outcomes

Evolution of the channel was analysed along the reach within the centre area of domain (half of the total domain) at 15 hours (0.625 days) interval. One fourth of the domain each close to the upstream and the downstream boundaries were excluded to minimize the boundary effects on channel

evolution. The effects of controlling factors on the channel evolution were assessed by analysing evolutions of channel width, bed level, water depth and sediment transport rate.

Channel width
Channel width has been computed as the width of the wetted part of the channel in a cross-section. Widths were computed in channel cross-sections 5m apart. Computed widths were then averaged along the reach to obtain a reach averaged channel width. Channel width change was computed by subtracting the initial channel width from the reach averaged channel width at any examined time step.

Bed level
Channel bed has to be distinguished from its banks to compute the changes in the bed level. The criteria explained in Chapter 3(section 3.2.3) were used to distinguish between the bed and banks. The point with the highest change of the transverse slope along both banks was used as thresholds to define channel bed and banks. The part of the cross-section between these points in opposite banks was considered as the bed and the rest as banks. The average level of the evolved channel bed was computed and subtracted from the initial bed level to obtain the average bed level change in a cross-section. The average bed level changes in the cross-sections were then averaged along the reach to obtain the reach averaged bed level changes. The reach average bed level changes were also plotted against the reach averaged change in width to obtain the combined evolution of channel width and bed level.

Water depth
Water depth in a cross-section was defined as the difference between water surface level and average bed level, the water surface being almost horizontal along the transverse direction. Water depths in cross-sections were averaged along the reach to obtain the reach averaged water depth.

Sediment transport rate
The evolution of total sediment transport rate through a cross-section, at the end of the $3/4^{th}$ of the computational domain, was analysed. The chosen cross-section was the downstream end of the domain used to analyze the channel evolution.

5.2.5 Model scenarios

The summary of experimental conditions of the explored scenarios is presented in Table 4. Initial channel width, discharge and sediment supply regime, and sediment sizes were varied among the scenarios. Bed width of initial channels were varied as 20 m (W0), 10 m (W1) and 40 m (W2) to study the effects of initial channel width on the channel evolution. Sediment size were varied as 30 mm (P) and 10 mm (S) to study the evolution of channel with higher and lower sediment mobility.

Uniform and non-uniform idealized hydrographs (H1 and H2) were used to investigate the effects of flow magnitude and of flow unsteadiness on the channel evolution. In the uniform-flow runs, a constant discharge of 217 m3/s was used which corresponds to the mean annual flood of River Severn. Hydrographs H1 and H2 were designed to explore the effects of the amplitude of non-uniform flow regime keeping the same duration of high and low flow stages (Figure 42). Both hydrographs during each cycle convey an equal total volume of water to the constant flow, under the same duration. Hydrograph H1 had low and high discharge of 163 m3/s and 271 m3/s (+/- 25% of uniform flow), respectively. Hydrograph H2 had low and high discharge of 108 m^3/s and 325 m^3/s (+/- 50% of uniform flow), respectively. Both high and low discharges had duration of 3.75 days. Scenarios were

explored without upstream supply of sediments and with upstream supply of sediments (*) to investigate the effects of sediment supply regime on channel evolution.

Table 7. List of modelled scenarios and related hydraulic, sediment and geometric characteristics.

Simulations	Bed Width	Low flow (Non-uniform runs)		Constant flow (Uniform runs)	High flow (Non-uniform runs)		Ds	Sediment feed	Domain*
	(m)	Q (m3/s)	T (days)	Q (m3/s)	Q (m3/s)	T (days)	(mm)		
P-W0	20	-	-	217			30	No	SD
P-W1	10			217			30	No	SD
P-W2	40			217			30	No	SD
P-W0*	20			217			30	Yes	SD
P-W1*	10			217			30	Yes	SD
P-W2*	40			217			30	Yes	SD
H1-W0*	20	271	3.75		163	3.75	30	Yes	LD
H2-W0*	10	325	3.75		108	3.75	30	Yes	LD
H2-W2*	40	325	3.75		108	3.75	30	Yes	LD
S-W0	20			217			10	No	LD
S-W1	10			217			10	No	LD
S-W2	40			217			10	No	LD
S-W0*	20			217			10	Yes	LD
S-W1*	10			217			10	Yes	LD
S-W2*	40			217			10	Yes	LD

*SD = Short domain, LD = Long domain

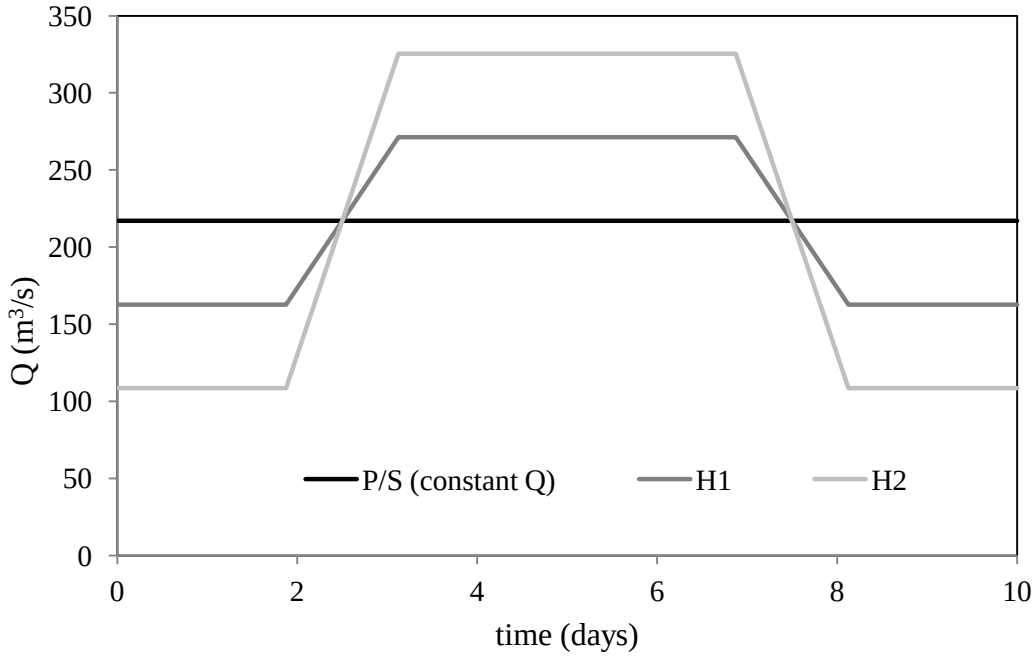

Figure 42. An illustration of the shape of the different flow hydrographs used for the numerical simulations

5.2.6 Results

Sensitivity analysis

Width evolution of the channel in the scenarios without morfac (MF ==1) and MF equal to 10 are presented in Figure 43. The simulations with MF equal to 10 resulted in a slightly narrower channel compared to the scenario without MF. The trends of width evolution in both scenarios are similar. This suggested that the value of MF equal to 10 was a reasonable choice for the modelling study on channel evolution allowing a reasonable computational cost.

Figure 44 shows the width evolution of channels with 1m, 2m and 5m wide grid cells. Simulations in all scenarios were carried out with an angle of repose equal to 26.5°. Scenario with the smallest grid cells (Δy = 1 m) showed a rather consistent trend in the width evolution. Scenarios with larger grids had stages where the bank erosion stopped during the width evolution. The channel width in the widest grid (Δy = 5 m) scenario was constant after a brief stage occurring at the beginning of channel evolution. The scenario with 2m wide grid cells continued to widen with some intermediate stages without bank erosion. The reason behind such difference is that wider grid cells could not represent slopes steeper than the critical slope required for bank erosion. So, higher volume of the sediment had to be eroded from the channel bed, closer to the banks, to steepen the bank slopes for initiating bank erosion. In the scenarios with wider grid cells, the areas close to the banks were represented by few cells. Since topography variations of channel bed close to the banks cannot be properly represented by coarse grid cells, the flow field was modelled less accurately The banks stopped to widen in the coarsest grid case because the flow near the bank was not able to erode sediments from the near bank bed cells to cause bank erosion.

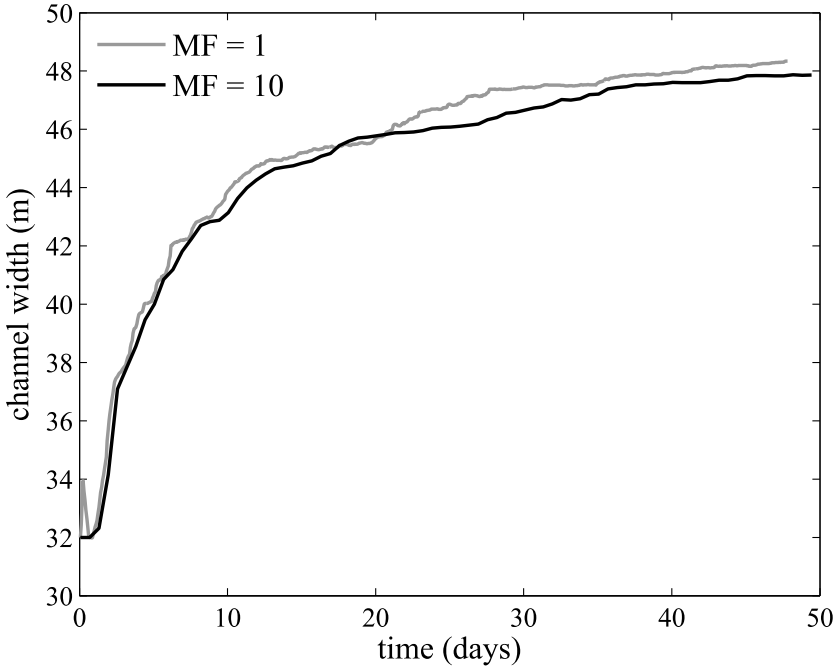

Figure 43. Effect of the Morphological-Acceleration-Factor coefficient on channel evolution. Channel width evolution in scenarios without Morphological-Acceleration-Factor (MF=1) and with MF equal to 10.

Width evolution of the channel in scenarios with angle of repose equal to 26.5°, 40° and 60° are presented in Figure 45. Simulations in all the scenarios were carried out with 1 m wide grid cells. Wider channels were obtained for smaller angle of repose scenarios.

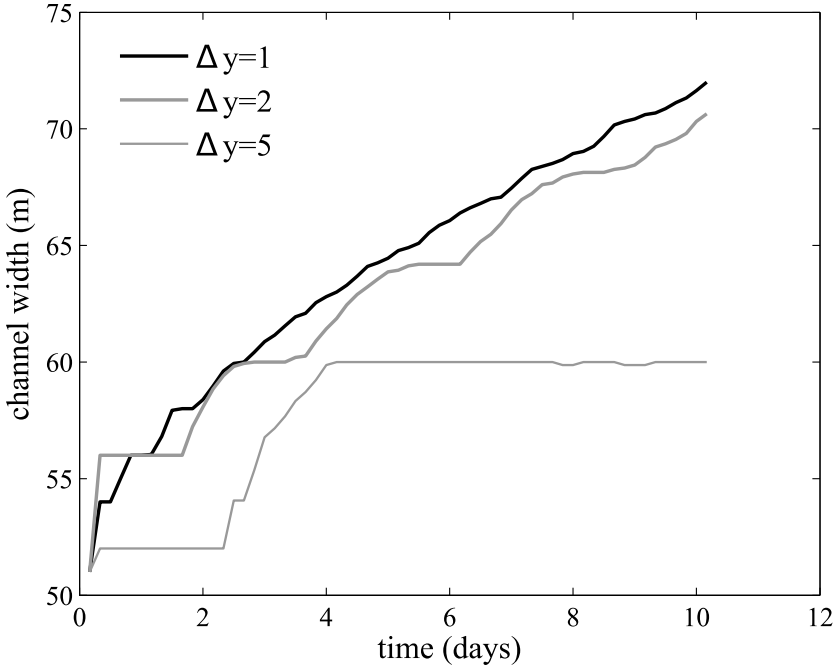

Figure 44. Effect of the transverse grid size Δy on simulated channel evolution. Channel width evolution in model descretized with 1m, 2m and 5m wide grids.

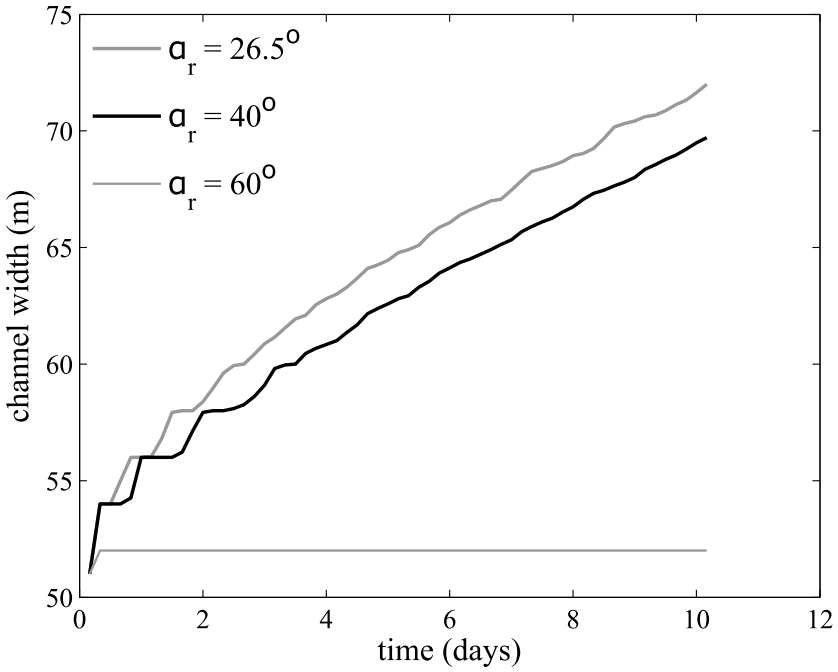

Figure 45. Effect of the angle of repose value chaosen for bank erosion simulations. Channel width evolution in scenarios with angle of repose of 26.5°, 40° and 60°.

Width evolution in scenarios with angle of repose 26.5° and 40° showed a consistent monotone behaviour, having similar evolution trend with the latter resulting in a narrower channel. Banks in scenario with the highest angle of repose (α_r = 60°) did not erode. Grids were too wide to represent the bank slope higher than 60° required for bank erosion.

Sensitivity analyses show that bank erosion formulation based on angle of repose is sensitive to both grid cell size and the value of angle of repose. In this sense, the angle of repose has the role of a numerical parameter rather than actually reflecting a physical property of a bank in the reach scale modelling of rivers where the sizes of computational grid size of several meters are used.

Planform development

Channels in all of the scenarios (Table 4) evolved to straight single thread channels. Scenarios with reduced sediment size (10 mm) resulted in wider channels. Channel width also varied along the reach always with upstream part of the reach narrower than the downstream part. Channel bed in the upstream part of the reach was plain but migrating alternate bars were observed along the downstream part of the reach. Scenarios with larger sediment diameter (30 mm) resulted in plain channel bed throughout the evolution except for scenarios with H-2 discharge hydrograph where migrating alternate bars were observed during the low flow stage.

The channel evolution in different scenarios starting from initial channel with 20 m bottom width is presented in Figure 46 as an example of planform evolution in the model. Scenarios starting from other initial channel widths resulted in similar qualitative planform. Changes in morphological features like channel width, depth, bed level and sediment transport rate during channel evolution in individual scenarios are described in the following sections.

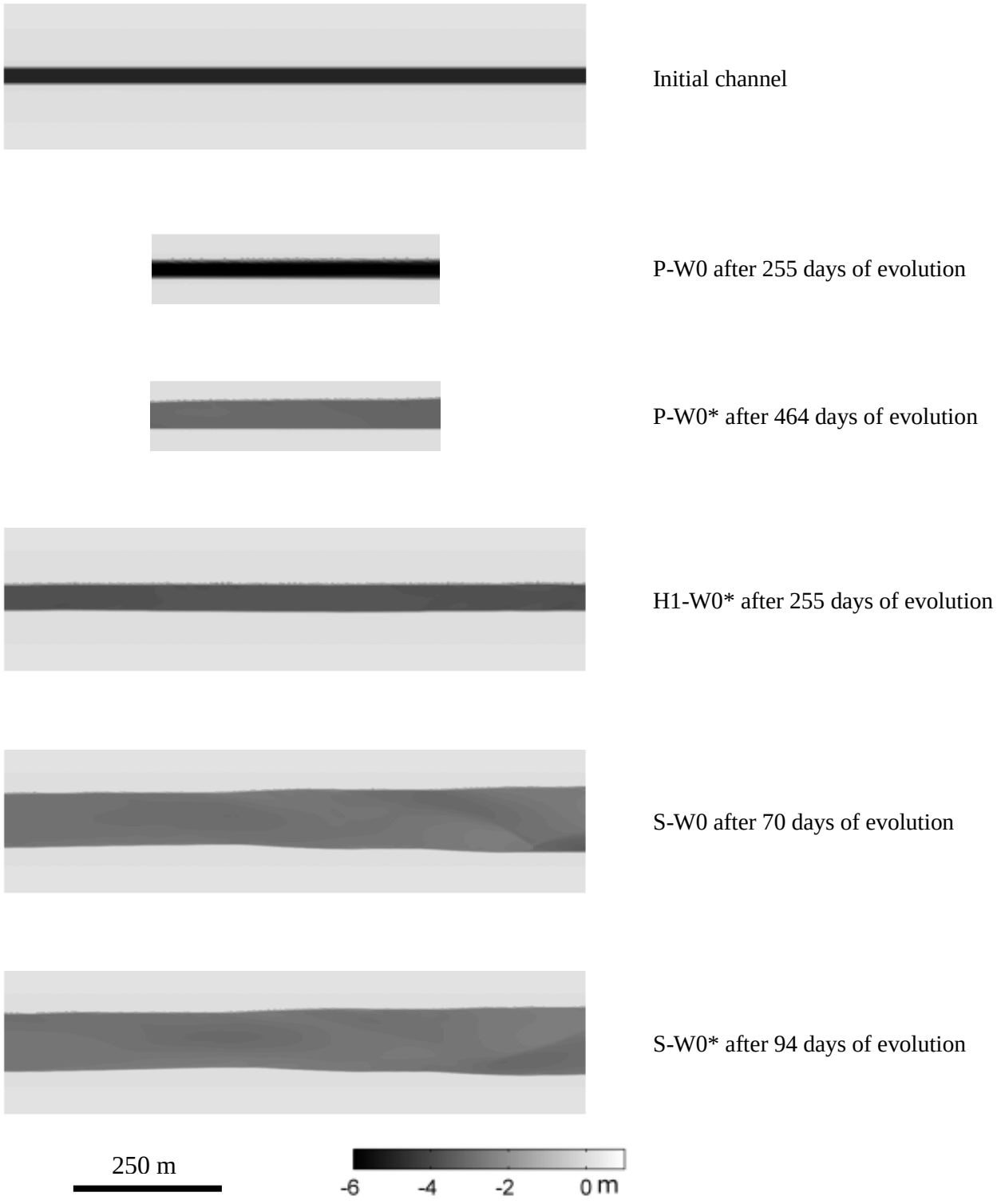

Figure 46. Two-dimensional plot of the simulated channel bed level computed after removing longitudinal slope in scenarios starting from 20 m wide initial channel. "P" runs have coarser sediment compared to "S" runs. The asterisk denotes the presence of upstream sediment supply, assumed to be at capacity with the local conditions in the inlet section.

Width evolution

Width evolution of channels starting from different initial channel width at uniform flow and without sediment supply is presented in Figure 47. Scenarios with narrower initial width (P-W0 and P-W1) rapidly widened during the early stage but narrowed at slower rate during the later stage of development. Both scenarios resulted in similar channel widths. Scenario starting from the widest initial channel width (P-W2) narrowed after 30 days of development. Channel beds in all of the scenarios were flat so the channel bed throughout the cross-section needs to be eroded to reduce channel width. Since P-W2 started from the widest channel, more amount of sediment needs to be eroded from its channel bed to result in similar width as in scenarios P-W1 and P-W2. P-W2 had smallest flow velocities so it had the lowest bed erosion rate which restrict its narrowing rate resulting in the widest channel among the scenarios.

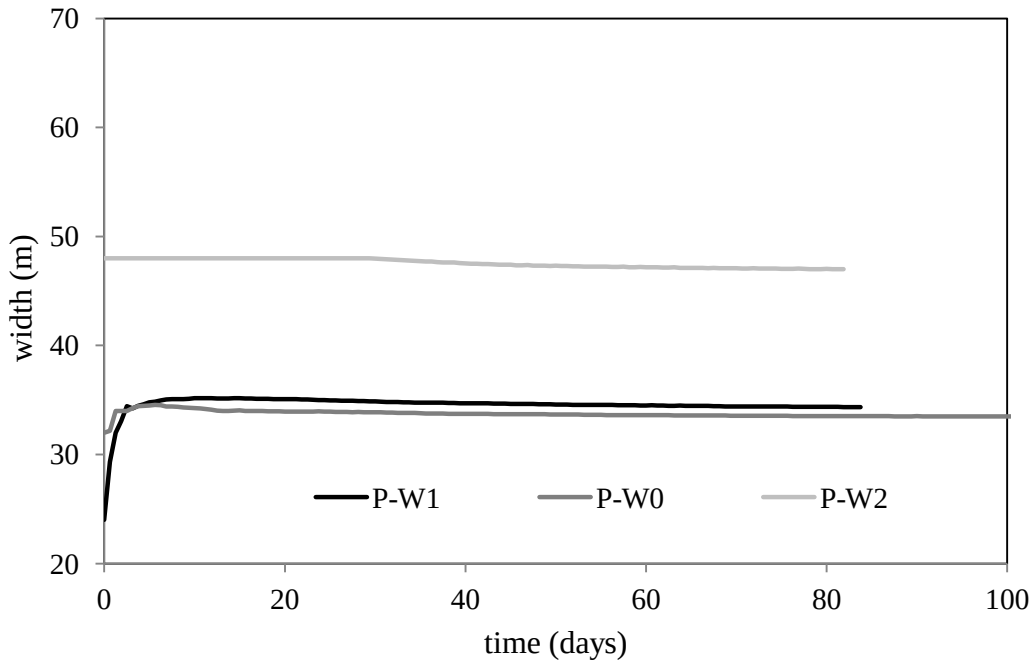

Figure 47. Channel width evolution in scenarios P-W0, P-W1 and P-W2. Uniform flow without upstream sediment supply.

Figure 48 shows the width evolution of channels starting from different initial width, uniform flow and with upstream sediment supply. The channels are wider than their counterparts without sediment supply. Scenarios starting from the narrower initial channel width (P-W0* and P-W1*) widened rapidly during the early stage of development (15 days) and continued to widen at a slower rate. P-W2* scenario did not widen and maintained its initial channel width. Scenario P-W0* resulted in the width similar to P-W2* scenario after 50 days of the evolution and continued to widen. Channel in P1-W1* scenario evolved by widening but resulted in narrower channel width than P-W0* and P-W2* scenarios.

Evolution of channels starting from different initial channel width, at non-uniform flow regimes with sediment supply is presented in Figure 49. Scenarios H1-W0* and H2-W0* start from same initial channel width but differ in flow regime. Scenario H2-W0* which had higher amplitude of flow variation than H1-W0* scenario resulted in wider channel. Scenario H2-W0* and H2-W2* were supplied with same discharge regime but started from different initial channel widths. Despite starting from narrower initial channel, H2-W0* scenarios result in wider channel than H2-W2* scenario at the later stage of the development. The widening and narrowing due to spreading and shrinking of the

water surface between the high and the low stage discharges was evident throughout the width evolution.

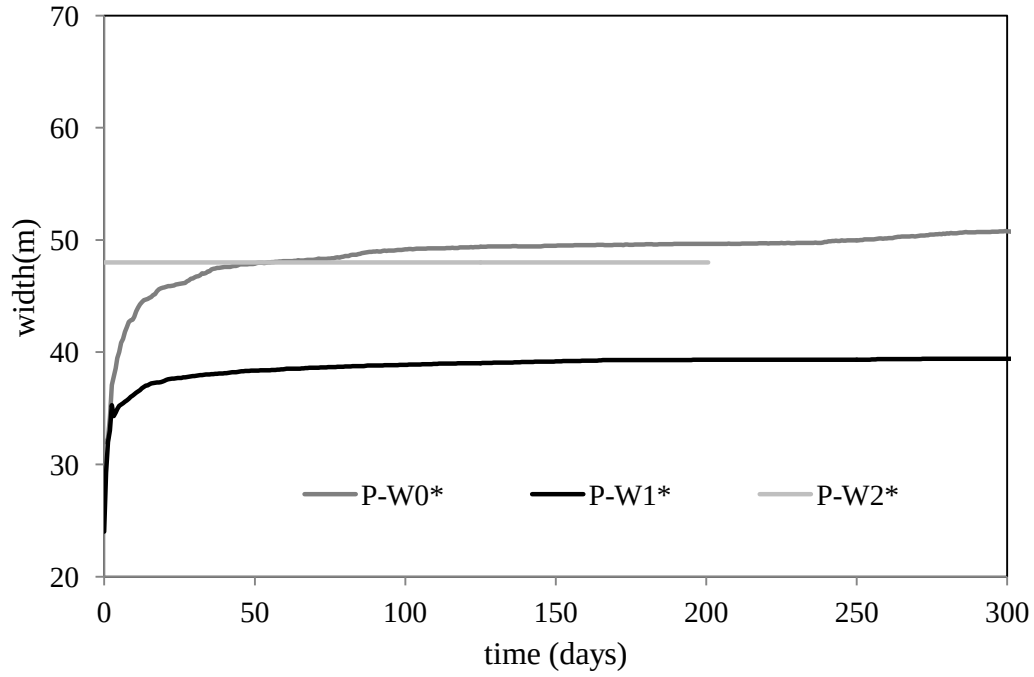

Figure 48. Channel width evolution in scenarios P-W0*, P-W1* and P-W2*. Uniform flow without upstream sediment supply.

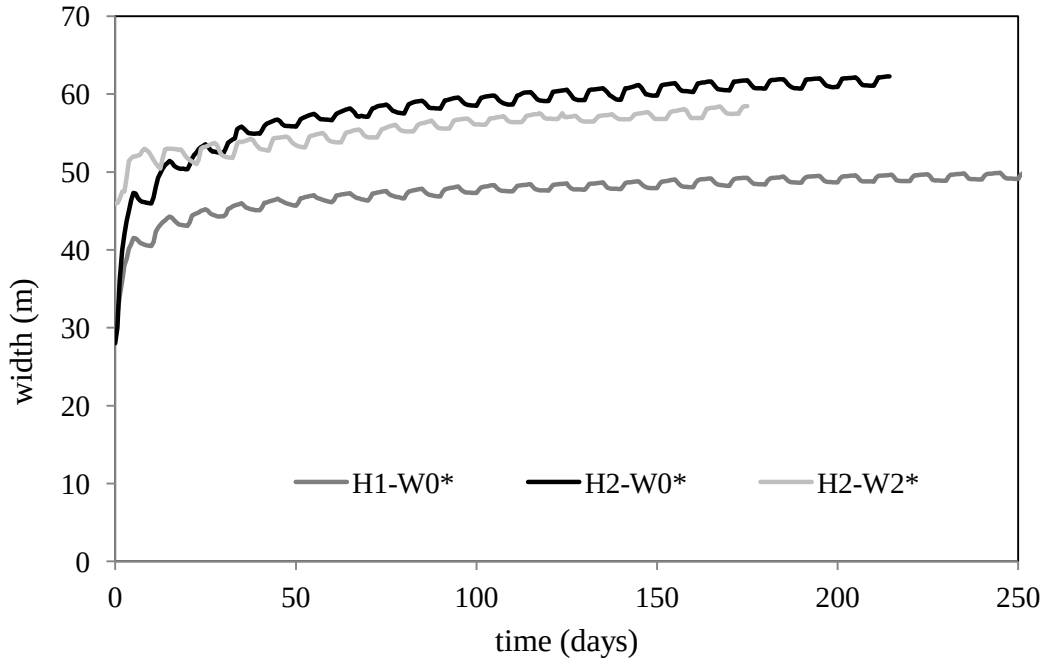

Figure 49. Channel width evolution in scenarios H1-W0*, H2-W0* and H2-W2*. Non-uniform flow regime with upstream sediment supply.

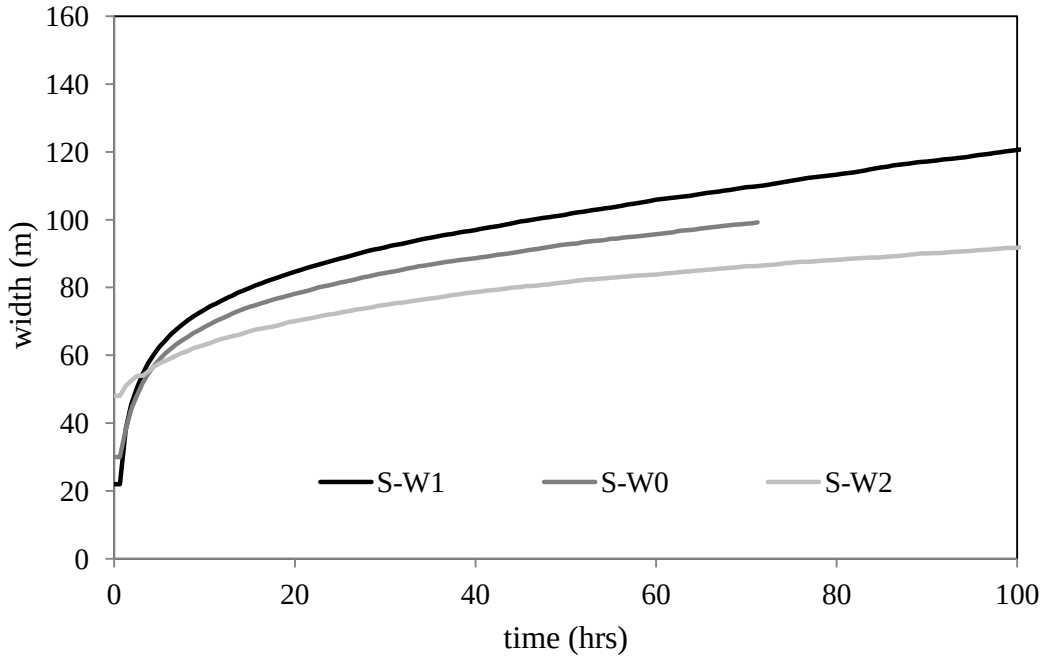

Figure 50. Channel width evolution in scenarios S-W1, S-W0 and S-W2. Uniform flow without upstream sediment supply.

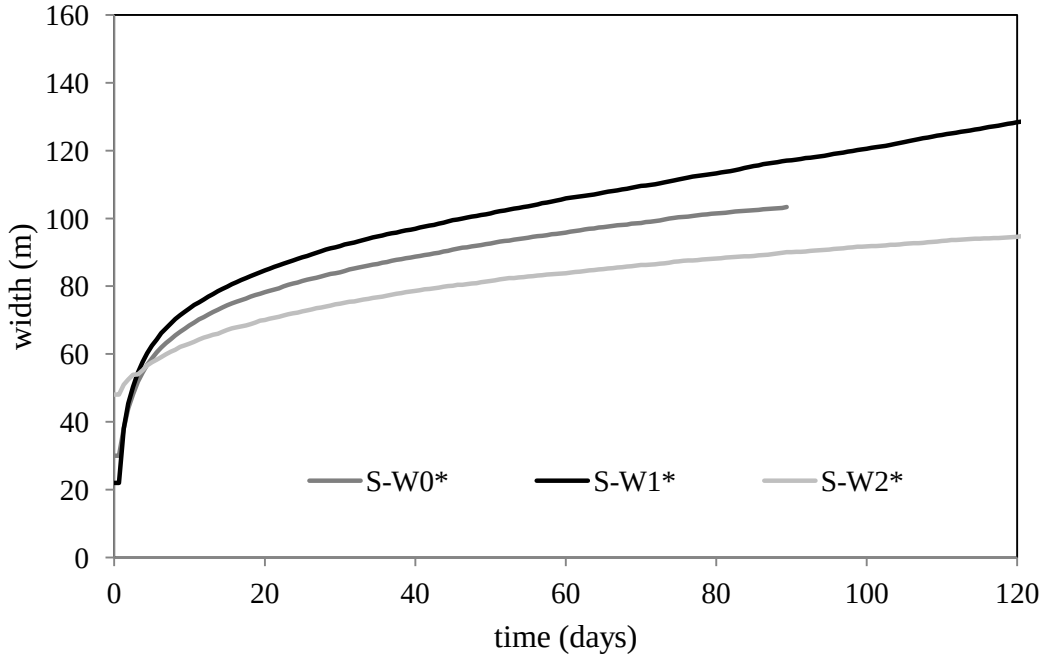

Figure 51. Channel width evolution in scenarios S-W1*, S-W0* and S-W2*. Uniform flow with upstream sediment supply.

Sediment size was reduced to 10 mm to investigate width evolution in a channel with higher widening rate. Earlier investigations were carried out with sediment diameter of 30 mm. The width evolutions in scenarios starting from different initial channel width, uniform flow at different sediment supply regime were analyzed. Width evolutions of channels starting from same initial width were similar in both sediment supply and without sediment supply regime (Figure 50 and Figure 51). This is because the higher rate of widening of the reach closer to the upstream boundary supplied sediment to the downstream reach preventing the incision. The effects of lack of sediment supply may become

prominent in the channel evolution at much longer time when the incision starts near the upstream boundary and advances further downstream. All scenarios widened rapidly during the early stage of the development and continued to widen at different rates. Scenarios with narrowest width (W1) resulted in the widest channel and continued to widen at highest rate. Scenario starting from the widest initial channel width resulted in the narrowest channel.

Channel width and bed level evolution

Bed level of the channel evolves simultaneously with its width. Change in channel width (ΔW) "relative width" is plotted against the change in bed level (Δη) "relative bed level" to analyze the combined evolution of channel width and bed. Positive and negative value of ΔW denote channel widening and narrowing, respectively. Positive and negative values of Δη signify bed aggradation and erosion, respectively. Evolution of relative channel width and bed level in scenarios starting from different inital channel width at uniform flow without sediment supply is presented in Figure 52. Scenarios starting from narrower initial width (P-W0 and P-W1) widen and aggraded during the early stage of the development. Both P-W0 and P-W1 scenarios resulted in similar channel widths. Scenario P-W1 widened and aggraded the most because it started from the narrowest initial width. Both scenarios show incision and narrowing trend during the later stage of the development. P-W2 scenario which started from the widest initial channel showed a brief aggradation during the early stage of development and continued to incise. Change in width was negligible until the channel incised by 0.5 m after which the channel started to narrow.

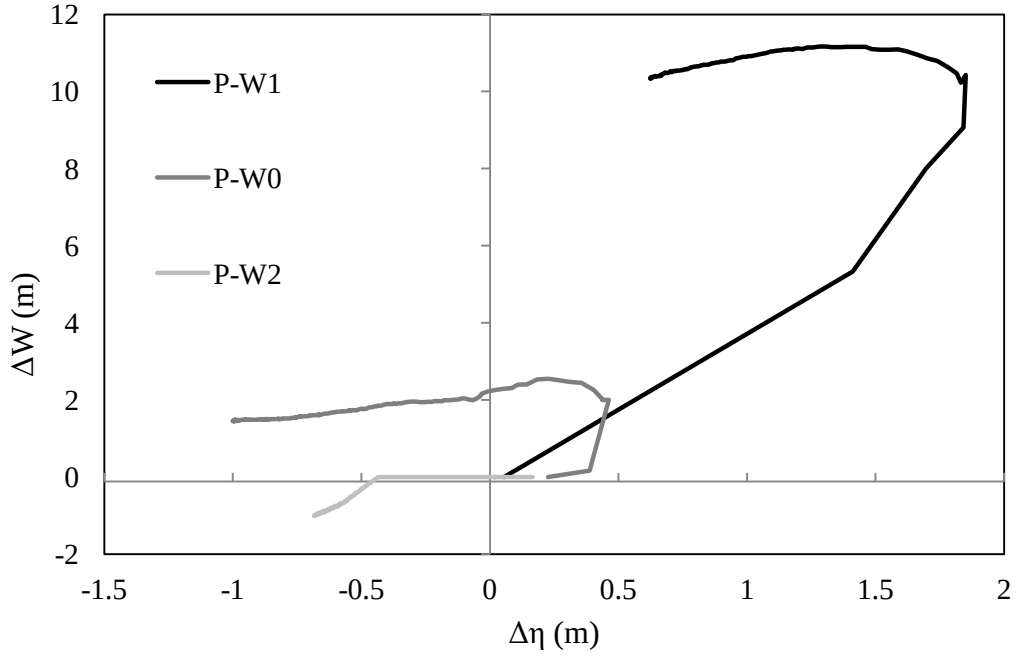

Figure 52. Relative changes in channel width and bed level during the channel evolution in scenarios P-W0, P-W1 and P-W2. Uniform flow without upstream sediment supply.

Figure 53 shows the relative channel width and bed evolution for scenarios starting from different initial widths at uniform flow with sediment supply. Scenarios P-W0* and P-W1* which started from narrower initial channel rapidly widened and aggraded during the early stage of the development. Aggradation rate was higher in P-W1* scenario. Bed aggradation rate decreased during the later stage of the development where the channel evolved mostly by widening. Scenario starting from the widest initial width (P-W2*) showed little bed aggradation even though it maintained its initial channel width throughout the development.

Relative width and bed level evolution of channels starting from different initial channel width, at non-uniform flow regimes with sediment supply is presented in Figure 54. Scenarios H1-W0* and H2-W0* start from same initial channel width but were supplied with non-uniform flow with different amplitude of discharge variations. Scenario with higher amplitude of flow variation (H2-W0*) resulted in wider and aggraded channel. Both high and low discharges widened and aggraded channel during the early stage of the development. The effect of the high and the low flow stage was evident during the later stage of the channel evolution. Channel width increased and bed level decreased during the rising limb of discharge hydrograph and channel width decreased but bed level increased during the falling limb of the discharge hydrograph. This resulted in a hysteresis characteristic of the relative channel width and bed evolution. The area of the hysteresis loop decreased during the later stage of the development.

Scenarios H2-W0* and H2-W2* were supplied with similar discharge hydrograph but start from different initial channel widths. Scenario starting from narrower initial channel width (H2-W0*) resulted in aggraded channel which is attributed to the higher width change. H2-W2* scenario, which started from the wider initial channel, showed irregular patterns without a clear hysteresis characteristics during the evolution.

The scenarios starting from different initial channel width at uniform flow are compared among the cases with smaller sediment diameter (S scenarios) and cases with the bigger sediment diameter (P scenarios). The cases with reduced sediment diameter all resulted in wider and aggraded channel compared to respective scenarios in the case with the bigger sediment diameter. In the case with smaller sediment size, the evolution trend of relative width and channel bed level were not affected by the sediment supply regime (Figure 55 and Figure 56). Scenario starting from the narrowest initial channel resulted in most widening and aggradation. Least widening and aggradation was observed in the scenario starting from the widest initial channel.

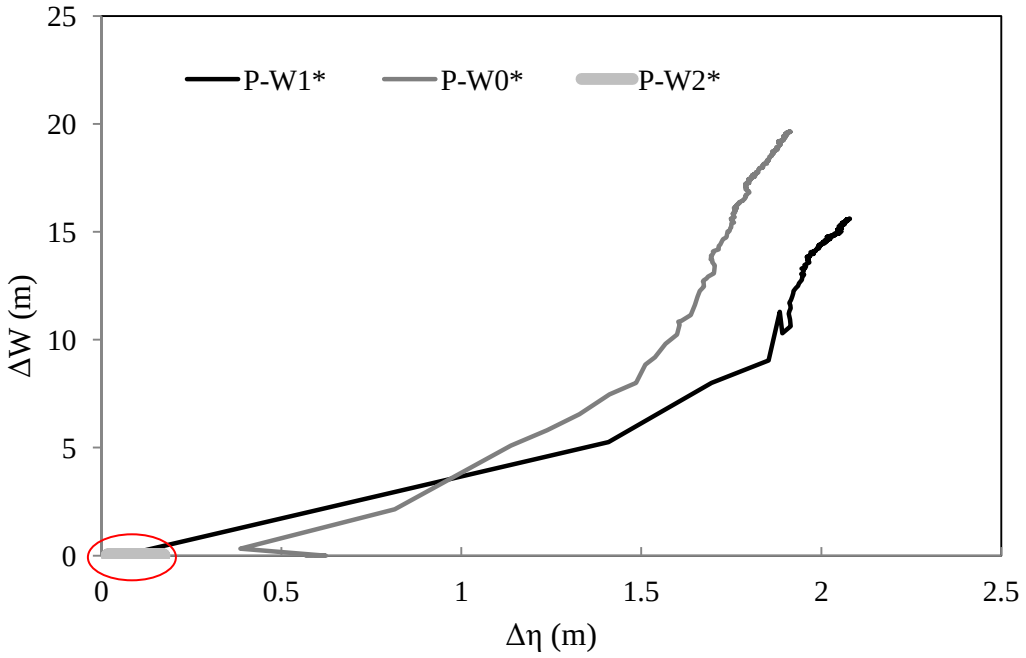

Figure 53. Relative changes in channel width and bed level during the channel evolution in scenarios P-W0*, P-W1* and P-W2*. Uniform flow with upstream sediment supply. The circled portion highlights the results in P-W2* scenario.

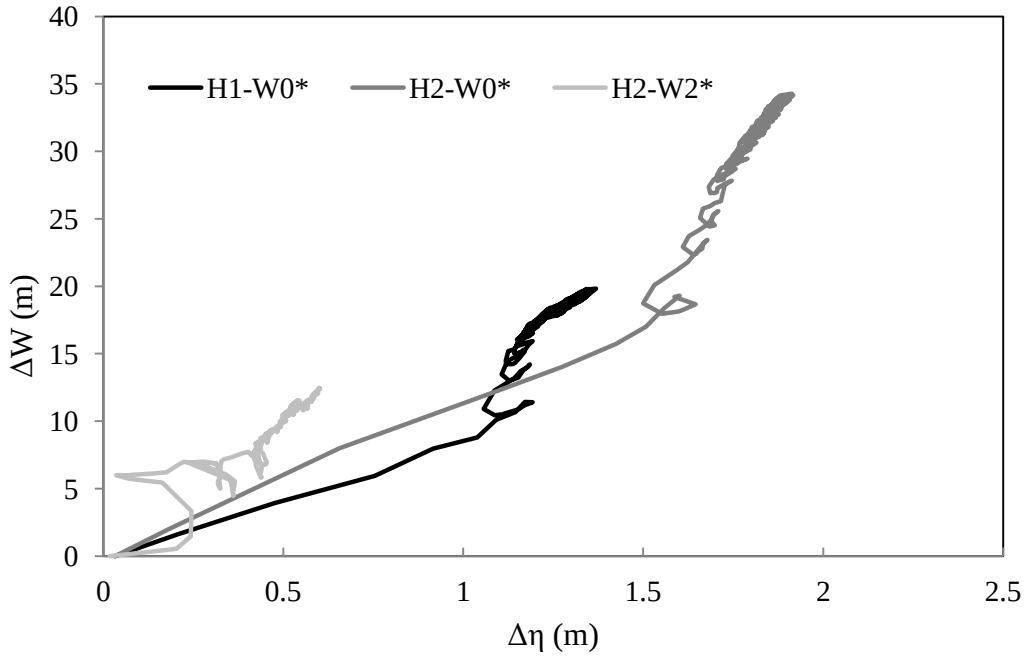

Figure 54. Relative changes in channel width and bed level during the channel evolution in scenarios H1-W0*, H2-W1* and H2-W2*. Non-uniform flow with upstream sediment supply.

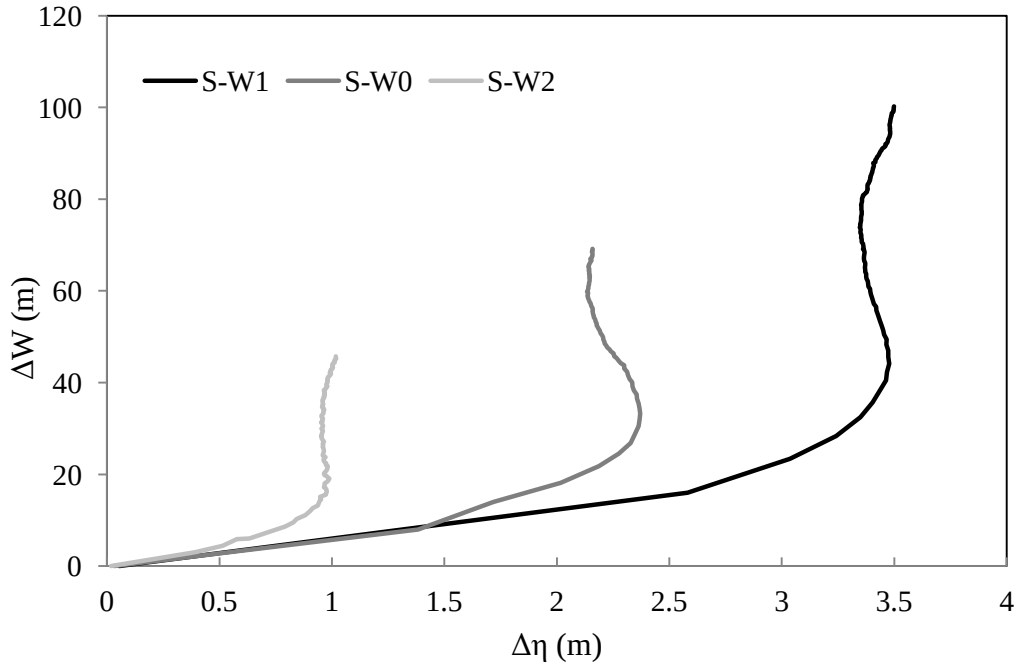

Figure 55. Relative changes in channel width and bed level during the channel evolution in scenarios a) S-W0, S-W1 and S-W2. Uniform flow without upstream sediment supply.

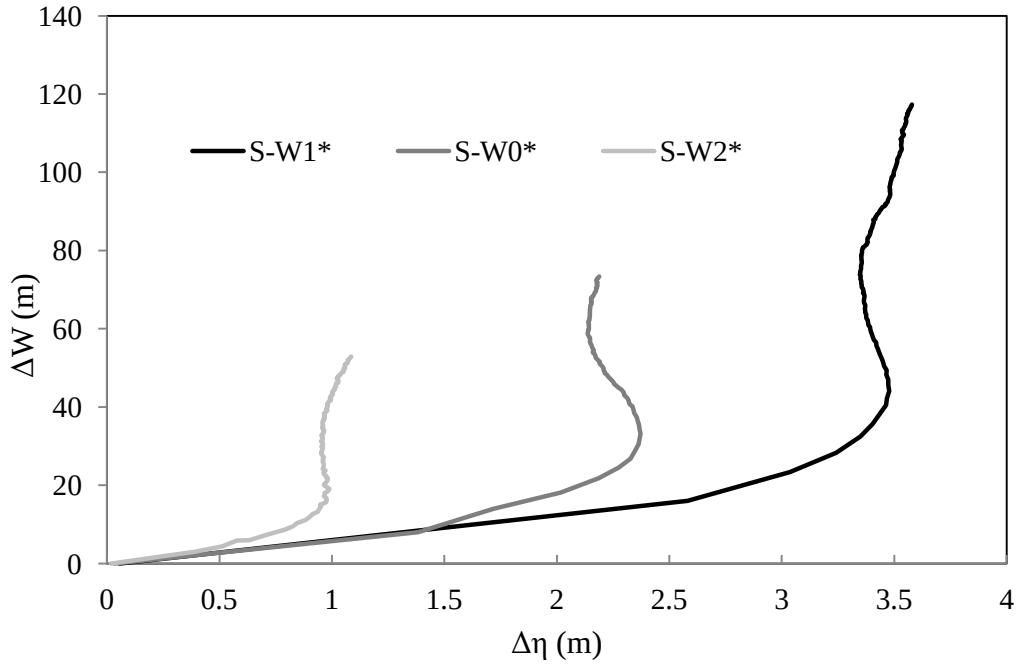

Figure 56. Relative changes in channel width and bed level during the channel evolution in scenarios a) S-W0*, S-W1* and S-W2*. Uniform flow with upstream sediment supply.

Depth evolution

Water depth evolution in the scenarios starting from different initial channel width at uniform flow without sediment supply is presented in Figure 57. Scenarios starting from narrower initial channel width (P-W0 and P-W1) which evolved to similar channel width also resulted in similar water depth. The decrease in water depth during the early stage of development is attributed to the widening of the channel. The water depth then gradually started to increase due to channel incision. Channel bed incised without changing its width during the early stage development in P-W2 scenario which caused increase in water depth. The rate of increase in water depth changed when the channel started to narrow. P-W2 scenario had wider channel so it resulted in shallower channels compared to P-W0 and P-W1 scenarios.

Figure 58 shows water depth evolution in the scenarios starting from different initial channel width without sediment supply. Scenarios P-W0* and P-W1* rapidly widened and aggraded during the early stage of the development which resulted in a rapid decrease of the water depth. Water depth was almost constant during the later stage of the development. Water depth in P-W2* scenario did not change because the channel did not change its width throughout the development. Scenarios P-W0* and P-W2* resulted in similar water depth because they evolved to similar channel width at the later stage of the development. Channel was narrower in P-W1# scenario which resulted in higher water depth.

Water depth evolution in scenarios starting from different initial channel width at non-uniform flow with sediment supply is presented in Figure 59. The variation in water depth due to discharge variation wass observed throughout the development. Scenario H1-W0* resulted in highest water depth because it evolved to the narrowest channel. Scenarios H2-W0* evolved to wider channel which resulted in slightly lower water depth compared to H2-W2* scenario.

Water depth evolution in smaller sediment size case for scenarios starting from same initial channel were similar in both sediment supply and the without supply regime (Figure 60 and Figure 61). Water

depth decreased during the initial stage of the development because of rapid widening and aggradation of the channel. Water depth continued to decrease during the later stage of the development. Scenario S-W2 evolved to narrowest channel so it resulted in the highest water depth. Scenarios S-W0 and S-W1 resulted in similar water depth despite evolving into channels with different widths.

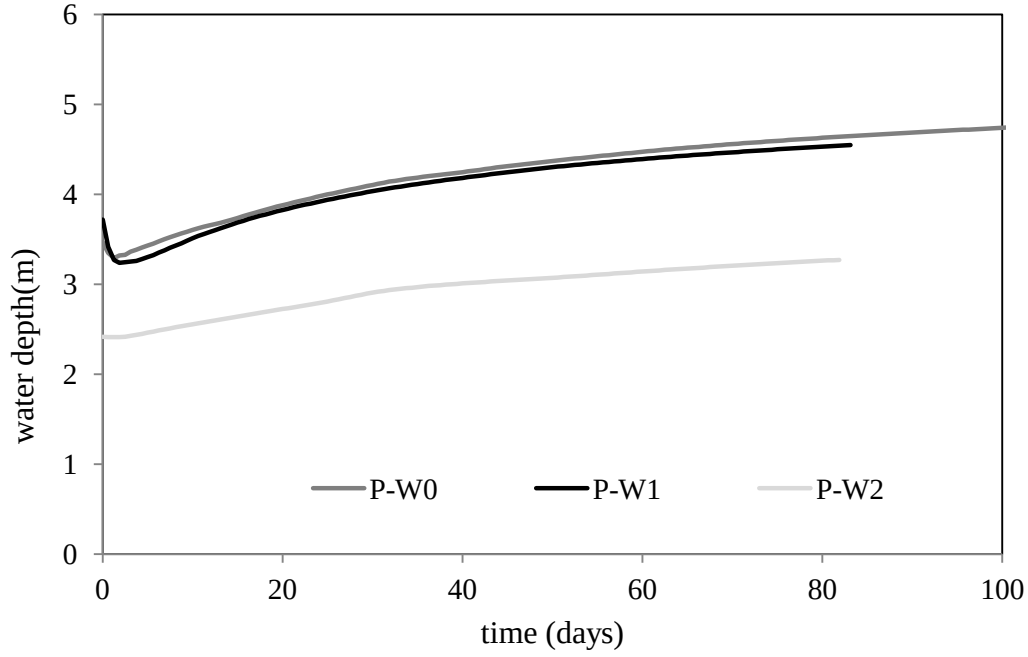

Figure 57. Water depth evolution in scenarios P-W1, P-W0 and P-W2. Uniform flow without upstream sediment supply.

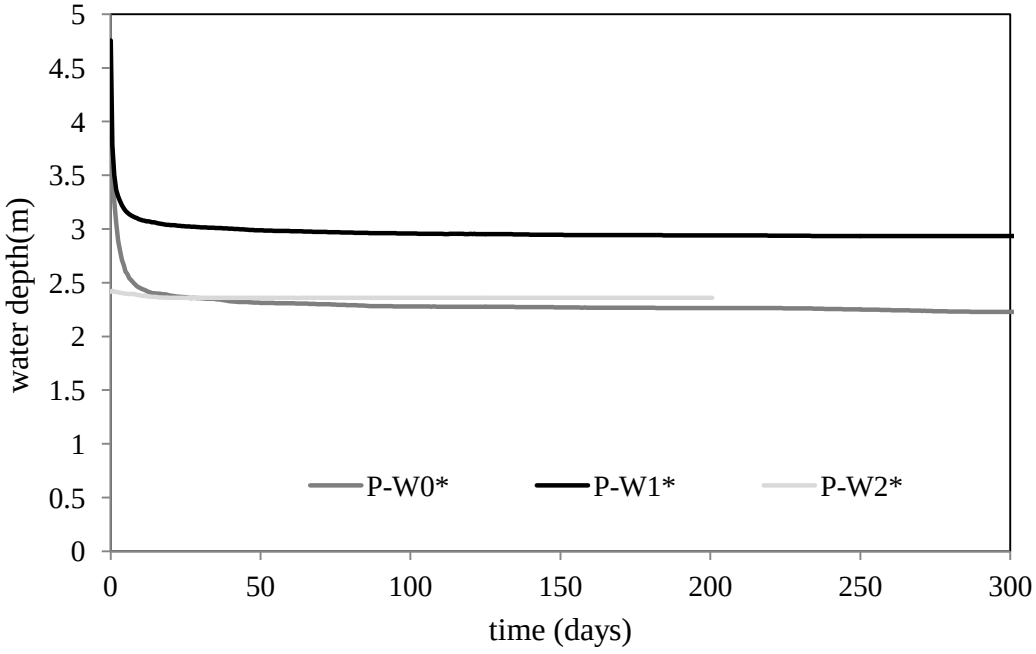

Figure 58. Water depth evolution in scenarios P-W1*, P-W0* and P-W2*. Uniform flow without upstream sediment supply.

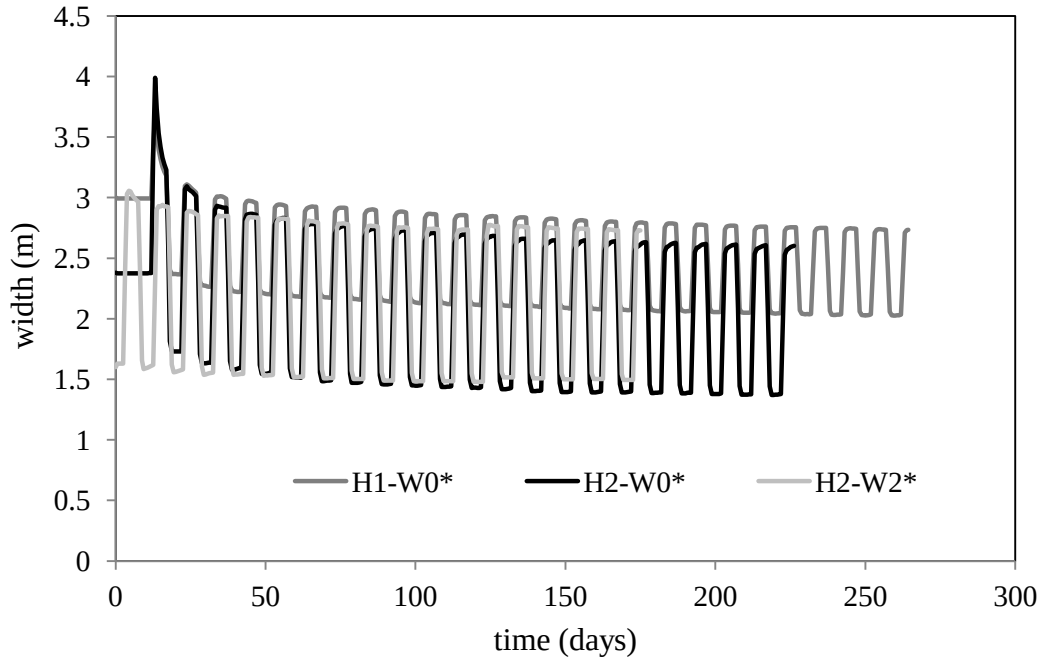

Figure 59. Water depth evolution in scenarios H1-W0*, H2-W0* and H2-W2*. Non-uniform flow with upstream sediment supply.

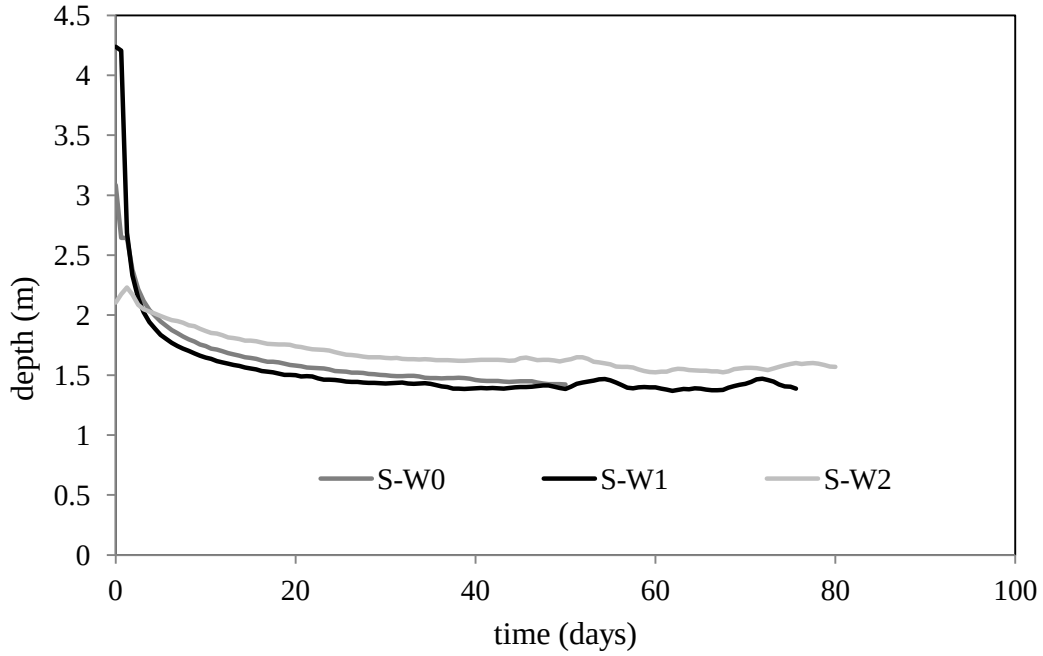

Figure 60. Water depth evolution in scenarios S-W0, S-W1 and S-W2. Uniform flow without upstream sediment supply.

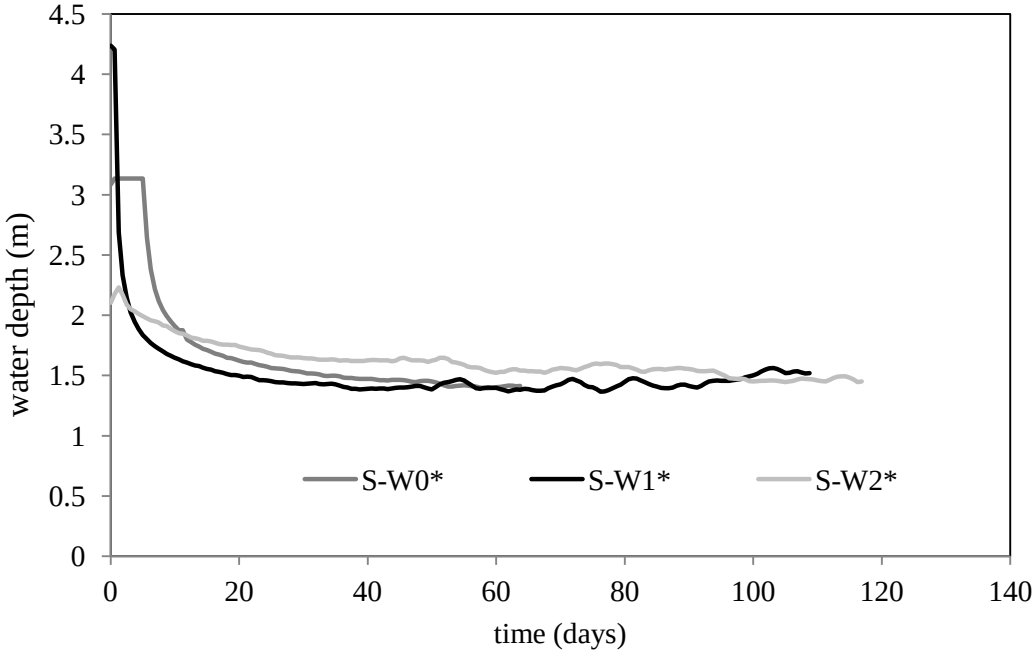

Figure 61. Water depth evolution in scenarios S-W0*, S-W1* and S-W2*. Uniform flow with upstream sediment supply.

Sediment transport rate evolution

Sediment transport rate exiting the reach for the scenarios starting from different initial channel widths at uniform flow without sediment supply is presented in Figure 62. High sediment transport rate occurred during the early stage of the development in scenarios P-W0 and P-W1 because they widened rapidly during this stage. Highest widening rate was observed in P-W1 scenario which resulted in the highest sediment transport rate. Bank erosion did not occur in scenario P-W2 so the sediment transport rate exiting the reach is entirely contributed by the bed incision. Since no sediment was supplied from the upstream boundary, sediment transport rate in all the scenarios approaches to zero at the later stage of the development.

Figure 63 shows the sediment transport exiting the reach for the scenarios starting with different initial channel widths at uniform flow with sediment supply. Scenario P-W0* evolved to the widest channel and also resulted in the highest sediment transport rate. Scenarios P-W1* and P-W2* resulted in similar sediment transport at the later stage of the development despite evolving into channels with different widths and water depths. Channel width and depths were similar in P-W0* and P-W2* scenarios but they result in different sediment transport rate. Rapid widening of channels during early stage of evolution resulted in higher sediment transport rate in scenarios P-W0* and P-W1*. Sediment transport rate increased in scenario P-W2* even though its width remained constant throughout the development.

Sediment transport exiting the reach for the scenarios starting with different initial channel widths at non-uniform flow with sediment supply is presented in Figure 64. Scenario with higher discharge amplitude (H2-W0* and H2-W2*) resulted in higher and lower sediment transport rate at high and low flow respectively compared to the scenario with lower discharge amplitude (H1-W0*). Negligible sediment transport rate was observed during the lower discharge stage in scenario H2-W2* indicate the channel evolution is entirely contributed by the high stage discharge.

Sediment transport exiting the reach in smaller sediment size case for the scenarios starting with different initial channel with sediment supply and without sediment supply are presented in Figure 65 and Figure 66, respectively. Higher sediment transport rate were observed during early stage development in the scenarios starting from narrower initial channel widths (W0 and W1). Scenario SW0 showed higher sediment transport rate compared to SW1 scenario. Sediment transport rate were similar in scenarios SW0* and SW1*. Scenarios starting from widest initial channel showed lowest sediment transport rate in the early stage of the development but resulted in the highest sediment transport rate at the later stage of the development.

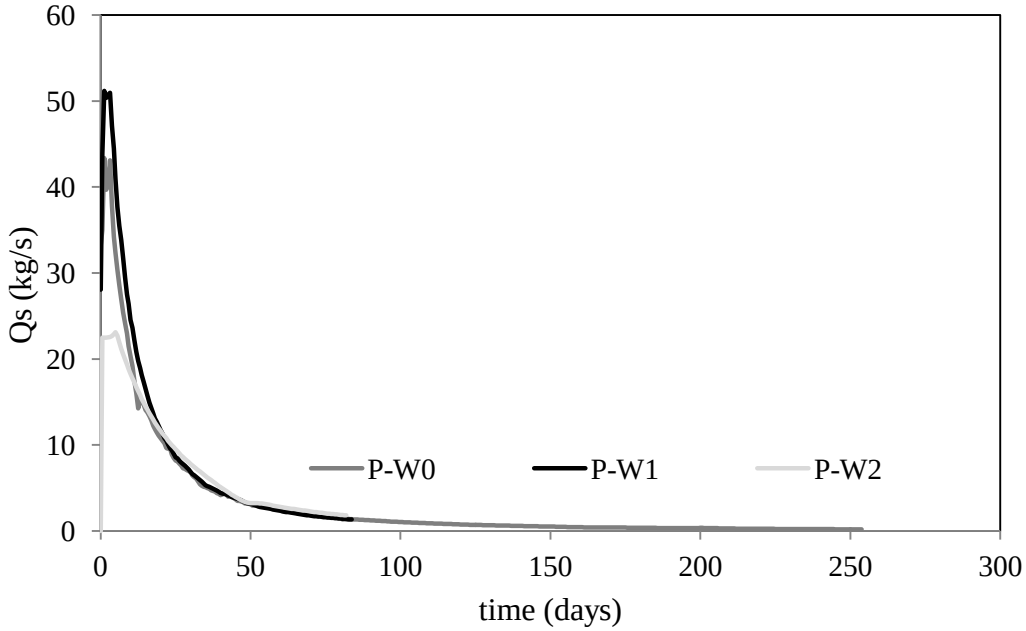

Figure 62. Sediment transport rate exiting the reach in scenarios P-W1, P-W0 and P-W2. Uniform flow without upstream sediment supply.

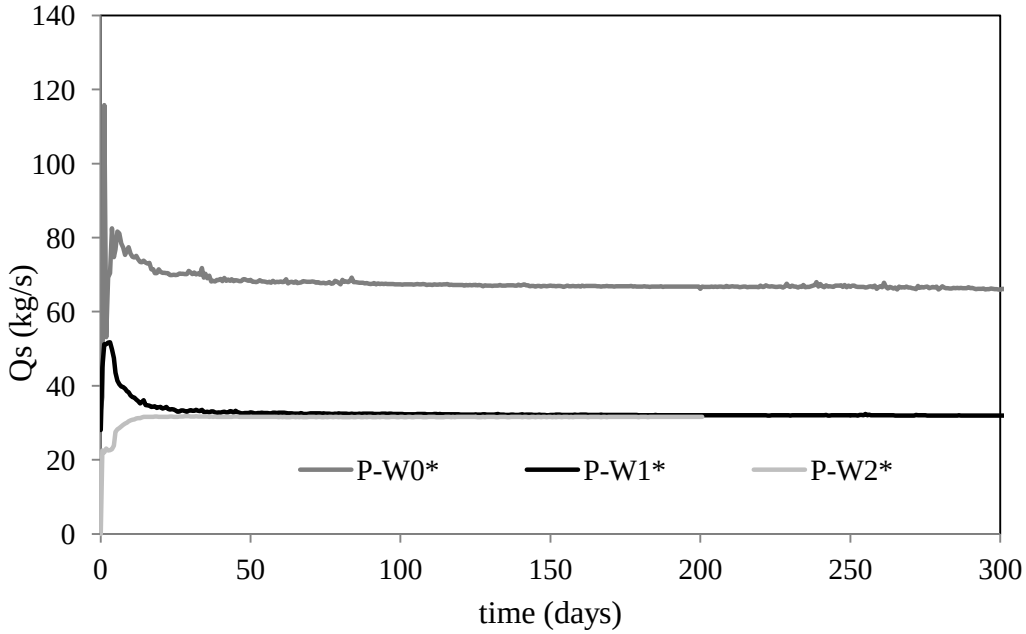

Figure 63. Sediment transport rate exiting the reach in scenarios P-W1*, P-W0* and P-W2*. Uniform flow with upstream sediment supply.

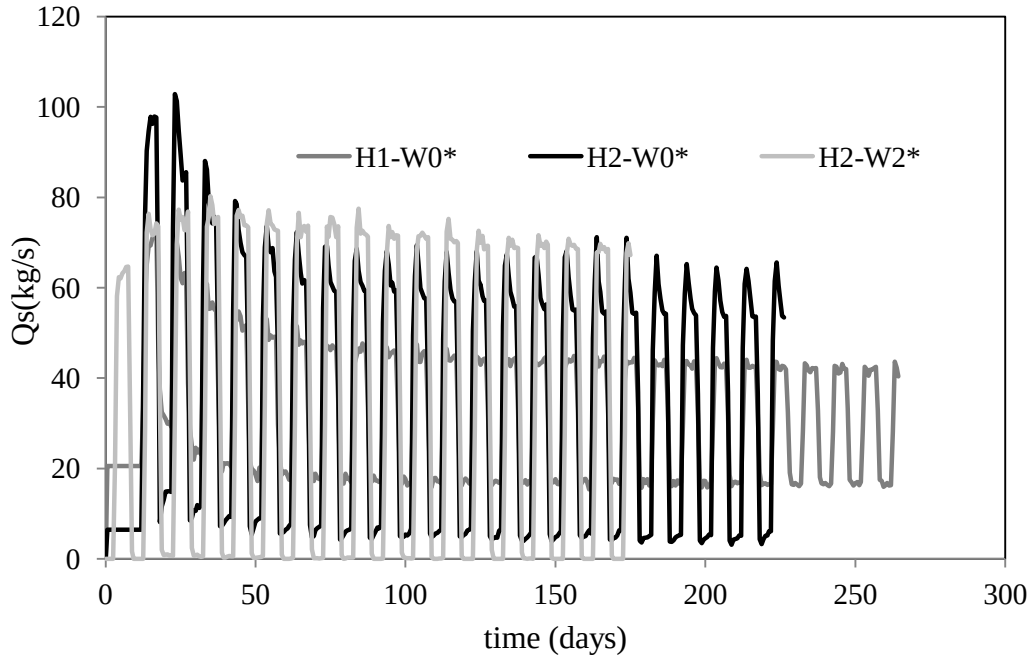

Figure 64. Sediment transport rate exiting the reach in scenarios H1-W0*, H2-W0* and H2-W2*. Non-uniform flow with upstream sediment supply.

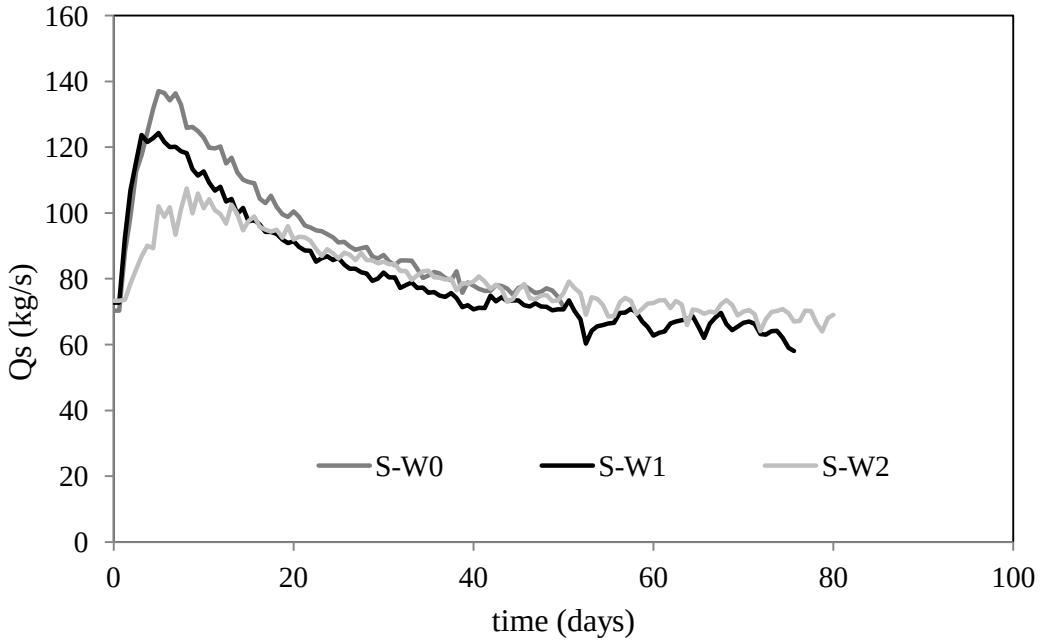

Figure 65. Sediment transport rate exiting the reach in scenarios S-W0, S-W1 and S-W2. Uniform flow without upstream sediment supply.

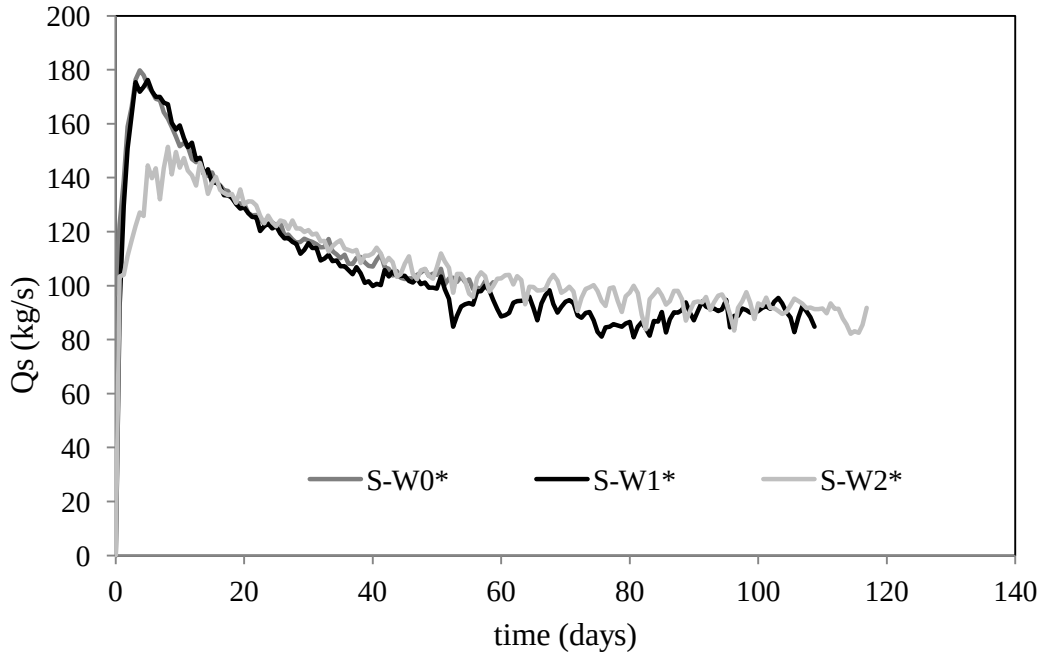

Figure 66. Sediment transport rate exiting the reach in scenarios S-W0*, S-W1* and S-W2*. Uniform flow with upstream sediment supply.

5.3 Summary of the results

The effects of controlling factors: Initial channel width, discharge and sediment regime, were investigated using numerical model and analytical model. Numerical model was used to simulated channel evolution of a gravel bed river at the field scale. The simulations were carried at scenarios similar to those explored in the experiments reported in Chpater-3. Analytical model was used to compute the channel evolution using the experimental data. The results from the investigations can be summarized in the following sections.

Effects of initial channel width

Results from the numerical model show that the long-term evolution of channel width in scenarios with uniform flow without sediment supply is less affected by the initial channel width. Channels starting from narrower initial width resulted in similar widths and water depth. Channel starting from widest initial channel however still resulted in wider channels compared to the channels starting from narrower initial channels. The bed levels of the channels starting from narrower channels were higher than those of the channels starting from wider initial channels.

Width evolution of channels in scenarios with uniform flow and sediment supply did not show clear relation with the initial channel width. The channel starting from the narrowest initial channel resulted in narrowest width and most aggraded bed levels with low sediment transport rate. Lower sediment transport rate in the channel despite being narrowest and most aggraded bed suggest the channel evolution is affected by the downstream boundary. A constant water level corresponding to the normal water depth at initial conditions in the channel is prescribed at the downstream boundary. Channel starting from narrowest initial width would have the highest water level for a same discharge. The narrowest channel also evolves rapidly to the largest width during the initial stage of the development resulting in rapid lowering of the water level in the channel. However the water level at the downstream boundary is fixed and very high compared to the water level in the evolved channel creating back water curve in a reach close to the downstream boundary. Since the domain used in this

scenario was short (1000 m) the back water curve propagated further upstream affecting the evolution of the channel.

Long-term channel evolutions in scenarios with higher sediment mobility at uniform flow were affected by the initial channel width. These simulations were carried out using longer domain (2000 m) to avoid boundary effects. Channels starting from narrow initial channel resulted in wider and more aggraded channels compared to the channels starting from wider channels. Higher rate of channel widening resulted in higher sediment transport rates in the narrower channels during the early stage of the development. The sediment transport rates were higher in the channels starting from wider initial channel after the long-term development.

Channels evolving at non-uniform flow with sediment supply were also showed that the channels starting from narrower initial width result in wider and more aggraded channels.

Effects of discharge regimes
Results from both numerical model show that the long-term width evolution is different for different discharge regimes. Channels evolving with higher amplitude discharge variations result in wider and more aggraded channels. Channel widening occurred mostly during the higher flow stage.

Effects of sediment supply regime
Sediment supply regime affected the channel evolution simulated in a shorter domain with lower sediment mobility. In scenarios without sediment supply, the channel incision at the upstream boundary, due to lack of sediment supply, propagated downstream resulting in incised and narrow channels. Channels evolving in the scenarios with sediment supply were wider compared to the channels in without sediment supply scenario.

The channels evolving in a longer domain with higher sediment mobility were less affected by the sediment supply regime. Evolutions of channel width and bed level were similar in sediment supply and without sediment supply scenarios. The sediment transport rate in the channel was observed lower in the without sediment supply scenario. Higher sediment mobility resulted in higher bank erosion which supplied more sediments into the channel. The widening and incision in the reach of the channel close to the upstream boundary, which is excluded from the analysis, supplied the sediment to more downstream reach preventing them from incision. The effect of lack of sediment supply might be evident in the channel evolution at much longer time scales when the channel bed incision occurring close to the upstream boundary progresses into a longer reach downstream.

6 RIVER BED TOPOGRAPHY ADAPTATIONS TO SMALL AMPLITUDE WIDTH VARIATIONS

6.1 Introduction

Previous chapters (3 and 4) investigate the evolution of the river channel width under different controlling factors, such as flow and sediment supply regime viewed as upstream boundary conditions, as well as of an initially imposed channel width viewed as an initial condition, using experimental, numerical and analytical approaches. The channel adjustment was a result of interactions between the evolutions of channel width, slope, depth and bed topography at the river reach scale. The variation of width along the channel and in time was strongly interacting with the topographic evolution.

Under the unifying topic of the key role of channel width, this chapter explores the response of the riverbed to an imposed small-amplitude, irregular width variability in space using a fully non-linear numerical morphodynamic model. The analysis aims to address two inter-related research gaps. The first is the reproducibility of alternate bars observed in laboratory flume experiments on straight channels through numerical morphodynamic models. The second is about the required amplitude of planform forcing to actually condition the dynamics of the resulting "hybrid" bars that reflect a mixed behavior between free and forced bars. The link between the two issues is related to the nature itself of the planform forcing consisting of small-amplitude width variations: is it possible to quantify a lower threshold amplitude below which the forcing effect is negligible, i.e. it does not represent a planform forcing anymore? Is such effect actually relevant in reproducing laboratory experiments on river bars? And what is its specific role?

The numerical model was setup using data of laboratory experiments. The emphasis of the investigation is on small-scale spatial width variations which has been suggested from an unexpected mismatch between the properties of alternate bars observed in the laboratory experiments and those reproduced in the numerical model. Small width variations, at the scale of cross-sectional averaged water depth, are imposed along one of the banks but keeping the reach averaged width and slope constant. The analysis reveals the unexpected role of apparently small spatial irregular oscillation of the channel width and to interpret such role into the conceptual framework of the free and forced morphodynamic response of the channel.

6.2 Methodology

6.2.1 Model description

Delft3D (open source version - 3.28.50.01) was used for the investigation. Delft3D is a fully nonlinear numerical model that includes a bed evolution component and a flow field component that are "semi coupled". The flow field is implemented by solving the unsteady shallow-water equations with hydrostatic approximation in two dimensions. The bed evolution component is implemented by solving sediment transport equations and Exner's sediment balance equations [*Lesser et al.*, 2004]. In semi-coupled approaches, the sediment transport equation and flow-field equations are solved separately assuming that the bed level changes occurring at a small computational time steps is small and does not affect the flow [*Kassem and Chaudhry*, 1998]. The choice of the model was based on the comparison between a fully coupled (GIAMT-2D) and semi-coupled model (Delft3D). Such comparison has been developed because of the hydraulic conditions of the target laboratory experiments, which fall very close to the super critical range. Under such conditions, semi-coupled

models often develop numerical errors that may be large enough to mask the physical solution. The comparison was made by investigating the ability of both models to reproduce the alternate bars observed in the experiments of *Garcia Lugo et al.*, [2015]. The comparison between the models show that Delft3D is capable to reproduce the alternate bars similar to GIAMT-2D, despite the semi-coupled nature of the model, which may lead to numerical errors close to Froude-critical conditions. More details about such comparison between GIAMT-2D and Delft3D models are presented in Appendix B.

Delft3D has been used to investigate bars in alluvial channels in wide range of scales, from laboratory experiments to real rivers [*Crosato and Saleh*, 2011; *Crosato et al.*, 2011; *Schuurman et al.*, 2012; *Verbruggen*, 2012] though most often far from the Froude-critical range. The description of the model is provided is Appendix B.

6.2.2 Model setup

Experiments

The model was setup in Delft3D code using data of the *Garcia Lugo et al.*, [2015] experiments. This allowed a choice of realistic values of the model parameters and to compare between the topography evolved in numerical models and in the experiments. Experiment Run# 11 of *Garcia Lugo et al.* [2015] was chosen to investigate the effects of small width variations on the evolution of alternate bars. The experiment carried out in 0.4 m wide channel with longitudinal slope of 1% and discharge of 2 l/s was selected for the investigation. Alternate bars were observed in the experiment at 4 hours of development. The width along the channels had small variations, up to 4% of the reach averaged channel width, due to the bulging of the plastic material used to construct non-erodible banks (Figure 67). The evolved channel bed was measured within a 15 m long reach at the centre of the flume. The measurements were carried out at two instances of time 16 minutes apart at the end of the experiments. The sediment transport rate at the downstream end of the flume was continuously recorded during the entire duration of the experiments. The spatial extensions of the dry areas were measured along the channel before the experiments were stopped for bed level measurements.

Three more experiments were chosen to study effects of small width variations on bed topography at different flow width-to-depth ratio. The experimental conditions of the simulated runs are summarized in Table 8. In Table 8 Run# refers to the Run ID of *Garcia Lugo et al.* [2015]; W is the width of the channel, m; Q is the discharge, l/s; H is the average flow depth, m; D_s is the sediment diameter, mm; S is the longitudinal bed slope; β denotes the flow width to depth ratio in the channel; βcr denotes the critical value of the flow width to depth ratio required for the instability of free bars. The value of critical width-to-depth ratio is computed for the experimental conditions using the analytical linear bar theory of *Colombini et al.* [1987]. βcr corresponds to twice the value of the computed critical width-to-depth ratio. More details about the experiments can be found in *Garcia Lugo et al.* [2015].

Table 8- Details of the experiments used for investigations by numerical model

Run #	W (m)	Q (l/s)	H (m)	D_s (mm)	S (-)	β (-)	β/βcr (-)	Bed form
3	0.15	2.5	0.028	1	0.01	5.4	0.5	No bars
7	0.3	1.5	0.013	1	0.01	23.1	3	Alternate bar
9	0.3	2.5	0.023	1	0.01	13	2	Alternate bar
11	0.4	2	0.013	1	0.01	30.8	5	Alternate bar

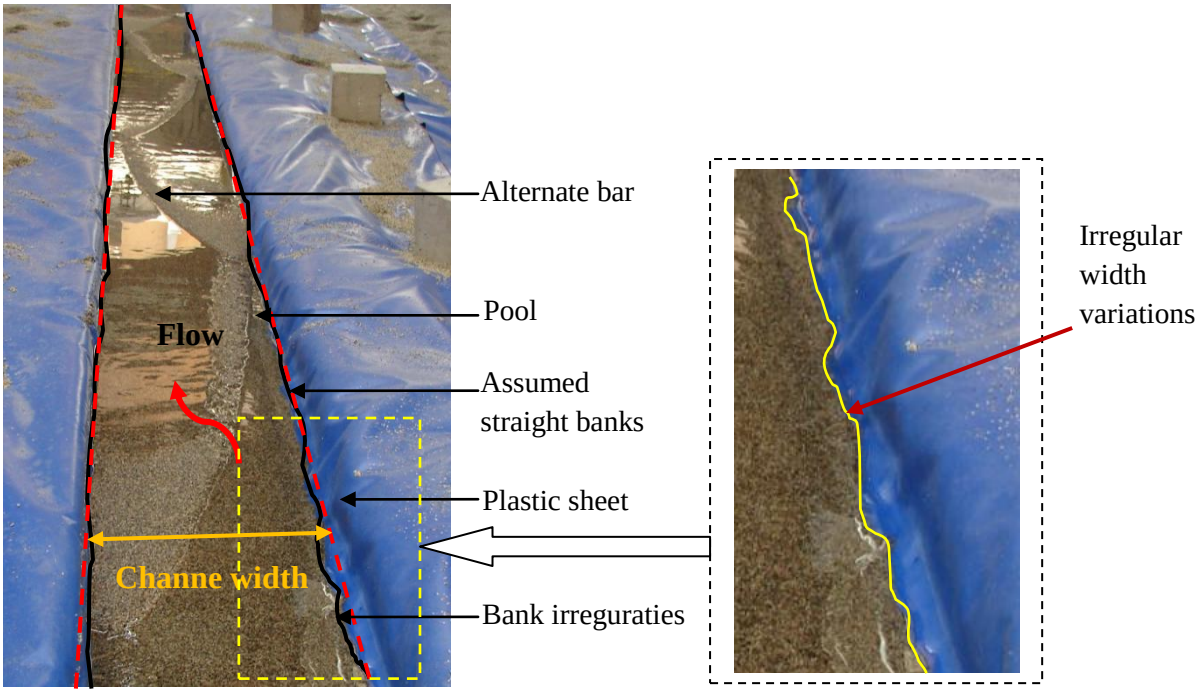

Figure 67. Image showing the alternate bars formed in the experiment and close up view illustrating the width variations near the banks.

Model domain and grid size

A 35 m long rectangular domain with 1% longitudinal slope and fixed banks were setup. A longer computational domain compared to the experimental flume is adapted to minimize the effects of errors propagating from the boundaries on a 15 long reach at the centre of the flume. Domains having 0.4 m, 0.3 m and 0.15 m width were used for the investigations. A random perturbation of 0.1% of sediment size (1mm) was imposed in the initial bed topography to trigger the development of bars.

The computational domain was spatially discretized using rectangular grid cells. *Schuurman and Kleinhans* [2011] show that the reach averaged bar characteristics, in numerical simulations of braided rivers, are largely independent of grid sizes. Shapes of bars were better obtained using finer grids, which however required much higher computational time. Computation grids 0.02 m wide in lateral direction and 0.05 m long in longitudinal directions were used. In the 0.4 m wide channel case, the computational domain would have 20 grid cells in the lateral direction, resulting in a representation of bars with reasonable spatial resolution while optimizing the computational time. Computation grids with the same cell dimensions were used to discretize 0.3 m and 0.15 m wide domains.

Small amplitude width variations measured along the bank lines in the experiments and a set of idealised width variations of prescribed dimension were implemented along the bank lines. Few grid cells close to each bank were locally added to further refine the grid to 0.005m in the lateral direction. Grid refinement below 0.005m was not possible because of the high computational cost and the numerical stability requirement of the model. Such local refinement allowed implementing smaller amplitude width variations along the banks. The new bank lines defined the extent of the computational domain in the lateral directions. The computational time step was chosen as 0.06 seconds, which ensured the stability in the model.

Boundary conditions

Discharge was prescribed along every cell at the upstream boundary. Discharge was varied in time and among each cell by adding random perturbations between -1% and 1% of the uniform discharge. Sediment transport rate in equilibrium with the local hydraulic conditions were imposed at the upstream boundary. A constant water level corresponding to normal water depth was prescribed at the downstream boundary. A no slip boundary condition was used along the lateral boundary of the domain. The partial-slip boundary condition in Delft3D is implemented in an explicit way which would require very small computational time step for the stability of the numerical model. This would largely increase the computational time of the model.

Hydrodynamic modelling

The hydrodynamic modelling in Delft3D solves continuity and horizontal momentum equations of water flow and a turbulence closure model. It requires choice of appropriate bed roughness, turbulence parameters and parameterization of spiral flow. Manning's roughness formulation with roughness coefficient equal to 0.014 $m^{1/3}/s$ was used in the model. The equivalent Chezy's roughness is computed by the model as $C = (h^{1/6})/n$, where C is the Chezy's roughness coefficient, h is the local water depth (m) and n is the Manning's roughness coefficient. Manning's roughness formulation allowed having depth dependent roughness, where deeper channels have low roughness and shallow channels have higher roughness. Information on flow depth and velocity were not available from the experiments to calibrate the roughness coefficient in the model. The measured extents of dry areas in the experiments were used to choose reasonable values of the Manning's roughness. A fixed bed hydrodynamic model was carried out on a bed topography obtained from the experiment. Manning's roughness coefficient was varied to reproduce the extent of measured dry areas. The coefficient which reproduced most extent of the dry areas was chosen. The details on the choice of roughness parameter are presented in Appendix B.

The diffusion due to turbulence was modelled by prescribing coefficient of horizontal eddy viscosity [*Lesser et al.*, 2004]. Horizontal eddy viscosity largely depends upon the grid size and the flow condition being modelled. *Verbruggen* [2012] used the value of 0.01 m^2/s to model alternate bars in the laboratory scale. Their choice was based upon the value which ensured stability in the model although they argue that the realistic value is two orders of magnitude less than the chosen value. The value of 0.001 m^2/s was used in model setup which ensured computational stability within the model.

Spiral flow produced by local streamline curvature plays an important role in modelling the realistic equilibrium shapes of alternate bars [*Nelson,* 1990]. The effect of spiral flow in Delft3D is implemented to correct the direction of the bed shear stress with respect to the direction of the depth averaged velocity as shown in equation (28). The intensity of the spiral flow motion is computed based upon the stream line curvatures as shown in equation (29).

$$Tan(\alpha_\tau) = \frac{-A}{\sqrt{u^2 + v^2}} \qquad (28)$$

$$A = \frac{2}{\kappa^2} E_{spir} \left(1 - \frac{\sqrt{g}}{2\kappa C} \right) \qquad (29)$$

Where, α_τ is the corrected angle of bed shear stress with respect to the direction of depth averaged velocity; u and v are the depth averaged velocity in stream wise (x) and transverse (y) direction respectively, m/s; κ is the Von Karman's constant; E_{spir} is the calibration parameter weighing the

intensity of spiral flow motion; g is the acceleration due to gravity, m/s^2; C is the dimensional Chezy's roughness coefficient, $m^{1/2}/s$.

The value of E_{spir} was chosen as 0.5 based upon previous numerical modeling studies of laboratory experiments [*Verbruggen*, 2012].

Sediment transport modelling

Sediment transport modelling directly affects the bed evolution through the Exner sediment balance equation. Here the temporal bed evolution depends on the horizontal divergence of the sediment transport rate vector. The later is modelled in terms of its intensity and of its direction with respect to the depth-averaged flow field. Uniform sediment size of 1 mm was used in the modelling. The sediment transport in the experiments was bed- load dominated because of the relatively low shields stress conditions (0.072 – 0.16). A *Meyer-Peter and Muller* [1948] type bed load formula was used to model sediment transport. Such general form of Meyer-Peter and Muller bed load transport formula is presented in equation (25).

$$q_s = a\sqrt{\Delta g D_s^3}(\theta - \theta_{cr})^b \qquad (30)$$

where, q_s is the sediment transport per unit width, $m^3/s/m$; $\Delta = (\rho_s - \rho)/\rho$ is the relative sediment density, ρ_s is the density of sediment, kg/m^3, and ρ is the density of water, kg/m^3; D_s is the sediment diameter, m; $\theta = u^2/(C^2 \Delta D_s)$ is the Shields stress, u is the module of the depth-averaged velocity vector, m/s, C is the dimensional Chezy's roughness coefficient, $m^{1/2}/s$; θ_{cr} is the threshold Shields stress for sediment motion (widely used as 0.047); a and b denote coefficients that can be calibrated to match the sediment transport rate observed in a specific situation. The classical Meyer-Peter and Muller bed load formula uses the values of coefficient a, θ_{cr} and b as 8, 0.047 and 3 respectively.

Meyer-Peter and Muller bed load formula has been successively modified [*Hunziker and Jaeggi*, 2002; *Wong and Parker*, 2006; *Huang*, 2010], with different modifications suggest different values of the above coefficients. In the model, the values of coefficient θ_{cr} and c were adopted as 0.047 and 3.2 [*Wong and Parker*, 2006] respectively and the coefficient a was varied to achieve the best matching between the reach progressive averaged sediment transport predicted by the model close with the one observed in the experiments. The results of sediment transport modelling are presented in section 6.3.

Direction of the bed load particles being transported along a sloping bed is affected by the influence of the gravity which acts according to the sloping bed surface [*Ikeda*, 1982]. The local bed slope effect plays an important role in modelling topography of the channel bed. Higher bed slope effect would direct more sediment particles along sloping bed, downwards to the channel, and lower bed slope effect would result in deviating less sediment particles to the channels. Consistently, higher transverse bed slope effects result in smoother bed topography with low amplitude bars [*Defina*, 2003; *Bernini et al.*, 2006; *Nicholas*, 2010]. *Schuurman et al.* [2013] show that modelling channel without transverse bed slope effects yields bed topographies with unrealistic pattern of bars having very steep side slopes. The transverse bed slope effects on the sediment transport direction were used to adjust the amplitude of the bed topography in the numerical model to match with the one observed in the experiments.

The transverse-bed slope effect on the direction of bed-load transport is modelled using *Ikeda* [1982] formulation modified by *van Rijn* [1993], which is presented in equation (27).

$$q_{s,n} = q_s \alpha_{bn} \sqrt{\frac{\theta_{cr}}{\theta}} \frac{\partial z}{\partial y} \quad (31)$$

Where, $q_{s,n}$ is the unit bed load transport component in the lateral direction (m3/s/m); α_{bn} is a calibration parameter; θ_{cr} is the critical Shield's stress; θ is the Shield's stress and $\partial z/\partial y$ is the transverse bed slope. Increasing the value of the α_{bn} coefficient corresponds to increase the transverse bed slope effect on the direction of bed load transport. The α_{bn} coefficient in the *van Rijn* [1993] is equivalent to $r/\sqrt{\theta cr}$ in the *Ikeda* [1982] formulation.

6.2.3 Data analysis methods

To assess the effects of small amplitude width variations on the channel bed development, the evolution of the following features were analysed.

Sediment transport

The reach averaged sediment transport rates observed during the numerical evolution of channel bed were compared with those observed in the experiments. It cannot be expected that the modelled sediment transport rate time series could be entirely compared with that observed in the experiments. Realistically, a closer correspondence can be aimed at between ensemble metrics, rather than instantaneous values of the sediment transport time series. For this reason, a progressive average (herein after "PA") of the sediment transport rate was compared between the numerical model and experiment. The PA sediment transport over a period T was calculated using equation (32).

$$q_s(T) = \frac{1}{T}\int_0^T q_s(t)dt \quad (32)$$

Where, $q_s(T)$ is the progressive averaged sediment transport rate, m^3/s, over the period T; $q_s(t)$ denotes the instantaneous value of the sediment transport rate, m3/s, which varies in time.

Analysis of the progressive averaged sediment transport time series allowed determining if the duration of the experiment and of the simulations were long enough to make an estimate of the average sediment transport rate characterizing each run. The choice of appropriate value of coefficients "a" in the sediment transport formula (equation 3) was also based upon the PA sediment transport rate comparison between the model and the experiment.

Bed topography statistics

The statistical distribution of the bed level was characterised by hypsometric curves. Hypsometric curves are the plot of bed level versus the bed surface area exceeding that value of the bed level. The spatial distribution of the bed level, obtained after removing the reach averaged longitudinal channel bed slope (detrended bed level) was used to compute the hypsometric curves. The areas with higher bed level corresponds to the bars (deposition surface) lumped together and the lower level areas denote the channels are lumped together. The bars are separated from channels by bed level close to zero. Hypsometric curves are commonly used to characterise the morphodynamic developments in tidal systems [e.g. *Marciano et al.,* 2005; *Wang et al.,* 2002]. One of the few cases of their use to characterize fluvial bed topography is reported by *Bertoldi et al.,* [2013].

Harmonic analysis of the bed topography

To assess the effects of amplitude of width variations on bed topography, width was varied at a desired amplitude and wavelength along left bank of the domain. To detect the bar wavelength, a longitudinal section of the channel was obtained close to the banks where the width variations have

been imposed. The reach-averaged channel bed slope was subtracted from such longitudinal bed profile. Harmonic analysis was carried out by performing Fast Fourier Transform (FFT) on the longitudinal section. The amplitude and wavelength of the three most dominating Fourier harmonics were analysed.

Wave length of bars can be one of the criteria to distinguish between the alternate bars resulting from free instability and those resulting from some external forcing. Alternate bars formed by free instability are mostly migrating, except at the resonance conditions where they are theoretically steady. Alternate bars as the result of forced instability are steady. In straight channels, forced alternate bars are also part of the intrinsic response of the system, but they are triggered by a local persistent perturbation of the channel geometry that acts as a forcing term in the longitudinal boundary conditions. Their amplitude in space can be growing (amplifying), decreasing (damping) and constant [*Mosselman et al.*, 2006]. The migrating bars in general are shorter than the steady bars. So, forced alternate bars are in general longer than the free alternate bars [*Blondeaux and Seminara*, 1985; *Lanzoni*, 2000a].

A non dimensional bar wave-length (L_b) was computed as the ratio between the wave-length (L_b*) and width of the channel (W_b). Similarly a non dimensional amplitude (A_b) was computed as the ratio between the bar amplitude (Ab*) and depth of the channel. Relative wave-length ($L_{b,r}$) and amplitude ($A_{b,r}$) were also computed as the ratio of the wave-length and amplitude respectively between the width variation cases and without width variation case. Factors $F = L_b \times A_b$ and $F_r = L_{b,r} \times A_{b,r}$ were computed to assess the effect of width variations on the channel bed topography.

6.2.4 Design of the numerical runs

The scenarios are named broadly based on the width of the channel and the type of width variations used along the banks (Figure 68).

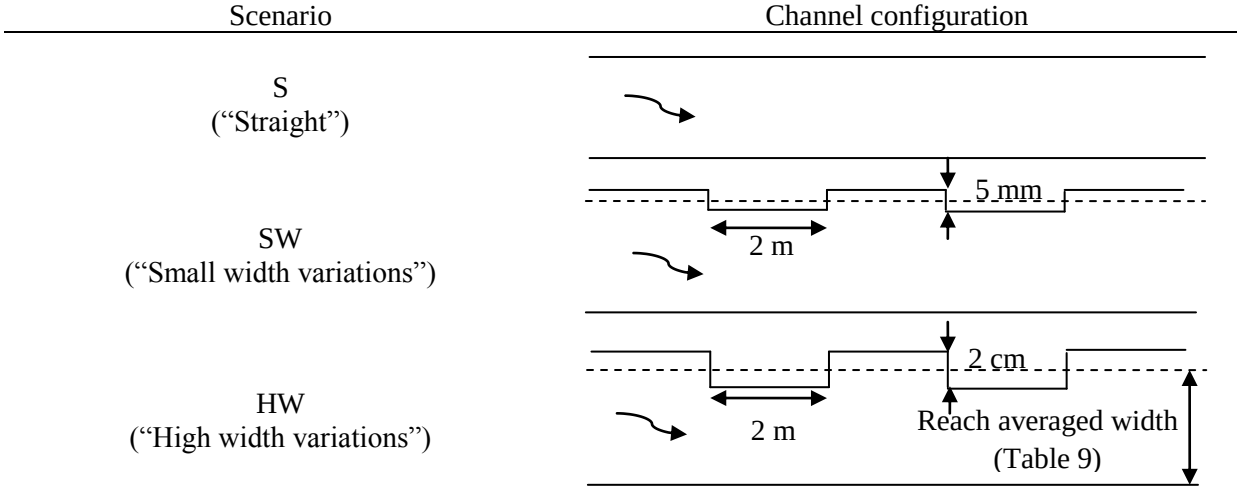

Figure 68. Channel configurations corresponding to different scenarios.

Scenarios S represent test cases in channels without width variations. Scenario Scenarios SW represent test cases with relatively small width variations along the left bank, having an amplitude of 2.5 mm. Scenarios HW were carried out by implementing varying width with an amplitude of 1cm along the left bank. The width was varied in the form of rectangular wave with 2 m wavelength. Suffixes 1, 2 and 3 in each scenario represent the channel width of 0.4, 0.3 and 0.15 m respectively. Scenarios with suffix 2' were also carried out in 0.3 m wide channel but at lower width to depth ratio (higher discharge) compared to scenarios with suffix 2. Scenario S1I was simulated using

experimental conditions of S1 scenario after implementing measured width variations along the banks. Scenario S1G and S1B were both simulated using experimental conditions of S1 scenario after implementing small groyne near upstream and increasing the roughness of narrow strip close to the banks, respectively. Numerical simulations were grouped under 3 major cases based upon the objectives of the simulations.

Effects of small irregular width variations

Two different scenarios were explored to assess the effects of small irregular width variations on the evolution of alternate bars in the flume experiments. Laboratory conditions of experiment-1(Table 8) were used to setup the model. The first scenario (S1) was setup using a reach averaged width of the channel without implementing small amplitude width variations (Figure 68). The second scenario (S1I) was setup by implementing the measured width variations along the bank lines of the channel (Figure 69). Width variations in the experimental channel were irregular with their highest amplitude up to 4% of the channel width. The effects of small irregular width variations on evolution of bed topographies were then assessed by comparing the results of both scenarios with the observed bed evolution in the experiment-1.

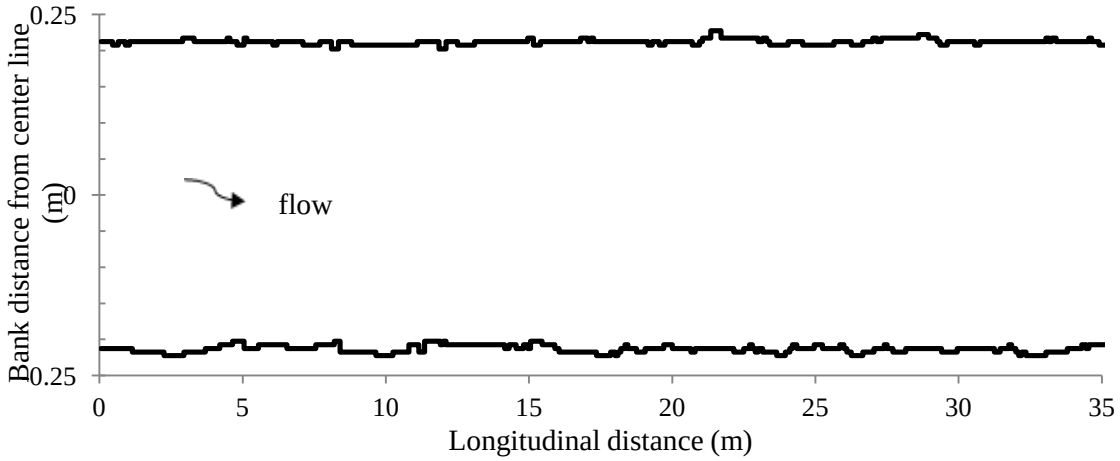

Figure 69. Irregular bank lines implemented in S1I scenario. The vertical scale is distorted on purpose for the sake of better visualization.

Effects of amplitude of width variations on bed topography

The objective of this case was to investigate the effects of different amplitude of width variations on the bed topography at different formative conditions of alternate bars. For each scenario regular width variations in space with amplitude 2.5 mm (SW runs in Table 9) and 5 cm (HW runs in Table 9) were imposed along one of the banks. The width variations were created through an idealized left bank where small-amplitude groyne-like structures having the same amplitude were placed at a regular spacing that corresponded to their longitudinal extension of 2 m (Figure 68). *Wu et al.* [2011] report that the amplitude of the width variations have more influences in the bed topography evolution more than the wavelength. The wave length of such imposed width variations were therefore 4 m in all the scenarios.

Potential parameterization of small amplitude width variations

It may not be convenient to include small amplitude width variations along the banks in the numerical modelling studies. Reach scale modelling is often carried out using larger computational grids for faster computation. In such cases the small amplitude width variations along the banks are at a sub-grid scale. This would require local refinement of grids which may not be desired from the

computational cost and model stability requirement. The parameterization of these variations would help to take into account their effects without geometrically implementing them in the model. Small amplitude width variations can behave as obstructions along the banks or can also be viewed in terms of an increase of the hydraulic roughness within a zone close to the banks. On this line of reasoning, two additional scenarios were investigated in a straight channel without geometrically implementing the small irregular width variations. The first scenario (S1G) was setup implementing one 0.02 m long groyne along the right bank close to the upstream boundary. The second scenario (S1B) was setup by increasing the roughness of a 2 cm wide strip close to the banks arbitrarily by 30%. The effects of obstruction and roughness variations on evolution of alternate bars were then assessed by comparing the results with the bed evolution in S1 scenario and in the lab experiments.

The details of all the numerical runs are presented in Table 9. The scenarios explored cover wide range of width to depth ratio (β) values. The ratio $\beta/\beta_{cr} > 1$ indicates formative conditions of free alternate bars are met. β_{cr} is the critical width-to-depth ratio value required for the formation of free alternate bars in straight channels.

Table 9. Scenarios explored to assess the effects of amplitude of width variation on bed topography

W	Q	D	Amplitude of width variation (A_w x W)				β	β/βcr
(m)	(l/s)	(m)	0	0.0025	0.01	Measured		
0.4	2	0.013	S1, S1G, S1B	SW1	HW1	S1I	30.8	4
0.3	1.5	0.013	S2	SW2	HW2		23.1	3
0.3	2.5	0.023	S2’	SW2’	HW2’		13	2
0.15	2.5	0.028	S3	SW3	HW3		5.4	0.5

6.3 Results

Appropriate parameters of the sediment transport rate formula (equation (25)) had to be selected to model the average sediment transport rate measured in the experiments. The PA sediment transport rate in the model were computed for 300 cross-sections which is represented by grey band in Figure 70. The fluctuation in the sediment transport mainly corresponds to the development of the bars in the model. PA sediment transport rate in the S1 numerical run was modelled close to PA sediment transport rate in experiment using value of coefficient a (equation (25)) as 7 (Figure 70-a).

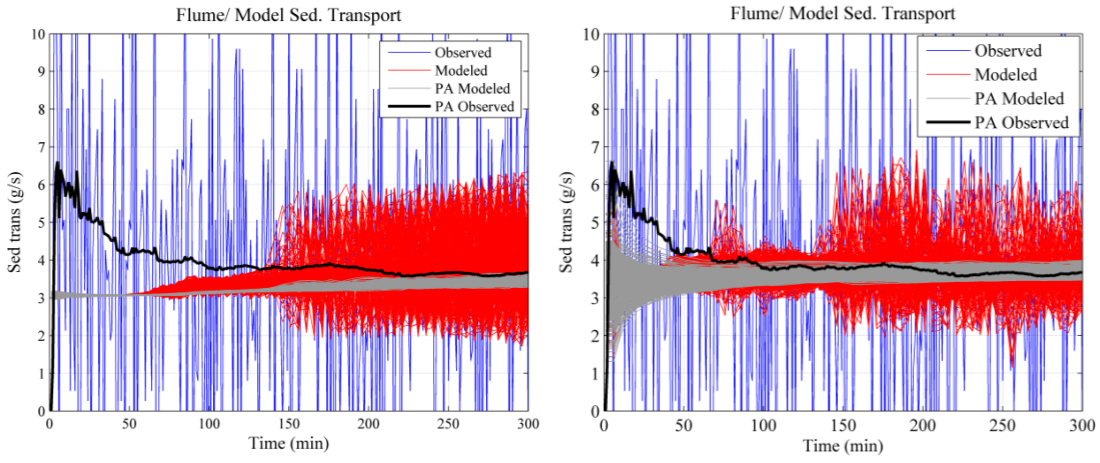

a) b)

Figure 70. PA sediment transport observed in the experiment compared with PA sediment transport rate in numerical model for a) S1 and b) S1I scenarios.

Using the same value of the coefficient a, after implementing the irregular width variations in scenario S1I, showed lower PA sediment transport rate. So, the value of the coefficient a was increased to 8 in run S1I which resulted in a PA sediment transport rate closer to the experiment (Figure 70-b).

The coefficient α_{bn} in transverse slope effect in the direction of bed-load transport (equation (27)) was adjusted for the modelled amplitude of bars to match at best that in the experiments.

6.3.1 Effect of small amplitude width variations

Bars in the S1 scenario were observed as the result of the free instability caused by flow over the mobile channel bed. The instability was triggered by the random perturbation provided in the channel bed and the flow at the upstream boundary. *Defina* [2003] and *Wu et al.*, [2011] used localised sediment bump to trigger the alternate bars in their models. Random disturbance of ± 1% in the flow rate at the upstream boundary varying both in time and in the lateral direction was used in the model. Such small disturbances were needed to continuously trigger alternate bars at the upstream boundary as the alternate bars continued to move downstream. Without the flow disturbances, the bars at the upstream boundary migrated downstream leaving the bed flat coherently with the convective nature of bar instability [*Federici and Seminara*, 2003] and the bars remained along a small reach close to the downstream boundary. Small disturbance in flow also exist in the flume experiments due to fluctuation in the pumping rates.

Small amplitude mid channel bars first appeared in the upstream part of the domain and started to migrate downstream. As the mid-channel bars continuously migrated downstream, alternate bars suddenly appeared along the remaining part of the flume. The mid channel bars merged to form larger alternate bars which continued to lengthen and migrate downstream. The bars were of diagonal shape with the downstream faces much steeper than the upstream faces (Figure 71-b and Figure 73-a). After two hours of development the bars stopped to lengthen and bars of similar wavelength were observed migrating at a constant celerity in the model. The bar evolution trends were similar to the trends of free alternate bars reported in the literature [e.g. *Defina*, 2003; *Bernini et al.*, 2006]. The wavelengths of bars in the model were almost half of the wavelength of bars observed in the experiments (Figure 73-a). The comparison of the statistical distribution of the bed level also shows that the pools were shallower and the bars were lower in the model compared to the experiment (Figure 74-a).

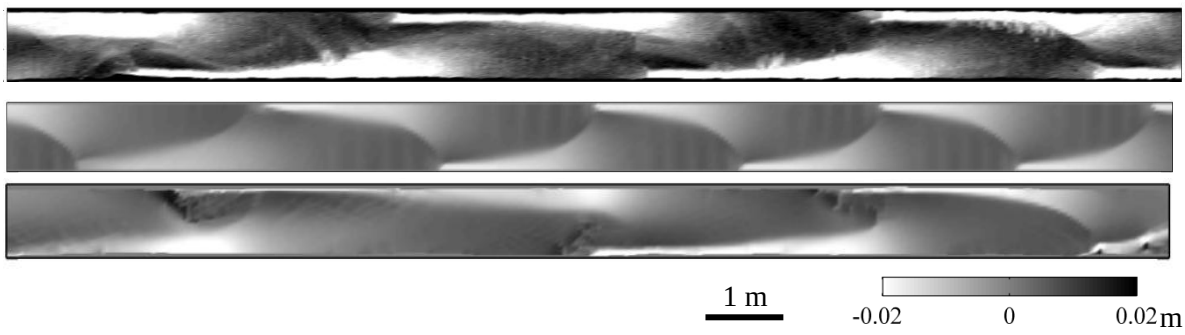

Figure 71. Bed topography in a) flume experiment, b) S1 scenario (straight channel with smooth banks) and c) S1I scenario (actual irregular width variations). Graphic scale represents longitudinal scale. The lateral scale is distorted by factor 2 to show details of topographic variation on later direction.

The early stage evolution trends of the bars in the S1I scenario were similar to the S1 scenario. As the development progressed, the bars became longer and steady starting from the upstream boundary. Evolution of the average wavelengths of the first three dominating Fourier harmonics in longitudinal

sections along left and right banks for scenarios S1 and S1I are presented in Figure 72. The evolution at the initial stage is similar for both scenarios. The evolution-trend started to deviate after half an hour when the wavelength of bars in S1I scenario start to grow longer. Steady bars were observed throughout the domain in S1I scenario after the 4 hours of development. The wave-lengths of the bars at the end of the S1I scenario were much closer to the experiments (Figure 71-c and Figure 73-b) compared to those in the run S1, with smooth banks. Also, bars at the end of run S1 were still migrating, while at the end of run S1I the longer bars were steady. It may be noted that some spikes of deposition are observed on few bar tops (Figure 73-b). Such spikes might be due to the numerical instability caused by the occurrence of trans-critical flow when bars start to emerge and dry, as also reported by *Verbruggen* [2012].

The comparison of statistical distribution of the bed topography (Figure 74-b) shows that the areas of bars and pools were modelled reasonably well compared to the experiments using the value of α_{bn} = 0.5. Pools in the model were still shallower. Figure 74 also highlights that the comparison between numerical and experimental bed topography distribution is improved when the small amplitude width variations are accounted for in the computational domain.

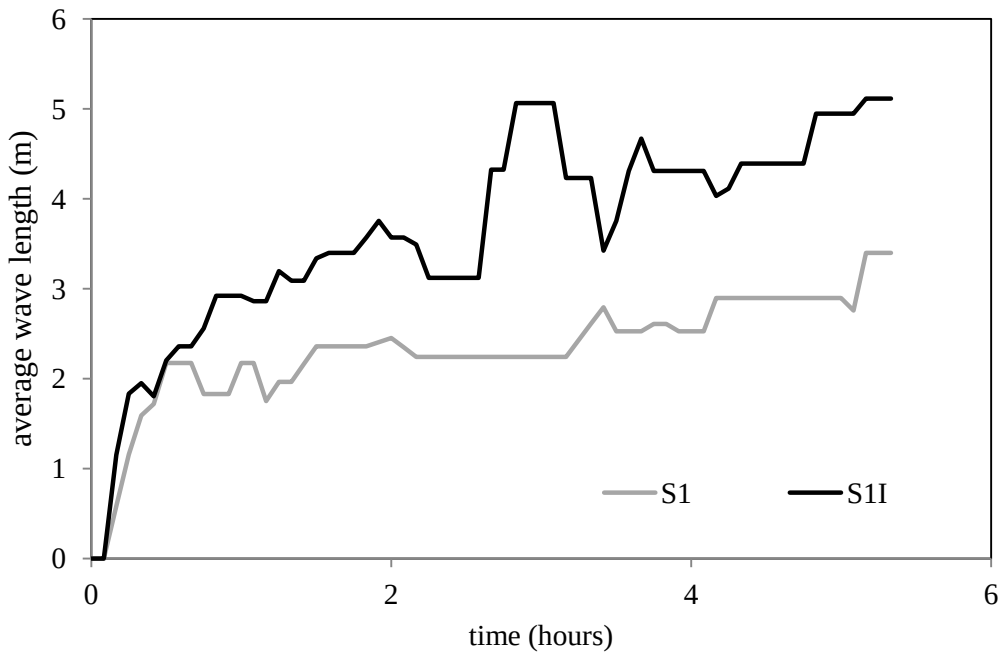

Figure 72. Evolution of average wavelength of the three most dominating Fourier harmonics in longitudinal section along left and right banks for a) S1 scenario (straight channel with smooth banks) and b) S1I scenario (actual irregular width variations).

b)

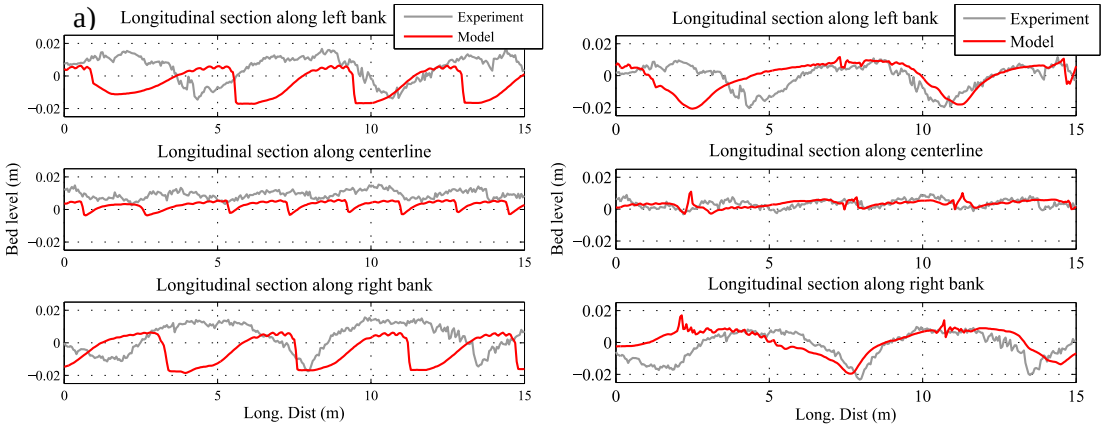

Figure 73. Longitudinal section along the left bank, center and right bank of the bed topography obtained in the model compared with flume experiment for a) S1 (without width variation) and b) S1I scenarios (actual irregular width variations)

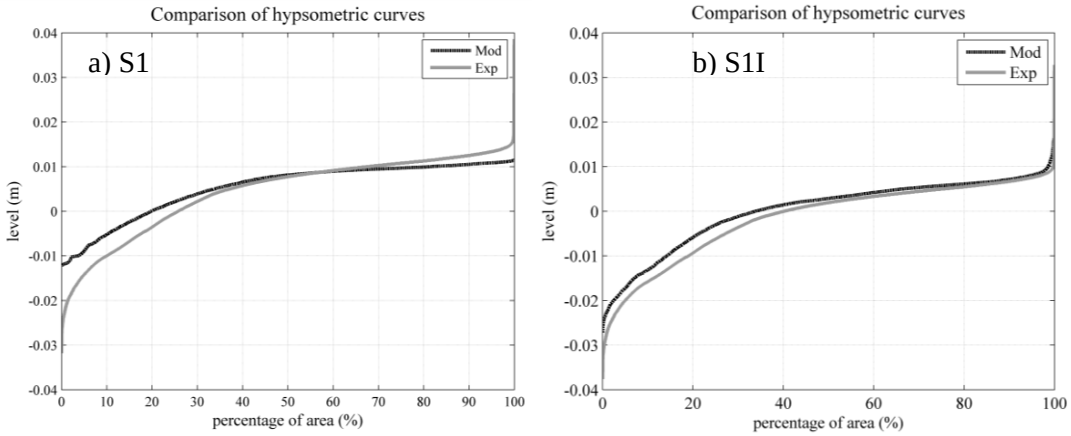

Figure 74. Bed elevation distribution in numerical model compared with the bed elevation distribution in the laboratory experiment: a) S1 scenario (without width variation) and b) S1I scenario (actual irregular width variations).

6.3.2 Effects of amplitude of width variations on bed topography

Effects of amplitude of width variations were determined by performing harmonics analysis of the longitudinal section of the channel bed close to the banks with varying width. The bed topography in scenario "S" is developed as the free instability and is referred as free scenario. Scenarios S3 and S2' did not develop alternate bars. Width to depth ratio (β) in scenario S3 was lower than the critical width to depth ratio required for the bar formation ($\beta/\beta_{cr} < 1$). Bedform waves with wavelength much smaller than the channel width were observed along the channel bed (Figure 76). Width to depth ratio in scenario S2' was higher than the critical width to depth ratio required for the bar formation (β/βcr = 2). Bedform wave with dominating longitudinal wavelength of 6.7 m was observed along the channel bed (Figure 76) but with negligible amplitude (Figure 77). Bars with wavelength of 1.5 m were observed in the laboratory experiments at similar settings. Bars might have been suppressed in the model due to the additional diffusion induced by numerical schemes. *Verbruggen et al.*[2012] also reported that the numerical model predicted higher value of resonance width to depth ratio (β_r) than analytical theory which they attribute to the numerical diffusion present in the model. Scenario S1 and S2 developed alternate bars with dominating longitudinal wavelengths 2.86m and 3.33 m, respectively.

Longitudinal wavelengths as well as the amplitude of the bed forms were different in scenarios SW and HW compared to S scenario (free scenario). So a factor F was computed as the product of dimensionless wave length (L_b) and dimensionless amplitude (A_b) of the Fourier harmonics to analyse the combined effects of the width variations. The amplitude of first 3 dominating harmonics in most of the cases had a small difference. So an average of factor F was computed for the first 3 dominating Fourier harmonics (Figure 77). Similarly average of the relative factor Fr was computed with respect to respective free scenarios for the first 3 dominating harmonics (Figure 78).

The width variation amplitude is 2.5 mm in all SW scenarios. The non-dimensional width variation amplitude (A_w) varies due to the channel-width difference among different scenarios (Figure 75). SW4 and SW1 have the highest and lowest A_w respectively. The dominating longitudinal wavelength is 5 m in both SW1 and SW2 scenarios which is significantly longer compared to S1 and S2 scenarios. Both F and relative F_r are higher in SW2 scenario compared to SW1 scenario. This might be because SW2 scenario as higher non dimensional amplitude of width variation (A_w) compared to SW1 scenario.

The dominating longitudinal wavelength in SW2' scenario is 1.8 m which is similar to half the wavelength of the imposed width variation. The decrease in F and F_r in SW2' scenario was observed because the magnitude of the decrease in the longitudinal wavelengths of bedforms were greater than the increase in their amplitudes, compared to the S2' scenario. The dominating longitudinal wavelength, F and F_r have increased in the SW3 scenario compared to S3 scenario.

Scenarios HW had higher amplitude of width variations compared to SW scenarios. The dominating longitudinal wavelengths in both HW1 and HW2 scenarios are 5 m which are similar to SW1 and SW2 scenarios. Similarly the dominating longitudinal wavelengths in both HW2' and HW3 scenarios are 1.8 m which is close to half the wavelength of the imposed width variations. All HW scenarios show increase in F and F_r compared to SW scenarios because A_w is higher in HW scenarios. The F_r decreases with the increase in β/β_{cr} ratio among HW scenarios. The effect of width variations is observed higher in the scenarios with higher A_w.

S1	SW1			HW1			4
S2		SW2			HW2		3
S2'		SW2'			HW2'		2
S3			SW3			HW3	0.5
0	0.006	0.008	0.017	0.025	0.033	0.067	

A_w

β/β_c

Figure 75. Diagram illustrating the simulated combinations of the relative amplitude of width variations A_w and the width-to-depth ratio β relative to the critical value for free bar instability β_c. The run IDs are reported for the sake of clarity (see also Table 9).

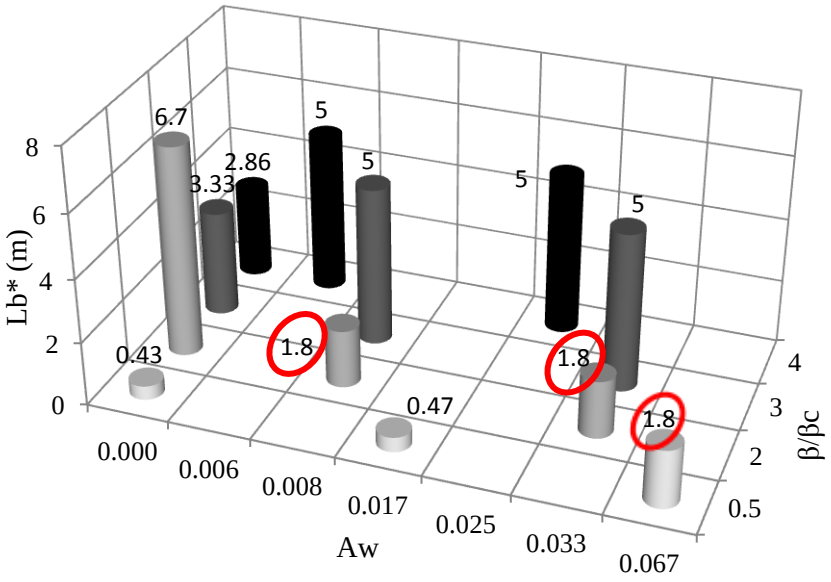

Figure 76. First dominating longitudinal wavelength in channel in different experimental condition and amplitude of width variations. Circled values are close to the half of wavelength of imposed width variations.

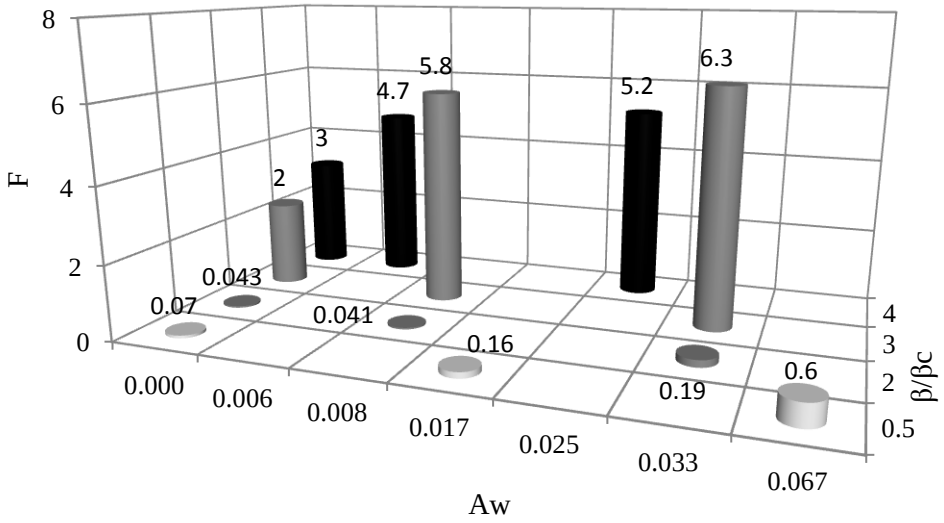

Figure 77. Average Product of Ab and Lb (F) of the 3 highest dominating harmonics in the channel bed along longitudinal direction at different experimental conditions and amplitude of width variations

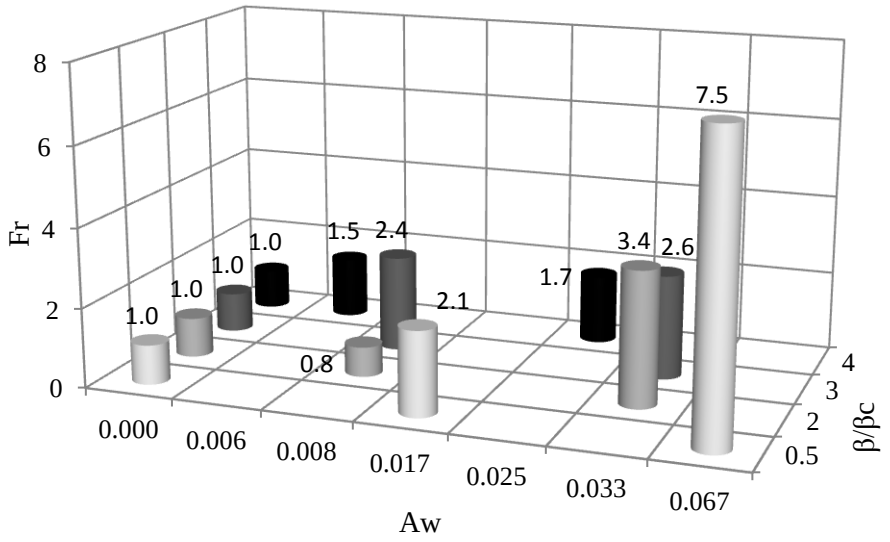

Figure 78. Average Product of relative Ab and relative Lb (F_r) of the 3 highest dominating harmonics in the channel bed along longitudinal direction at different experimental conditions and amplitude of width variations

6.3.3 Parameterization of the small amplitude width variations

In S1G scenario bar first appeared just downstream of the small groyne. The width of the bar was equal to the length of the groyne (0.02 m). Development of the first bar triggered the development of free bars within the domain which migrated in the downstream direction. The bars started to become longer and steady starting from the upstream boundary. After 4 hours the entire domain contained steady alternate bars. The PA sediment transport rate (Figure 79-a) and the wave-length of the alternate bars were similar to the experiment (Figure 80-b). The statistical distribution of the bed topography (Figure 81) shows that the area of the bars are well represented in the model however the area of the pools are much shallower compared to the experiments.

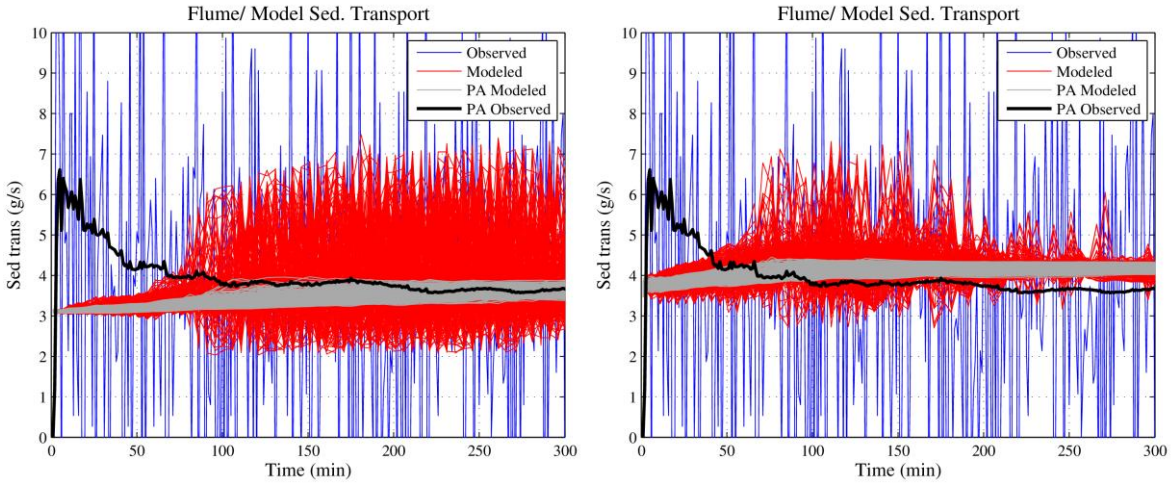

Figure 79. PA sediment transport observed in the experiment compared with PA sediment transport rate in numerical model for a) S1G and b) S1B scenarios.

Free bars in S1B scenario were triggered by the small flow variations at the upstream boundary. The bars formed near the upstream boundary further triggered free alternate bars within the domain. The

bars grew in amplitude and length as they migrated in downstream direction. The bars close to the upstream boundary stopped elongating and migrating and developed into steady bars. The development of the steady bars moved further downstream of the domain. After 4 hours steady bars were observed along the entire domain. The sediment transport in the model was observed slightly higher than the experiments (Figure 79-b). The wave-length of the bars were observed shorter than the experiments but 50% longer than the bars in S1 scenario (Figure 80-c). The comparison of the statistical distribution of the bed topography shows that the highest areas of the bars were predicted higher and the area of the pools shallower compared to the experiment (Figure 81).

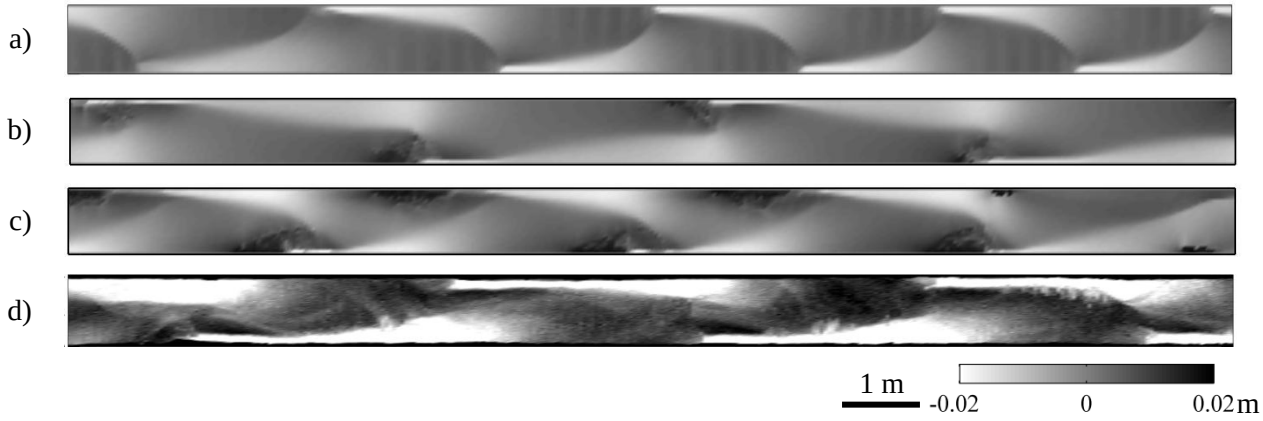

Figure 80. Bed topography in a) S1, b) S1G, c) S1B scenarios; and d) laboratory experiments. Flow is from left to right. Graphic scale represents longitudinal scale. The lateral scale is distorted by factor 2 to show details of topographic variation on later direction.

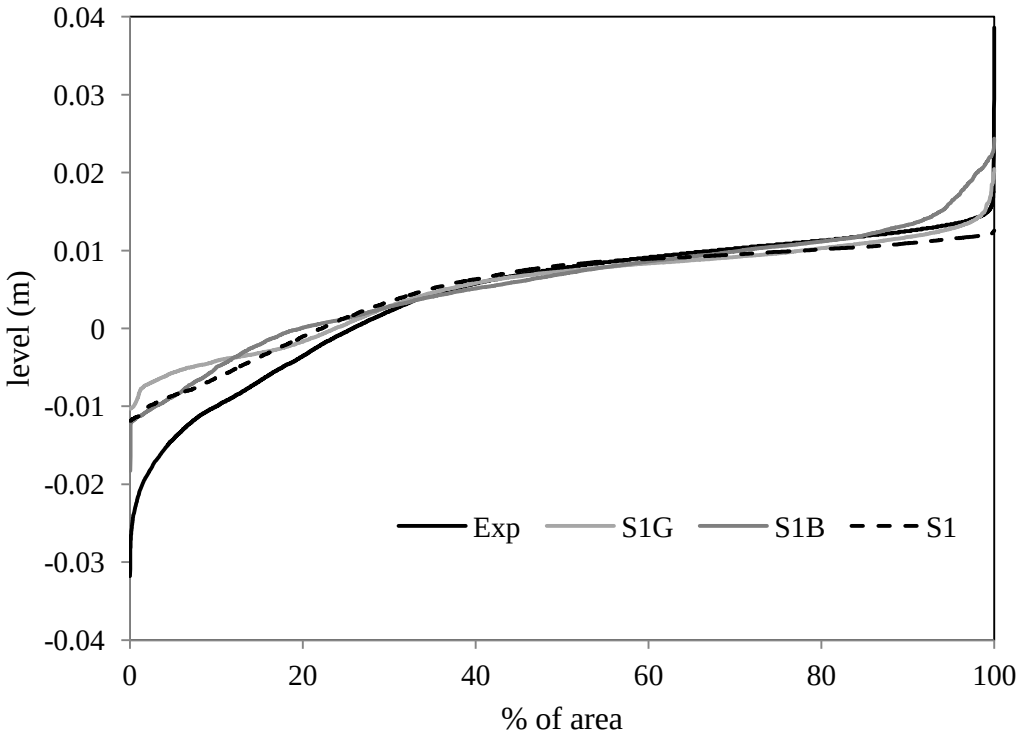

Figure 81. Statistical distribution of channel bed elevation in scenarios S1G, S1B compared with scenario S1 and the experiment

6.4 Summary of results

Alternate bars observed in the laboratory experiments of *Garcia Lugo et al.* [2015] were reproduced using a 2D-depth-averaged morphodynamic model. The first step in numerical modeling of alternate bars involved the choice of roughness values to model the flow field with reasonable accuracy. In the absence of flow depth measurements in the experiments, the value of the roughness coefficient was estimated through an alternative, indirect method based on the comparison of of dry areas measured in the experiments and simulated with the hydraulic model under conditions of the fixed bed geometry measured at the end of the experiment. The second step involved calibration of the sediment transport rate predictor to achieve a reasonable reproduction of the sediment transport measured in the experiment. The final step involved adjusting the coefficient of transverse bed slope effects on the direction of the bed load transport to accurately model the amplitude of the bed forms in the experiments.

The channel in the experiments had small amplitude width variations (amplitude less than 4% of channel width) whose effects were never analyzed previously and that was initially assumed to have a negligible effect. In a first attempt alternate bars were modeled using constant reach-averaged channel width. Despite the reasonable choice of the roughness parameter value and modeling the average sediment transport rate, the properties of alternate bars in the model were unexpectedly different compared the experiments. Bars in the numerical model were much shorter (half of the observed wavelength) and had steep downstream slope compared to those in experiments. They were migrating in the downstream direction. In the second approach, the actual, small-amplitude width variations present in the experiment were implemented in the numerical model. Alternate bars developed in the second simulations set were steady and longer compared to those in the first approach. However with the same sediment transport formula, the sediment transport rate were modeled 25% less in the second approach. This suggested that the sediment transport rate is higher in channels with migrating alternate bars compared to the channels with steady alternate bars. The coefficient in the sediment transport predictor had to be increased to model the sediment transport rate closer to that observed in the experiment. The length and amplitude of the alternate bars were modeled similar to the experiments. Although the width varied in small amplitudes (less than 4% of channel width), it was sufficient to accelerate the development of steady alternate bars whose wavelength and amplitude were similar to the bars in the experiment. This suggested that, despite appearing as "small" the irregular width variations might provide a forcing effect able to affect the dynamics of the free migrating bars and to promote a markedly different morphological development of the river bed. It was therefore necessary to investigate more systematically the effect of such width oscillations by isolating the role of their amplitude, symmetry and also to understand to which extent they could be viewed as an additional near-bank roughness in a numerical model.

To study the effects of amplitude of width variations on bed topography, several scenarios were then explored by implementing varying amplitude of regular, idealized width variations along one bank of the channel, keeping their wavelength constant. Channel width-to-depth ratios were varied to study the effects on scenarios with characterized by the presence of morphodynamic instability of "free" alternate bars. The results show that the amplitude of width variations as small as 0.6 % is sufficient to influence the alternate bar characteristics and to produce "hybrid" bar patterns between purely free and forced. They increased wavelength and amplitude of the alternate bars compared to the free alternate bars. The effects were stronger when the amplitude of the width variations was increased. In the channels without alternate bars, the width variations forced bed forms with wavelengths similar to half the wavelengths of width variations.

The possibility of parameterising the effects of small amplitude width variations in the numerical model were explored by two additional scenarios: i) increasing the near-bank roughness and ii) implementing a small obstruction along the banks. Despite adopting the arbitrary values of increased roughness of the cells closer to the banks, steady bars were observed in the model. Wavelength of the bars were shorter compared to the experiment. The bars were represented higher and the channels were represented shallower. Similarly implementing a small groyne, equal to 5% of the channel width, near the upstream boundary also accelerated the development of steady bars in the model. The wavelengths of alternate bars were observed longer and similar to the experiment. Bars in the model were represented similar to the experiment but the channels were represented shallower. It is concluded that the effect of spatially distributed, irregular width variations can be to a certain extent captured also by parameterizing them in the form of increased roughness close to the banks or as small obstructions along the banks.

Despite alternate bars being widely studied, this study presents one of few cases where alternate bars observed in the specific experiments are reproduced using numerical. To reproduce alternate bars in the experiments the model was calibrated on different morphological processes that were measured by direct or indirect methods during the measurement. This allowed us to adjust the parameters in the numerical model in a controlled and structured manner. Modelling also required realistic information on the lateral banks which contained small amplitude oscillations. The statistical comparison of the bed level distribution allowed validation of the evolved topography in both longitudinal and lateral directions. Previous studies for instance, *Defina* [2003] used experimental data of *Lanzoni* [2000a] to qualitatively compare the evolution trend. Their objectives were to rather explore evolution trend of alternate bars using numerical model, otherwise studied conducting laboratory experiments, and assess the sensitivity of the parameters and initial conditions in bar evolution. *Jang and Shimizu* [2005b] and *Wu et al.*[2011] show examples of bars in numerical models in fair agreement with experimental observations, comapring the longitudinal and cross-sectional profiles. This study strengthens their findings by reproducing the three-dimensional topographic features as well as the sediment transport transport rate in good agreement with those observed in the experiments.

7 CONCLUSIONS AND DISCUSSIONS

A self-formed river flowing through an alluvium adapts its width, depth and slope based on hydrological conditions, sediment characteristics, riparian vegetation and bank material [*Parker et al.*, 2007]. The flow over alluvial beds at higher width to depth causes morphodynamic instability, resulting in bars which scale with the cross-section of the river [*Tubino et al.*, 1999; *Colombini and Stocchino*, 2012]. Bars are largest of the bedforms which strongly interact with the width during the planimetric evolution of the river.

The practical and engineering interest on stable cross-section of alluvial channels has attracted a considerable amount of research since late 19th century [*Kennedy*, 1895]. Much of the research has focused in development of the width predictor methods mostly based on empirical approaches and methods based on extremal hypothesis and to lesser extent on mechanistic methods. In past two decades, research has advanced in development of models including geotechnical as well as fluvial processes to simulate bank failure mechanism more accurately. Despite significant development on the width predictors, research in controls on width evolution of channel cannot still be considered a fully settled issue. The effect of spatial width variability on river bars has mainly been based on assessing the role of such planform forcing effect to the bed topography, both in case of straight and meandering river channels. The amplitude of with variability has been related to fundamental questions as those behind the transition between single- and multi-thread river morphologies, and most studies consider regular spatial variations of the channel width. The limits of what can actually be considered a "planform forcing" effect, or has instead a too small variability have never been clarified, as well as its role on the resulting channel morphodynamics. For instance, the effects of small amplitude width variations on straight channels, which may be due to imperfect bank lines or protrusion due to vegetations, on morphodynamics of river bed has been neglected so far.

The first aim of the thesis is to analyse the effects of controlling factors on the channel evolution of bed-load dominated river focusing on the channel width. The investigations were carried out by conducting laboratory experiments (Chapter 3), analytical modelling (Chapter 4) and numerical modelling (Chapter 5).

The second aim of the thesis is to analyse the effects of small width variation on the morphodynamics response of the channel bed focusing on alternate bars. The investigations were carried out using two dimensional fully non-linear numerical model.

Based on the research outcomes following conclusions can be drawn:

7.1 Conclusions

Hydro-morphological controls on reach-averaged evolution of alluvial channel geometry

Regarding the effects of the initial channel width, the results from the experiments have shown that the long-term equilibrium channel widths were independent of the initial channel width in the experiments with constant discharge and without upstream sediment supply. The experiments starting from narrower initial width first widened during the early stage followed by narrowing and the experiments starting from wider initial width narrowed by bed incision, all eventually resulting in similar long-term equilibrium width. Similar trends were observed in the numerical simulations starting from narrower channels carried in a shorter domain.

The results from both numerical modelling (Chapter 5) and laboratory experiments (Chapter 3) have shown that the width evolution is affected by the initial channel width in the scenarios with constant discharge and upstream sediment supply. The channel starting from the narrowest initial channel resulted in the widest and the most aggraded channels. The equilibrium amount of sediment supplied from the upstream allowed the channel bed to remain aggraded. Though these scenarios could not be investigated for long-term in the experiments but the initial development trends are in line with the results of the numerical model.

Results from laboratory experiments have shown that at similar variable discharge regimes without sediment supply, the experiments starting from a wider channel resulted in wider channels compared to the ones starting from the narrower channels. However, in the scenarios with similar variable discharge with sediment supply, numerical model results show that channels starting from narrower initial width eventually results in wider channels. These scenarios could not be investigated for long-term in the experiments but the initial development trends are in agreement with the results of the numerical model.

Regarding the effects of discharge regimes, all flow regimes explored supplied same volume of water in the experiments during each cycle. Results from experiments carried out without upstream sediment supply show that the channels evolved at variable discharge are wider compared to those formed at constant discharge. Channels with higher amplitude of flow variability resulted in the largest final width in the experiments starting from narrower initial conditions. The trend of evolution of same sets of experiments computed by analytical model show similar results. In the experiments starting from wider initial channel, the evolution at variable discharge was different from that of channel starting from narrower initial channel. For instance, channels evolved under variable discharges with similar low discharge resulted in similar channel widths. Results from numerical modelling have shown in the scenarios starting from narrower initial channel at variable discharge with sediment supply, channels are obtained wider with higher amplitude of flow variations.

Effects of small width variations on the bed morphodynamics of alluvial channels

Alternate bars observed in the laboratory experiments were reproduced on the numerical model reasonably well at a similar time scale. This required accounting for the presence of small amplitude width variations along the banks. The first step of the modelling involved the choice of reasonable roughness value. The second step involved implementing the minor width variations measured along the banks of the experiments (< 4% of channel width) which were not initially expected to play a relevant control. The third step involved calibrating the sediment transport formula based on the sediment transport rate exiting the flume. The final step involved the choice of appropriate coefficient to adjust the transverse bed slope effects on the sediment transport direction. Results from the numerical modelling have shown that small width variations present along the banks of the experiments accelerated the development of steady bars in the flume experiments. The sediment transport rate is greatly affected by the type of bed forms. At similar flow and sediment characteristics, channels with migrating alternate bars transport more sediment than the channels with steady alternate bars.

Further investigation shows that even small width variations, less than 0.6% of the channel width is sufficient to develop steady bars in the channels. The width variations, though very small, provide a continuous forcing which interact with the free bars in the channel bed to eventually result in steady bars which are longer than the free bars. The effects are more dominating for the scenarios with width to depth ratio closer to critical width to depth ratio. In the scenario of weak instability or below the

formative conditions of bars, the width variations impose bed forms. The effects of width variation increase with the increase in amplitude of width variations.

7.2 Discussion and recommendation

Hydro-morphological controls of reach-averaged evolution of alluvial channel geometry

The Shields stress during the initial conditions of uniform flow experiments, computed using median grain size, ranged between 0.05 and 0.1. These values of Shields stress corresponding to median grain size of sediment at bank full conditions are common in gravel bed rivers [*Garcia*, 1999]. The natural sand-bed rivers usually have Shields stresses an order of magnitude higher than those observed in gravel-bed rivers. The bed and banks of the experimental channels were composed of the same non-cohesive material. So the banks and the bed had same degree of erodibility. In most natural gravel-bed rivers, the bank materials differ from the to the material forming the bed. The bank material may contain fine cohesive sediment or composite layers of different materials which make them less erodible compared to the channel bed [*Hey and Thorne*, 1986; *Leyland et al.*, 2015]. In addition, in real rivers the presence of vegetation greatly influences the erodibility of the banks [*Rinaldi and Darby*, 2007]. So, the channel in our experiments would correspond to natural gravel-bed rivers with bed and banks composed of similar materials and without riparian vegetation. Such conditions are commonly found in pro-glacial streams [*Chew and Ashmore*, 2001] The aim is however, not to reproduce any specific type of river but to study channel evolution processes considering it as 1:1 scale experiments. Numerical simulations were also carried out at the initial Shields stress equal to 0.09.

The size of the laboratory experiments imposed several restrictions during the investigation. The experiments especially with the sediment feed could not be carried out for a longer period of time. The reach of the channel is shorter and can be easily influenced by the processes at the upstream and the downstream boundary. The experiments carried out on a larger experimental flume might allow investigation on channel evolution at longer time scale with less effects from the imperfections at the boundaries.

Laboratory experiments were conducted using non-uniform sediment. Sediment of uniform size was used in the numerical model. Processes like armouring, selective transport occurring in the non-uniform sediment might have effects on the channel evolution in the experiments which were not represented in the numerical model. *Sun et al.* [2015] show that bed armouring near the banks influence the width evolution of a braided channel. Numerical modelling with graded sediments could allow reproducing processes similar to those observed in the experiments.

Bars were observed in the experiments which played an important role in the channel evolution. Channel widening occurred at higher rate in the experiments with sediment feed because of the growth of bars in the channels. Channel narrowing occurred at higher rate in the experiments starting with wide channels due to channel incision along the deeper parts leaving area of the bars dry. Bars did not form in the channels in the numerical model. So the channel narrowing in the numerical model occurs by lowering entire bed level. On the other hand lack of bars in the model resulted in symmetric widening of the channel caused by bank erosion on both banks. The numerical modelling in scenarios allowing bar developments could allow simulating incision and bank erosion process closer to those in the experiments.

A constant water level corresponding normal flow depth of a discharge in an initial channel was provided at the downstream boundary. The widening of the channel causes decrease in the water level

in the channel. The fixed water level induces a back water effect in the channel. The back water will affect longer reach close to the downstream boundary in the scenario starting from narrower initial channel. The influence of the back water effect can be avoided using a longer domain. The use of small grid cells to simulate bank erosion process is already computationally expensive. Increasing the length of the domain will tremendously increase the computational time making the long-term investigation on channel evolution practically not feasible. Numerical modelling allowing flow depth at the downstream boundary would allow having better results at lower computational cost.

Results from the analytical model suggest that the channel width in the variable discharge conditions can be represented by using constant discharge corresponding to the peak flow conditions. The model is based on simplified physical processes so the experimental and numerical investigations can explain the validity of the findings and shed light on the representation of the non-uniform discharge with a uniform discharge.

Effects of small width variations on the bed morphodynamics of alluvial channels

Results from the numerical model show that bank irregularities accelerate the development of non migrating bars suggesting that they have affected the dynamics of alternate bars in the experiments. The two dimensional numerical model used for the investigation in the framework of this study does not model the sub grid scale phenomena like turbulence (although the diffusion due to turbulence is taken into account). Very often eddies occur near the disturbances causing flow separation and smoothening the effect of disturbances. Numerical modeling including the modeling turbulence structure in the flow field would further improve the understanding on the effects of small amplitude width variations. A flume experiment under similar conditions but with constant width (straights banks) would also verify the findings from this study.

The numerical investigation also suggest that increasing roughness close to the banks and implementing small obstruction along the bank can simulate the steady bars with properties closer to those observed in the experiments. The roughness value was arbitrarily chosen so the investigation varying the roughness values could verify if the small width variations could be represented in the model increasing the roughness close to the banks. The small width variations may act as the forcing equivalent to small groynes distributed along the space. The investigations implementing several small groynes along the channels can improve the understanding on the effects of the small width variations on channel bed topography.

The effects of width variations were investigated by imposing a width variation of certain amplitude and wave length along one of the banks of the channel. Investigations were carried out in the channels with different width. The use of similar amplitude of width variation resulted in different relative amplitude of width variations, with respect to the channel width, among different scenarios. This caused difficulty in the analysis since both relative amplitude of width variations and width to depth ratio were varying among the scenarios. The investigations at similar relative amplitude of width variation among the scenarios can allow better understanding.

List of Symbols

a and b	Coefficients
B_b	Bottom width of the channel
C	Chezy's roughness coefficient
D	Sediment diameter
$D_{i,0}$ / $D_{i+1,0}$	Initial depth of the channel at adjacent cross-section i/ cross-section i+1 (m)
D_i / D_{i+1}	Depth of the channel at adjacent cross-section i/ cross-section i+1after time T (m)
D_s	Sediment diameter (mm)
D90	90^{th} percentile sediment diameter
E	Error of the estimation of net volume of the sediment (%)
E_{spir}	Calibration parameter weighing the intensity of spiral flow motion
F_s,bed,i	Relative volume of the sediments reworked in the channel bed within the sub-reach i (%)
F_s,bank,i	Relative volume of the sediments reworked from the channel banks within the sub-reach i (%)
g	Acceleration due to gravity (m/s^2)
h	Local water depth (m)
H	Average flow depth (m)
k_s	Roughness height
L_i	Longitudinal distance between cross-section i/ cross-section i+1 (m)
L_x	Length of the reach
M	Absolute weight of dry sand
M_r	Relative weight
M_T	Weight of basket at time T (kg)
M_{T+1}	Weight of the basket at time T+1(kg)
n	Manning's roughness coefficient
n_r	Exponents and coefficient in the formulation of dimensional roughness coefficient
n_k	Coefficient
N	Number of sub reaches
q_s	Sediment transport per unit width
$q_{s,n}$	Unit bed load transport component in the lateral direction ($m^3/s/m$)
q_{bx}	Sediment transport rate in bed along longitudinal directions
q_{sx}	Sediment transport rate in side slopes along longitudinal directions
$q_s(t)$	Instantaneous value of the sediment transport rate (m^3/s)
$q_s(T)$	Progressive averaged sediment transport rate (m^3/s)
$q_{s,n}$	Bed load transport on lateral direction ($m^3/s/m$);
Q	Discharge (l/s)
Q_s	Sediment transport rate (kg/ min)
r	Coefficient weighing the sediment transport in side slopes in the transverse direction
S	Longitudinal bed slope
S_s	Side slope of the channel
u	Module of the depth-averaged velocity vector (m/s)
u	Depth averaged velocity in stream wise (x) direction
u	Depth-averaged velocity (m/s)
U	Mean flow velocity in the cross-section
v	Depth averaged velocity in stream transverse (y) direction
V	Voltage (volts)
V_t	Transversal mean velocity along side walls
$w_{s,i}$	Net change of sediment in cross-section i (kg)
W	Width of the channel (m)
$W_{i,0}$ /$W_{i+1,0}$	Initial width of the channel at adjacent cross-section i/ cross-section i+1 (m)

W_i / W_{i+1}	Width of the channel at adjacent cross-section i/ cross-section i+1, after time T (m)
W_s	Computed total net change of sediment in flume (kg)
$W_{s,obs}$	Weight of the sediment collected at the downstream end of the flume (kg)
z	distance (m)
α_{bn}	Calibration parameter
α_r	Coefficient in the formulation of dimensional roughness coefficient
α_τ	Corrected angle of bed shear stress with respect to the direction of depth averaged velocity
β	Flow width to depth ratio in the channel
βcr	Critical value of the flow width to depth ratio required for the instability of free bars
$\partial z/\partial y$	Transverse bed slope
Δ	Relative sediment density
κ	Von Karman's constant
$\bar{\eta}_b$	Reach averaged bed level of the channel
η t	Top level of the channel
θ	Shield's stress
θ_b	Shields stress in channel bed
θ_{cr}	Critical Shield's stress
θ_s	Shields stress in side slopes
ρ_s	Density of sediment (kg/m^3)
ρ	Density of water (kg)
$\hat{q}_{syb}$	Sediment transport rate in the side slope integrated between y_w and y_b
ΔT	Time interval (min)
$\Delta V_{s,i}$	Total change of the sediment volume in a sub-reach i (m)
$\Delta V_{s,bank,i}$	Total change of the sediment volume in a sub-reach contributed by channel banks (m)
$\Delta V_{s,bed,i}$	Total change of the sediment volume in a sub-reach contributed by channel bed (m)

APPENDIX A

A-1 Pump calibration

Pump calibration was performed to derive pumping rate with respect to the frequency of the current provided to the pump. Following steps were carried out to calibrate the pump:

Step 1: Pumping rate is determined by the head difference between the pump inlet and the pump outlet. The inlet level was fixed by maintaining the water level in the bucket at the downstream end of the flow by providing a overflow and continous supply of discharge into the bucket. The pump outlet was fixed at a level at the upstream part of the flume. Same pump inlet and outlet level were used in all of the experiments carried out.

Step 2: Sand from the flume was emptied to carry out pump calibration in a fixed bed.

Step 3: A known frequency of the current was supplied to the pump and the pump was started. The pump supplied discharge from the bucket at the downstream end of the flume to the inlet of the flume. After 5 minutes of pumping, a bucket with volume marked at 10 litres was used to collect discharge exiting the flume. The time required to fill the bucket upto 10 liters mark was noted. The procedure was repeated two more times and average time was computed. The pumping rate was computed by dividing the volume collected (10 litres) by average time.

Step 4: The current frequency was varied increasing by 2.5 Hz and the procedures in step 3 were repeated for each increament.

Step 5: The pumping rate was plotted against current frequency. A best fit curve was obtained from the scattered plot. The equation of the best fit curved defined the relation between the pumping rate and the current frequency.

Table A-1 Pump calibration

SN	Freqency	vol (l)	time (s)				Discharge (l/s)			
			t1	t2	t3	t avg	Q1	Q2	Q3	Qavg
1	15	10	50.25	49.16	52.39	50.6	0.20	0.20	0.19	0.20
2	17.5	10	34.43	34.52	34.57	34.50667	0.29	0.29	0.29	0.29
3	20	10	27.72	27.64	27.6	27.65333	0.36	0.36	0.36	0.36
4	22.5	10	22.52	22.29	21.76	22.19	0.44	0.45	0.46	0.45
5	25	10	20.63	20.54	20.99	20.72	0.48	0.49	0.48	0.48
6	30	10	16.77	17.13	17.07	16.99	0.60	0.58	0.59	0.59
7	35	10	13.69	14.38	14.42	14.16333	0.73	0.70	0.69	0.71
8	40	10	13.04	13.03	13.25	13.10667	0.77	0.77	0.75	0.76
9	45	10	11.96	12.26	12.33	12.18333	0.84	0.82	0.81	0.82
10	50	10	12.16	12.09	11.89	12.04667	0.82	0.83	0.84	0.83

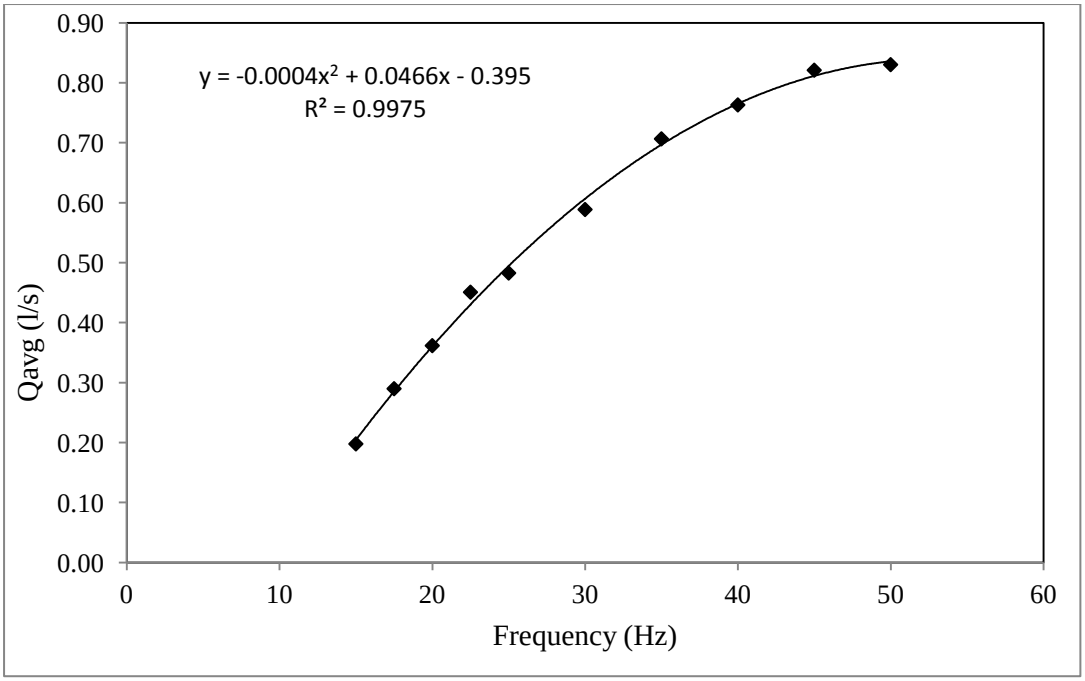

Figure A-1 Average pumping rate plotted against supplied frequency.

The relationship between the pumping rate (Q) and the supplied current frequency (F) is obtained as:

$Q = -0.00043883F^2 + 0{,}0466F - 0.395$

A-2 Sediment weighing calibration

A weighing sensor was used to weigh the collected sediment in the basket. The output of the weighing sensor is in voltage. A voltage weight relation has to be determined to convert the voltage data into weight. The relation was obtained as follows:

Step 1: The weighing sensor was connected to the voltmeter and the measuring voltage was set at 0.5 V.
Step 2: A known weight was hung on the weight sensor and the voltage reading was noted.
Step 3: The weight was increased by adding known weight and the voltage reading was noted.
Step 3: The weight was plotted against output voltage. A best fit curve was obtained from the scattered plot. The equation of the best fit curved defined the relation between the weight and the voltage output.

Table A-2 Weighing machine callibration

Weight (g)	Voltage (V)
1891	756.4
1972	788.8
3863	1545.2
4863	1945.2

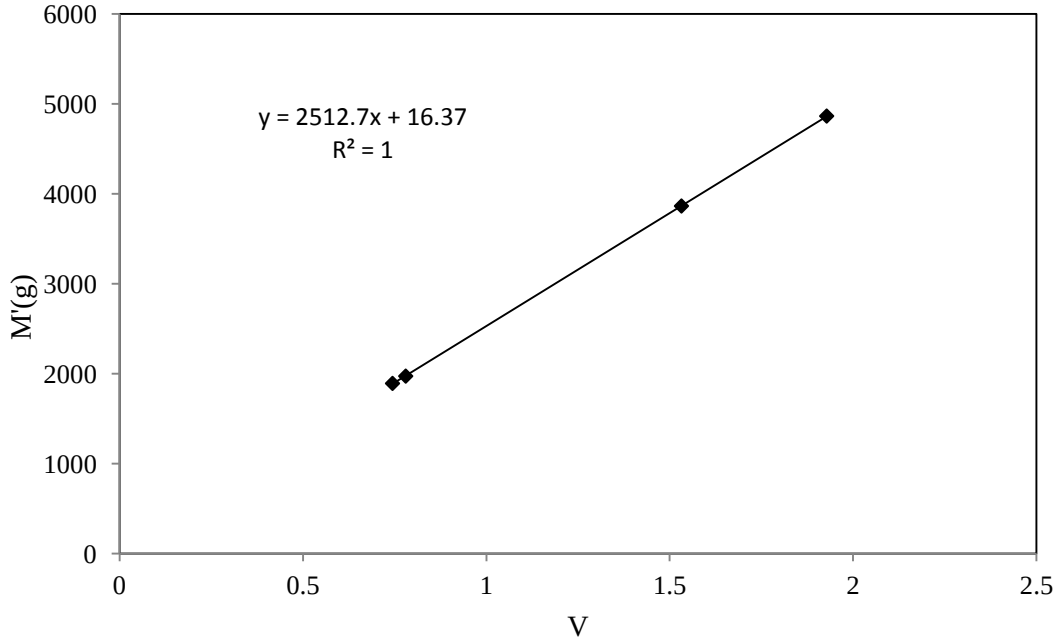

Figure A-2 Average pumping rate plotted against supplied frequency.

The relationship between weight (M) and voltage (V) was obtained as:

$M_r = (2512.7V + 16.37)/1000$

Weight of the sediments measured in the experiments are the submerged weight of the sediment. The absolute weight was computed as:

$$M = M_r \frac{2635}{1635}$$

Where M = Absolute weight of dry sand (kg), M_r = Relative weight (kg), V = Volts (V)

The temporal variation of the weight is affected by noises due to the turbulence in the bucket caused by the overflowing water. Due to the noise the recorded cumulative weight signal shows frequent reduction in value at short time interval, even progressing forward in time. So, a low pass filter was used to remove the high frequency noise from the temporal weight signal. The sediment transport rate is then computed from the filtered signal as follows.

$$Q_s = \frac{M_T - M_{T+1}}{\Delta T}$$

Where,

ΔT = the time interval (min), M_T = weight of basket at time T (kg), M_{T+1} = weight of the basket at time T+1(kg) and Q_s = sediment transport rate (kg/ min).

The low pass filter is still not able to reduce the noise completely from the weight signal. The sediment transport rate computed at very small interval (in the order of seconds) would still result,

unrealistic, negative sediment transport rate. So sediment transport rate is computed per minute time interval avoids the negative values in the sediment transport rate.

A-3 Width computation

The temporal evolution of the channel width was computed from the images captured by the video camera. The images of uniform flow experiment were extracted at the interval of 30 minutes from the start of the experiments. Whereas, images of non-uniform discharge experiments were extracted at the end of each low and high flow stages. Width was then extracted from the images using Arc GIS 9.1 as follows:

Step 1: Images were geo-referenced assigning the known coordinates of the control points installed within the flume.

Step 2: The right bank and left bank of the wet part of the channel were digitized

Step 3: The center line of the channel was traced as the midpoint between the left and the right bank of the channel

Step 4: Cross-section line perpendicular to the center line of the channel was drawn every 20 cm from the inlet of the flume

Step 5: The distance between the intersection point of the perpendicular line at the left and the right bank is defined as the width of the channel at that cross-section.

Step 6: The width of the channel was then averaged within a reach between 1m and 4 m from the inlet of the flume to obtain a reach averaged width from the image.

Step 7: The relative change in width was then computed by subtracting with the initial width of the channel.

A-4 Width evolution

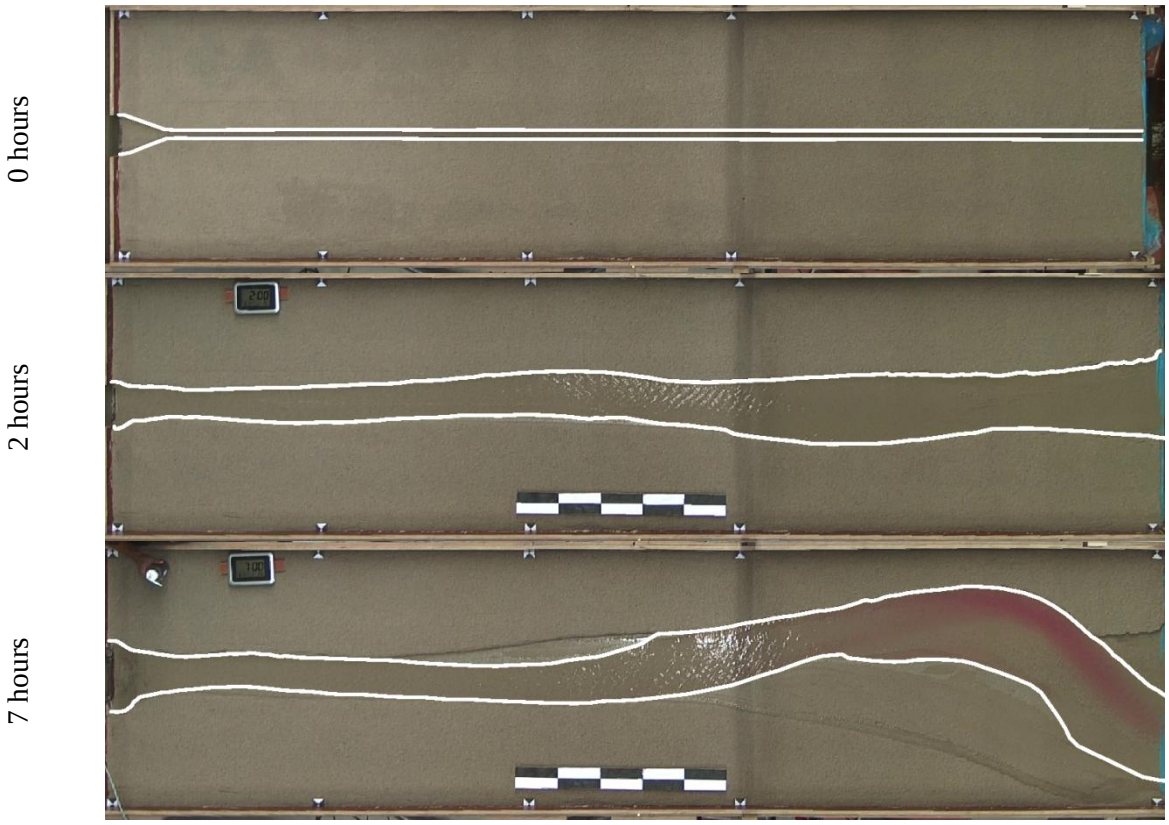

Figure A-4.1 Width evolution in UNI-0.04 scenario after 2 hours and 7 hours

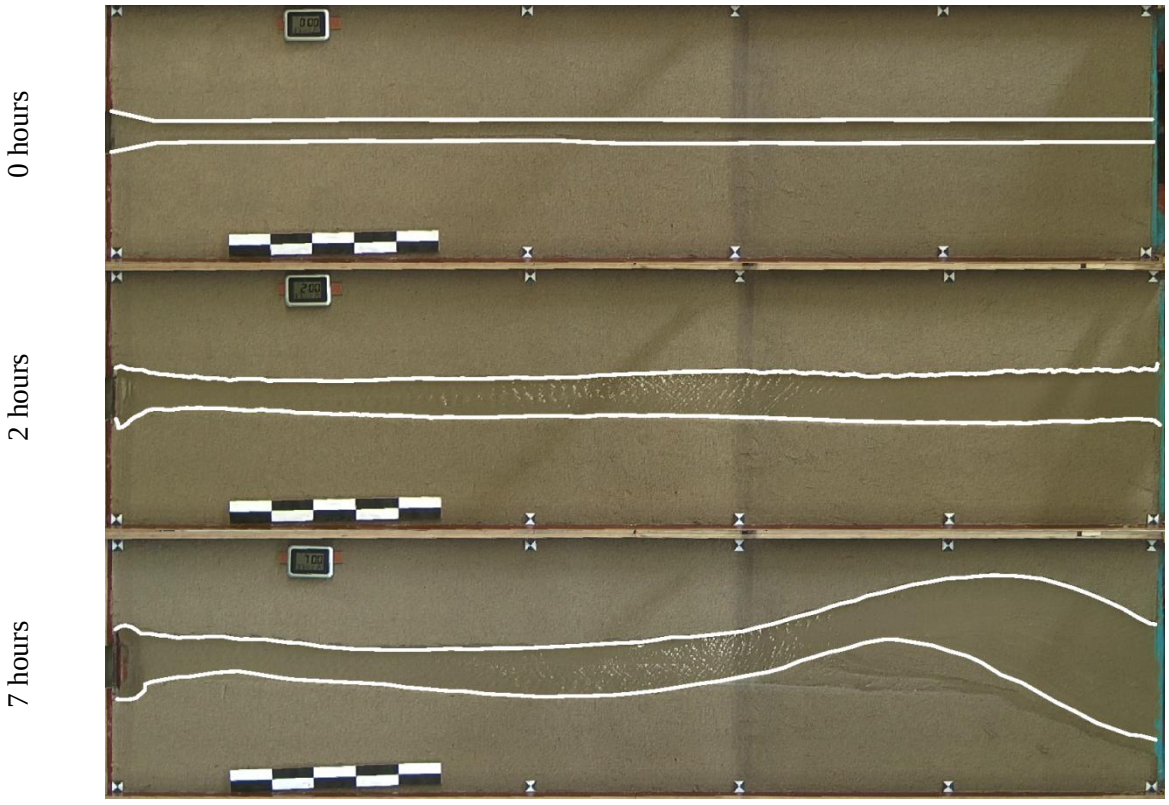

Figure A-4.2 Width evolution in UNI-0.1 scenario after 2 hours and 7 hours

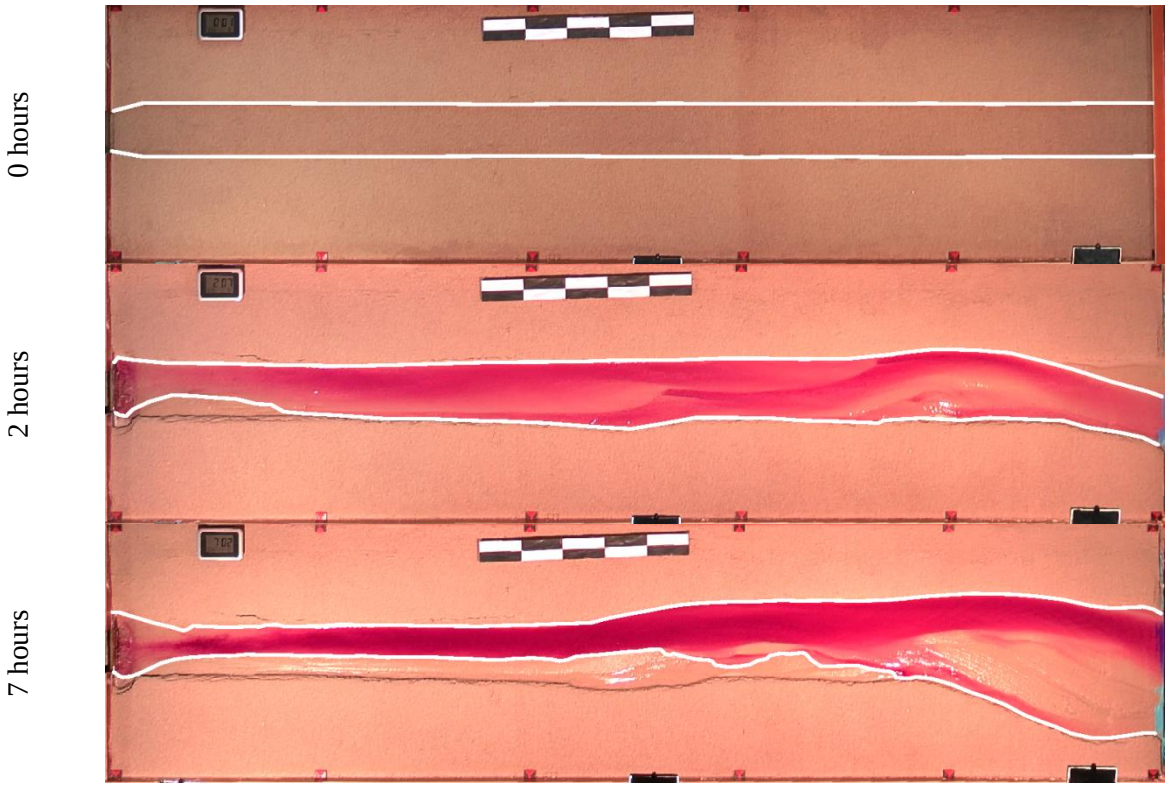

Figure A-4.3 Width evolution in UNI-0.25 scenario after 2 hours and 7 hours

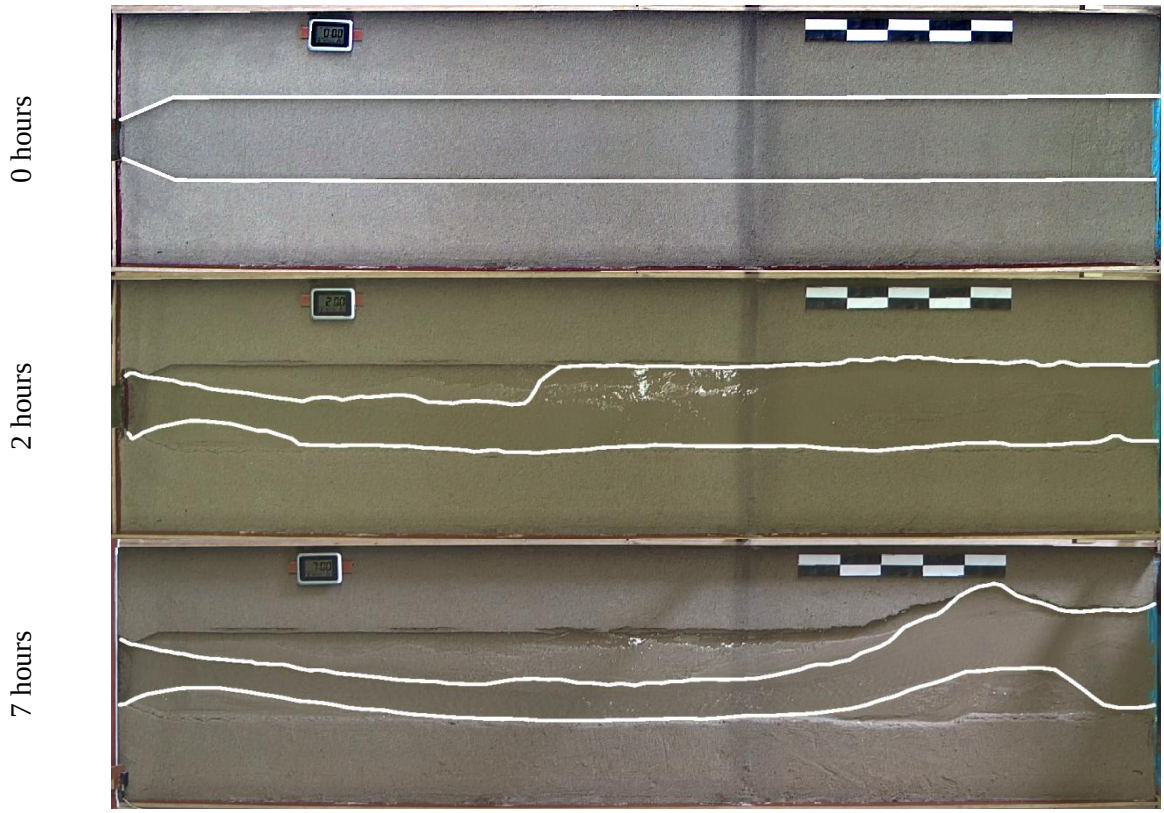

Figure A-4.4 Width evolution in UNI-0.4 scenario after 2 hours and 7 hours

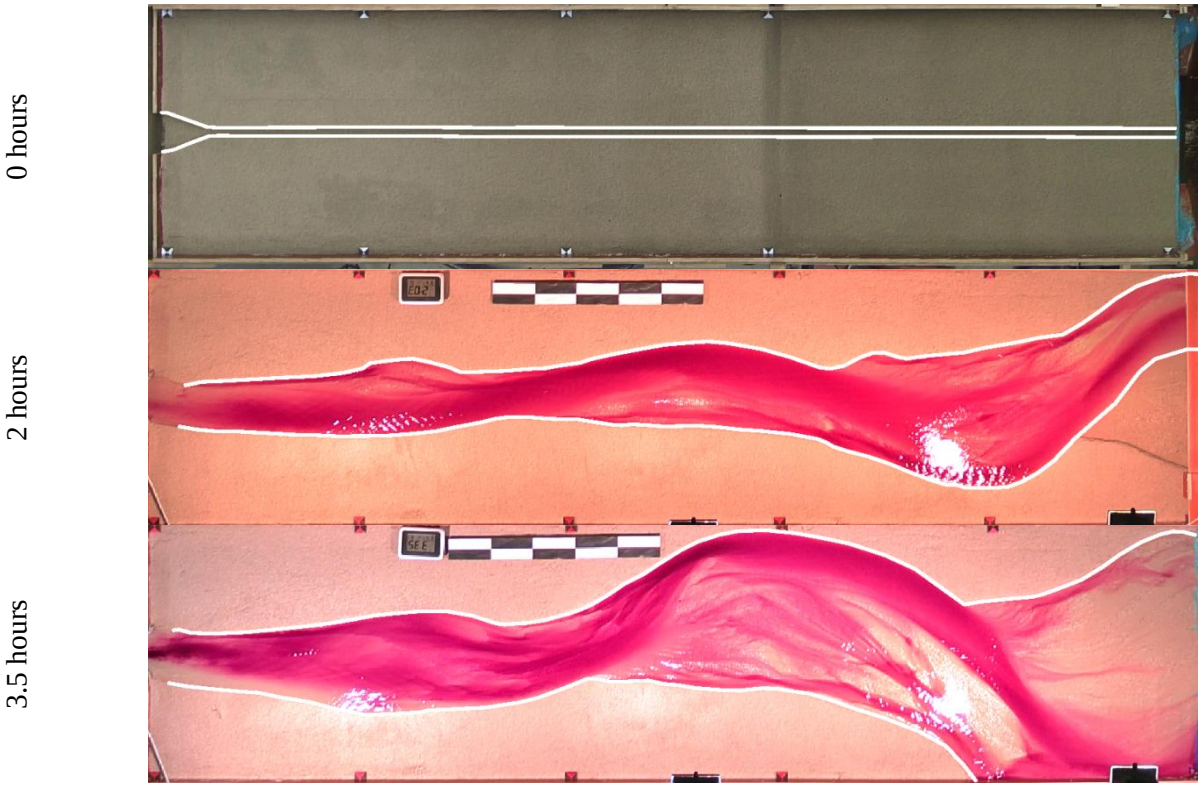

Figure A-4.5 Width evolution in UNI-0.04* scenario after 2 hours and 3.5 hours

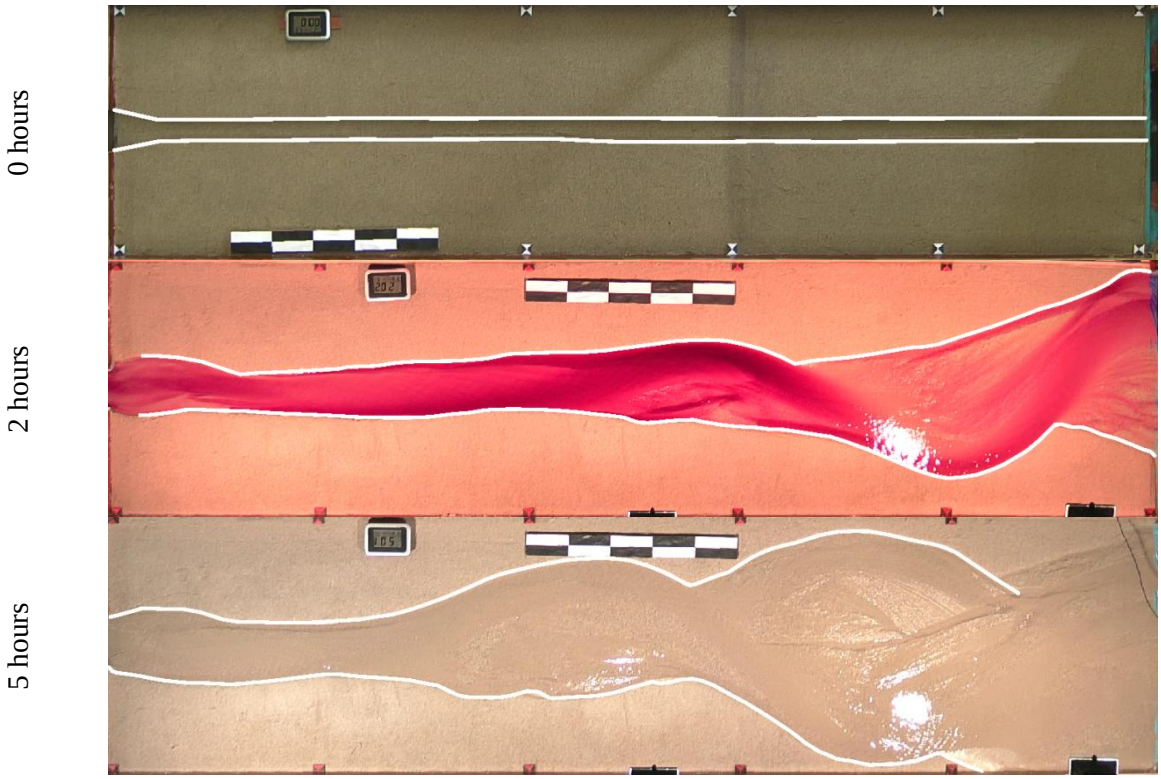

Figure A-4.6 Width evolution in UNI-0.1* scenario after 2 hours and 5 hours

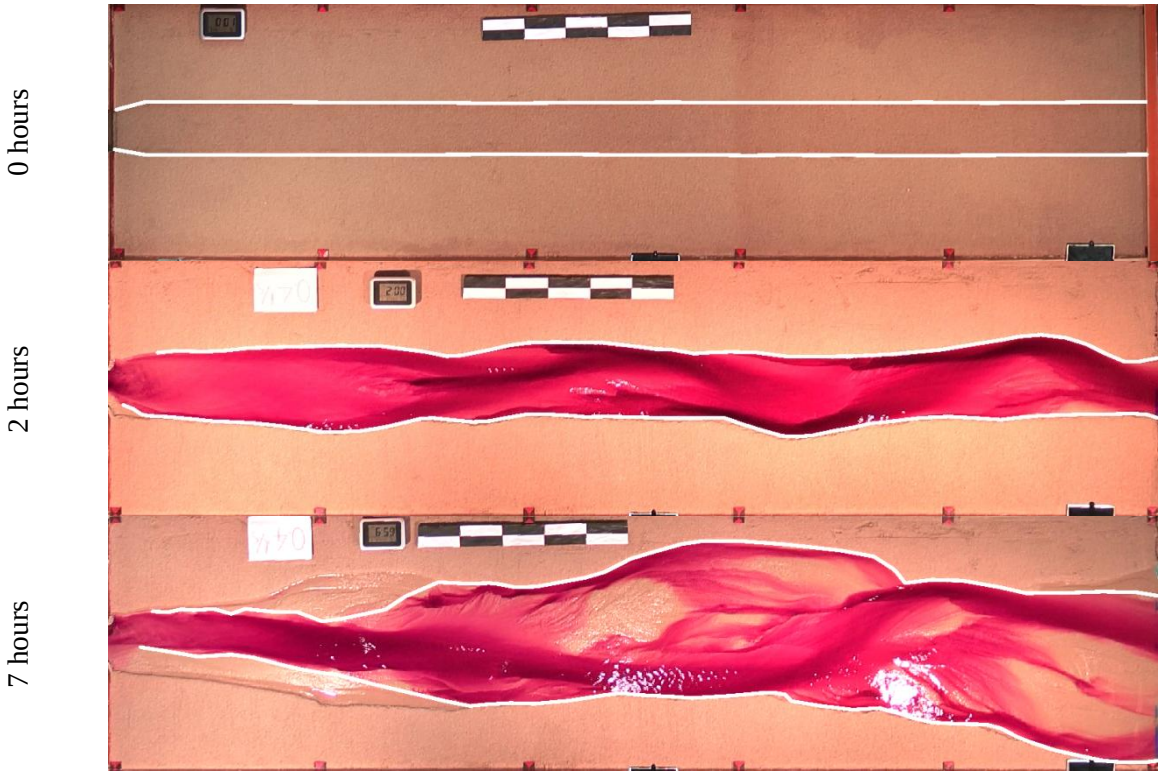

Figure A-4.7 Width evolution in UNI-0.25* scenario after 2 hours and 7 hours

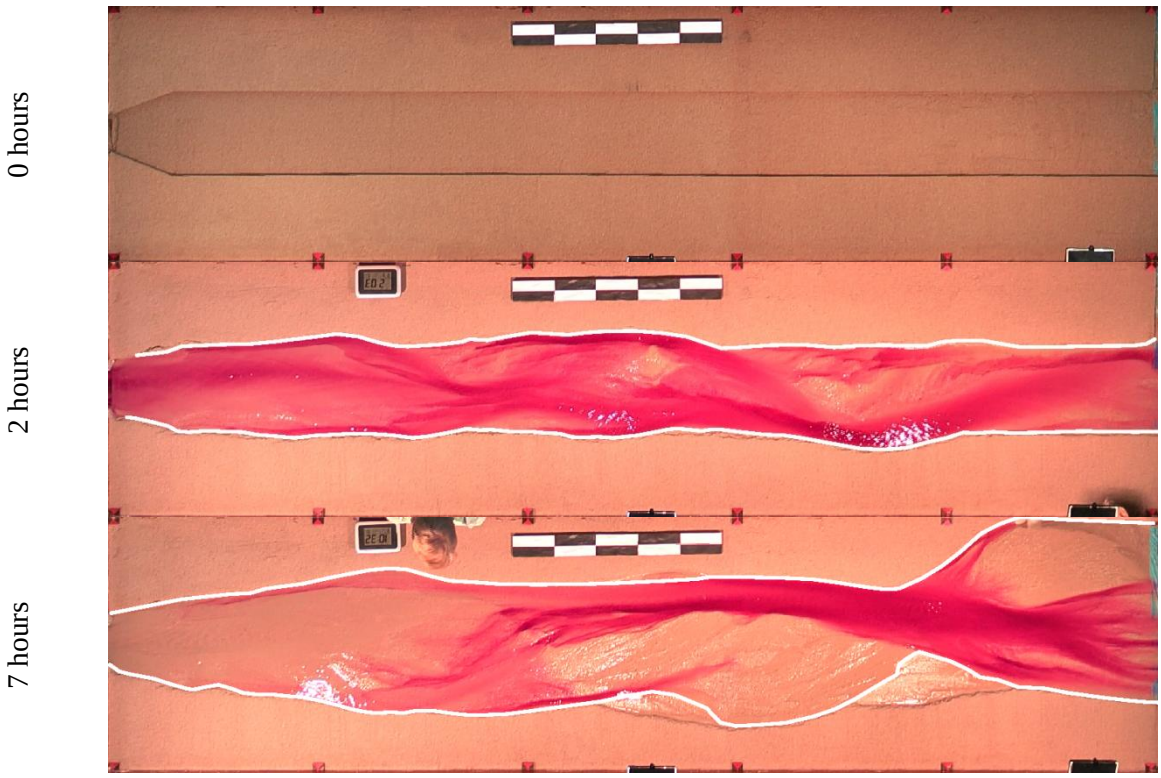

Figure A-4.8 Width evolution in UNI-0.4* scenario after 2 hours and 7 hours

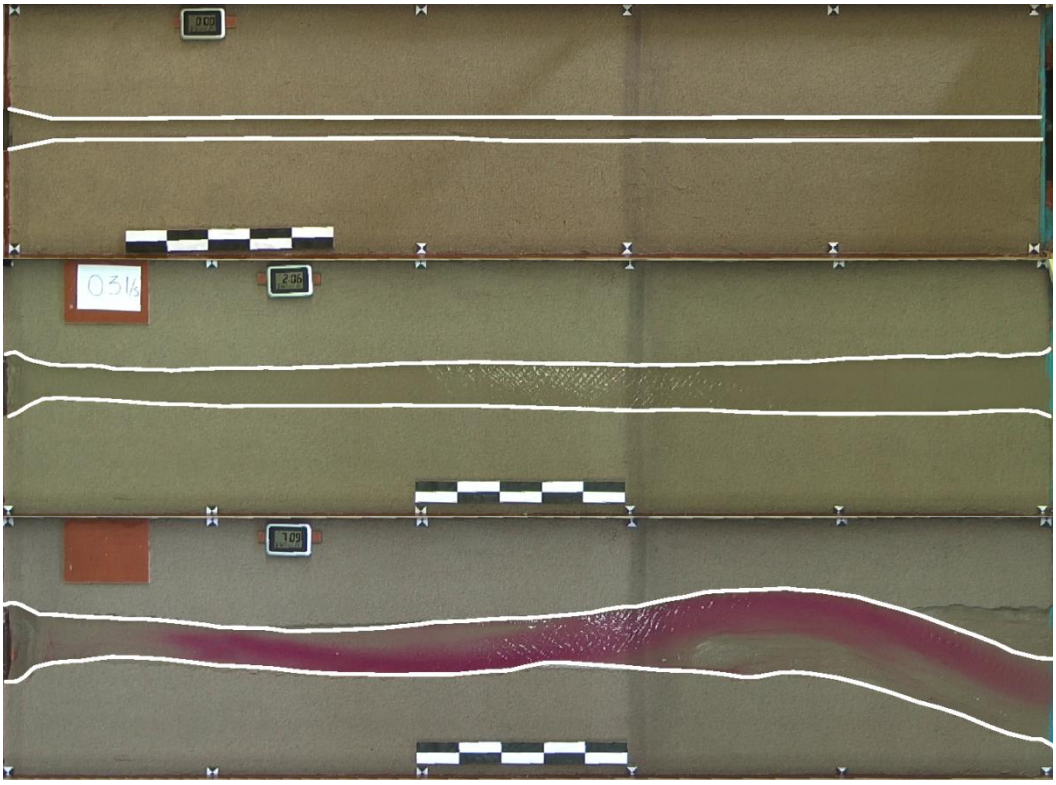

Figure A-4.9 Width evolution in H1-0.1 scenario after 2 hours and 7 hours

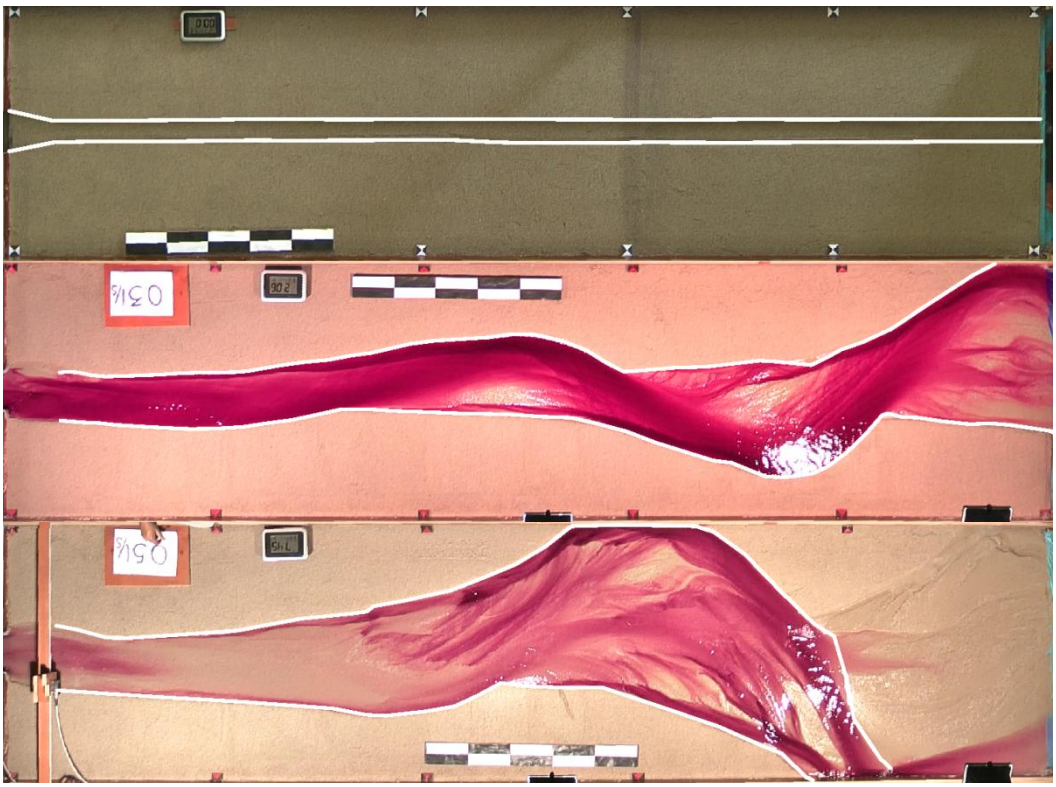

Figure A-4.10 Width evolution in H1-0.1* scenario after 2 hours and 5 hours

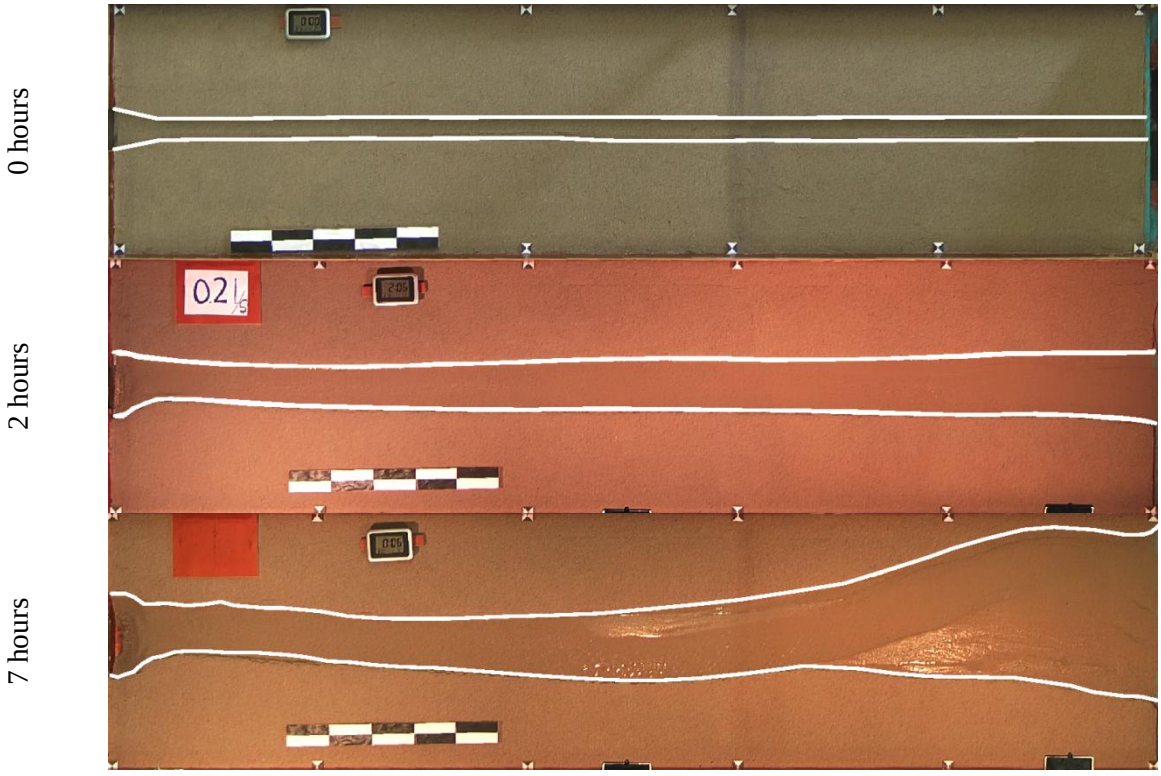

Figure A-4.11 Width evolution in H2-0.1 scenario after 2 hours and 7 hours

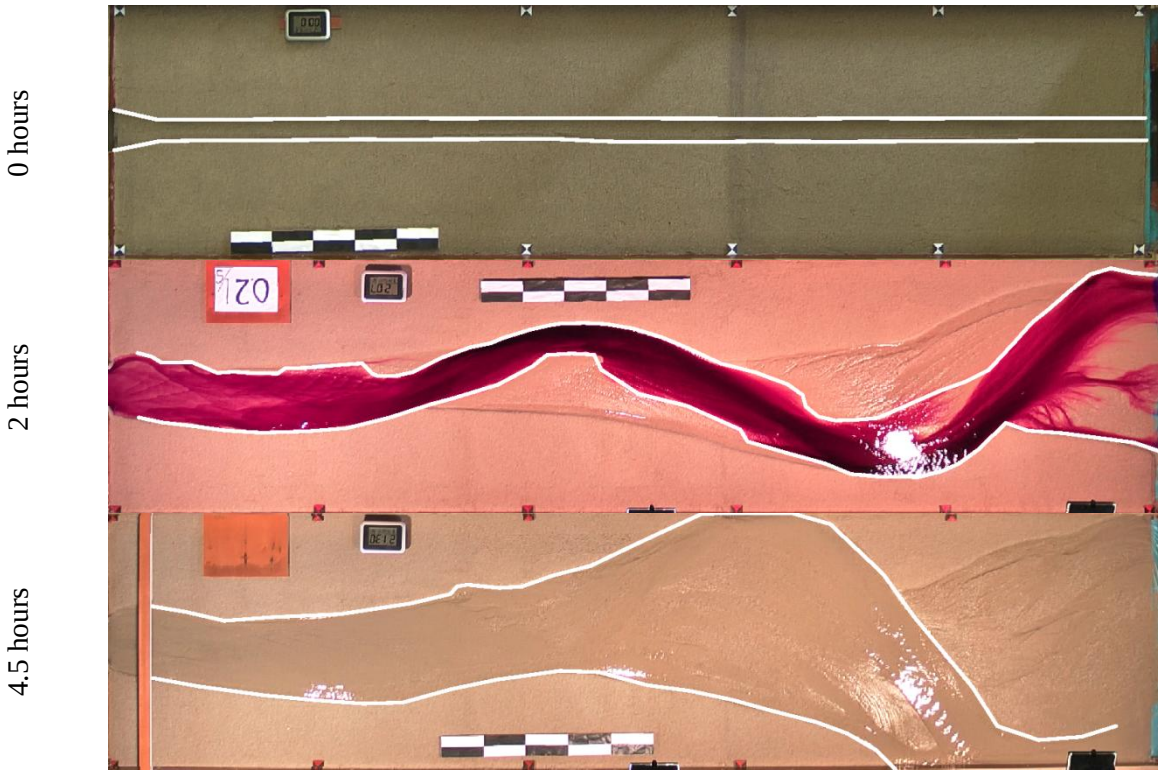

Figure A-4.12 Width evolution in H2-0.1* scenario after 2 hours and 4.5 hours

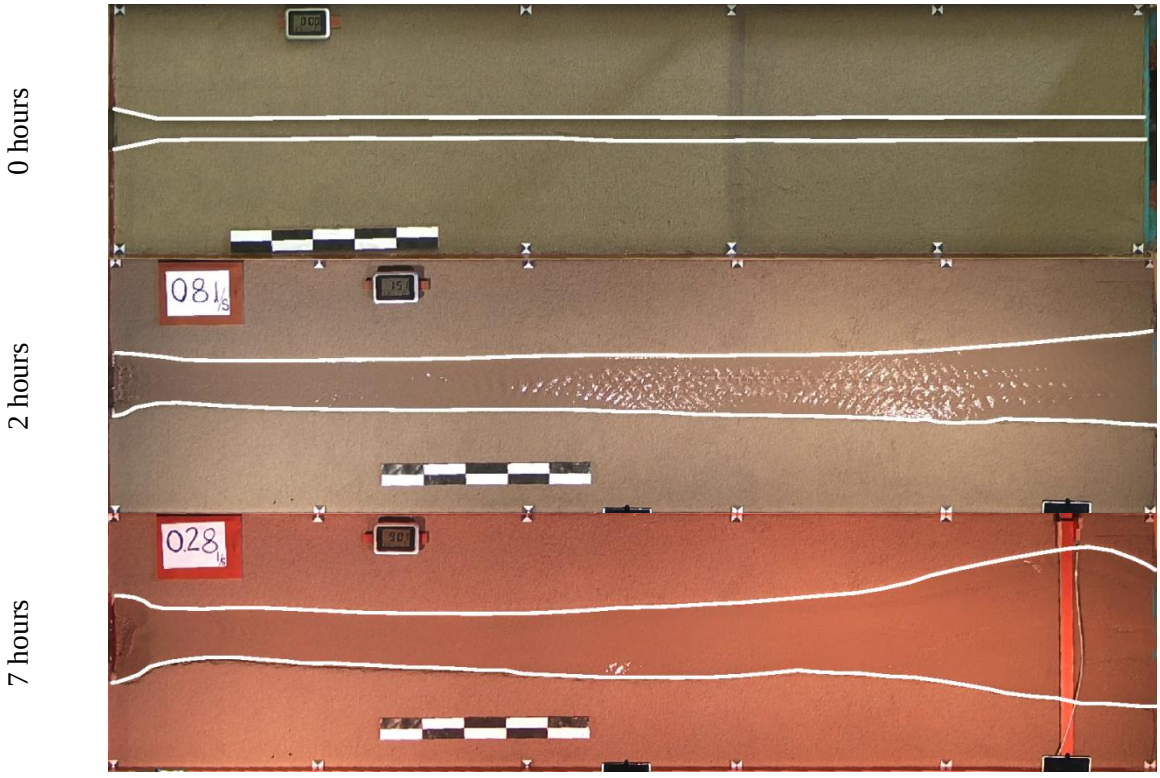

Figure A-4.13 Width evolution in H3-0.1 scenario after 2 hours and 7 hours

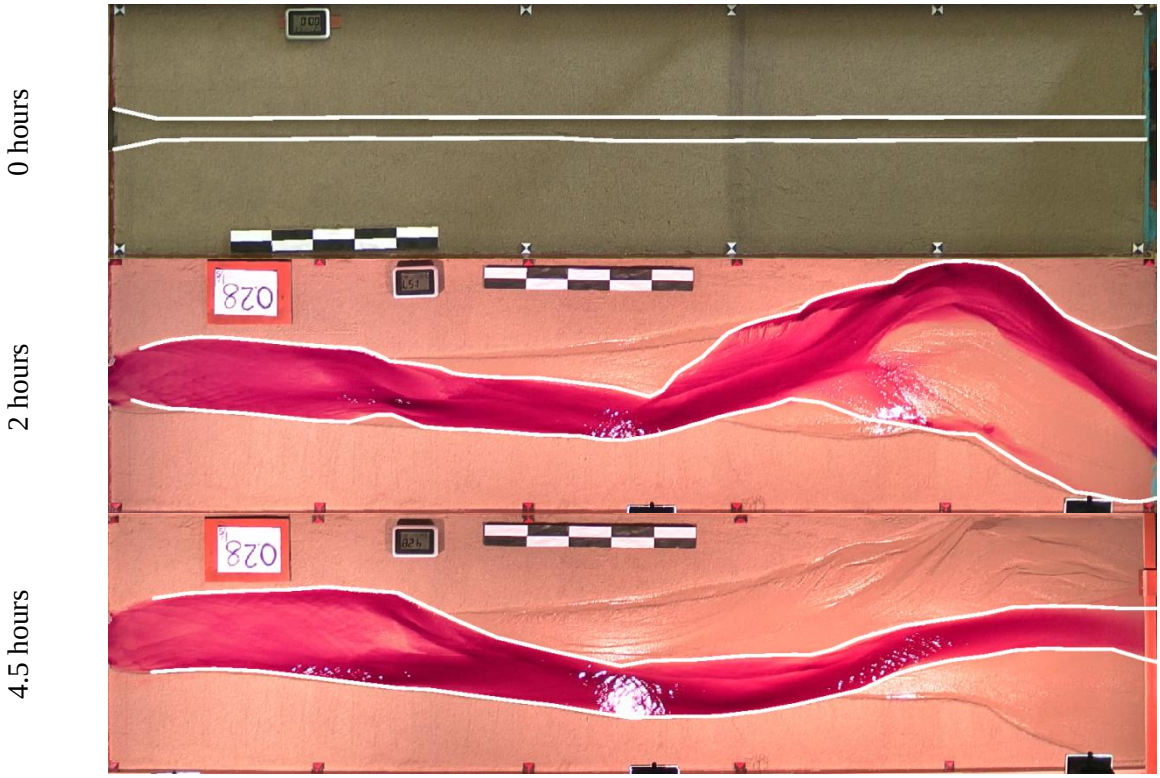

Figure A-4.14 Width evolution in H3-0.1* scenario after 2 hours and 4.5 hours

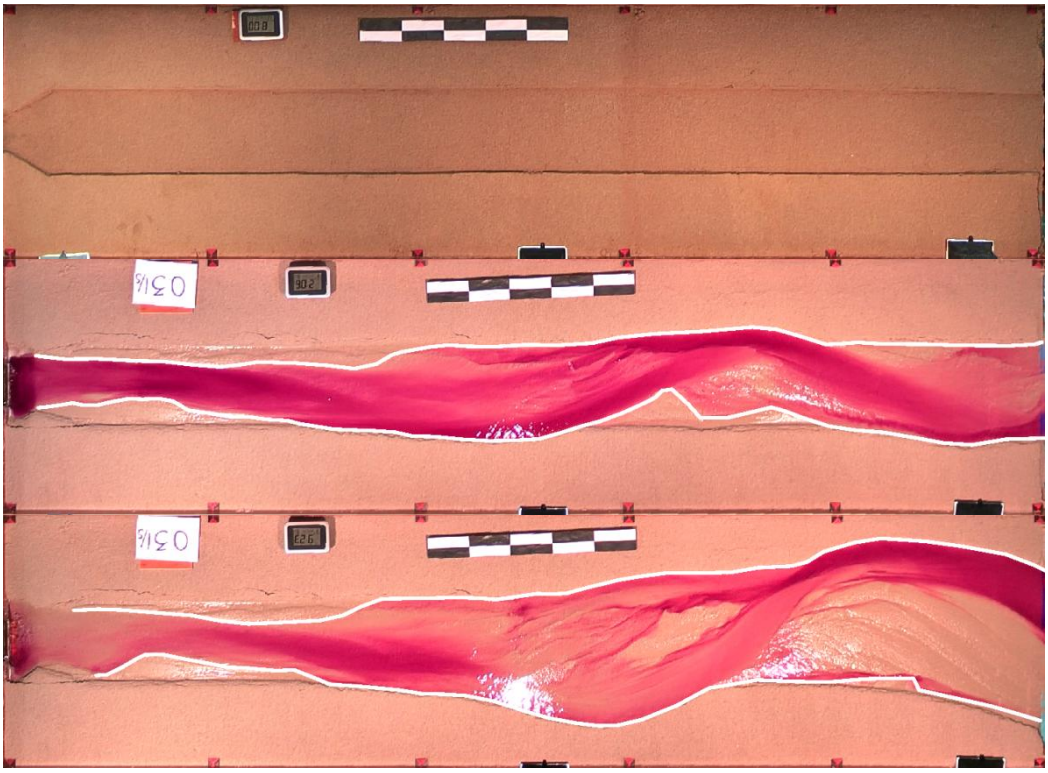

Figure A-4.15 Width evolution in H1-0.4 scenario after 2 hours and 7 hours

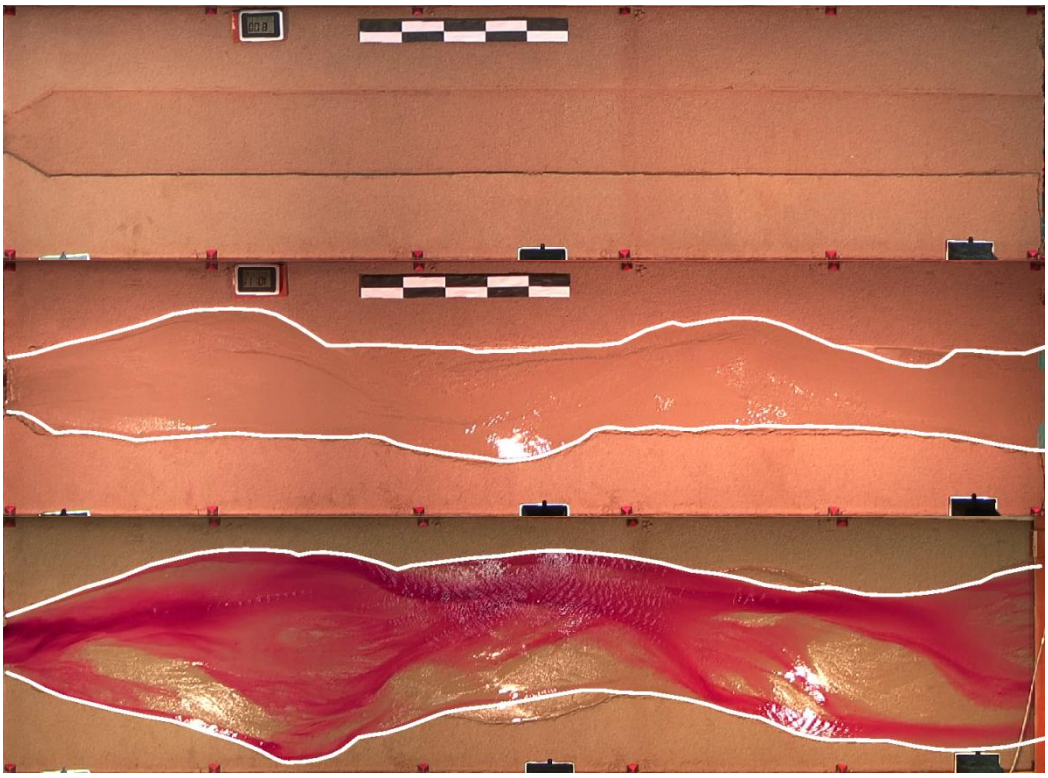

Figure A-4.16 Width evolution in H1-0.4* scenario after 2 hours and 7 hours

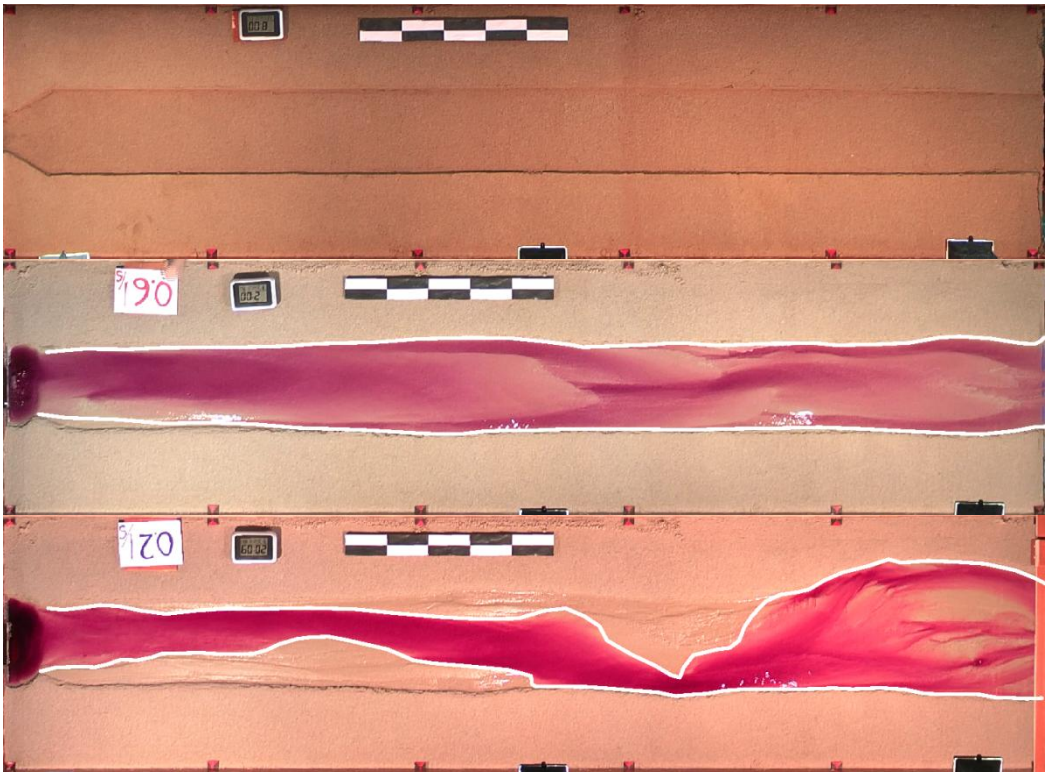

Figure A-4.17 Width evolution in H2-0.4 scenario after 2 hours and 7 hours

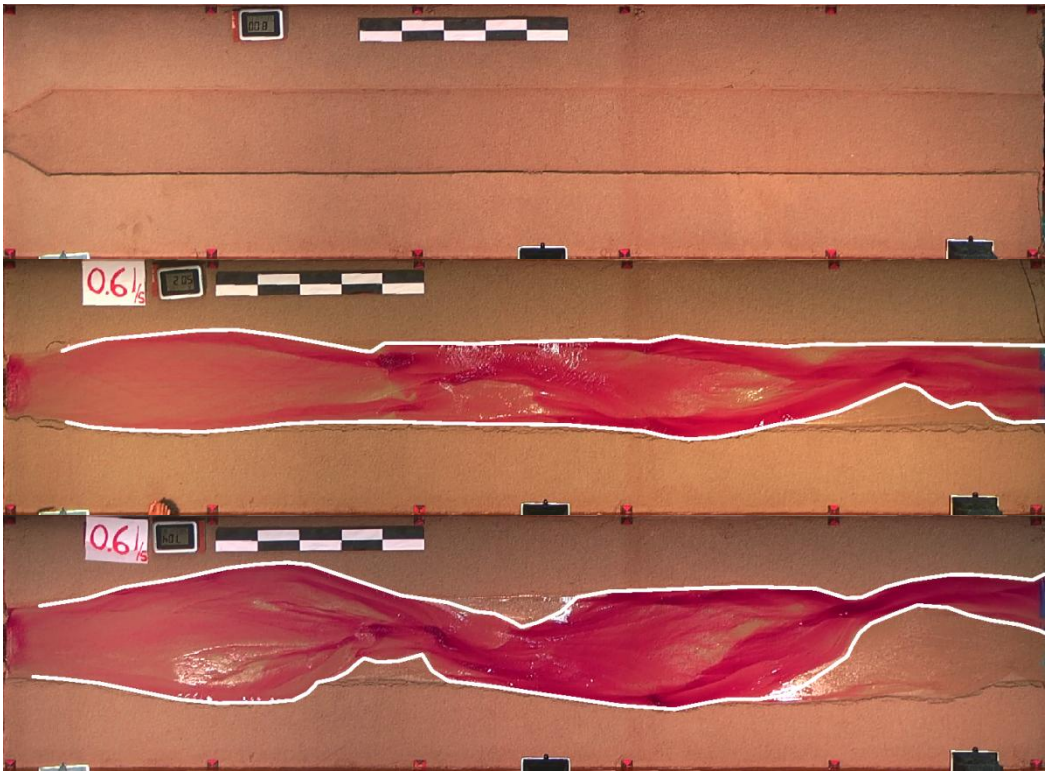

Figure A-4.18 Width evolution in H2-0.4* scenario after 2 hours and 7 hours

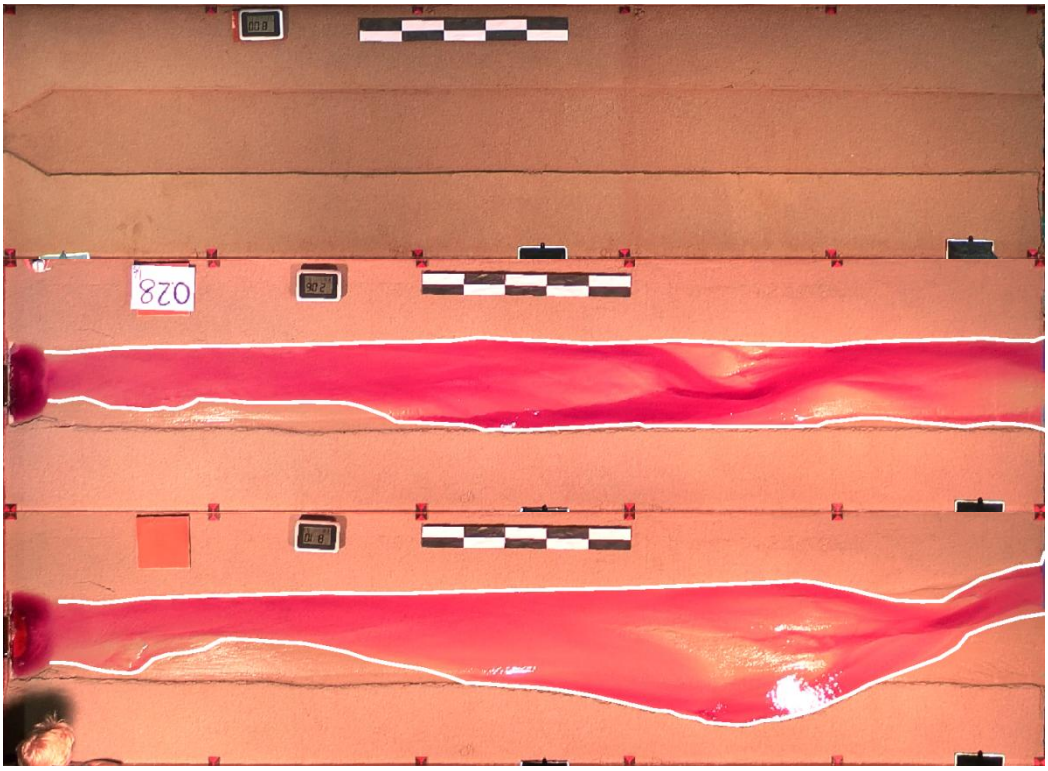

Figure A-4.19 Width evolution in H3-0.4 scenario after 2 hours and 7 hours

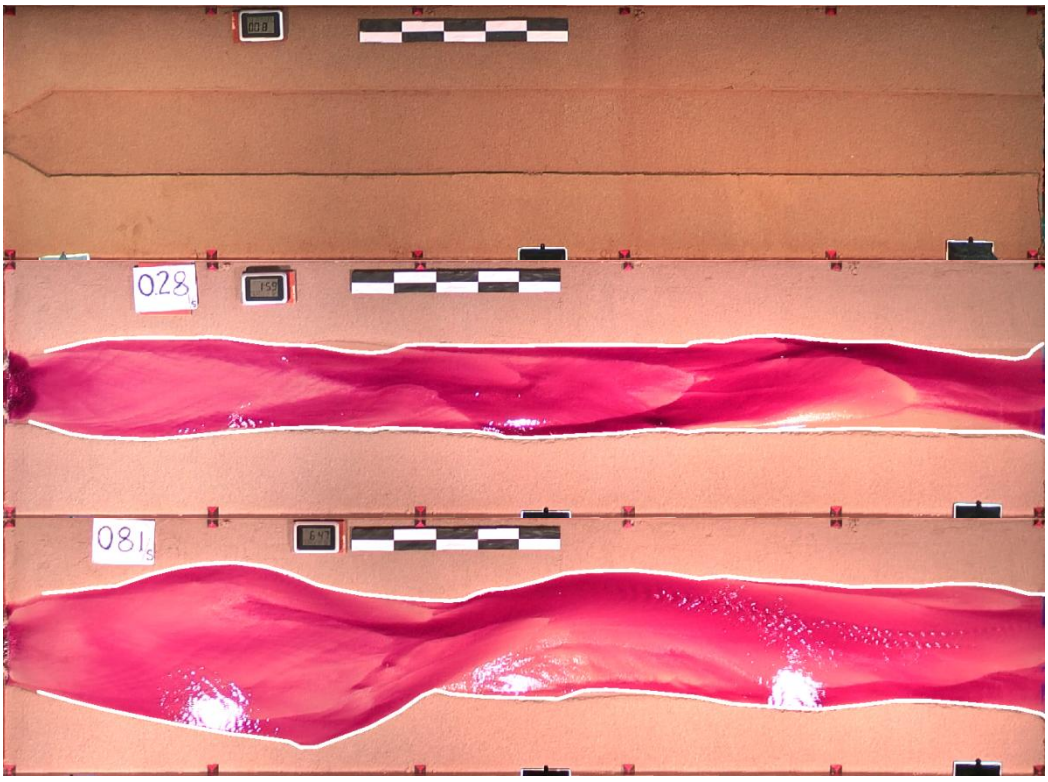

Figure A-4.20 Width evolution in H3-0.4* scenario after 2 hours and 7 hours

A-5 Topography measurement

Topographic measurement were carried out in cross-sections at an interval of 0.5 m from the discharge inlet of the flume. The measurement was carried out using a laser scanner. The device measures distance in terms of voltage (V), The voltage-distance relation for the device is:

$Z = (2.5\ V + 1)/100$

Where, Z is the distance measured between tip of the laser to the target, V is the voltage output from the device.

The measured topography was then used to determine the volume of sediment reworked from the bank and the bed of the channel which is explained as follows:

Sediment reworking model:

A simple model, was developed to quantify reworking of sediment from the banks and the bed of the channel. Entire flume was first subdivided into sub reaches. Sub reaches were defined by the reach between two adjacent measured cross-sections. The volume was computed using following relations:

$$\Delta V_{s,i} = \Delta V_{s,bed,i} + \Delta V_{s,bank,i}$$

$$\Delta V_{s,bed,i} = \frac{W_{i,0} \times \Delta D_i + W_{i+1,0} \times \Delta D_{i+1}}{2} \times L_i$$

$$\Delta V_{s,bank,i} = \frac{D_i \times \Delta W_i + D_{i+1} \times \Delta W_{i+1}}{2} \times L_i$$

$$\Delta D_i = D_i - D_{i,0}$$

$$\Delta D_i = D_i - D_{i,0}$$

$$\Delta D_{i+1} = D_{i+1} - D_{i+1,0}$$

$$\Delta W_i = W_i - W_{i,0}$$

$$\Delta W_{i+1} = W_{i+1} - W_{i+1,0}$$

Where,

$\Delta V_{s,i}$ = Total change of the sediment volume in a sub-reach i (m^3)

$\Delta V_{s,bed,i}$ = Total change of the sediment volume in a sub-reach contributed by channel bed (m^3)

$\Delta V_{s,bank,i}$ = Total change of the sediment volume in a sub-reach contributed by channel banks (m^3)

$W_{i,0}/W_{i+1,0}$ = Initial width of the channel at adjacent cross-section i/ cross-section i+1 (m)

W_i/W_{i+1} = Width of the channel at adjacent cross-section i/ cross-section i+1, after time T (m)

$D_{i,0}/ D_{i+1,0}$ = Initial depth of the channel at adjacent cross-section i/ cross-section i+1 (m)

D_i/ D_{i+1} = Depth of the channel at adjacent cross-section i/ cross-section i+1after time T (m)

L_i = Longitudinal distance between cross-section i/ cross-section i+1 (m)

Since we are analyzing the volume of the reworked sediment, the width of the channel for this model is computed as distance between the left and the right bank at a level half of the depth of the channel. The relative volumes of sediment reworked from bed and banks, along each sub-reach of the channel, was then computed as:

$$F_{s,bed,i} = \frac{\Delta V_{s,bed,i}}{\left|\Delta V_{s,bed,i}\right| + \left|\Delta V_{s,bank,i}\right|} \times 100$$

$$F_{s,bank,i} = \frac{\Delta V_{s,bank,i}}{\left|\Delta V_{s,bed,i}\right| + \left|\Delta V_{s,bank,i}\right|} \times 100$$

Where

$F_{s,bed,i}$ = Relative volume of the sediments reworked in the channel bed within the sub-reach i (%)

$F_{s,bank,i}$ = Relative volume of the sediments reworked from the channel banks within the sub-reach i (%)

To assess the accuracy of the method, the computed net amount of sediment exiting the flume was compared to the amount of sediment collected at the downstream end of the flume. For the comparison, the change in volume of sediment within a sub reach was converted to weight using equation **Error! Reference source not found.** and **Error! Reference source not found.**.

$$w_{s,i} = \Delta V_{s,i} \times (1 - \underset{porosity}{0.41}) \times 2635$$

$$W_s = \sum_{i=1}^{N} w_{s,i}$$

Where,

$w_{s,i}$ = net change of sediment in cross-section i (kg)

W_s = computed total net change of sediment in flume (kg)

N = number of sub reaches.

The error in the estimation of the net volume of the sediment is computed as.

$$E = \frac{(W_s - W_{s,obs})}{W_{s,obs}} \times 100$$

Where,

E = error of the estimation of net volume of the sediment (%)

$W_{s,obs}$ = Weight of the sediment collected at the downstream end of the flume (kg)

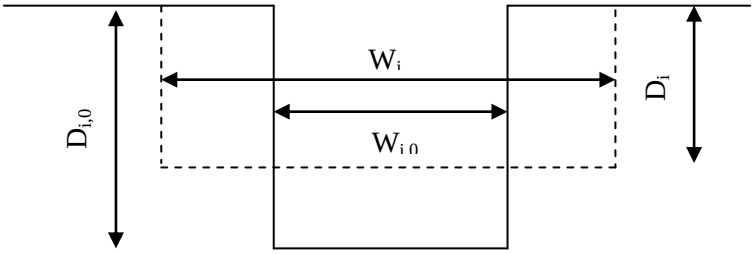

Figure A-5.1. Schematic diagram showing the definition of depth and width used in the simple sediment budget model

MODELLING OF ALTERNATE BARS IN STRAIGHT CHANNEL USING DIFFERENT MORPHODYNAMIC MODELS

1 INTRODUCTION

The objectives of this research is to investigate the morphodynamics of alternate bars using differnt physics based numerical models. Physics-based numerical models potentially provide a powerful tool to support the investigation of the temporal evolution of bars in a single (e.g. Defina, 2003) and multi-thread channels (e.g. Schuurman et. al, 2013) in a controlled manner. Although models include a simplified description of the complex physical processes, they provide the flexibility to investigate morphodynamics under variable forcing and initial conditions. Recently Nicholas (2013) has shown that physics based numerical model coupled with vegetation and bank dynamics is able to reproduce spectrum of realistic channel planforms from meandering to braided. The models are based upon data of flume experiments carried out by Garcia et al (2014).

The major numerical tools adopted in this work are two different numerical models, one semi-coupled (Delft3D) and another fully-coupled (GIAMT2D). In semi-coupled models, the sediment transport equation and flow-field equations are solved seperately assuming that the bed level changes occuring at a small computational time steps is small and does not affect the flow field. Whereas, in the case of fully-coupled model, flow-field equations and sediment transport equations are solved together in single time steps (Kaseem and Chaudhary, 1998). At higher froude number (>1), the time scale of the bed level change is comparable to the time scale of hydrodynamics changes, so the fully-coupled model is more robust and stable to simulate morphodynamic processes during super critical flows.

This chapter presents the investigation of bar dynamics in single-thread channels. The chapter is organized in three different sections: methodology, results and conclusion and discussion. The methodology section explains the experiments, numerical models and the model setup. The results section elaborates the comparison between results of two different numerical models and the experiments and finally the conclusion and discussion section elaborates the context of validity of results.

2 METHODOLOGY

2.1 General methodology

The research methodology is based upon physics-based numerical modeling. The morphodynamics of alternate bars were investigated using two-dimensional physics based numerical models. Numerical models were rigorously calibrated using the laboratory experiment data of Garcia (2014) to reproduce the characteristics of alternate bars observed in the experiments. In the first approach we used a well validated and robust semi-coupled model, based on the DELFT3D code designed for small Froude numbers (<0.8). In the second approach we used a fully-coupled model (GIAMT2D) that can handle supercritical flows (Fr>1). The results of both models are then compared with the experiments to make a choice of the numerical model for the detail investigation of the morphodynamics of alternate bars observed in the experiments.

2.2 Laboratory Experiments

Experiments of Garcia (2014) were used to construct numerical models to simulate realistic dynamics of bars. The experiments were carried out in a flume facility, 2.90 m wide and 25 m long, at the University of Trento. Details of the flume facility are explained in Bertoldi et al, (2009). The experiments were conducted within a narrower width than the width of the flume facility. The channel of desired width was excavated at the centre of the flume. A plastic sheet was then laid on the excavated channel and layer of sand of desired thickness was then laid on the plastic bed (figure 1). Thus the constructed channels have mobile bed with non-erodible banks. The experiments consist of a series of runs performed at many different configurations characterized by different value of channel width with three different discharge values for each planform configuration. Increasing channel width has allowed obtaining a series of channel morphologies ranging from single-thread with alternate bars to braiding planforms with different braiding intensities.

The development of the channel bed is influenced by the boundary conditions of the flume. To avoid the influence of the boundaries, the bed topography of 15 m reach in the center of the flume was measured using the laser scanner, at two times during the experiments (figure 2a and 2b). The measurements were made at the resolution of 5 mm in lateral direction and 50 mm in longitudinal directions. Some parts of the channel were dry due to the bars emerging above the water level. The dry areas were measured from the still photographs taken before the measurement of the bed topography. The time-series data of the sediment transport was also measured at downstream end of the flume (figure 3).

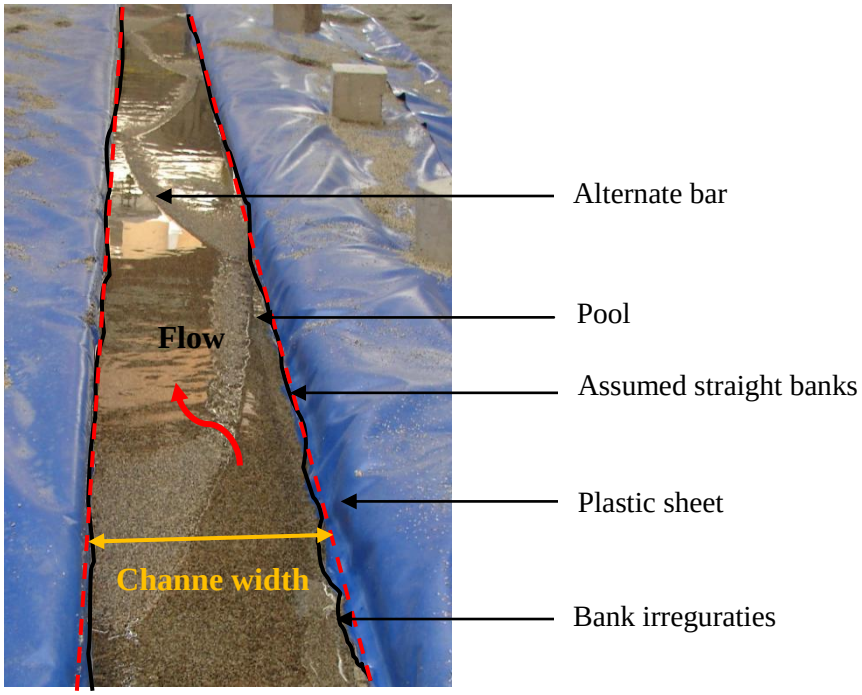

Figure -1 Flume experiments showing alternate bars and the plastic banks with irregularities

These data were used to setup numerical model reproducing realistic alternate bar dynamics and are discussed in the sections below.

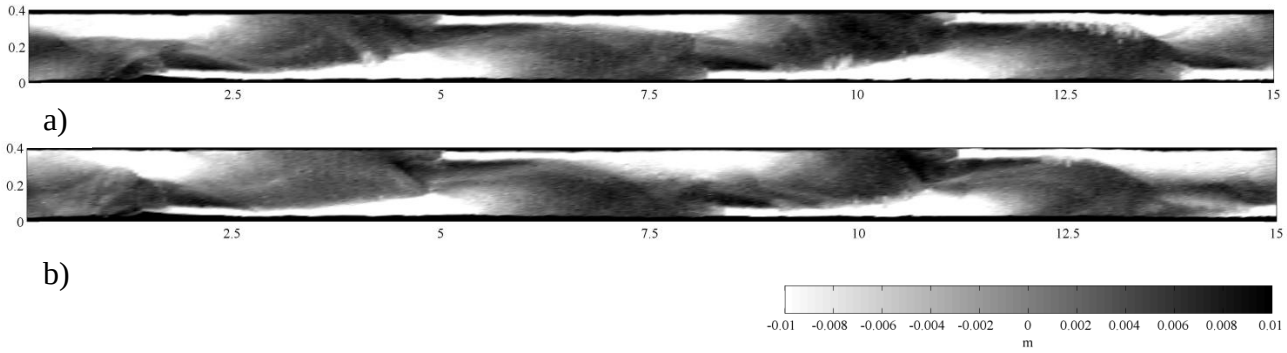

Figure -2 Bed topography showing alternate bars in experiment measured a) after 275 minutes and b) after 300 minutes (the bed topography is de-trended with the longitudinal slope)

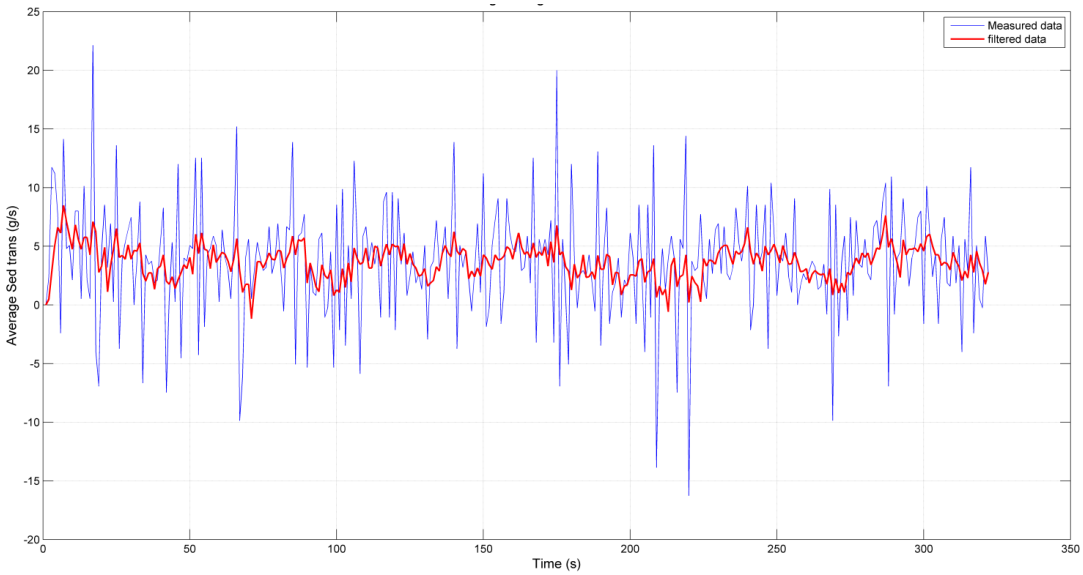

Figure – 3 Sediment transport rate signal observed at the downstream end of the flume

We choose three different experimental runs: channel with alternate bars (single-thread channel), wandering channel (transition between single thread and multi-thread channel) and braided channel (multi-thread channel). Details of the experimental conditions for the three different configurations are presented in table 1. The alternate bar case was used for the investigation using numerical models. Since the flow depth and velocities were not measured during the experiments, the hydrodynamic calibration in the numerical models were performed by reproducing dry areas observed in the experiments (e.g. Zilliani et al, 2013,Williams et al,2013). The alternate bars in the experiment were submerged so wandering channel and braided channel cases, which had dry areas due to emergence of bars above the water surface, were used for the hydrodynamic calibration (figure 4a, 4b and 4c).

Table 1: Details of flume experiments selected for this study

Q (l/s)	**W (cm)**	**D (cm)**	**Fr (-)**	**β (-)**	**ds50 (mm)**	**S (%)**	**DA (%)**	**T (min)**	**Qs (g/s)**	**Pattern**
2.0	40	1.25	1.14	16	1.05	1	0	320	3.568	Alternate
1.5	60	0.85	1.08	35	1.05	1	2.5	900	1.568	Wandering
2.0	125	0.7	1.04	90	1.05	1	18	3500	1.706	Braided

Q = Liquid discharge provided at upstream boundary, W= width of the channel, D = water depth, Fr = Froude number, β = half width to depth ratio, ds_{50} = median sediment diameter, S = longitudinal slope of the channel, DA = Percentage of the dry bar area with respect to the total area of the channel, T = duration of the experiments and Qs = solid discharge measured at the downstream boundary of the flume.

The experiments were run more than 10 times the Exner-time scale. The Exner-time scale estimates the time scale of the development of the channel bed considering the width scale of the flume. It is computed as:

$$T = D \times W/qs \quad (1)$$

Where, T = Exner time scale (min), D = water depth (m), W= channel width (m), qs=sediment transport rate per unit width ($m^3/m/s$)

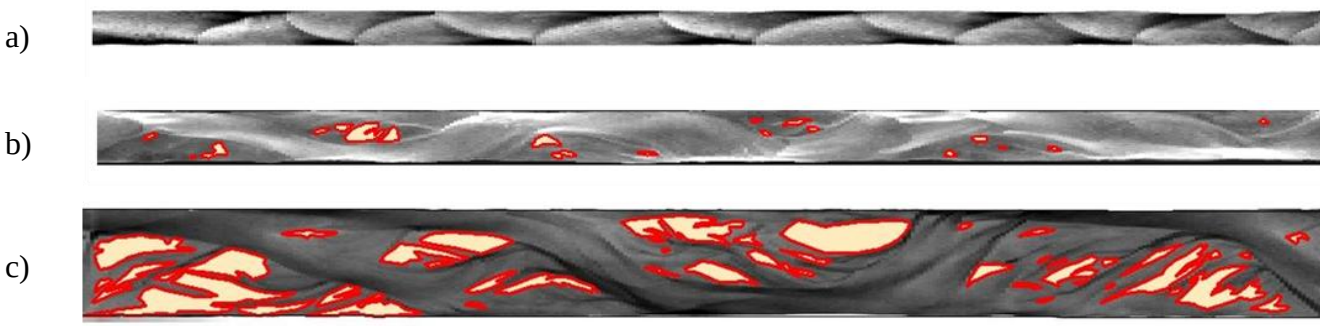

Figure 4 Bed topography showing dry areas (in red) measured in the experiment for a) alternate bars case b) wandering case and c) after braided case.

2.3 Model descriptions

This section describes the semi-coupled model, Delft3D, and fully-coupled model, GIAMT2D, makes a comparison between different characteristics of the two models.

2.3.1 Semi-coupled model (Delft3D)

DELFT3D solves unsteady depth averaged shallow-water equations in two dimensions (2DH) with hydrostatic approximation, and sediment transport and bottom updating is calculated in an semi-coupled way with respect to the flow-field. The differential equations are solved in semi-implicit way using finite difference based alternating direction implicit (ADI) method in structured computational grids. The model has been validated on several analytical solutions and series of laboratory

experiment tests. The details of the numerical aspects and validation of Delft3D code is explained well by Lesser et al., (2004) and van der Wegen and Roelvink, (2008). The hydrodynamic and morphodynamic model of Delft3D are explained as follows:

a) Hydrodynamic model

The hydrodynamic model of Delft3D solves the unsteady shallow-water equations in two dimensions (2DH) with hydrostatic approximations. The two dimensional form of conservation of momentum and continuity equations can be written as:

$$\frac{\partial u}{\partial t} + u\frac{\partial u}{\partial x} + v\frac{\partial u}{\partial y} + g\frac{\partial z_w}{\partial x} + c_f\frac{u\sqrt{u^2+v^2}}{h} - v_e\left(\frac{\partial^2 u}{\partial x^2} + \frac{\partial^2 u}{\partial y^2}\right) = 0 \qquad (2)$$

$$\frac{\partial v}{\partial t} + u\frac{\partial v}{\partial x} + v\frac{\partial v}{\partial y} + g\frac{\partial z_w}{\partial x} + c_f\frac{v\sqrt{u^2+v^2}}{h} - v_e\left(\frac{\partial^2 v}{\partial x^2} + \frac{\partial^2 v}{\partial y^2}\right) = 0 \qquad (3)$$

$$\frac{\partial z_w}{\partial t} + \frac{\partial hu}{\partial x} + \frac{\partial hv}{\partial y} = 0 \qquad (4)$$

Where,

$$cf = g\frac{n^2}{h^{3/2}} \qquad (5)$$

In which, x is longitudinal coordinate (m), y is the lateral coordinate (m), t is the time (s), u is the depth averaged flow velocity in longitudinal direction (m/s), v is the depth averaged flow velocity in lateral direction (m/s), h is the water depth (m), z_w is the free water surface level (m), g is the acceleration due to gravity (m^2/s), v_e is the horizontal eddy viscosity (m^2/s), cf is the friction coefficient (-) and n is mannings roughness coefficient ($m^{-1/3}s$).

b) Morphodynamic model

The flow velocity obtained from the hydrodynamic model is used to compute the sediment transport field in the morphodynamic model. The sediment transport can be computed using Meyer Peter Muller type formulas as follows:

$$q_s = A(\theta - \theta_{cr})^B\sqrt{g\Delta d_s^3} \qquad (6)$$

Where,

$$\theta = \frac{u^2 n^2}{h^{1/3}\Delta d_s} \qquad (7)$$

$$\Delta = \frac{\rho_s - \rho}{\rho} \qquad (8)$$

In which, qs is the magnitude of sediment transport rate per unti width (m^3/s/m), A is the callibration coefficient (-), Θ is the dimensionless bed shear stress (-), Θcr is the critical dimensional bed shear stress for the sediment motion (0.047), B is the calibration exponent (-), ds is the sediment diameter (m), Δ is the relative density of the sediment (2.65), ρs is the density of sediment (kg/m3)and ρ is the density of water (kg/m3).

The direction of sediment transport occurring on a transverse bed slope deviates due to gravity effects. The effect of transverse bed slope on direction of bed load transport is modeled using Ikeda (1982) formulation as presented by van Rijn(1993) as follows:

$$q'_y = q_{sx}\alpha_{bn}\sqrt{\frac{\theta_{cr}}{\theta}}\frac{\partial z_b}{\partial y} \qquad (8)$$

Where, q'y is the additional bed-load transport vector and the direction is towards the down slope (m^3/s/m) , α_{bn} is the callibration coefficient whose default value is 1.5, z_b is the bed level (m).

The sediment balance is then computed using Exner principle in two directions as follows:

$$\left(1-\Lambda_p\right)\frac{\partial z_b}{\partial t} + \frac{\partial q_{sx}}{\partial x} + \frac{\partial q_{sy}}{\partial y} = 0 \qquad (9)$$

Where, qsx is the sediment transport rate per unit width in x direction (m3/s/m) and qsy is th sediment transport rate per unit width in y direction (m3/s/m) and Λ_p is the porosity (40%).

The bed level is then updated at each time step using a constant porosity and computed bed load transport gradient along the computational grid cell.

2.3.2 Fully-coupled model

GIAMT2D solves the momentum balance and continuity of water and sediment in coupled way. The model solves the differential equations in explicit way using finite volume based centered type with upwind biased method in unstructured triangular computational mesh. The model has been validated in several analytical test, including analytical model of free and forced bars in straight channel, and several experimental tests. The details of the numerical aspects and validation of GIAMT2D is explained well in Siviglia et al. (2013). Since the model solves the 2D shallow water equation and Exner equation in coupled way, the continuity equation of liquid discharge also contains the solid discharge (equation 10). The momentum balance equation of water and continuity of sediment and water in two dimensional can be written as:

$$\frac{\partial z_w}{\partial t} + \frac{\partial}{\partial x}\left(q_x + q_{sx}\right) + \frac{\partial}{\partial y}\left(q_y + q_{sy}\right) = 0 \qquad (10)$$

$$\frac{\partial q_x}{\partial t} + \frac{\partial}{\partial x}\left(\frac{q_x^2}{h} + \frac{1}{2}gz_w^2 - gz_w z_b\right) + \frac{\partial}{\partial y}\left(\frac{q_x q_y}{h}\right) + gz_w\frac{\partial z_w}{\partial x} + ghS_{fx} = 0 \qquad (11)$$

$$\frac{\partial q_y}{\partial t} + \frac{\partial}{\partial y}\left(\frac{q_y^2}{h} + \frac{1}{2}gz_w^2 - gz_w z_b\right) + \frac{\partial}{\partial x}\left(\frac{q_x q_y}{h}\right) + gz_w \frac{\partial z_w}{\partial y} + ghS_{fy} = 0 \qquad (12)$$

$$\frac{\partial z_b}{\partial t} + \frac{\partial q_{sx}}{\partial x} + \frac{\partial q_{sy}}{\partial y} = 0 \qquad (13)$$

Where, x is the coordinate in longitudinal direction (m), y is the coordinate in lateral direction (m), qx and qy are flow discharge per unit width in x and y direction respectively (m3/s/m), zw is the water surface elevation (m), zb is the bottom surface elevation (m), h is the water depth (m), qsx and qsy are sediment transport rate per unit width in x and y direction respectively (m3/s/m), Sfx and Sfy are dimensionless frictional term (-).

The dimensional frictional terms are computed as:

$$S_{fx} = \frac{q_x n^2}{h^{10/3}} \qquad (14)$$

$$S_{fy} = \frac{q_y n^2}{h^{10/3}} \qquad (15)$$

Where n is the mannings roughness coefficient ($m^{-1/3}s$).

The sediment transport rate can be computed as the Myer-Peter like formula as:

$$q_S = \frac{A(\theta - \theta_{cr})^B \sqrt{g\Delta d_s^3}}{1 - \Lambda_p} \qquad (16)$$

Where,

$$\theta = \frac{h\sqrt{S_{fx}^2 + S_{fy}^2}}{\Delta d_s} \qquad (17)$$

In which, qs is the magnitude of sediment transport rate per unti width ($m^3/s/m$), A is the callibration coefficient (-), Θ is the dimensionless bed shear stress (-), Θcr is the critical dimensional bed shear stress for the sediment motion (0.047), B is the calibration exponent (-), ds is the sediment diameter (m), Δ is the relative density of the sediment (2.65).

The direction of sediment transport along the transverse bed slope is adjusted using Ikeda(1983) formulation as follows:

$$q'_{sy} = -\frac{r}{\sqrt{\theta}}\left(\frac{\partial z_b}{\partial x}, \frac{\partial z_b}{\partial y}\right) \times \overrightarrow{n_q} \qquad (18)$$

Where, q'sy is the additional sediment transport rate due to transverse bed slope effects, $\overrightarrow{n_q}$ =(-sinϒ,cosϒ) is the unit vector perpendicular to q, ϒ is the angle of bottom shear stress with respect to x direction, r is the callibration coefficient.

2.3.3 Comparison of models

The basic difference between the two models is the way how the shallow water equation and sediment continuity equations are solved. GIAMT2D solves with the coupled approach and Delft3D solves using semi-coupled approach. In addition to the coupling of shallow water and Exner equations, the models differ in several numerical aspects. The comparison between Delft3D and GIAMT2D is presented in table 2.

Delft3D is based upon finite difference semi-implicit numerical scheme and uses structured grids (cartesian or curvilinear grids) for the computation. GIAMT2D is build using finite volume explicit scheme and uses unstructured (triangular) grids for the computation. Transverse bed slope effect in both models can be modeled using Ikeda (1983) formulations. DELFT3D has parameterization of the effects of spiral flow in flow and sediment-transport direction and also has lateral bank erosion implementation which is not available in GIAMT2D.

Both numerical models can handle the drying and wetting phenomenon and have been validated by reproducing sets of experiments having analytical solutions. GIAMT2D is validated for the free bar development at the initial case and the influence of obstruction on the morphodynamics of forced bars on the basis of analytical solutions. Detail descriptions of the tests are presented in Siviglia et al (2013). Both validation tests were performed in super critical flow conditions. Since we are studying bar dynamics using experimental data under super-critical flow condition, same validation tests were repeated with DELFT3D code to check the limitation of the code in simulating bar dynamics under super-critical flow conditions. The results of the test are explained later in the section 3.2.

Table 2 Comparison of model characteristics between GIAMT2D and Delft3D models

Model/ Characterisitcs	**GIAMT2D**	**Delft3D**
Numerics	Finite volume, fully-coupled, explicit scheme	Finite difference, semi coupled, semi-implicit scheme
Mesh	Unstructured triangular mesh	Structured, curvilinear mesh
Spiral flow parameterization	Not available	Based upon stream line curvature
Lateral bank erosion	Not available	Parameterised by simple factor
Sediment transport	Mayer Peter Muller like formulas, Parker (1990)	Meyer Peter Muller like formulas, Englund and Hansen, van Rijn 1984 & 1993, Bijker, Soulsby and Ashida Michue
Transverse bed slope effects on direction of bed load	Ikeda (1982)	Ikeda (1982) modified by vajn Rijn (1993)
2D-Roughness formulation	Manning's formulation	Chezy, Manning and white-Colebrook formulation.
2D-Turbulence	Not available	Constant value assigned or turbulence closure models including algebraic forms can be used
Wetting and drying	Capable	Capable

2.4 Model setup and calibration

The models were setup in Delft3D code and GIAMT2D code using the physical parameters of the alternate bar case of the laboratory experiments shown in table 1. The physical and numerical parameters were kept as similar as possible to make a robust comparison between results of the two models. A 0.4 m wide and 35 m long channel was used for model setup in Delft3D. The domain was chosen longer to isolate 15m long reach, the domain of interest, from the boundary effects. Cartesian rectangular grids of 2 cm wide (in lateral direction) and 5 cm long (in longitudinal direction) were used in DLEFT3D. So, the computational domain has 20 grids in lateral direction which is sufficient to properly capture the lateral features of alternate bars. In the case of GIAMT2D, the influence of boundary was stronger so the domain length had to be increased to 75 m (additional 30 m in each side).

A 0.4 m wide and 75 m long channel was used for model setup in GIAMT2D. The longer domain was adopted to isolate the effects of the boundary, which were stronger in the case of GIAMT2D, from the reach of interest. GIAMT2D uses unstructured triangular meshes and is optimized for the Delaunay mesh generating algorithms. The algorithm generates equilateral triangular grid elements and the grid size cannot be refined in the lateral direction alone. The length of the channel in GIAMT2D is twice of the channel implemented in DELFT3D. The computational time requirement of the fully-coupled model is very high compared to the semi-coupled models and it is strongly determined by the number of grid elements in the domain. Thus, number of grid elements along the lateral direction was restricted to 10 to obtain reasonable computational time in the model.

Flat channel bed with the slope of 1% along the longitudinal directions was provided as initial conditions in both the models. The bed was also randomly perturbed by noise of ± 10% of sediment diameter to trigger the bar development. Uniform discharge of 2 l/s was provided at the upstream boundary section and the fixed water level corresponding to normal water level was provided at the downstream boundary. The discharge at the upstream boundary was also randomly perturbed by ± 1% of uniform discharge in DELFT3D model. At the upstream boundary, sediment discharge equal to the local sediment transport capacity near the boundary was provided in both the models. The Manning's roughness formulation was implemented in Delft3D and the corresponding value of Gaukler's Strickler formulation was implemented in GIAMT2D. Since the bed-load process were dominant in the experiments the Wong and Parker (2006) transport formulations was used to compute the sediment transport rate in both the models.

$$Qs = \alpha d_s \sqrt{\Delta g d_s}\,(\theta - 0.047)^{1.6} \qquad (19)$$

$$q_s = a\sqrt{\Delta g D_s^3}\,\sqrt{(\theta - b)^c} \qquad (33)$$

$$\Delta = (\rho_s - \rho)/\rho \qquad (34)$$

$$\theta = \frac{u^2}{C^2 \Delta D_s} \qquad (35)$$

Where,

q_s = sediment fraction transport per unit width ($m^3/s/m$)

Δ = relative sediment density

ρ_s = density of sediment (kg/m^3)

ρ = density of water (kg/m$^{3)}$

D_s = sediment diameter (m)

Θ = Shields stress

u = depth-averaged velocity (m/s)

C = Chezy's roughness coefficient (m$^{1/2}$/s

b = critical Shields stress for threshold of motion

a and c = coefficients

Where Qs = sediment transport rate per unit width (m^3/s/m), ds = sediment diameter (m), Δ = relative density of the sediment (1.65), g = acceleration due to gravity (9.81 m/s^2), Θ= shields number, α = callibration coefficient.

The consistent international standard practice does not exist on validation of morphological models (Mosselman, 2012). We perform model calibration in three different stages. The choice is based upon the data available from the experiments. The morphodynamics of bars are sensitive to the formulation and magnitude of roughness (e.g. Nicholas et al., 2013, Schuurman et al., 2013). The Manning's roughness formulation is chosen to be consistent with both the models. So, the first stage of calibration was performed to make the choice of the magnitude of roughness parameter. The flow depth and velocity was not measured in the experiments which makes it difficult to estimate the value of roughness in the experiments. So the value of roughness was estimated indirectly based upon the estimation of measured dry areas. Alternate bars were submerged throughout the experiment, so the wandering and braided cases, having dry areas, were used for the analysis. A fixed bed hydrodynamic model, in DELFT3D code, was setup using the measured bed topography to investigate a reasonable value of the roughness coefficient in the experiments. The model was run with different values of roughness coefficient to reproduce the dry areas observed in the experiments. Both braided and wandering case resulted highest correlation with the measured dry areas of bars for the value of Manning's coefficient of 0.014. Due to computational time limitations the first stage of calibration was not repeated for the GIAMT2D case. So, the Manning's value of 0.014 was used in DELFT3D and the corresponding Gauckler's stricklers value of 71.5 was used in GIAMT2D models.

In the second stage, the calibration of sediment transport formula was performed to reproduce the average value of the sediment transport rate in the model close to the average value of sediment transport rate measured in the experiment. Value of α, in equation 19, was varied in the Delft3D model until the average transport rate in the model resulted close to the observed sediment transport rate at the downstream boundary of the experiments. The value of α was optimized at 7 in Delft3D. The value of α equal to 7 also resulted the average sediment transport rate in the GIAMT2D model close to the average value of observed sediment transport rate at the downstream boundary of the experiment. The results are presented later in the section 3.3.

Effect of the transverse bed slope on the bed-load transport direction is a sensitive parameter in modeling of bars. Higher transverse bed slope effect results in smoother bed topography and lower

transverse bed slope effect results in unrealistic steep bed topography (Defina, 2003). So, the third stage of calibration is performed by varying αbn, equation 8, in Delft3D and varying r parameter, equation 18, in GIAMT2D to reproduce the topography observed in the experiments. Hypsometric curves were used to compare the observed and modeled bed topography. Hypsometric curve is a plot of sorted bed elevation and their respective cumulative area. Since channel has a longitudinal slope, the bed topography has to be detrended with the initial bed slope before performing such statistical analysis. Use of hypsometric curve is widely used to quantify the developed topography in morphodynamic studies (Marciano, et al., 2005, Wang, et al., 2002). The results are presented later in the section 3.3.

3 RESULTS

3.1 Two dimensional benchmark tests for Delft3D

DELFT3D code simulated the initial development of free bars as predicted by the analytical free bar theories (figure 6), like GIAMT2D, as reported by Siviglia et al (2013). The code was also able to simulate the influence of obstruction in the sub-resonant case but failed to simulate the upstream influence of the obstruction for the super- resonant case. However, Verbrugen (2012) was able to simulate the upstream influence of obstruction on the morphodynamics of alternate bars under sub critical flow and super-resonant conditions using DELFT3D code.

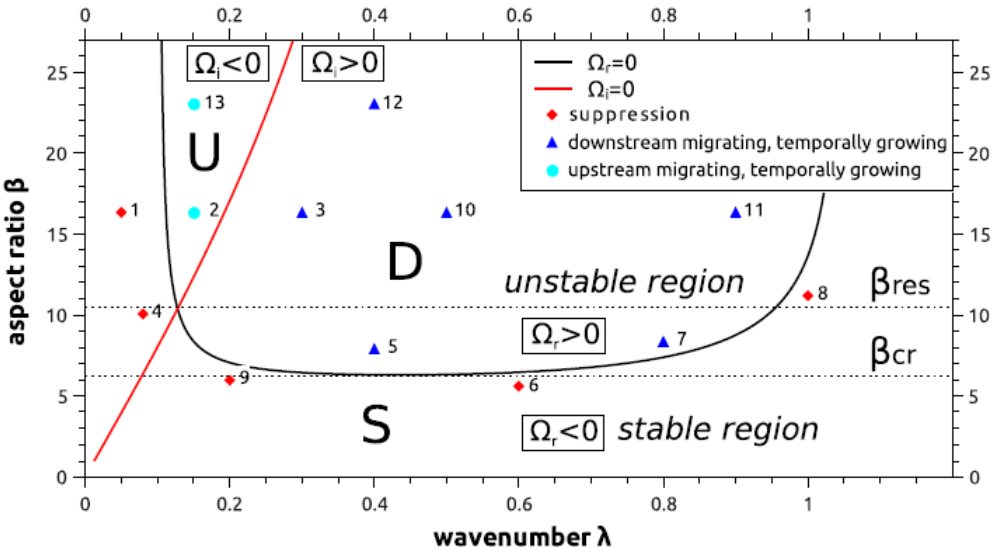

Figure – 5 Free bar instability tests performed by Siviglia et al (2013) for GIAMT2D

3.2 Numerical models

Results of the investigations of morphodynamics of alternate bars carried out using semi-coupled model and fully-coupled numerical models are presented in this section. After the choice of roughness parameter based upon reproduction of dry areas, the sediment transport rate measured at the downstream end of the flume is used to calibrate the Wong and Parker (2006) transport formula in the model. We adjusted values of coefficient α to reproduce the long-term average sediment transport observed at the downstream end of the flume. A progressive average of the observed sediment transport was compared with the progressive average of the modeled total sediment transport in cross-sections at every 5 cm (longitudinal grid resolution) along the reach. The progressive average (PA) sediment transport is computed at each time step progressing from beginning to the end of the

sediment transport rate signal. At each progress along with the time, sediment transport rate observed form the beginning to that location in time is averaged. The progressive average allows us to analyze if the observed signal is long enough to determine the average value of the signal. Prog ressive average of sediment transport rate both in experiment and numerical model achieve constant value closer to 300 minutes which indicate that observation duration of the sediment transport rate is sufficient to compute the average sediment transport rate. Coefficient α equal to 7 reproduced closest average sediment transport rate in both numerical models compared to the average of the observed sediment transport rate in the experiment (figure 7 a and b). The sediment transport rate in the fully-coupled model is slightly higher than the sediment transport rate in the semi-coupled model.

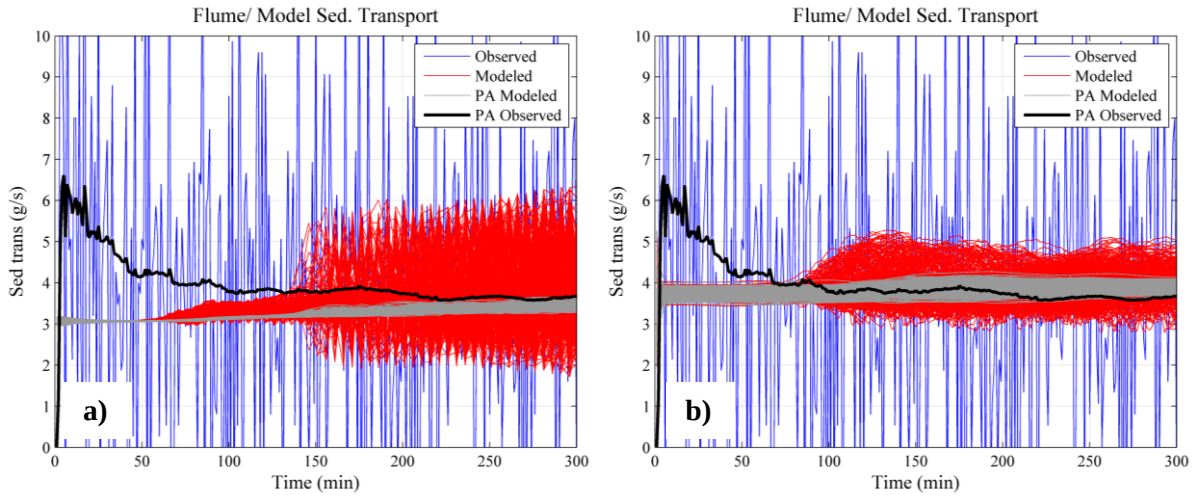

Figure – 6 Comparison of sediment transport rate observed in the experiment and modeled using a) semi-coupled model (DELFT3D) and b) fully-coupled model (GIAMT2D)

The topography of the channel bed was modeled in detail adjusting the coefficient of transverse bed slope effect on direction of bed load transport as discussed in the earlier section. Hypsometric curves were used to compare the modeled bed topography with the observed bed topography. The best resemblance was observed for the value of r = 0.108 (figure 8 a and b). The two dimensional topography, detrended with longitudinal slope, of bars modeled using semi-coupled and fully-coupled model are shown in figure 9, a and b.

The percentage of area below and above zero level in the hypsometric curves represents the area of channels and bars respectively. The hypsometric curves show that both Delft3D and GIAMT2D models are not able to model the bed level distribution correctly as observed in the experiments. However, hypsometric curves from Delft3D model output shows that the model was able to reproduce areas of channels closer to experiments than GIAMT2D model. On the other hand the hypsometric curve from GIAMT2D model shows that it was able to reproduce bar areas closer to experiment than Delft3D model.

Longitudinal profiles along the left bank center and the right bank of both numerical models are compared with those observed in the experimental runs (figure 10 a and b). The bars reproduced by both Delft3D and GIAMT2D models are shorter than those observed in the experiments. The bars reproduced by Delft3D model have steep downstream slope and mild upstream slope. It indicates that bars are migrating in downstream direction at faster rate. However, the heights of bars in Delft3D are closer to the bar heights in experiments which are also reflected in the hypsometric curve (figure 8a). The bars reproduced by GIAMT2D have similar slope both in upstream and downstream direction,

closer to the experiments, which indicates that the bars are migrating downstream at slower speed (figure 10b). The height of bars is however lower compared to those of experiments which is the reason why the hypsometric curve of bed topography modeled by GIAMT2D matches closer to that of experiments in the bar portion than in channel portion(figure 8b).

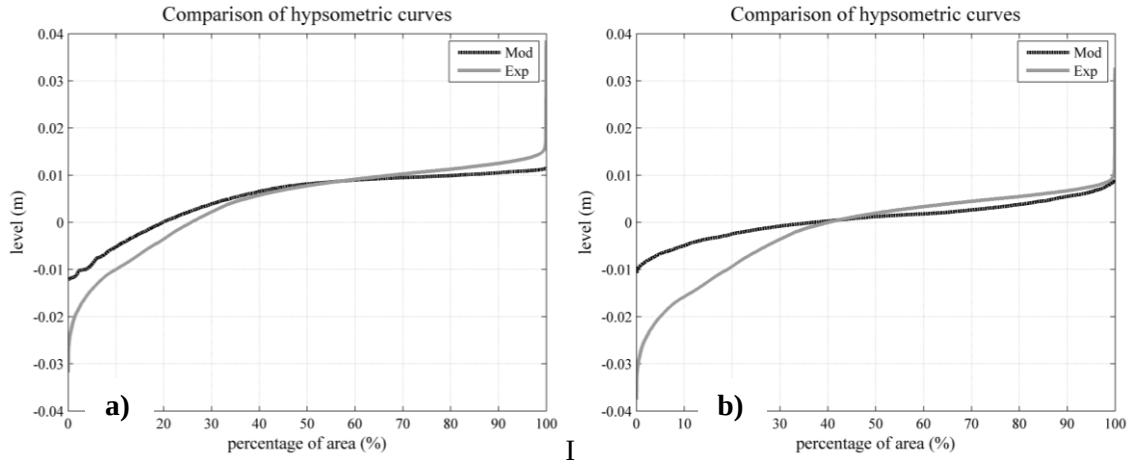

Figure – 7 Comparison of hypsometric curves of bed topography observed in the experiment and modeled using a) semi-coupled model (DELFT3D) and b) fully-coupled model (GIAMT2D) for straight bank case

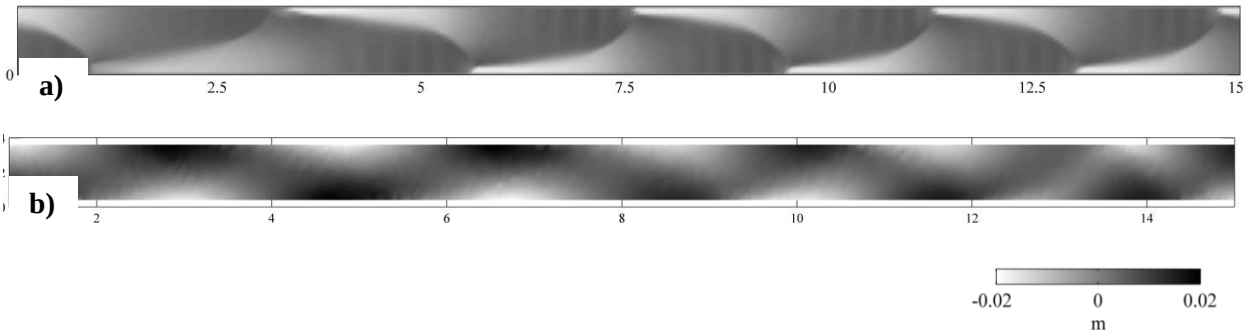

Figure – 8 Detrended bed topography modeled using a) DELFT3D and b) GIAMT2D, flow is from left to right

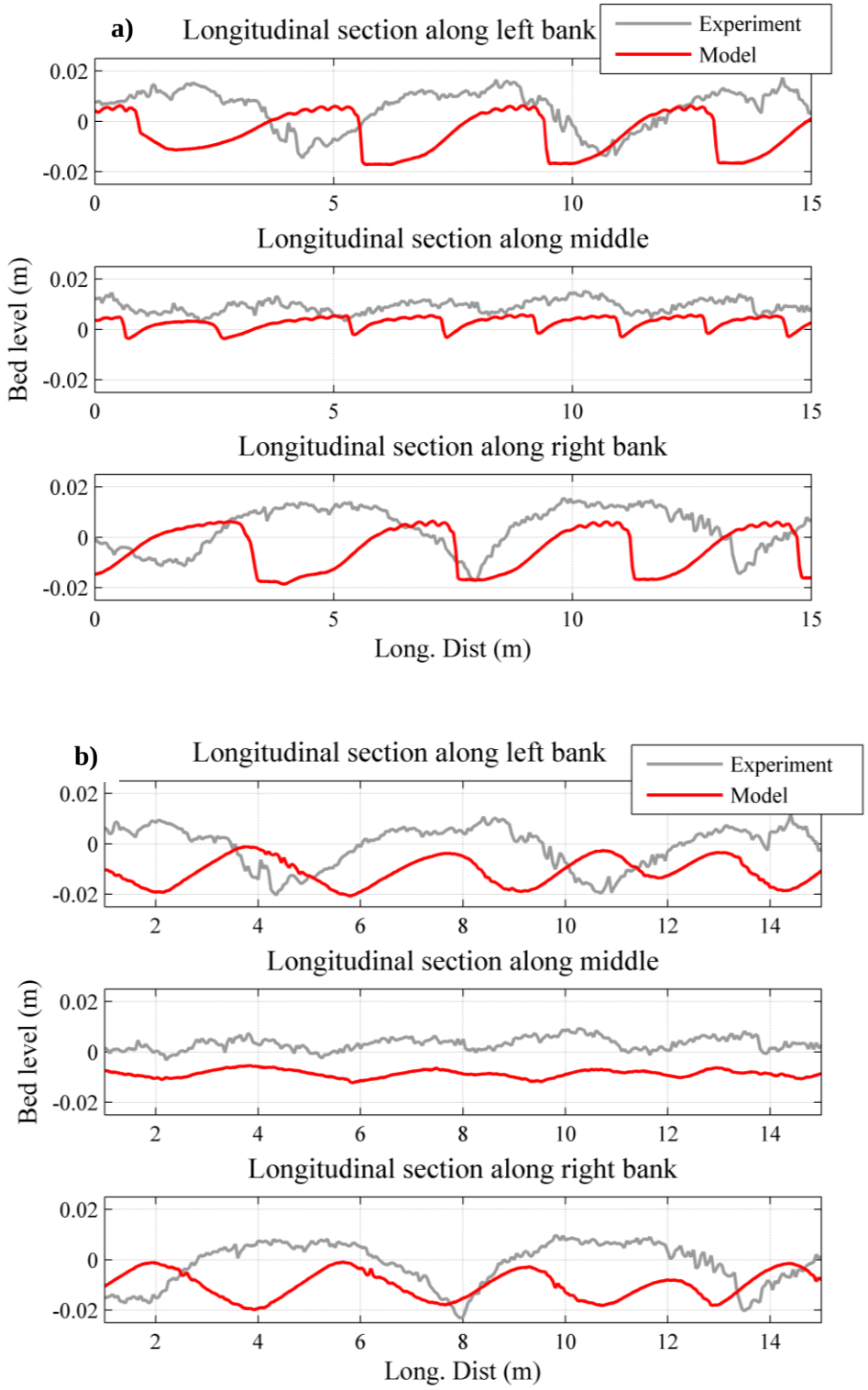

Figure – 9 Comparison of longitudinal profile, along the left bank, center and the right bank, between the experiment and modeled topography using a) DELFT3D and b) GIAMT2D, flow is from left to right

4 CONCLUSION AND DISCUSSION

This study aims to study morphodynamics of alternate bars using different morphological models. We used two 2D numerical models, one semi-coupled and another fully-coupled for the investigation. The

semi-coupled model, based on the DELFT3D code designed for small Froude numbers (<0.8). A fully-coupled model based upon GIAMT2D code, which can handle supercritical flows (Fr>1) is also used for the investigation. The physical and numerical parameters in both numerical models are kept as similar as possible for the robust comparison between the results from both the numerical models. GIAMT2D does not have parameterization of spiral flow effects and lateral bank erosion compared to Delft3D. The stream line curvatures are relatively mild in the case of alternate bars (straight channels) due to the absence of sharp curves. So, spiral flow may have less effect on the alternate bar dynamics. Since the bank is non-erodible and no emerged bars are observed, the effect of lateral bank erosion on the dynamics of alternate bars is no more significant in our case. So, both parameters were not implemented also in Delft3D model. They may be relevant in modeling the wandering and braiding channels. Curvatures are relatively high due to the presence of the mid-channel bars which might increase the effect of spiral flow on the dynamics of bars. Bars were immersed from water surface for both the cases and the interface between the dry and wet part of the bar also behaves as a bank inside a channel. So, the effect of the lateral bank erosion can play an important role in the bar dynamics.

Data of flume experiments were used to setup the numerical models to reproduce the observed experiments. Manning's formulation was chosen to be consistent with both numerical models. However, Manning's coefficient is converted to Chezy's coefficient in DELFT3D code using water depth, which makes roughness depth dependent unlike in GIAMT2D where the Manning's formulation is not depth dependent. The flow field and roughness parameters were not measured in the experiments. The value of roughness is the results of calibration based on the reproduction of the extension of dry areas measured in the final bed topography of the braided and the wandering case. Although the experiments were conducted using the same sediment, the value of the roughness may be different due to the presence of more mid channel bars (additional form roughness) and differences in water depth. The adopted method of hydrodynamic calibration is still a tentative estimation of the hydraulic roughness parameters because the flow velocity may deviate significantly even if the flow depth is modelled with a reasonable accuracy in a numerical model (Papanicolau et al., 2011).

Linear bar theory shows that the width to depth ratio (β) of the experiments are high compared to the critical width to depth ratio for alternate bar instability. The value of β in the analyzed experimental tests might also lie above the β critical value of higher bar modes. Indeed in the numerical runs we first observed small mid channel bars appearing within the domain. These small mid channel bars later merged to form larger alternate bars as the development progressed. Even thoguh β of the experiment is higher than the resonant value of β, the observed alternate bars fall in sub resonant region because alternate bars with wave number 1.04 are observed, which is higher than the resonant wave number. The bed topography in experiments measured at two different times (figure 2 a and b) also show the alternate bars elongating and migrating downstream.

The bar properties in the numerical models were significantly different compared to those observed in laboratory experiments, even if the average sediment transport rate predicted in the model was quite close to the one observed in the laboratory experiment. Bars reproduced by both Delft3D and GIAMT2D had wave length between 3 to 5 m and were shorter compared to the bars in the laboratory experiments. Bars in DELFT3D had longer wave lengths compared to bars simulated by GIAMT2D. DELFT3D bars had asymmetric shape with steeper slope at downstream part and were migrating downstream at higher speed in DELFT3D (figure 10 a). GIAMT2D bars had more symmetrical shape and had even slope both in upstream and downstream direction and were migrating downstream with a slower speed (figure 10 b) compared to Delft3D. Higher migration speed of bars in DELFT3D might be due to the imposed discharge perturbation at the upstream boundary in addition to the initial bed perturbation. The bed topography measured at two instances near the end of the experiments

show that the bars in the experiment were migrating downstream at slower rate than those observed in the experiments. The wavelengths of non-migrating bars are longer compared to those of free bars which indicate that the alternate bars in experiment are non-migrating alternate bars.

Bibliography

Alonso, C. V., and C. T. Combs (1986), Channel width adjustment in straight alluvial channels, in *4th Federal Interagency Sedimentation Conference*, pp. 345–357.

Amiri-Tokaldany, E., S. E. Darby, and P. Tosswell (2003), Bank Stability Analysis for Predicting Reach Scale Land Loss and Sediment Yield, *J. Am. Water Resour. Assoc.*, 897–909.

Anderson, R. J., B. P. Bledsoe, and W. C. Hession (2005), Anderson2004_JAWRA, , *05405*.

Andrews, E. D. (1984), Bed-material entrainment and hydraulic geometry of gravel-bed rivers in Colorado., *Geol. Soc. Am. Bull.*, *95*(3), 371–378, doi:10.1130/0016-7606(1984)95<371:BEAHGO>2.0.CO;2.

Ashmore, P. (1991), Channel Morphology and Bed Load Pulses in Braided, Gravel-Bed Streams, *Geogr. Ann. Ser. A, Phys. Geogr.*, *73*(1), 37, doi:10.2307/521212.

Ashmore, P. E. (1982), Laboratory modelling of gravel braided stream morphology, *Earth Surf. Process. Landforms*, *7*(3), 201–225, doi:10.1002/esp.3290070301.

Van den Berg, J. (1995), Prediction of alluvial channel pattern of perennial rivers, *Geomorphology*, *12*(4), 259–279, doi:10.1016/01695-55X9(50)0014V-.

Bernini, A., V. Caleffi, and A. Valiani (2006), Numerical Modelling of Alternate Bars in Shallow Channels, in *Braided Rivers*, pp. 153–175.

Bertoldi, W., and M. Tubino (2005), Bed and bank evolution of bifurcating channels, *Water Resour. Res.*, *41*(7), n/a–n/a, doi:10.1029/2004WR003333.

Bertoldi, W., a. M. Gurnell, and M. Welber (2013), Wood recruitment and retention: The fate of eroded trees on a braided river explored using a combination of field and remotely-sensed data sources, *Geomorphology*, *180-181*, 146–155, doi:10.1016/j.geomorph.2012.10.003.

Bittner, L. D. (1994), River bed response to channel width variations: Theory and experiments, University of Illinois at Urbana-Champaign.

Blanckaert, K., and H. J. de Vriend (2003), Nonlinear modeling of mean flow redistribution in curved open channels, *Water Resour. Res.*, *39*(12), 1–14, doi:10.1029/2003WR002068.

Blench, T. (1969), *Mobile-bed Fluviology*, University of Alberta Press, Edmonton, Alberta, Canada.

Blondeaux, P., and G. Seminara (1985), A unified bar–bend theory of river meanders, *J. Fluid Mech.*, *157*(-1), 449, doi:10.1017/S0022112085002440.

Bolla Pittaluga, M., R. Luchi, and G. Seminara (2014), On the equilibrium profile of river beds, *J. Geophys. Res. Earth Surf.*, *119*(2), 317–332, doi:10.1002/2013JF002806.

Borah, D. K., and P. K. Bordoloi (1989), Stream bank erosion and bed evolution model, in *Sediment Transport Modeling*, edited by S. Wang, pp. 612–617.

Bray, D. I. (1982), Regime relations for gravel-bed rivers, in *Gravel-Bed Rivers*, edited by R. D. Hey, J. C. Bathurst, and C. R. Thorne, pp. 517–542, John Wiley, Chichester, U. K.

Byishimo, P. (2014), Effects of variable discharge on the width formation and cross-sectional shape of sinuous rivers, UNESCO-IHE.

Callander, R. a. (1969), Instability and river channels, *J. Fluid Mech.*, *36*(03), 465, doi:10.1017/S0022112069001765.

Cantelli, a., M. Wong, G. Parker, and C. Paola (2007), Numerical model linking bed and bank evolution of incisional channel created by dam removal, *Water Resour. Res.*, *43*(7), 1–16, doi:10.1029/2006WR005621.

Cao, S., and D. W. Knight (1996), Regime theory of alluvial channels based upon the concept of stream power and probability, *Proc. ICE - Water Marit. Energy*, *118*(3), 160–167, doi:10.1680/iwtme.1996.28683.

Chew, L. C., and P. E. Ashmore (2001), Channel adjustment and a test of rational regime theory in aproglacial braided stream, *Geomorphology*, *37*(1-2), 43–63, doi:10.1016/S0169-555X(00)00062-3.

Church, M., and R. I. Ferguson (2015), Morphodynamics: Rivers beyond steady state, *Water Resour. Res.*, *6*(4), n/a–n/a, doi:10.1002/2014WR016862.

Colombini, M., and a. Stocchino (2008), Finite-amplitude river dunes, *J. Fluid Mech.*, *611*, 283–306, doi:10.1017/S0022112008002814.

Colombini, M., and a. Stocchino (2011), Ripple and dune formation in rivers, *J. Fluid Mech.*, *673*, 121–131, doi:10.1017/S0022112011000048.

Colombini, M., and a. Stocchino (2012), Three-dimensional river bed forms, *J. Fluid Mech.*, *695*, 63–80, doi:10.1017/jfm.2011.556.

Colombini, M., G. Seminara, and M. Tubino (1987), Finite-amplitude alternate bars, *J. Fluid Mech.*, *181*(-1), 213, doi:10.1017/S0022112087002064.

Coulthard, T. J., and M. J. Van De Wiel (2006), A cellular model of river meandering, *Earth Surf. Process. Landforms*, *31*(1), 123–132, doi:10.1002/esp.1315.

Coulthard, T. J., and M. J. Van De Wiel (2013), Numerical Modeling in Fluvial Geomorphology, in *Treatise on Geomorphology*, vol. 9, pp. 694–710, Elsevier Ltd.

Couperthwaite, J. S. (1997), Downstream change in channel hydraulics along the River Severn, UK, University of Birmingham.

Crosato, A., and E. Mosselman (2009), Simple physics-based predictor for the number of river bars and the transition between meandering and braiding, *Water Resour. Res.*, *45*(3), 1–14, doi:10.1029/2008WR007242.

Crosato, A., and M. S. Saleh (2011), Numerical study on the effects of floodplain vegetation on river planform style, *Earth Surf. Process. Landforms*, *36*(6), 711–720, doi:10.1002/esp.2088.

Crosato, A., E. Mosselman, F. Beidmariam Desta, and W. S. J. Uijttewaal (2011), Experimental and numerical evidence for intrinsic nonmigrating bars in alluvial channels, *Water Resour. Res.*, *47*(3), 1–14, doi:10.1029/2010WR009714.

Crosato, A., F. B. Desta, J. Cornelisse, F. Schuurman, and W. S. J. Uijttewaal (2012), Experimental and numerical findings on the long-term evolution of migrating alternate bars in alluvial channels, *Water Resour. Res.*, *48*(6), doi:10.1029/2011WR011320.

Dapporto, S., M. Rinaldi, and N. Casagli (2001), Failure mechanisms and pore water pressure conditions: Analysis of a riverbank along the Arno River (Central Italy), *Eng. Geol.*, *61*(4), 221–242, doi:10.1016/S0013-7952(01)00026-6.

Darby, S. E., and C. R. Thorne (1996), Numerical Simulation of Widening and Bed Deformation of Straight Sand-Bed Rivers. I: Model Development, *J. Hydraul. Eng.*, *122*(4), 184–193, doi:10.1061/(ASCE)0733-9429(1996)122:4(184).

Darby, S. E., M. Rinaldi, and S. Dapporto (2007), Coupled simulations of fluvial erosion and mass wasting for cohesive river banks, *J. Geophys. Res. Earth Surf.*, *112*(3), 1–15, doi:10.1029/2006JF000722.

Darby, S. E., H. Q. Trieu, P. a. Carling, J. Sarkkula, J. Koponen, M. Kummu, I. Conlan, and J. Leyland (2010), A physically based model to predict hydraulic erosion of fine-grained riverbanks: The role of form roughness in limiting erosion, *J. Geophys. Res. Earth Surf.*, *115*(4), 1–20, doi:10.1029/2010JF001708.

Defina, A. (2003), Numerical experiments on bar growth, *Water Resour. Res.*, *39*(4), 1–12, doi:10.1029/2002WR001455.

Diplas, P. (1990), Characteristics of Self- Formed Straight Channels, *J. Hydraul. Eng.*, *116*(5), 707–728, doi:10.1061/(ASCE)0733-9429(1990)116:5(707).

Diplas, P., and G. G. Vigilar (1992), Hydraulic Geometry of Threshold Channels, *J. Hydraul. Eng.*, *118*(4), 597–614, doi:10.1061/(ASCE)0733-9429(1992)118:4(597).

Duro, G., A. Crosato, and P. Tassi (2015), Numerical experiments to explore bar management by channel width variations, in *E-proceedings of the 36th IAHR World Congress*, pp. 28–31, The Hague, the Netherlands.

Duró, G., A. Crosato, and P. Tassi (2015), Numerical study on river bar response to spatial variations of channel width, *Adv. Water Resour.*, doi:10.1016/j.advwatres.2015.10.003.

Eaton, B. C., and M. Church (2007), Predicting downstream hydraulic geometry: A test of rational regime theory, *J. Geophys. Res. Earth Surf.*, *112*(3), 1–18, doi:10.1029/2006JF000734.

Eaton, B. C., and R. G. Millar (2004), Optimal alluvial channel width under a bank stability constraint, *Geomorphology*, *62*(1-2), 35–45, doi:10.1016/j.geomorph.2004.02.003.

Eaton, B. C., R. G. Millar, and S. Davidson (2010), Channel patterns: Braided, anabranching, and single-thread, *Geomorphology*, *120*(3-4), 353–364, doi:10.1016/j.geomorph.2010.04.010.

Engelund, F. (1970), Instability of erodible beds, *J. Fluid Mech.*, *42*(02), 225, doi:10.1017/S0022112070001210.

Exner, F. M. (1925), Über die Wechselwirkung zwischen Wasser und Geschiebe in Flüssen (On the interaction between water and sediment in streams), in *Akad. Wiss Wien*, pp. 165–205.

Federici, B., and G. Seminara (2003), On the convective nature of bar instability, *J. Fluid Mech.*, *487*, S0022112003004737, doi:10.1017/S0022112003004737.

Ferguson, R. I. (1986), *Hydraulics and hydraulic geometry*.

Foley, J. a. (2005), Global Consequences of Land Use, *Science (80-.).*, *309*(5734), 570–574, doi:10.1126/science.1111772.

Fredkin, J. F. (1945), *A laboratory study of the meandering of alluvial rivers*.

Fredsøe, J. (1978), Meandering and braiding of rivers, *J. Fluid Mech.*, *84*(04), 609, doi:10.1017/S0022112078000373.

Fujita & Muramoto (1982), Experimental Study on Stream Channel in Alluvial Rivers, *Bull. Disaster Prev. Res. Inst.*, *32*(288), 49 – 96.

Fujita, Y. (1989), Bar and Channel Formation in Braided Streams, in *River Meandering*, vol. 12, pp. 417–462.

Fujita, Y., and Y. Muramoto (1985), Studies on the Process of Development of Alternate Bars, *Bull. Disaster Prev. Res. Inst.*, 55–86.

Garcia Lugo, G. A., W. Bertoldi, A. J. Henshaw, and A. M. Gurnell (2015), The effect of lateral confinement on gravel bed river morphology, *Water Resour. Res.*, *51*(9), 7145–7158, doi:10.1002/2015WR017081.

Garcia, M. H. (1999), Closure to "The Legend of A. F. Shields" by John M. Buffington, *J. Hydraul. Eng.*, *126*(9), 721–723, doi:10.1061/(ASCE)0733-9429(2000)126:9(721.2).

García, M. H. (2008), Sediment Transport and Morphodynamics, *Sediment. Eng.*, *54*(110), 21–163, doi:doi: 10.1061/9780784408148.ch02.

Glover, R. E., and Q. L. Florey (1951), *Stable channel profiles*, Denver, Colorado.

Griffiths, G. A. (1984), Extremal Hypotheses for River Regime: An Illusion of Progress, *Water Resour. Res.*, *20*(1), 113–118, doi:10.1029/WR020i001p00113.

Gurnell, A. M., W. Bertoldi, and D. Corenblit (2012), Changing river channels: The roles of hydrological processes, plants and pioneer fluvial landforms in humid temperate, mixed load, gravel bed rivers, *Earth-Science Rev.*, *111*(1-2), 129–141, doi:10.1016/j.earscirev.2011.11.005.

Hey, R. D., and C. R. Thorne (1986), Stable Channels with Mobile Gravel Beds, *J. Hydraul. Eng.*, *112*(8), 671–689, doi:10.1061/(ASCE)0733-9429(1986)112:8(671).

Hoey, T. B., and A. J. Sutherland (1991), Channel morphology and bedload pulses in braided rivers: a laboratory study, *Earth Surf. Process. Landforms*, *16*(5), 447–462, doi:10.1002/esp.3290160506.

Huang, H. Q. (2010), Reformulation of the bed load equation of Meyer-Peter and M??ller in light of the linearity theory for alluvial channel flow, *Water Resour. Res.*, *46*(9), 1–11, doi:10.1029/2009WR008974.

Huang, H. Q., and G. C. Nanson (1997), Vegetation and channel variation; a case study of four small streams in southeastern Australia, *Geomorphology*, *18*(3-4), 237–249, doi:10.1016/S0169-555X(96)00028-1.

Huang, H. Q., C. Deng, G. C. Nanson, B. Fan, X. Liu, T. Liu, and Y. Ma (2014), A test of equilibrium theory and a demonstration of its practical application for predicting the morphodynamics of the Yangtze River, *Earth Surf. Process. Landforms*, *39*(5), 669–675, doi:10.1002/esp.3522.

Hunziker, R. P., and M. N. R. Jaeggi (2002), Grain Sorting Processes, *J. Hydraul. Eng.*, *128*(12), 1060–1068, doi:10.1061/(ASCE)0733-9429(2002)128:12(1060).

Ikeda, H. (1989), Sedimentary Controls on Channel Migration and Origin of Point Bars in Sand–Bedded Meandering Rivers, *River Meand.*, *12*, 51–68, doi:10.1029/WM012p0051.

Ikeda, S. (1981), Self-formed straight channels in sandy beds, *J. Hydraul. Div. Am. Soc. Eng.*, *107*(4), 389–406.

Ikeda, S. (1982), Lateral bed load transport on side slopes, *J. Hydraul. Div. Am. Soc. Civ. Eng.*, *108*(11), 1369–1373.

Ikeda, S., and N. Izumi (1990), Width and depth of self-formed straight gravel rivers with bank vegetation, *Water Resour. Res.*, *26*(10), 2353–2364, doi:10.1029/90WR00812.

Ikeda, S., and N. Izumi (1991), Stable channel cross sections of straight sand rivers, *Water Resour. Res.*, *27*(9), 2429–2438, doi:10.1029/91WR01220.

Ikeda, S., G. Parker, and Y. Kimura (1988), Stable width and depth of straight gravel rivers with heterogeneous bed materials, *Water Resour. Res.*, *24*(5), 713, doi:10.1029/WR024i005p00713.

Iwasaki, T., Y. Shimizu, and I. Kimura (2015), Numerical simulation of bar and bank erosion in a vegetated floodplain: A case study in the Otofuke River, *Adv. Water Resour.*, 1–17, doi:10.1016/j.advwatres.2015.02.001.

Jaeggi, M. N. R. (1984), Formation and Effects of Alternate Bars, *J. Hydraul. Eng.*, *110*(2), 142–156, doi:10.1061/(ASCE)0733-9429(1984)110:2(142).

Jang, C., and Y. Shimizu (2005a), Numerical Simulation of Relatively Wide, Shallow Channels with Erodible Banks, *J. Hydraul. Eng.*, *131*(July), 565–575.

Jang, C.-L., and Y. Shimizu (2005b), Numerical simulations of the behavior of alternate bars with different bank strengths, *J. Hydraul. Res.*, *43*(6), 596–612, doi:10.1080/00221680509500380.

Jansen, P. P., L. Van Bendegom, J. van den Berg, M. De Vries, and A. Zanen (1979), *Principles of river engineering: non tidal alluvial river*, Pitman, London.

Jia, D., X. Shao, H. Wang, and G. Zhou (2010), Three-dimensional modeling of bank erosion and morphological changes in the Shishou bend of the middle Yangtze River, *Adv. Water Resour.*, *33*(3), 348–360, doi:10.1016/j.advwatres.2010.01.002.

Julien, P. (2002), *River Mechanics*, Cambridge University Press.

Kaless, G., L. Mao, and M. a. Lenzi (2014), Regime theories in gravel-bed rivers: Models, controlling variables, and applications in disturbed Italian rivers, *Hydrol. Process.*, *28*(4), 2348–2360, doi:10.1002/hyp.9775.

Kassem, A. A., and M. H. Chaudhry (1998), Comparison of Coupled and Semicoupled Numerical Models for Alluvial Channels, *J. Hydraul. Eng.*, *124*(8), 794–802, doi:10.1061/(ASCE)0733-9429(1998)124:8(794).

Kean, J. W., and J. D. Smith (2006a), Form drag in rivers due to small-scale natural topographic features: 1. Regular sequences, *J. Geophys. Res. Earth Surf.*, *111*(4), 1–13, doi:10.1029/2006JF000467.

Kean, J. W., and J. D. Smith (2006b), Form drag in rivers due to small-scale natural topographic features: 2. Irregular sequences, *J. Geophys. Res. Earth Surf.*, *111*(4), 1–15, doi:10.1029/2006JF000467.

Kennedy, R. G. (1895), The prevention of silting in irrigation canals, *Minutes Proc.*, *119*(1895), 281–290, doi:10.1680/imotp.1895.19850.

Klaassen, G. J., E. Mosselman, and H. Brühl (1993), On the prediction of planform changes in braided sand-bed rivers, in *Advances in Hydro-Science and -Engineering*, pp. 134–146.

Kleinhans, M. G. (2010), Sorting out river channel patterns, *Prog. Phys. Geogr.*, *34*(3), 287–326, doi:10.1177/0309133310365300.

Kleinhans, M. G., and J. H. van den Berg (2011), River channel and bar patterns explained and predicted by an empirical and a physics-based method, *Earth Surf. Process. Landforms*, *36*(6), 721–738, doi:10.1002/esp.2090.

Van Der Klis, H. (2003), Uncertainty Analysis applied to Numerical Models of River Bed Morphology, Delft University of Technology.

Klösch, M., B. Blamauer, and H. Habersack (2015), Intra-event scale bar-bank interactions and their role in channel widening, *Earth Surf. Process. Landforms*, n/a–n/a, doi:10.1002/esp.3732.

Kovacs, A., and G. Parker (1994), A new vectorial bedload formulation and its application to the time evolution of straight river channels, *J. Fluid Mech.*, *267*(-1), 153, doi:10.1017/S002211209400114X.

Lacey, G. (1930), Stable channels in alluvium, *Minutes Proc.*, *229*(1930), 259–292, doi:10.1680/imotp.1930.15592.

Lane, E. W. (1955), Design of Stable Channels, *Trans. Am. Soc. Civ. Eng.*, *120*(1), 1234–1260.

Langendoen, E., and a Simon (2008), Modeling the Evolution of Incised Streams . II : Streambank Erosion, *J. Hydraul. Eng.*, *134*(7), 905–915, doi:10.1061/(ASCE)0733-9429(2008)134:7(905).

Langendoen, E. J., and C. V. Alonso (2008), Modeling the Evolution of Incised Streams: I. Model Formulation and Validation of Flow and Streambed Evolution Components, *J. Hydraul. Eng.*, *134*(6), 749–762, doi:10.1061/(ASCE)0733-9429(2008)134:6(749).

Langendoen, E. J., A. Mendoza, J. D. Abad, P. Tassi, D. Wang, R. Ata, K. El kadi Abderrezzak, and J.-M. Hervouet (2015), Improved numerical modeling of morphodynamics of rivers with steep banks, *Adv. Water Resour.*, doi:10.1016/j.advwatres.2015.04.002.

Lanzoni, S. (2000a), Experiments on bar formation in a straight flume: 1. Uniform sediment, *Water Resour. Res.*, *36*(11), 3351, doi:10.1029/2000WR900161.

Lanzoni, S. (2000b), Experiments on bar formation in a straight flume: 2. Graded sediment, *Water Resour. Res.*, *36*(11), 3351, doi:10.1029/2000WR900161.

Leopold, B. L., and M. G. Wolman (1957), *River Channel Patterns: Braided, Meandering, and Straight*.

Leopold, L. B., and T. J. Maddock (1953), The Hydraulic Geomtry of Stream Channels and Some Physiographic Implications, *Geol. Surv. Prof. Pap. 252*, 1–56.

Lesser, G. R., J. a. Roelvink, J. a T. M. van Kester, and G. S. Stelling (2004), Development and validation of a three-dimensional morphological model, *Coast. Eng.*, *51*(8-9), 883–915, doi:10.1016/j.coastaleng.2004.07.014.

Leyland, J., S. E. Darby, L. Teruggi, M. Rinaldi, and D. Ostuni (2015), A self-limiting bank erosion mechanism? Inferring temporal variations in bank form and skin drag from high resolution topographic data, *Earth Surf. Process. Landforms*, n/a–n/a, doi:10.1002/esp.3739.

Li, S., and R. G. Millar (2011), A two-dimensional morphodynamic model of gravel-bed river with floodplain vegetation, *Earth Surf. Process. Landforms*, *36*(2), 190–202, doi:10.1002/esp.2033.

Lindley, E. S. (1919), Regime Channels, in *Punjab Engineering Congress*, vol. 7, pp. 63–74.

Lundgren, H., and I. G. Jonsson (1964), Shear and velocity distribution in shallow channels, *J. Hydraul. Div. Am. Soc. Eng.*, *901*, 1–21.

Meyer-Peter, E., and R. Müller (1948), Formulas for Bed-Load Transport, *Int. Assoc. Hydraul. Struct. Researach - Zweite Tagung - Second Meet. - Deuxième réunion*.

Millar, R. G. (2000), Influence of bank vegetation on alluvial channel patterns, *Water Resour. Res.*, *36*(4), 1109–1118, doi:10.1029/1999WR900346.

Millar, R. G. (2005), Theoretical regime equations for mobile gravel-bed rivers with stable banks, *Geomorphology*, *64*(3-4), 207–220, doi:10.1016/j.geomorph.2004.07.001.

Millar, R. G., and M. C. Quick (1993), Effect of Bank Stability on Geometry of Gravel Rivers, *J. Hydraul. Eng.*, *119*(12), 1343–1363, doi:10.1061/(ASCE)0733-9429(1995)121:4(382).

Mosselman, E. (1998), Morphological modelling of rivers with erodible banks, *Hydrol. Process.*, *12*(8), 1357–1370, doi:10.1002/(SICI)1099-1085(19980630)12:8<1357::AID-HYP619>3.0.CO;2-7.

Mosselman, E. (2004), Hydraulic geometry of straight alluvial channels and the principle of least action, *J. Hydraul. Res.*, *42*(2), 219–222, doi:10.1080/00221686.2004.9728386.

Mosselman, E., M. Tubino, and G. Zolezzi (2006), The overdeepening theory in river morphodynamics : Two decades of shifting interpretations, *Group*, (1998), 1175–1181.

Murray, A. B., and C. Paola (1994), A cellular model of braided rivers, *Lett. to Nat.*, 54–57.

Nanson, G. C., and E. J. Hickin (1983), Channel Migration and Incision on the Beatton River, *J. Hydraul. Eng.*, *109*(3), 327–337, doi:10.1061/(ASCE)0733-9429(1983)109:3(327).

Nelson, J. (1990), The initial instability and finite-amplitude stability of alternate bars in straight channels, *Earth-Science Rev.*, *29*(1-4), 97–115, doi:10.1016/0012-8252(90)90030-Y.

Nicholas, a. P., P. J. Ashworth, G. H. Sambrook Smith, and S. D. Sandbach (2013), Numerical simulation of bar and island morphodynamics in anabranching megarivers, *J. Geophys. Res. Earth Surf.*, *118*(4), 2019–2044, doi:10.1002/jgrf.20132.

Nicholas, A. P. (2010), Reduced-complexity modeling of free bar morphodynamics in alluvial channels, *J. Geophys. Res. Earth Surf.*, *115*(4), doi:10.1029/2010JF001774.

Nicholas, A. P. (2013), Modelling the continuum of river channel patterns, *Earth Surf. Process. Landforms*, *38*(10), 1187–1196, doi:10.1002/esp.3431.

Nienhuis, P. H., and R. S. E. Leuven (2001), River restoration and flood protection: controversy or synergism, *Hydrobiologia*, *444*(1998), 85–99, doi:10.1023/A:1017509410951.

Niezgoda, S. L., and P. A. Johnson (2005), Improving the Urban Stream Restoration Effort: Identifying Critical Form and Processes Relationships, *Environ. Manage.*, *35*(5), 579–592, doi:10.1007/s00267-004-0088-8.

Osman, A. M., and C. R. Thorne (1988), Riverbank Stability Analysis. I: Theory, *J. Hydraul. Eng.*, *114*(2), 134–150, doi:10.1061/(ASCE)0733-9429(1988)114:2(134).

Papanicolaou, A. N., M. Elhakeem, and R. Hilldale (2007), Secondary current effects on cohesive river bank erosion, *Water Resour. Res.*, *43*(12), 1–14, doi:10.1029/2006WR005763.

Parker, G. (1976), On the cause and characteristic scales of meandering and braiding in rivers, *J. Fluid Mech.*, *76*(03), 457, doi:10.1017/S0022112076000748.

Parker, G. (1978a), Self-formed straight rivers with equilibrium banks and mobile bed. Part 1. The sand-silt river, *J. Fluid Mech.*, *89*(01), 109–125, doi:10.1017/S0022112078002499.

Parker, G. (1978b), Self-formed straight rivers with equilibrium banks and mobile bed. Part 2. The gravel river, *J. Fluid Mech.*, *89*(01), 127, doi:10.1017/S0022112078002505.

Parker, G. (1979), Hydrulic geometry of active gravel rivers, *J. Hydraul. Div. Am. Soc. Eng.*, *105*, 1185–1201.

Parker, G., P. R. Wilcock, C. Paola, W. E. Dietrich, and J. Pitlick (2007), Physical basis for quasi-universal relations describing bankfull hydraulic geometry of single-thread gravel bed rivers, *J. Geophys. Res. Earth Surf.*, *112*(4), 1–21, doi:10.1029/2006JF000549.

Peakall, J., P. Ashworth, and J. Best (1996), Physical Modeling in Fluvial Geomorphology: Principles, Applications and Unresolved Issues, *Sci. Nat. Geomorphol.*, (September 1996), 34.

Piégay, H., S. E. Darby, E. Mosselman, and N. Surian (2005), A review of techniques available for delimiting the erodible river corridor: a sustainable approach to managing bank erosion, *River Res. Appl.*, *21*(7), 773–789, doi:10.1002/rra.881.

Pierre-Louis, V. (2005), *Water Engneering in Ancient Civilizations 5,000 years of history*.

Pizzuto, J. E. (1990), Numerical simulation of gravel river widening, *Water Resour. Res.*, *26*(9), 1971–1980, doi:10.1029/90WR00462.

Pizzuto, J. E. (1994), Channel adjustments to changing discharges, Powder River, Montana, *Geol. Soc. Am. Bull.*, *106*(11), 1494–1501, doi:10.1130/0016-7606(1994)106<1494:CATCDP>2.3.CO;2.

Prins, A., and M. De Vries (1971), On dominant discharge concepts for rivers, in *14th Congress IAHR*, p. C20, Paris.

Redolfi, M., and M. Tubino (2014), A diffusive 1 D model for the evolution of a braided network subject to varying sediment supply, in *River Flow 2014*, edited by A. J. Schleiss, G. De Cesare, M. J. Franca, and M. Pfister, pp. 1153–1162, CRC Press, Lausanne, Switzerland.

Repetto, R., M. Tubino, and C. Paola (2002), Planimetric instability of channels with variable width, *J. Fluid Mech.*, *457*, 79–109, doi:10.1017/S0022112001007595.

Van Rijn, L. (1993), *Principles of Sediment Transport in Rivers, Estuaries and Costal Seas*, Aqua Publications.

Rinaldi, M., and N. Casagli (1999), Stability of streambanks formed in partially saturated soils and effects of negative pore water pressures: the Sieve River (Italy), *Geomorphology*, *26*(4), 253–277, doi:10.1016/S0169-555X(98)00069-5.

Rinaldi, M., and S. E. Darby (2007), Modelling river-bank-erosion processes and mass failure mechanisms: progress towards fully coupled simulations, in *Developments in Earth Surface Processes*, vol. 11, pp. 213–239.

Rinaldi, M., B. Mengoni, L. Luppi, S. E. Darby, and E. Mosselman (2008), Numerical simulation of hydrodynamics and bank erosion in a river bend, *Water Resour. Res.*, *44*(9), 1–17, doi:10.1029/2008WR007008.

Rinaldi, M., C. Simoncini, and H. Piégay (2009), Scientific design strategy for promoting sustainable sediment management: The case of the magra river (Central-Northern Italy), *River Res. Appl.*, *25*(5), 607–625, doi:10.1002/rra.1243.

Schielen, R., a. Doelman, and H. E. de Swart (1993), On the nonlinear dynamics of free bars in straight channels, *J. Fluid Mech.*, *252*(-1), 325, doi:10.1017/S0022112093003787.

Schumm, S. A. (1985), Patterns of alluvial rivers, *Annu. Rev. Earth Planet Sci.*, *13*, 5–27.

Schumm, S. A., and H. R. Khan (1972), Geological Society of America Bulletin Experimental Study of Channel Patterns, *America (NY).*, *83*(6), 1755, doi:10.1130/0016-7606(1972)83.

Schuurman, F., and M. G. Kleinhans (2011), Self-formed braided bar pattern in a numerical model, in *RCEM*, pp. 1647–1657.

Schuurman, F., M. G. Kleinhans, and W. A. Marra (2012), Morphodynamic modeling of large braided sand-bed rivers,

Schuurman, F., W. a. Marra, and M. G. Kleinhans (2013), Physics-based modeling of large braided sand-bed rivers: Bar pattern formation, dynamics, and sensitivity, *J. Geophys. Res. Earth Surf.*, *118*(4), 2509–2527, doi:10.1002/2013JF002896.

Seminara, G., and M. Tubino (1989), Alternate Bars and Meandering : Free , Forced and Mixed Interactions, in *River Meandering*, vol. 12, pp. 267 – 320.

Seminara, G., and M. Tubino (1992), Weakly nonlinear theory of regular meanders, *J. Fluid Mech.*, *244*, 257, doi:10.1017/S0022112092003069.

Shields, F. D., R. R. Copeland, P. C. Klingeman, M. W. Doyle, and A. Simon (2003), Design for Stream Restoration, *J. Hydraul. Eng.*, *129*(8), 575–584, doi:10.1061/(ASCE)0733-9429(2003)129:8(575).

Simon, A. (1989), A model of channel response in disturbed alluvial channels, *Earth Surf. Process. Landforms*, *14*(1), 11–26, doi:10.1002/esp.3290140103.

Simon, A. (1995), Adjustment and recovery of unstable alluvial channels: Identification and approaches for engineering management, *Earth Surf. Process. Landforms*, *20*(7), 611–628, doi:10.1002/esp.3290200705.

Simon, A., and a. J. C. Collison (2002), Quantifying the mechanical and hydrologic effects of riparian vegetation on streambank stability, *Earth Surf. Process. Landforms*, *27*(5), 527–546, doi:10.1002/esp.325.

Simon, A., and C. R. Thorne (1996), Channel Adjustment of an Unstable Coarse-Grained Stream: Opposing Trends of Boundary and Critical Shear Stress, and the Applicability of Extremal Hypotheses, *Earth Surf. Process. Landforms*, *21*, 155–180, doi:10.1002/(SICI)1096-9837(199602)21:2<155::AID-ESP610>3.0.CO;2-5.

Simon, A., W. J. Wolfe, and A. Molina (1991), Mass-wasting algortihms in an alluvial channel model, in *5th Federal Interagency Sediment Conference, Subcomm on Sedimentation*, pp. 22–29, Las Vegas, Nevada.

Simon, A., A. Curini, S. E. Darby, and E. J. Langendoen (2000), Bank and near-bank processes in an incised channel, *Geomorphology*, *35*(3-4), 193–217, doi:10.1016/S0169-555X(00)00036-2.

Simon, A., R. E. Thomas, A. Curini, and F. D. Shields (2002), Case Study: Channel Stability of the Missouri River, Eastern Montana, *J. Hydraul. Eng.*, *128*(10), 880–890, doi:10.1061/(ASCE)0733-9429(2002)128:10(880).

Singh, V. P. (2004), On the theories of hydraulic geometry, *Int. J.*, *18*(3), 196–218.

Siviglia, A., G. Stecca, D. Vanzo, G. Zolezzi, E. F. Toro, and M. Tubino (2013), Numerical modelling of two-dimensional morphodynamics with applications to river bars and bifurcations, *Adv. Water Resour.*, *52*, 243–260, doi:10.1016/j.advwatres.2012.11.010.

Sloff, K., and E. Mosselman (2012), Bifurcation modelling in a meandering gravel-sand bed river, *Earth Surf. Process. Landforms*, *37*(14), 1556–1566, doi:10.1002/esp.3305.

Struiksma, N., and A. Crosato (1989), Analysis of a 2-D bed topography model for rivers, in *River Meandering*, pp. 153–180.

Struiksma, N., P. Engineer, K. W. Olesen, S. Officer, and C. Flokstra (1985), Bed deformation in curved alluvial channels D ´ eformation des lits fluviaux dans les courbes 1 Introduction 2 Description of the bed deformation, , *1*, 57–79.

Sun, J., B. Lin, and H. Yang (2015), Development and application of a braided river model with non-uniform sediment transport, *Adv. Water Resour.*, doi:10.1016/j.advwatres.2014.12.012.

Surian, N., and M. Rinaldi (2003), Morphological response to river engineering and management in alluvial channels in Italy, *Geomorphology*, *50*(4), 307–326, doi:10.1016/S0169-555X(02)00219-2.

Takebayashi, H., and T. Okabe (2008), Numerical modelling of braided streams in unsteady flow, *Proc. Inst. Civ. Eng. Water Manag.*, *000*, 1–10, doi:10.1680/wama.2009.00011.

Tal, M., and C. Paola (2010), Effects of vegetation on channel morphodynamics: Results and insights from laboratory experiments, *Earth Surf. Process. Landforms*, *35*(9), 1014–1028, doi:10.1002/esp.1908.

Tealdi, S., C. Camporeale, and L. Ridolfi (2011), Long-term morphological river response to hydrological changes, *Adv. Water Resour.*, *34*(12), 1643–1655, doi:10.1016/j.advwatres.2011.08.011.

Thomas, R., and A. P. Nicholas (2002), Simulation of braided river flow using a new cellular routing scheme, *Geomorphology*, *43*, 179–195.

Thorne, C. R. et al. (1998), River Width Adjustment. I: Processes and Mechanisms, *J. Hydraul. Eng.*, *124*(9), 881–902, doi:10.1061/(ASCE)0733-9429(1998)124:9(881).

Tubino, M. (1991), Growth of Alternate Bars in Unsteady Flow, *Water Resour. Res.*, *27*(1), 37–52, doi:10.1029/90WR01699.

Tubino, M., R. Repetto, and G. Zolezzi (1999), Free bars in rivers, *J. Hydraul. Res.*, *37*(6), 759–775, doi:10.1080/00221689909498510.

Valentine, E. M., I. a. Benson, C. Nalluri, and J. C. Bathurst (2001), Regime theory and the stability of straight channels with bankfull and overbank flow, *J. Hydraul. Res.*, *39*(3), 259–268, doi:10.1080/00221680109499829.

Verbruggen, W. (2012), Numerical nonlinear analysis of alternate-bar formation and overdeepening under superresonant conditions, Delft University of Technology.

Vigilar, Jr., G. G., and P. Diplas (1998), Stable Channels with Mobile Bed: Model Verification and Graphical Solution, *J. Hydraul. Eng.*, *124*(11), 1097–1108, doi:10.1061/(ASCE)0733-9429(1998)124:11(1097).

Visconti, F., C. Camporeale, and L. Ridolfi (2010), Role of discharge variability on pseudomeandering channel morphodynamics: Results from laboratory experiments, *J. Geophys. Res. Earth Surf.*, *115*(4), 1–18, doi:10.1029/2010JF001742.

Walling, D. E. (1999), Linking land use, erosion and sediment yields in river basins, *Hydrobiologia*, *410*, 223–240, doi:10.1023/A:1003825813091.

Wang, H., G. Zhou, and X. Shao (2010), Numerical simulation of channel pattern changes Part II: Application in a conceptual channel, *Int. J. Sediment Res.*, *25*(4), 380–390, doi:10.1016/S1001-6279(11)60005-X.

Williams, R. D., J. Brasington, M. Hicks, R. Measures, C. D. Rennie, and D. Vericat (2013), Hydraulic validation of two-dimensional simulations of braided river flow with spatially continuous aDcp data, *Water Resour. Res.*, *49*(9), 5183–5205, doi:10.1002/wrcr.20391.

Wilson, I. G. (1973), Equilibrium Cross-section of Meandering and Braided Rivers, *Nature*, *241*(5389), 393–394, doi:10.1038/241393a0.

Wohl, E., S. N. Lane, and A. C. Wilcox (2015), The science and practice of river restoration, *Water Resour. Res.*, n/a–n/a, doi:10.1002/2014WR016874.

Wolman, M. G., and L. M. J. Brush (1961), *Factors controlling the size and shape of stream channels in coarse noncohesive sands*.

Wong, M., and G. Parker (2006), Reanalysis and Correction of Bed-Load Relation of Meyer-Peter and Müller Using Their Own Database, *J. Hydraul. Eng.*, *132*(11), 1159–1168, doi:10.1061/(ASCE)0733-9429(2006)132:11(1159).

Wu, F., and T. Yeh (2005), Forced bars induced by variations of channel width : Implications for incipient bifurcation, , *110*, doi:10.1029/2004JF000160.

Wu, F. C., Y. C. Shao, and Y. C. Chen (2011), Quantifying the forcing effect of channel width variations on free bars : Morphodynamic modeling based on characteristic dissipative Galerkin scheme, , *116*, 1–20, doi:10.1029/2010JF001941.

Young, W. J., and J. Warburton (1996), Principles and practice of hydraulic modelling of braided gravel-bed rivers, *Int. J. Multiph. Flow*, *35*(2), 175–198, doi:10.1016/S0301-9322(97)80098-5.

Zarfl, C., A. E. Lumsdon, and K. Tockner (2015), A global boom in hydropower dam construction, *Aquat. Sci.*, (77), 161–170, doi:10.1007/s00027-014-0377-0.

Zolezzi, G., and G. Seminara (2001), Downstream and upstream influence in river meandering. Part 1.General theory and application to overdeepening, *J. Fluid Mech.*, *438*, 183–211, doi:10.1017/S0022112001004281.

Zolezzi, G., W. Bertoldi, and M. Tubino (2012), Morphodynamics of Bars in Gravel-Bed Rivers: Bridging Analytical Models and Field Observations, in *Gravel-Bed Rivers: Processes, Tools, Environments*, pp. 69–89.